1994

Nonlinear Analysis Of Piles With Application Of Offshore Tower Response

Nagger Mohamed El

NONLINEAR ANALYSIS OF PILES WITH APPLICATION TO OFFSHORE TOWER RESPONSE

BY

Mohamed Hesham Hamed El Naggar

Faculty Of Engineering Science

Civil Engineering Department

Submitted in partial fulfilment
of the requirements for the degree of
Doctor of Philosophy

Faculty of Graduate Studies
The University of Western Ontario
London, Ontario
November 1993

ISBN 0-315-90555-7

Canada

ABSTRACT

Three main areas are addressed in this study:

1- Statnamic Test Analysis: In recent years a new type of pile test employing a short-duration load was developed that became known as pile Statnamic test. A method of dynamic analysis has been formulated for this test. The aim of the analysis is twofold: to calculate the pile head displacements in such a way that a satisfactory match with the data measured during the test is obtained; and using the model parameters established from this comparison to predict the pile capacity. The model is one-dimensional and accounts for slip and energy dissipation in the far field. The parameters of the model are, for the most part, directly related to standard geotechnical parameters. The case studies described in this research indicate that the proposed mathematical model works very well and that the Statnamic test may become a useful tool for pile capacity prediction.

2- Nonlinear Behavior of Piles: An analysis of pile axial and lateral response to transient dynamic loading and to harmonic loading is presented allowing for nonlinear soil behavior, energy dissipation through radiation damping, soil hysteresis, and the loading rate dependency of the soil resistance. Furthermore, the discontinuity conditions at the pile-soil interface are accounted for. In addition, the effect of neighbouring piles is taken into account for piles in a group. The approach is employed to analyze the pile response to harmonic forces, pile driving, and Statnamic loading and to establish the bearing Capacity and load-deflection curves. Equivalent linear stiffness and damping

parameters as well as interaction factors for approximate nonlinear analysis of pile groups are established and presented.

3. Effect of Foundation Nonlinearity on Offshore tower response: The response of a fixed offshore tower is greatly affected by the nonlinear behavior of the supporting piles. The nonlinear analysis developed in this study is utilized to model the response of foundation piles. A model for the evaluation of wave forces on the tower members that takes into account the spatial incoherence effect on wave forces is described and used in the analysis. The effect of different foundation parameters on the dynamic characteristics of the tower is investigated. Also, the tower response to random wave forces is conducted and the effect of foundation parameters on the tower response is examined. The dynamic characteristics of the tower and its response to wave forces were found to be greatly influenced by the foundation nonlinearity and by the pile-soil-pile interaction as well.

ACKNOWLEDGEMENTS

I would like to express my sincerest gratitude to Professor M. Novak for his support, guidance, and encouragement throughout the course of this study. Conducting this work under his guidance was a rewarding experience.

My deep appreciation for my wife for her support, patience and encouragement as well as caring and sharing all the way along the road.

The author wishes to thank Dr. H. Mitwally for making his computer programs for the wave forces evaluation available. I would also like to thank all my colleague graduate students (Khaled, Hazem, Ahmad, Ashraf, and Yasser) for their fruitful discussions, help and friendship.

Finally, I would like to express my love and appreciation to my father, without his encouragement and support this work would not have been possible.

TABLE OF CONTENTS

LIST OF FIGURES

CHAPTER ONE

INTRODUCTION

1.1. General

Offshore structures are widely used for a variety of purposes. Oil production facilities are the main application, however, the use of offshore structures is not limited to this industry. Other important applications also exist for military and navigational purposes. The ever increasing demand for oil has forced offshore oil exploration and production activities to go into deeper sites in oceans and seas. As offshore structures go to increasing water depths, they encounter severe environmental conditions. Many difficulties arise in design and construction due to these conditions. These difficulties and the potential of major catastrophic failures, both in terms of human safety as well as economic loss, underline the importance of launching extensive research programmes.

The strength of any structure is a major factor in assessing its reliability; and the supporting foundation is crucial for providing the safety of an offshore structure. In most cases, piles are used as the supporting foundation. Piles used in the offshore construction industry have huge cross sections and embedded depths. The assessment of their drivability using a certain hammer system and the prediction of their capacities are major problems in offshore piling. Pioneer work done by Smith [1] to solve the pile driving problem is still widely used, however, extensive research programmes are needed to understand the complicated behavior of piles.

The interaction between the structure and the foundation system, widely known as soil-structure interaction, has a very significant impact on the response of offshore

structures to environmental loads such as wave forces and earthquake excitation. The dynamic characteristics of the structure are greatly affected by this interaction. This in turn affects the structural response according to the intensity and the dominant frequency of the excitation and its relationship to the fundamental natural frequency at the specific load level. In storm conditions, it has been observed that a drop in the fundamental natural frequencies of offshore structures occurs. This drop is mainly attributed to softening in the foundation system due to excessive deflections or loads, and it needs to be more understood because it has a great influence on the response of offshore structures subjected to, frequently encountered, storm conditions.

1.2. Objectives of the Study and Organization of the Thesis

This study is divided into two main parts. The first part deals with the nonlinear behavior of piles under loads that exceeds the linear limit. The second part is devoted to the exploration of the effect that this nonlinear behavior has on the dynamic characteristics of supported structures and their response to environmental loads. The objectives of the first part are:

1-To provide an analytical tool to be implemented in conjunction with the STATNAMIC test, a newly invented device which tests piles dynamically, to predict pile capacities in an accurate and quick way.

2-To provide an improved approach to assess the drivability of piles and to predict pile capacities using driving records in a rational way. Soil nonlinearity as well as different sources of energy dissipation in the soil are accounted for.

3-To formulate a nonlinear analysis for the dynamic axial and lateral pile responses and

to produce equivalent linear impedance functions as well as interaction factors suitable for the implementation in the super structure analysis. The analysis takes into account the nonlinear behavior of the soil in the vicinity of the pile and considers the discontinuity conditions at the soil-pile interface such as slippage and gapping in a rational way.

In the second part of the study, the analysis is concerned with the template offshore towers supported by piles, and the objectives are:

1-To investigate the effect of the nonlinear behavior of the supporting piles on the dynamic properties of the tower such as fundamental natural frequencies and damping ratios.

2-To implement the equivalent linear foundation parameters and an approach that can evaluate the wave forces accounting for the spatial incoherence in order to study the effect of the nonlinear soil-structure interaction on the tower response to wave forces.

Chapter 2 gives an extensive review of the available approaches for the analysis of single piles and pile groups and different techniques to evaluate their impedance functions and response to different types of loading. Also, a brief review of different types of offshore structures and the main sources of environmental loads is given in this chapter. Chapter 3 addresses the pile driving problem. An approach is developed to assess pile drivability and to predict its capacity using pile driving records. Also, Statnamic load test results are analyzed employing this approach to predict bearing capacities of the tested piles. The results obtained using this approach are compared with static load test results and other analytical techniques.

A time domain non-linear analysis of axial response of single piles and pile

groups is developed and presented in chapter 4. The soil reactions are modelled using a slip element to model the pile-soil interface, a nonlinear element for the soil adjacent to the pile and a viscoelastic element to model the wave propagation away from the pile. To account for the pile-soil-pile interaction, a link element is developed based on the plane strain assumption and a Fourier inverse process. Comparison with experimental and analytical results is presented. A set of equivalent linear impedance functions and interaction factors graphs are produced.

In chapter 5, a nonlinear analysis of lateral response of piles is formulated in the time domain to facilitate modelling of the nonlinear behavior of the soil as well as slippage and gapping at the soil-pile interface. The model is similar to that developed for the axial response, except that the soil reactions on both sides of the pile are modelled separately. The effect of the soil nonlinearity on the pile impedances and interaction between piles is demonstrated through a parametric study.

A review of the available models used for the evaluation of the random wave loads on offshore structures is presented in Chapter 6. Spectra of wave forces on offshore structures using different models are presented. These forces are used for the response analysis of the tower. The method used to evaluate the tower response is presented in Chapter 7. In Chapter 8, the effect of the pile foundation on the tower response is explored and the effect of nonlinearity on the modal properties of the tower is discussed. In Chapter 9, a summary of the study is given and conclusions are drawn.

CHAPTER TWO

LITERATURE REVIEW

2.1. Previously Developed Methods for Response Analysis of Piles

Soil-pile models for the dynamic response analysis of pile foundations may be categorized into four groups; elastic continuum models, boundary element models, Winkler models and finite element models. A brief review of these models is given herein.

2.1.1.Elastic Continuum Models

The response of single piles and pile groups to harmonic loads at pile heads was calculated applying the three-dimensional wave equations solutions. Assuming elastic conditions, the response for each vibration mode is computed as a function of frequency. Tajimi [2] assumed axisymmetric geometry in the soil-pile system and linear viscoelastic stratum, also, the vertical component of the soil motion is neglected when calculating the horizontal response. Novak [3] assumed a linear elastic soil layer composed of independent infinitesimally thin horizontal layers extending to infinity. Nogami and Novak [4], and Novak and Nogami [5] included material damping in the solutions for vertical and horizontal vibrations, respectively. Kobori et al. [6] studied the lateral response of piles considering all components of motion of an infinitely long pile and obtained the solution in the form of an infinite series of multiple integrals. Novak and Aboul-ella [7] extended the plane strain approach to include layered media. Novak and Sheta [8] included a massless, weak, cylindrical boundary zone around the pile to

approximately account for the soil nonlinearity in the region of the highest stresses. Akiyoshi [9] introduced the nonlinear effects due to slippage at the soil-pile interface during vertical vibration of single piles. The frictional stress was used as the boundary condition associated with perfect slipping in solving a continuum equation. The soil was assumed to be a linear elastic material in this study. Dynamic group effects of piles are studied using, in most cases, extensions of the approaches used for single piles and they are mostly linear approaches.

In conclusion, the elastic continuum model is convenient for developing explicit solutions which can accommodate the dynamic effects such as inertial forces and damping. However, the inclusion of the non-linear behavior in these models is very difficult.

2.1.2. Boundary Element Models

Boundary element models were developed to analyze the dynamic response of single piles and pile groups. The pioneer work was done by Banerjee [10] using a boundary element approach to analyze the response of piles. Kaynia and Kausel [11] extended the work done by Kobori et al. [6] and included cylindrical loads to study group effects. Sen et al. [12] and Mamoon et al. [13] used a Green's function in the boundary element method to study pile groups in homogeneous and nonhomogeneous soils. Sanchez-Salinero [14] computed the dynamic response of a plane strain medium using the boundary element method in the frequency domain and studied the group effects.

Boundary element models have the drawback that many integrations have to be evaluated and this may not be economical for the nonlinear time domain analysis.

2.1.3. Winkler Models

Winkler [15] has developed a soil model in which the deflection of the soil medium at any point on the soil-structure interface is proportional to the stress applied at that point and independent of stresses applied at other locations.

Penzien et al. [16] developed a multi-degrees of freedom lumped mass model and solved the equations of motion in the time domain for seismic excitations at the bedrock. They used Mindlin's solution [17] to define the soil spring stiffness. Prakash and Chandrasekaran [18] used a discrete element model for lateral response of the pile and used a transfer matrix approach to solve the fourth order differential equation. Novak [19] solved the vertical vibration employing the dynamic solutions developed by Baranov [20] for the soil in the formulation of pile motion analysis. This work was extended by Novak et al. [21] to derive more suitable forms for all vibration modes such as vertical, horizontal, torsional and rocking motions in a systematic way which includes material damping. Kagawa and Kraft [22,23] developed a nonlinear dynamic Winkler model for pile foundations in the frequency domain using an iterative linear equivalent method. Nogami [24] developed a frequency domain nonlinear Winkler model for horizontal vibration. This model uses a static p-y curve and consistent mass for the near field and dynamic plane strain solution for the far field. Matlock et al. [25] developed a nonlinear time domain model consisting of a dashpot and a unit curve to produce a nonlinear force-displacement relationship. The unit curve consists of a parallel series of springs and coulomb friction-blocks. The effects of gapping and degradation due to cyclic loading were included. Nogami and Konagai [26,27] developed time domain plane strain solutions for both vertical and horizontal excitations. They considered slippage at the

pile-soil interface and used these solutions to solve the axial response of pile groups [28].

The response analysis of pile groups is investigated by many researchers using the Winkler model assumptions. Nogami [29] derived an analytical solution for the response of floating piles by assuming a soil-column extending to the bedrock and later improved it using more rigorous expressions [30]. Sheta and Novak [31] introduced the model with a softer remolded area around the pile shaft. Dobry et al. [32] developed a simple expression for the horizontal stiffness and damping of piles on a Winkler model. They used a Voigt type model employing a spring and dashpot with coefficients derived from finite element analysis. Gazetas and Dobry [33] extended this model to include layered media. Nogami et al. [34] developed a nonlinear time domain model for pile groups based on Nogami and Konagai [26,27] solutions for the far field and non-linear element for the near field with stiffness constants derived from empirical p-y curves and finite element analysis.

2.1.4. Finite Element Models

The finite element method is widely used because of its versatility in representing geometry and boundary conditions. Also, it is possible to account for non-linear behavior and discontinuity conditions. Blaney et al. [35] analyzed laterally loaded end bearing piles using the consistent boundary matrix developed by Kausel et al. [36] to simulate the effect of the radiation condition of waves. Kuhlemeyer used the same approach [37] and introduced a special bending element for pile shafts. Wolf and Von Arx [38] developed a pile group response analysis method using a finite element method for the first time. Angelides and Roesset [39] developed a nonlinear finite element

method and compared its results with the dynamic p-y curve developed by Stevens and Audibert [40]. This finite element method was an extension of work by Blaney et al. [35] and a linear equivalent method was applied to take into account the nonlinearity of soil but discontinuities such as gapping and slippage were not considered.

The finite element method is a powerful technique not only for piles response analysis, but also for a variety of problems in different fields; however, it is very expensive to use when the nonlinear behavior of a group of piles is analyzed in the time domain by the step-by-step method.

2.2. Types of Offshore Structures

Offshore technology has experienced a remarkable growth in the last five decades to meet the increasing needs of the oil production industry for a wide variety of offshore structures to be installed in ever increasing water depths. These offshore structures are subjected to extremely hostile environments. The majority of the early offshore structures are of the steel jacket type. These towers have fundamental periods in the range of 1 to 5 seconds. Due to the fact that waves of high energy content have periods ranging from 6 to 25 seconds, the response of these structures to extreme waves is mainly static with little dynamic magnification. The natural period of the jacket type structure increases as the water depth increases, until it lies within the peak wave energy zone which leads to a large dynamic magnification and alternatively, compliant structures have to be used. In this study, only the response of the jacket type offshore structure is studied; however, the main types of offshore structures are briefly described herein for completeness.

2.2.1. Steel Jacket (Template) Platform

A jacket platform comprises of a space frame structure with piles driven through its legs which extends from the sea bottom to above the water surface Fig. 2.1. These piles transfer loads to the soil and fix the structure in place against lateral loads due to wind, waves, currents and collisions with ships or icebergs. To increase the lateral stiffness of the structure, piles are connected rigidly to the structure and are placed as far away from each other as possible. Template type platforms are suitable for water depths of up to 350 m. Some platforms may contain enlarged legs to provide for self-buoyancy during installation. Jacket platforms are located throughout the world.

2.2.2. Tension Leg Platform (TLP)

A tension leg platform is a compliant platform that withstands environmental loads by its ability to accommodate large deflections. It consists of a large floating hull which is pulled down by highly tensioned vertical tethers, Fig. 2.2. One advantage of the TLP is that it can be installed in deeper water depths without a proportional increase in the cost. These platforms have longer natural periods, which are well above the highest peak wave periods to avoid the dynamic amplification on the response to wave loads.

The foundation system for a TLP may consist of piles or gravity type footings and it also serves as an anchor to fix the tethers to the sea bed. In the case of piled foundations, a base template is first positioned at the sea bed then piles are driven through sleeves in the template and grouted in. The main foundation loading consists of the dead load and a constant tensile force due to buoyancy of the hull in addition to cyclic wave loads.

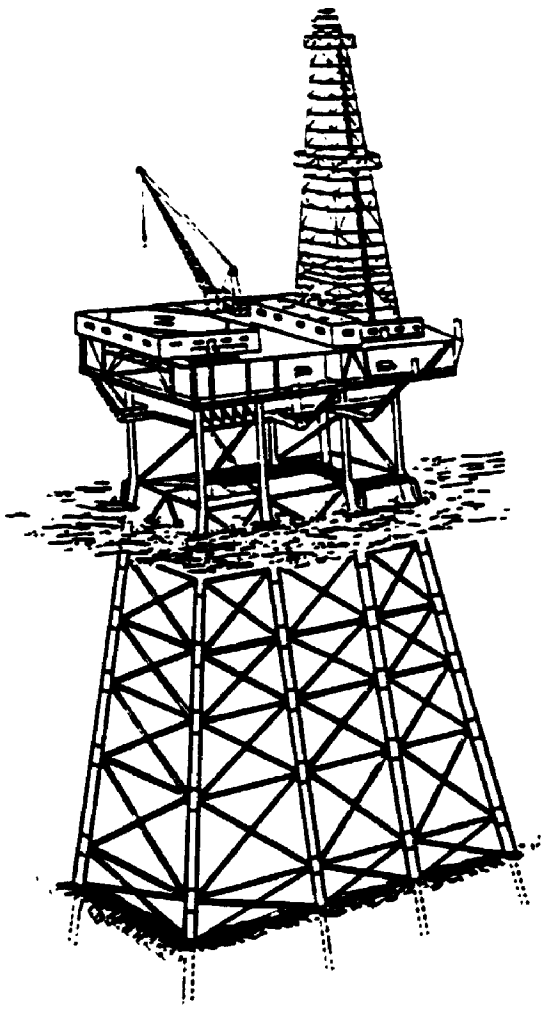

Figure 2.1 Steel Jacket Offshore Platorm (Dawson [108])

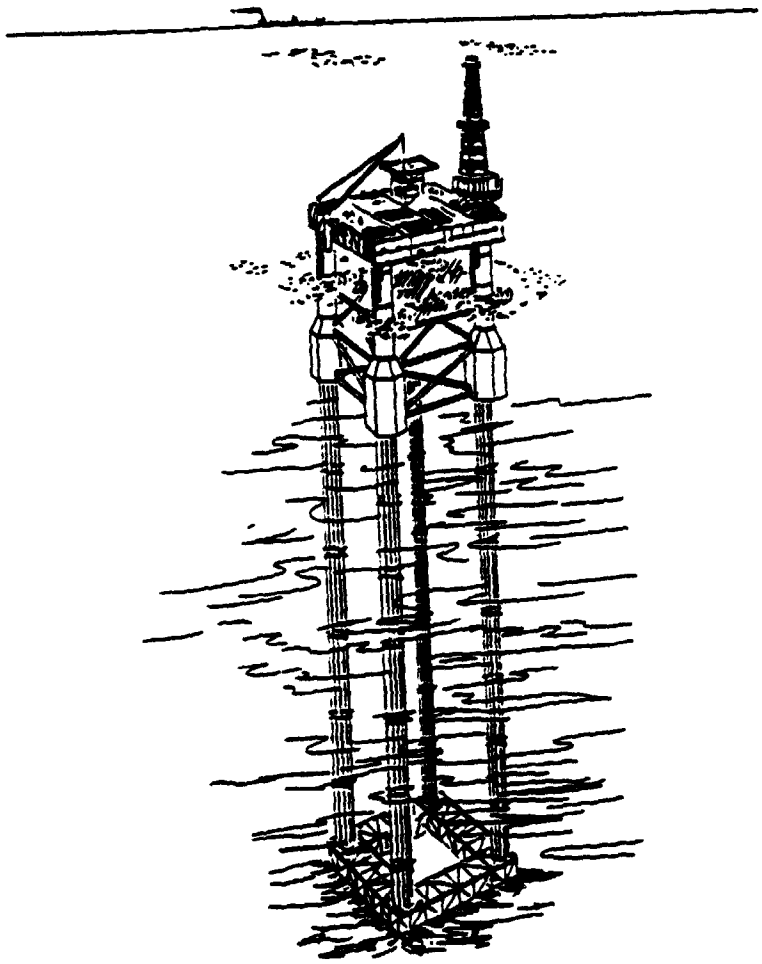

Figure 2.2 Schematic of a Tension Leg Platform (Dawson[108])

2.2.3. Guyed Tower Platform

It consists of a slender steel tower held upright by anchor cables with clump weights resting on the sea bed, Fig. 2.3. These clump weights allow the tower to tilt gradually in case of extreme waves. Thus, the tower acts as a pinned tower at its base. This design requires that piles are not rigidly connected to the tower at the base but are pinned. Guyed towers are compliant structures and are allowed to moor laterally, thus resisting wave loads by their inertia rather than their stiffness. It is estimated that guyed towers will be cost effective in the range of 350 to 450 m of water [41].

2.2.4. Gravity Platforms

These are concrete structures with a large diameter base resting on the sea bed. The base usually consists of cylindrical cells of which only a few extend above the mean water level to support the deck section which is made of steel modules, Fig. 2.4. Gravity base structures do not need to be anchored to the sea floor as they are stable under their immense weight. The cylindrical cells are used for the storage of crude oil. Tankers can load crude oil directly from the platform, thus saving the cost of extending a pipeline to an onshore facility.

2.3. Environmental Loads

The environmental loads on offshore structures are mainly due to waves, currents, wind, icebergs, earthquakes and mud slides. Some of them are briefly discussed in the following.

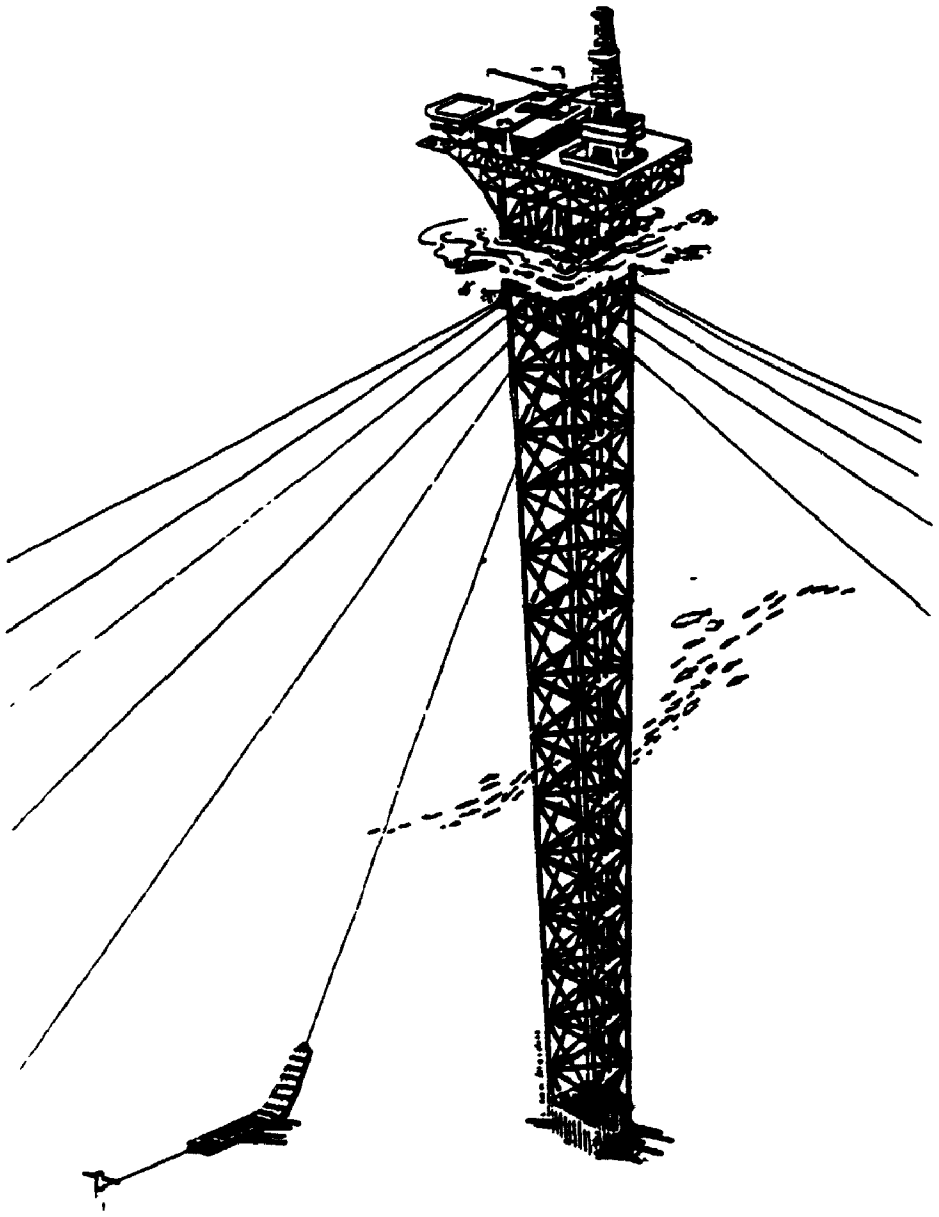

Figure 2.3 Guyed Tower Platform (Dawson [108])

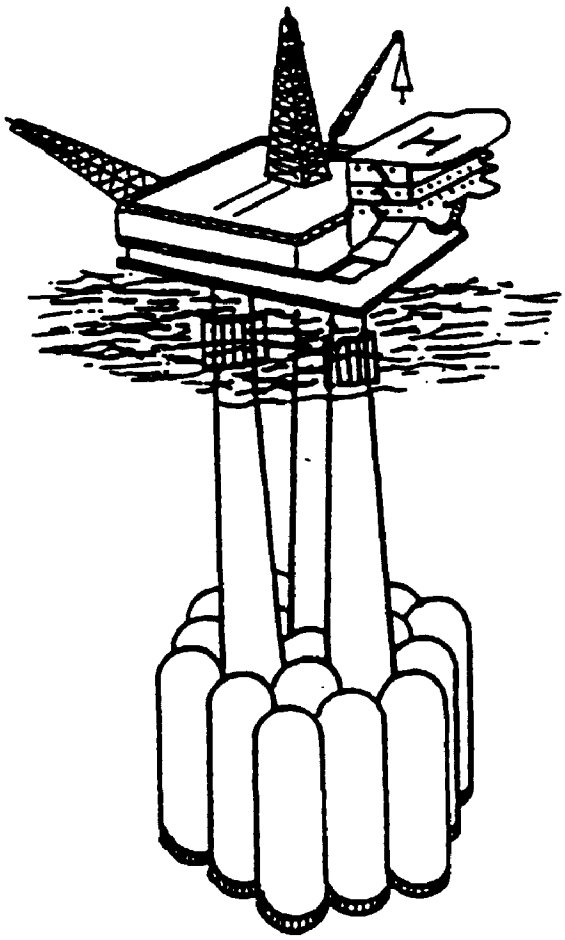

Figure 2.4 Schematic of a Concrete Gravity Platform (Dawson[108])

2.3.1. Wave Loads

Two approaches can be used to describe the wave loads. The first one is the deterministic approach, in which a design wave is selected based upon a certain return period and may be specified by a nonlinear wave theory. The second one is the stochastic approach, in which the spectrum of the sea surface elevation is related to the mean wind speed and is specified for the spectral analysis to be performed.

The dominant environmental loads on fixed offshore towers are the wave loads. Shorter waves with little energy content have periods that coincide with the natural periods of fixed offshore structures. Since their number of occurrences per year is greater than that for longer waves, fatigue analysis is very important for fixed offshore towers.

2.3.2. Wind Loads

Wind loads are the dominant environmental loads for compliant structures with fundamental periods greater than approximately 40 seconds [42]. These natural periods are close to the peak periods of the wind spectrum. However, further research is needed to get more understanding of wind loads on structures with such high natural periods.

2.3.3. Ice Forces

These will be predominant in areas subject to severe ice conditions. Ice forces depend on many factors such as the mechanical properties of ice and geometry and type of ice formations [43]. Ice forces on a sloping structure (cone like) are less than those on a vertical structure since the ice sheets are broken by bending in the former case while

they are broken by direct compression in the latter case. That is why ice resistant structures often have a conical geometry in the area subjected to ice sheets collision.

CHAPTER THREE

ONE DIMENSIONAL ANALYSIS OF STATNAMIC TEST AND PILE DRIVING

3.1. Introduction

The static loading test is the most reliable method to determine the bearing capacity of a pile. Because it is time consuming as well as expensive, only a limited number of piles are tested per site. A common alternative to predict the bearing capacity of driven piles is the use of pile driving formulae, but these formulae are empirical and their accuracy varies considerably.

The first rational approach to assess the pile drivability as well as its bearing capacity is generally attributed to Smith [1]. In his model, Smith suggested a finite difference solution for the pile driving problem idealized by a one dimensional wave equation model. The soil resistance to pile motion is represented by a series of springs and dashpots whose constants are empirically determined from back analysis of pile driving records and pile load tests. The total resistance to driving comprises two components, a static component and a dynamic one to represent the damping of the soil. Forehand and Reese [44] used the Smith model to predict the bearing capacity as the static component of the soil resistance. Again, this is an experience dependent approach based on matching model parameters to the data observed in the field. Other soil models were proposed subsequently. The soil model adopted in the Texas Transport Institute (TTI) computer program accounts for the nonlinearity of the soil damping force with penetration velocity. The WEAP program, developed at Case Western University,

employs a soil model, in which the damping force is uncoupled from the spring force and is only dependent on the pile particle velocity. The soil parameters required for these models are essentially empirical and have little analytical or physical basis.

A few researchers attempted to remedy this deficiency by using plane strain soil reactions given by Novak et al [21] to model the soil resistance. Among them Meynard and Corte' [45]; Mitwally and Novak [46]; Simons and Randolph [47]; and Lee et al [48]. These authors considered a horizontally homogeneous soil medium. This may lead to overestimation of radiation damping because large displacements and plastic deformations occur around the pile shaft reducing the effective soil shear modulus. Mitwally and Novak [49] approximated this effect using plane strain soil reactions that incorporate a weakened zone around the pile, i.e. radial nonhomogeneity.

All the above models deal with driven piles. They use the driving records and the hammer data to predict the bearing capacity of piles. However, there is a need for an inexpensive, fast, and reliable method to assess the bearing capacity of driven piles as well as cast in situ piles. To this end, a new method for pile testing was developed and described in Horvath et al [50] and Janes et al [51]. This method is analyzed in this study and an approach to predict the bearing capacity of piles is presented.

3.2. Statnamic Test Description

Berminghammer Corporation Limited, Canada and TNO-IBBC, the Netherlands, with financial assistance provided by the NRC-IRAP developed an innovative device to test piles dynamically but in a manner similar to a static environment, thus calling this method, the STATNAMIC test. The Statnamic apparatus consists of a pressure chamber

and a reaction mass placed on top of the pile (Fig. 3.1). Fuel is burned in a controlled manner within the pressure chamber. This creates a well defined force acting equally against the pile head and the reaction mass accelerating the latter upward and pushing the pile downward. After the fuel is burned, an exhaust port is opened and the gas is vented upward. The test lasts approximately 100 milliseconds with a low loading frequency ranging from 0 to 10 Hertz. Pile velocity and acceleration are below 2.0 m/s and 1.0 g respectively. A calibrated load cell, housed in the piston base, is used to monitor the applied load. A displacement transducer consisting of a light-sensitive cell is placed at the centre axis of the pile. A remote laser light source is stationed 10 to 20 m from the pile and provides a stationary datum isolated from any ground vibrations. Both load and displacement measurements are accurate to 0.1 %. A rugged field computer and signal conditioner acquire and digitize raw signals at a rate of 4000 Hertz, providing immediate load versus displacement plots or time histories and store the data on disk. Typical load and displacement time histories are shown in Fig. 3.2. Further details on the test can be found in Horvath et al [50] and Janes et al [51].

3.3. Theoretical Model

For theoretical analysis of the pile response, a one dimensional pile model is developed in this study. This model is based on the approach developed by Mitwally and Novak [49] but is extended to accommodate rate dependent parameters, loading generated by the statnamic test and some other refinements. The elements of the model are defined below.

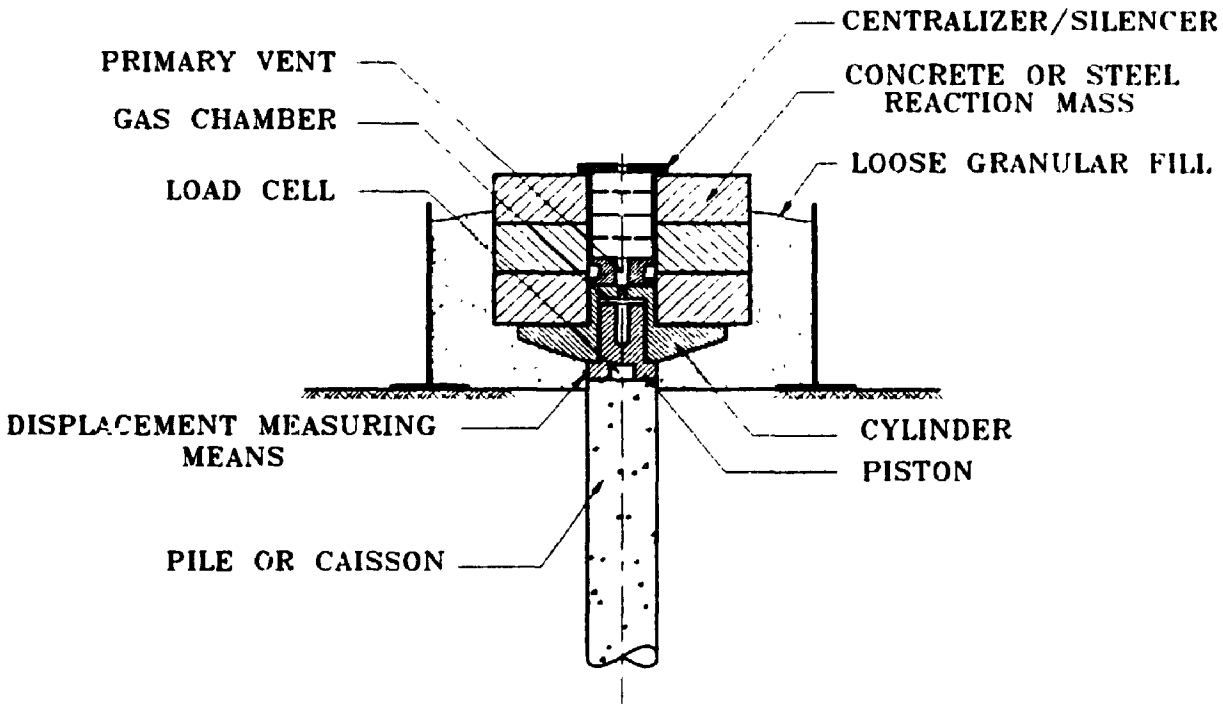

Figure 3.1 Cross-Sectional View of Statnamic Device

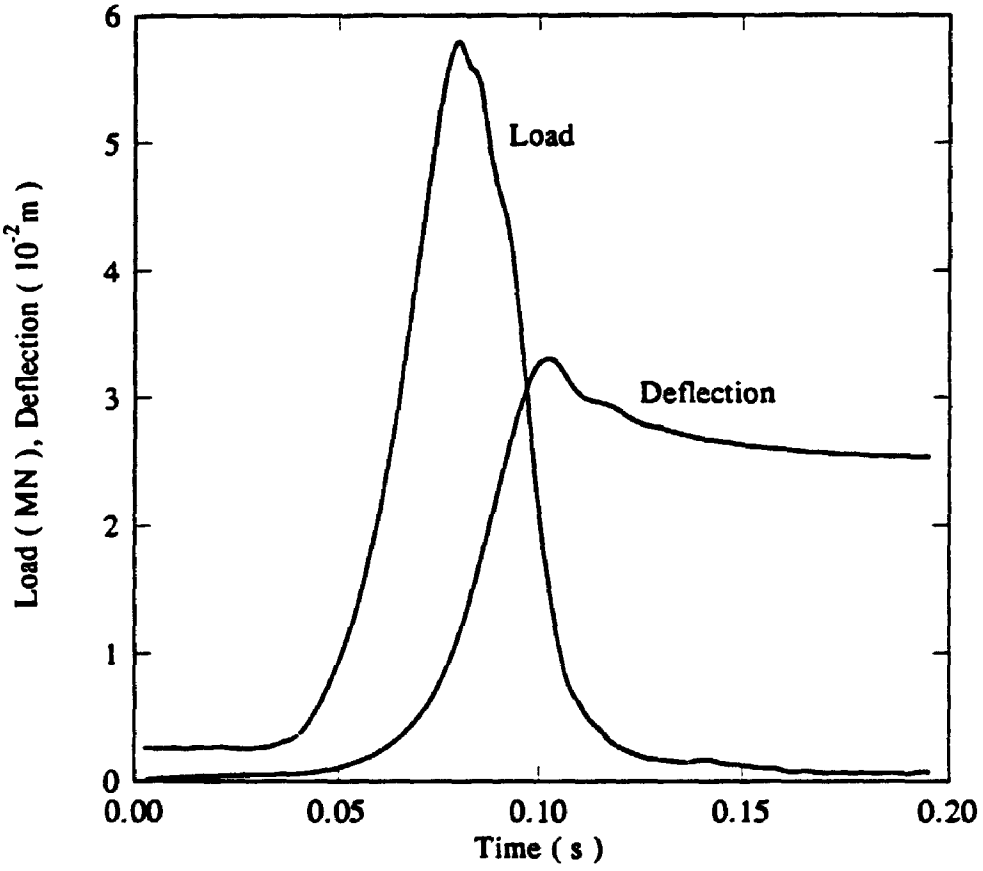

Figure 3.2 Typical Load and Deflection Time Histories for Statnamic Test

3.3.1. Soil Resistance

For the vertical response, the soil resistance to a harmonically vibrating cylinder is expressed under the plane strain assumption. This assumption yields the complex stiffness K as

$$K = G\,(\,S_{v1} + i\,S_{v2}\,) \tag{3.1}$$

where, G, is the soil shear modulus, i, the imaginary unit, and, S_{v1}, and S_{v2}, are dimensionless parameters that represent soil stiffness and damping, respectively, and are frequency dependent. For a homogeneous soil medium (Fig. 3.3a), the complex vertical stiffness is (Novak et al [21])

$$K = 2\,\pi\,G\,(1 + i\,2\,\beta\,)\,\frac{a_o^*\,K_1(a_o^*)}{K_o(a_o^*)} \tag{3.2}$$

where which K_1 and K_o are the modified Bessel functions of order one and zero, respectively. The complex dimensionless frequency is

$$a_o^* = a_o\,\frac{i}{\sqrt{1 + i\,2\,\beta}} \tag{3.3}$$

in which the real dimensionless frequency is

$$a_o = \omega\,\frac{r_o}{V_s} \tag{3.4}$$

In Eqs. 3.3 and 3.4 V_s is the soil shear wave velocity, r_o is the outer pile radius, β, is the soil material damping ratio assumed to be frequency independent, and ω is the circular frequency. To allow for soil nonlinearity near the pile, the radially nonhomogeneous medium incorporates a massless weakened soil zone of radius b and a reduced shear modulus G_m and an outer zone extending to infinity with a shear modulus G (Fig. 3.3b). The complex stiffness of the composite medium is (Novak and Sheta [8])

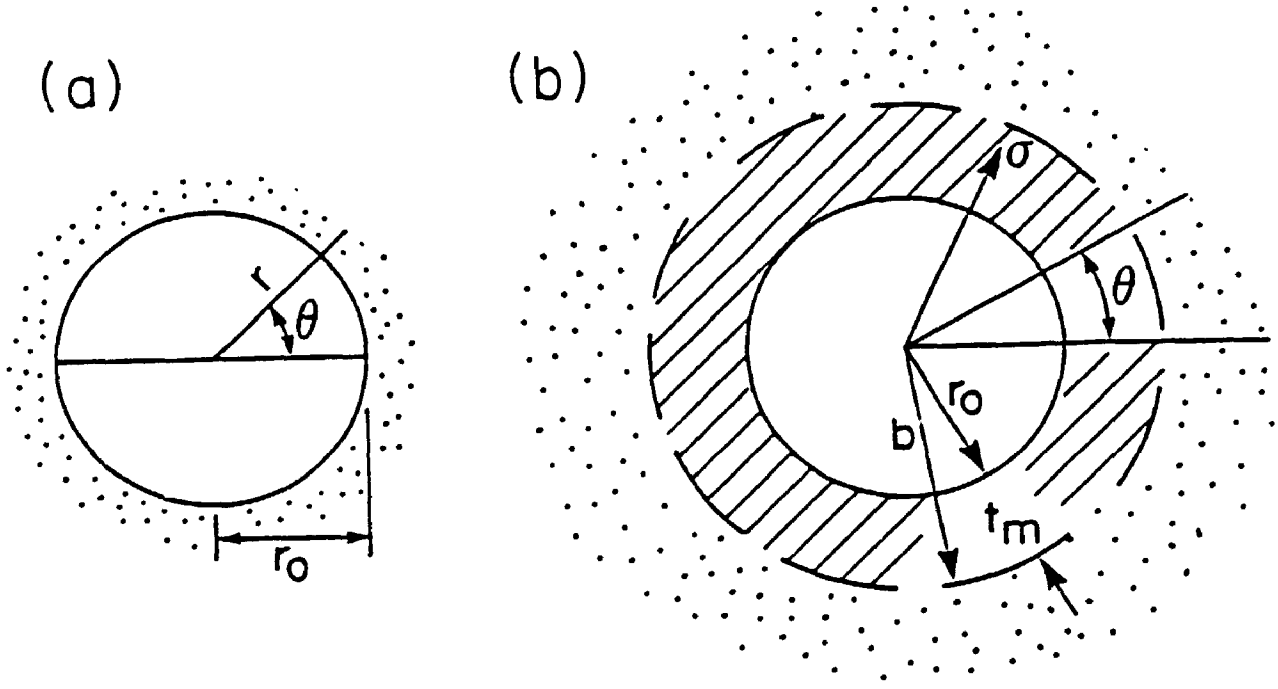

Figure 3.3 Notations for (a) Homogeneous and (b) Nonhomogeneous media

$$K = \frac{2\pi G_m^*}{-\ln\left(\frac{r_o}{b}\right) + \left(\frac{G_m^*}{G^*}\right)\frac{K_o(sb)}{sb\,K_1(sb)}} \tag{3.5}$$

in which $G^* = G(1 + i\,2\beta)$ is complex shear modulus and

$$s = i\,\frac{\omega}{V_s\sqrt{1 + i\,2\beta}} \tag{3.6}$$

Fig. 3.4a shows the variation in S_{v1} and S_{v2} for the homogeneous medium and an example of S_{v1} and S_{v2} for composite soil medium both plotted versus dimensionless frequency. The stiffness of the composite medium, being only one part of the total medium resistance, is less than that of the homogeneous medium at lower frequencies but is larger at higher frequencies. The damping of the composite medium is drastically less than that of the homogeneous medium. The absolute value (amplitude) of the total soil resistance is always reduced by the weak zone (Fig. 3.4b). The assumption of a massless inner zone was adopted to prevent spurious wave reflections from the boundary between the weakened zone and the outer soil zone which is a fictitious boundary and not a real physical one (Novak and Han, [52]). The mass of the weak zone, neglected in Eq. 3.5, can be lumped in full or in part into the soil node introduced later, but its effect is small. Soil layering is readily accounted for by substituting pertinent soil parameters in Eqs. 3.1 to 3.6.

At the pile tip, the soil resistance before plastic yield is modelled by the reaction of an elastic halfspace to a rigid massless circular disc undergoing harmonic vibration. For low dimensionless frequencies, typical of the pile response, the tip resistance can be described approximately by frequency independent parameters. This is also desirable

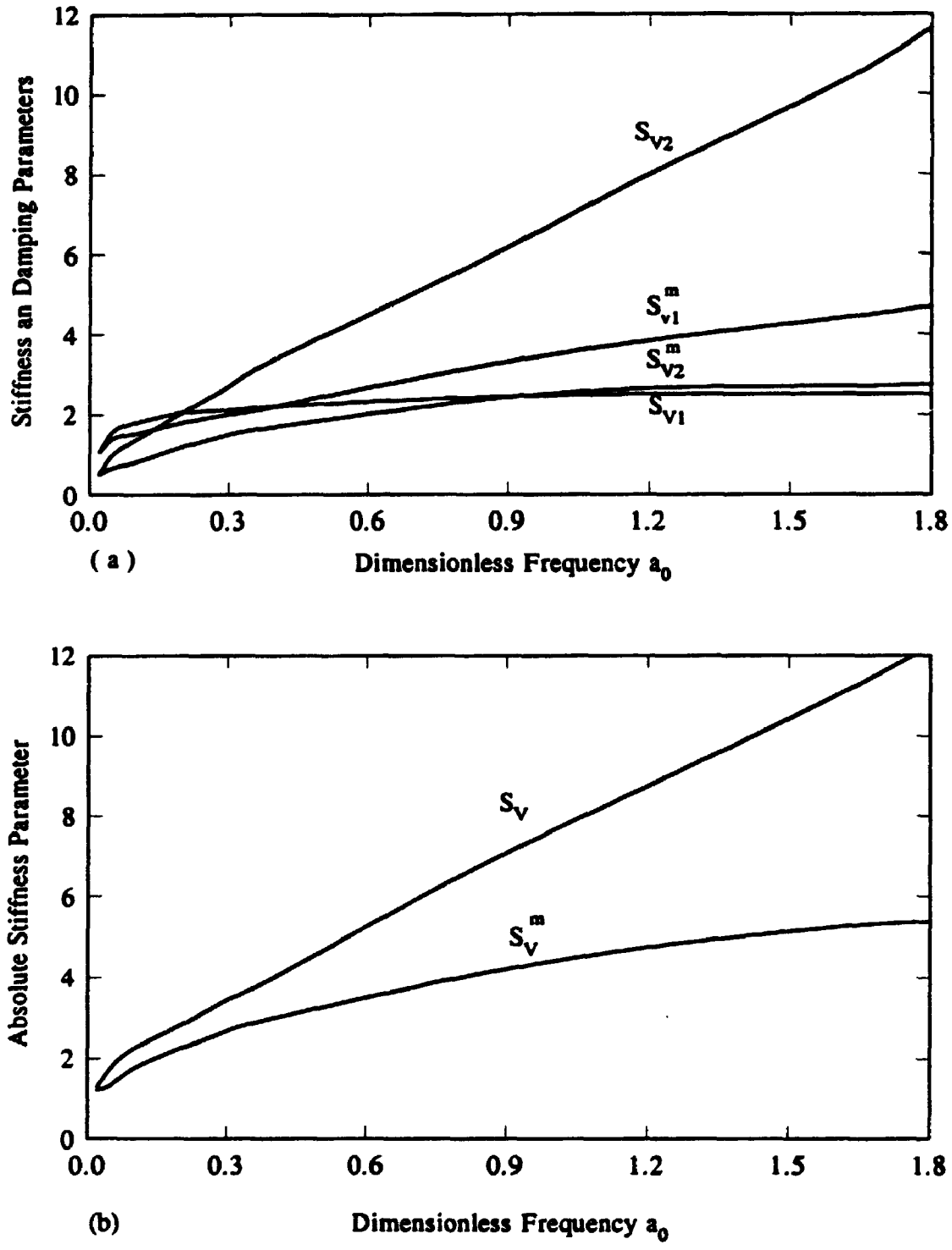

Figure 3.4 (a) Stiffness and Damping Parameters for Homogeneous and Non-homogeneous Media (b) Absolute Value of the Soil Resistance $G/G_m = 0.1$; $t_m/r_0 = 0.1$; $2\beta = 0.1$, 1 and 2 for Real and Imaginary Parts, Respectively

because the pile response is nonlinear and hence, a time domain analysis is called for. Thus, the disc stiffness can be taken as static, while for damping the formula due to Lysmar and Richart [53] can be used giving

$$K_t = \frac{4\ G\ r_o}{(1 - \nu_s)} \tag{3.7}$$

$$C_t = \frac{3.4\ r_o^2\ \sqrt{G\ \rho_s}}{(1 - \nu_s)} \tag{3.8}$$

In Eq. 3.7 and 3.8 K_t and C_t are the pile base stiffness and damping coefficients, respectively, ν_s is soil Poisson's ratio ,and ρ_s is soil density. Equations 3.7 and 3.8 are applicable for closed-ended piles. For open-ended piles, the stiffness and damping coefficients for a rigid ring may be introduced. The static stiffness coefficient for the rigid ring, proposed by Egorov [54], is

$$K_t = \frac{2\ G\ r_o}{(1 - \nu_s)\ \Omega} \tag{3.9}$$

in which Ω is a factor accounting for the thickness of the ring. The damping coefficient for the ring is approximated by the expression proposed by Gazetas and Dobry [55] as

$$C_t = \frac{3.4\sqrt{G\ \rho_s}\ (r_o^2 - r_i^2)}{(1 - \nu_s)} \tag{3.10}$$

in which r_i is the internal radius of the pile.

3.3.2. Loading Rate Effects

During the Statnamic test, the soil surrounding the pile is subjected to various loading rates. These rates affect the soil increasing its resistance to failure which results in the total soil resistance becoming higher than the static one. Coyle and Gibson [56] proposed a power law for the ultimate soil resistance given by

$$R_t = R_u (1 + J^* V^N) \tag{3.11}$$

where R_u is the static soil resistance, J^* is the rate effect factor, V is the penetration velocity and N is an experimentally determined exponent. Other researchers provided results supporting this formulation (e.g. Litkouhi and Poskitt [57] and Heerema [58,59]). Coyle and Gibson [56] found this effects in their triaxial experiments, which gave rise to the belief that these effects occur in addition to radiation damping. In the subsequent section, these rate effects are incorporated in the proposed model to define the limiting failure resistance and also the soil resistance during slippage.

3.3.3. Proposed Shaft Model

The pile is idealized by a system of discrete masses connected by linear springs. The soil resistance to pile motion is represented by a series of springs and dashpots (Fig. 3.5a) whose constants are established using the plane strain soil reactions described earlier. A weakened soil zone around the pile shaft is considered to account for the high strains and reduction in the soil shear modulus in this zone.

The motion of the soil adjacent to the pile shaft is traced independently from that of the pile. This is achieved by assigning an extra degree of freedom at each pile

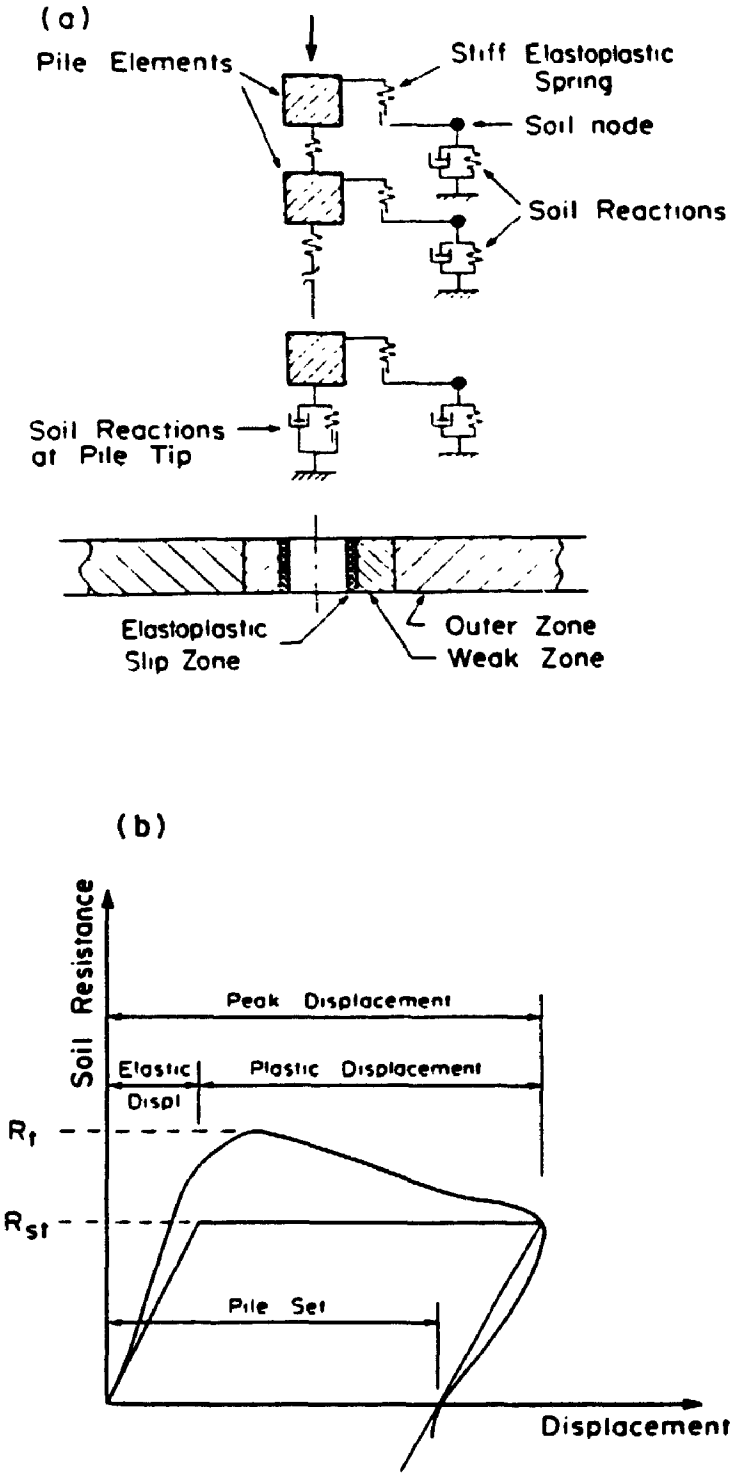

Figure 3.5 (a) Pile Shaft Model (b) Force-Displacement Relationship of Rate-dependent Elastoplastic Soil Spring

segment (the soil node) that represents the soil motion adjacent to the pile shaft. The limiting soil resistance is specified as

$$R_t = R_{st} (1 + J V_r^N) \tag{3.12}$$

where J is a coefficient representing the rate effects, N is an exponent representing the nonlinearity of this effect, and V_r is the relative velocity between the pile segment and the adjacent soil element. Before this limiting resistance is reached, motions of the pile segment and the adjacent soil are the same. This is ensured by linking the pile segment to the adjacent soil by a rate dependent elasto-plastic spring (Fig. 3.5b) which is assigned a high value of stiffness. The force in this link is equal to :

$$F_l = K_l W_r (1 + J V_r^N) \tag{3.13}$$

in which K_l is the spring stiffness coefficient and W_r is the relative displacement between the pile segment and the adjacent soil. Once the limiting resistance is attained, slip occurs. The pile and adjacent soil then move independently and the force in the link is equal to the limiting resistance given by Eq. 3.12. Rebonding occurs when the force in the link is less than the limiting resistance. The stiffness of the elasto-plastic spring should be sufficiently high so that the connection between the pile segment and the adjacent soil behaves almost rigid as long as the interface force is less than the limiting resistance. The motion in the degree of freedom representing the soil is resisted by the reactions of the outer layers modelled by a spring and a dashpot in parallel. Slip and plastic deformations are confined to the soil-pile interface. The spring and dashpot representing the outer zone soil reactions are considered to behave elastically all the time.

Soil nonlinearity associated with large displacements outside the slippage zone is accounted for by the reduction in the soil shear modulus in the weakened zone and increase in the material damping. Tracing the soil motion in this manner facilitates the determination of the condition for slippage and rebonding since the force in the elasto-plastic spring depends on the relative displacement and relative velocity between the pile segment and the adjacent soil. The modelling of the soil-pile interface behaviour in this manner is close to the physical situation. Before the slippage and after rebonding, the pile and soil move together and radiation damping is proportional to the pile (and soil) velocity. During slippage the soil resistance is not constant due to the rate effects specified above.

Soil resistance at the pile tip is modelled differently. Radiation damping at the pile tip continues to occur during plastic deformation as the soil just underneath the pile does not move independently from the pile. The soil spring, on the other hand, is considered to be elasto-plastic and the force in the spring exhibits some nonlinearity due to the rate effects also.

3.4. Equations of Motion

Pile and soil displacements are evaluated in the time domain using the linear acceleration assumption and the Newmark β method for direct time integration of the equations of motion. The modified Newton-Raphson iteration scheme is used to derive the governing equilibrium equations which are written as (Bathe [60])

$$[M]\{\ddot{W}\}^{(k)}_{t+dt} + [C]\{\dot{W}\}^{(k)}_{t+dt} + [K]_t\{dW\}^{(k)} = \{R\}_{t+dt} - \{F\}^{(k-1)}_{t+dt} \quad (3.14)$$

In equation 3.14, $\{\dot{W}\}$ and $\{\ddot{W}\}$ are the vectors of velocities and accelerations, respectively, [M] and [C] are the mass and damping matrices, respectively, and $[K]_t$ is the updated stiffness matrix at time t; k is the iteration number, dt is the time step and {dW} is the vector of displacement increments. $\{R\}_{t+dt}$ and $\{F\}_{t+dt}$ are the vectors of external and internal elastic forces, respectively. The following incremental relationship holds

$$\{W\}^{(k)}_{t+dt} = \{W\}^{(k-1)}_{t+dt} + \{dW\}^{(k)}_t \quad (3.15)$$

with the initial conditions

$$\{W\}^{(0)}_{t+dt} = \{W\}_t \quad (3.16)$$

and

$$\{F\}^{(0)}_{t+dt} = \{F\}_t \quad (3.17)$$

At the end of each time step, the stiffness matrix is updated by setting the stiffness terms corresponding to the yielding elasto-plastic springs to zero within each time step, iterations are repeated until convergence is achieved. The external input force, specified on the basis of the Statnamic test, is introduced as a pulse force digitized at each time step. The excitation frequency is assumed to be constant through the event and taken as the dominant frequency at which most of the energy delivered to the pile is concentrated. Fig. 3.6 shows the energy distribution of the force with the frequency. It is noticeable that most of the energy is concentrated at low frequency range, thus the frequency dependent soil reactions can be determined with a sufficient accuracy at a

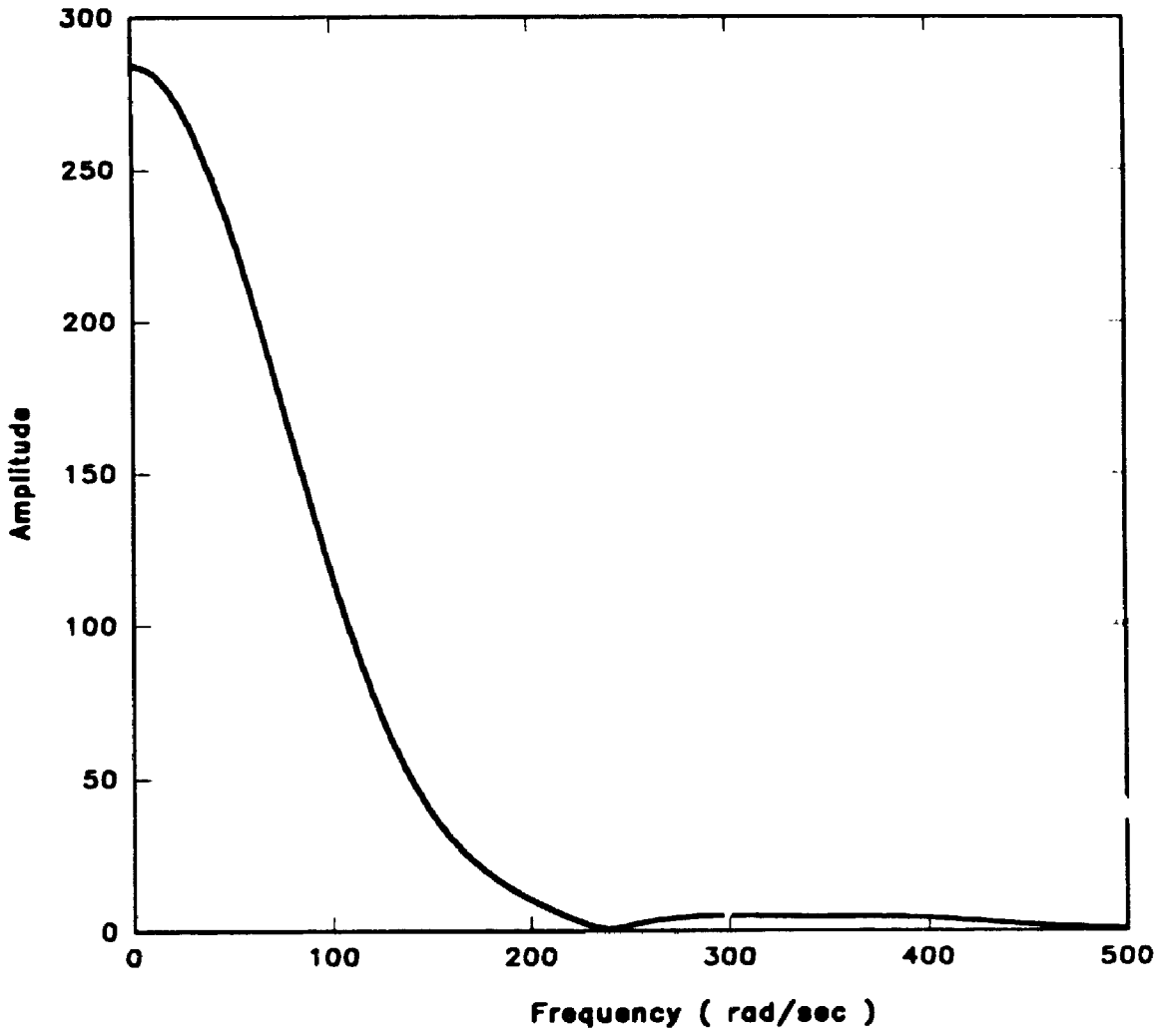

Figure 3.6 Fourier Spectrum of Load for Pile 4, Site 3

specific frequency pertinent to the test loading time history. To find this frequency, the loading time history is approximated by a sine curve and the frequency is calculated as

$$f = \frac{\pi}{t_p} \tag{3.18}$$

Where t_p is the event duration ranging from 60 ms to 120 ms. Examples of the calculated pile response will be given later.

3.5. Bearing Capacity Prediction

Based on the theoretical model described above, a pile bearing capacity prediction method is formulated. The main idea of this method is to achieve an adequate match not, only for the final set but also for the entire displacement time history. Using the measured displacement time history as a guide and adjusting the model parameters in a way described below, a satisfactory agreement between the measured and predicted time histories can be achieved proceeding in two main stages. The first one involves the elastic portion of the pile response while the second stage is the failure or slippage phase of the pile response. A flow chart describing the above mentioned method is shown in Fig. 3.7. Notice that the procedure for sands and clays is almost identical, except that different parameters need to be established. This procedure essentially differs from that of Chow et al [61] in that the match is achieved for the entire displacement time history and not just the final set. Also, no static load test is required and no setup factor has to be established. The whole procedure is described in full detail below.

3.5.1. Elastic Stage

Displacement match for the first portion of the time history (the elastic portion)

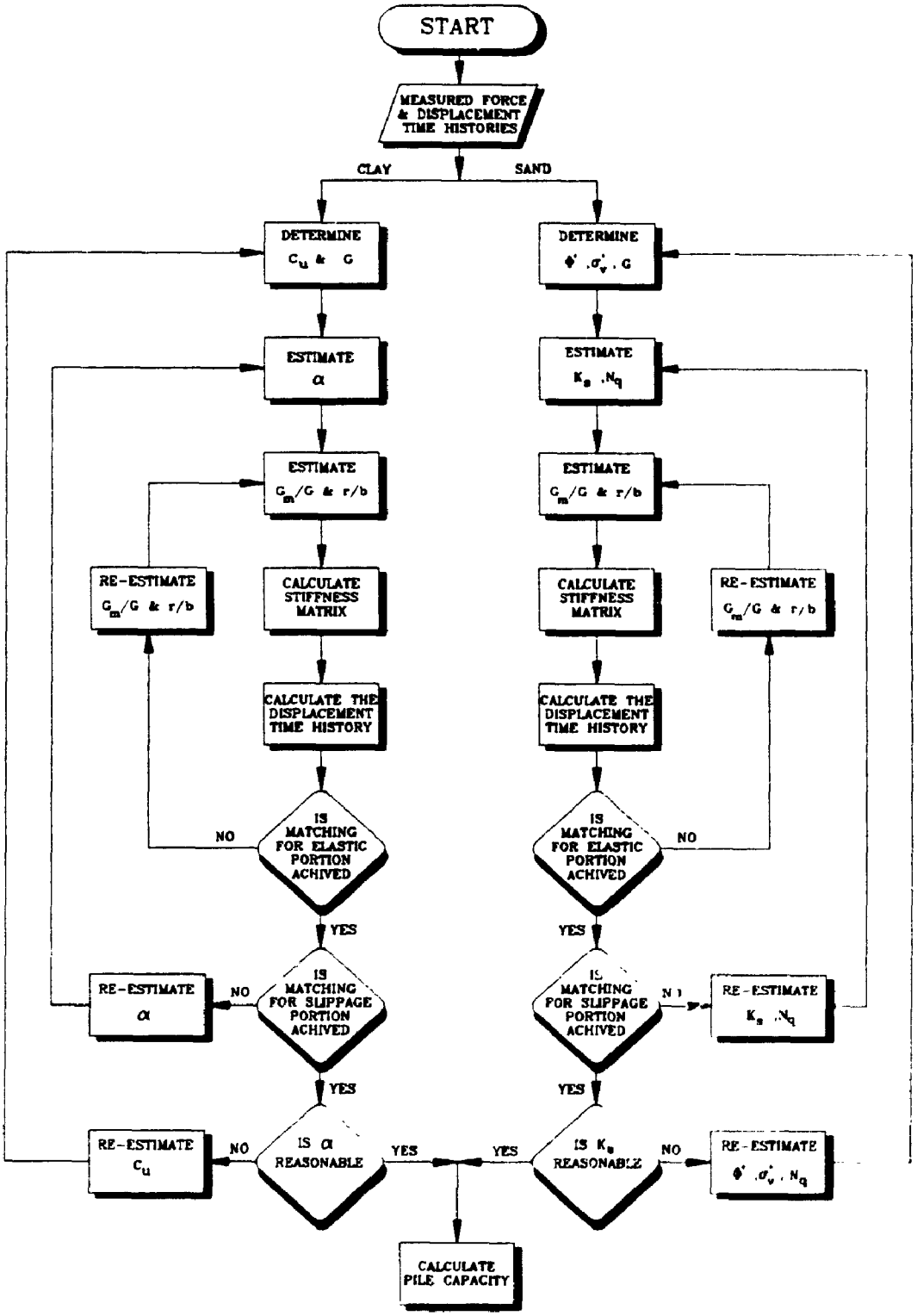

Figure 3.7 Flow Chart for Proposed Model for Pile Capacity Prediction

is tried first. The soil spring parameters are adjusted until a reasonable match for that part of the displacement time history (up to say the first 5.0 mm) is achieved. These parameters are; soil initial shear modulus G = G_{max}, shear modulus reduction ratio for the weakened zone G_w/G, and the weakened zone width ratio r_o/b. Typical values for G range from 100 to 250 c_u for cohesive soils, where c_u = undrained shear strength, and from 70 to 140 σ_v' for cohesionless soils, where σ_v' = effective stress in the soil layer. The shear modulus reduction ratio ranges from 0.15 to 0.8 according to the strain level. This means gradual variation with depth as the strain level varies with depth. The weak zone width ratio ranges from 0.5 to 0.9 according to the pile diameter (inversely) and also with the soil stiffness (also inversely). The effect of the variation of these parameters on the pile response is as follows:

1- Increasing the soil shear modulus decreases the elastic part of the displacement, but for constant shear strength, it may increase the final set.

2- Increasing the weak zone width and decreasing its shear modulus increases the elastic part of the displacement but reduces the final set if the shear strength is kept constant.

3.5.2. Slippage Stage

To achieve a desirable agreement in this stage, the soil parameters affecting the limiting resistance are to be suitably chosen. These parameters may be categorized into two groups: parameters that can be established in laboratory experiments and parameters that have to be assumed. The first group comprises the undrained shear strength for clay, c_u, and the angle of internal friction for sand, ϕ', as well as the unit weight, γ. The second group comprises the adhesion coefficient, α, for clay and the earth pressure

coefficient, k_s, for the sand as well as the base resistance factors, N_d, and, N_q, for clay and sand respectively. The static soil resistance, R_{st}, appearing in Eq. 3.13 may be defined as follows

for clayey soil

$$R_{st} = \alpha\, c_u\, \pi\, d \qquad \textit{(for the shaft)}$$

$$\textit{and} \qquad (3.19)$$

$$R_t = N_d\, c_u\, \pi \frac{d^2}{4} \qquad \textit{(for the tip)}$$

here, N_d is assigned the numerical value of 9.0 .

For sandy soil

$$R_{st} = k_s\, \sigma'_v \tan\delta \qquad \textit{(for the shaft)}$$

$$\textit{and} \qquad (3.20)$$

$$R_t = N_q\, \sigma'_v \frac{\pi\, d^2}{4} \qquad \textit{(for the tip)}$$

where $\delta = \phi' - 5°$.

A satisfactory agreement between the measured data and predicted pile response can be achieved by determining the first group of parameters from the tests and adjusting the parameters of the second group. The values of the parameters of the second group should lie within the range commonly employed in static design. However, if an adequate agreement cannot be achieved using values within the range, the parameters of the first group have to be adjusted. Thus the matching procedure works as a fine tuning process for the soil parameters predicted on the basis of laboratory experiments. This procedure is repeated until the match along the entire displacement time history is

attained. The bearing capacity of the pile can now be calculated from Eqs. 3.19 or 3.20 according to the soil type. The rate effects coefficient, J, was found to range from 0.50 to 0.78 for clay for both the shaft and the base, and from 0.1 to 0.15 for sand for the base only, and negligible for the shaft. The value of the exponent, N, was found to be in the vicinity of 0.5 and was assigned this value.

3.6. Case Studies

The procedure previously described was applied to a total of nine piles, six of which were driven and three drilled, installed on three different sites. These piles were tested by M. Janes and P. Bermingham both of Berminghammer Co., Ltd, Hamilton, Ontario using the Statnamic test and analyzed by the writer using the approach outlined herein and subjected to static loading capacity test.

First site

This site is located on the campus of McMaster University, Hamilton, Ontario. The subsurface soil profile at the site consists of mainly interbedded silty clay, clayey silt, silt, and silty fine sands (Fig. 3.8a). Weathered Queenston shale bedrock is encountered at a depth of about 19 m. Four driven closed-end steel pipe piles, each of 178 mm outside diameter with the wall thickness of 8.0 mm and 18.3 m length, were tested on this site. More details on this site are given by Horvath et al [50] .

Second site

The test site is located on Lulu Island within the Fraser River delta at Vancouver. This site belongs to The University of British Columbia. As shown in Fig. 3.8b, below a surface layer of sand fill there is a prevalent deposit of organic silty clays to a depth

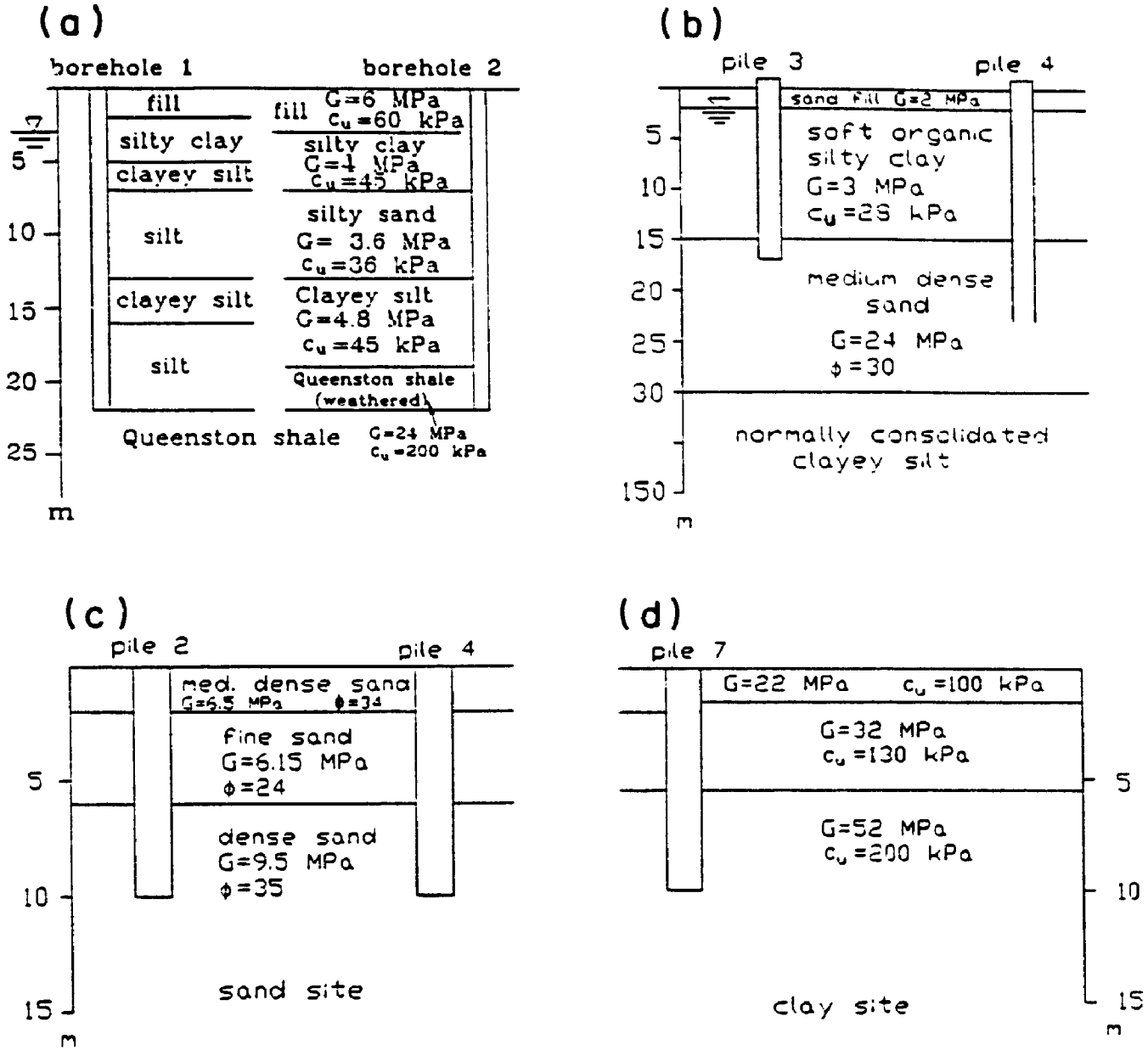

Figure 3.8 Soil Profiles for Different Sites (a) McMaster University (b) University of British Columbia, Lulu Island (c and d) Texas A&M University

of 15 m. Underlying this layer, a medium dense sand deposit, locally silty, prevails to a depth of 30 m. Extending to 150 m below the sand layer, a normally consolidated clayey silt was found . Two driven steel pipe piles, each of 324 mm outside diameter with the wall thickness of 9.5 mm, were tested on this site. More details on this site are given by Robertson et al [62] .

Third site

This site is located on the riverside campus at the Texas A&M University. The soil profile details are shown in Fig. 3.8C. Three drilled concrete piles, each of 909 mm diameter and 10 m length, were tested on this site, two of them were installed in sand and one in clay. The Statnamic test was a part of a large experimental program, described by J. Briaud [63] .

3.6.1. Results and discussion

Displacements

As an example, the calculated displacements are compared with measured values in Fig. 3.9. The displacements are plotted vs. the force on the pile head (Fig. 3.9a) and vs. time (Fig. 3.9b). The agreement between the theory and measured data is excellent. As can be seen from the figure, displacement varies in the time and force in a smooth way without the oscillations typical of pile driving records. The velocity, shown in Fig. 3.9c, was more oscillatory and was not compared with experimental data because velocities were not monitored. Analogous observations can be made for other piles (Figs. 3.10 and 3.11). The agreement between the theory and experiments is, for the

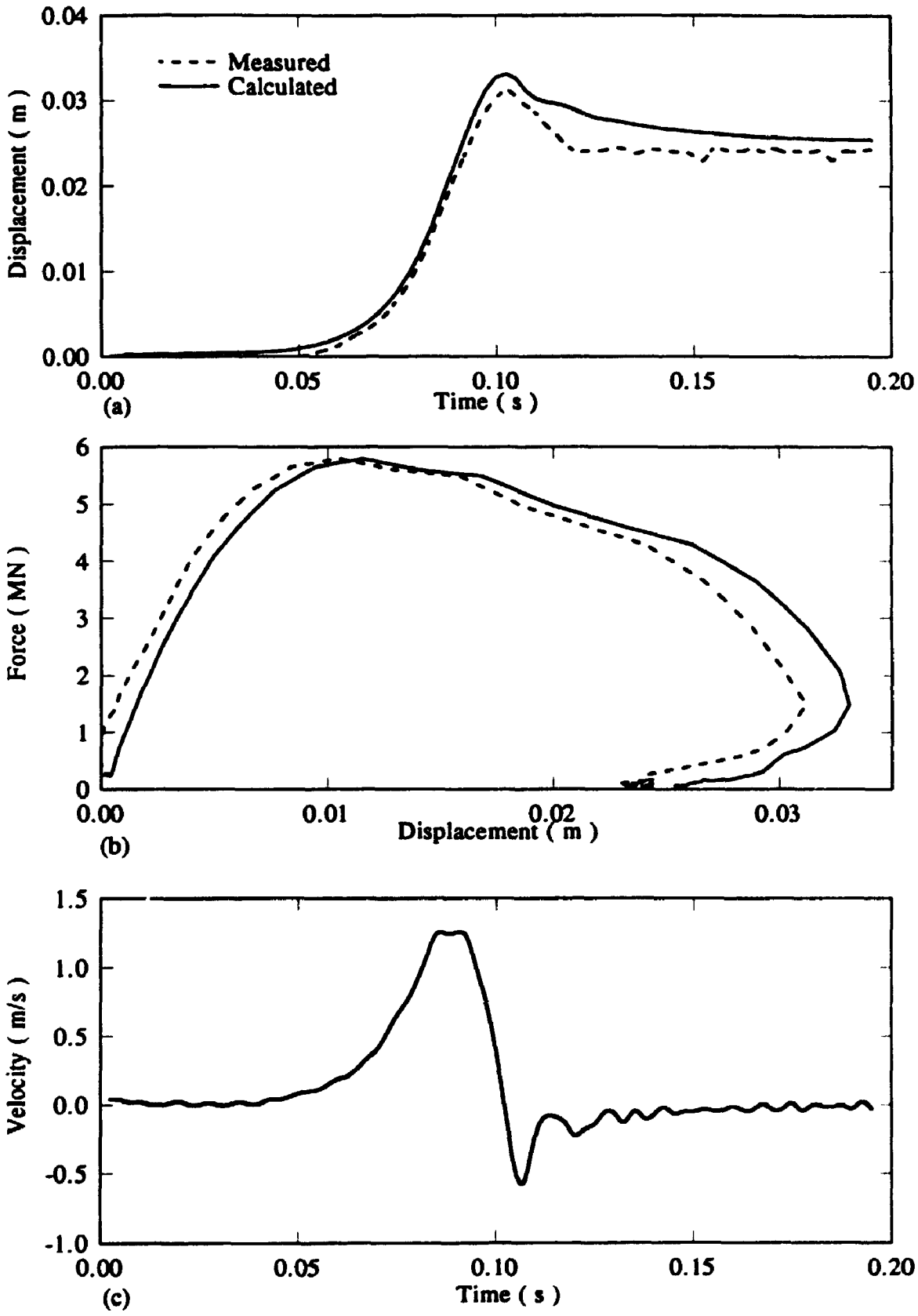

Figure 3.9 Measured and Predicted Response of Pile 4, Site 1. (a) Displacement vs. Time (b) Displacement vs. Force. (c) Predicted Velocity-Time History.

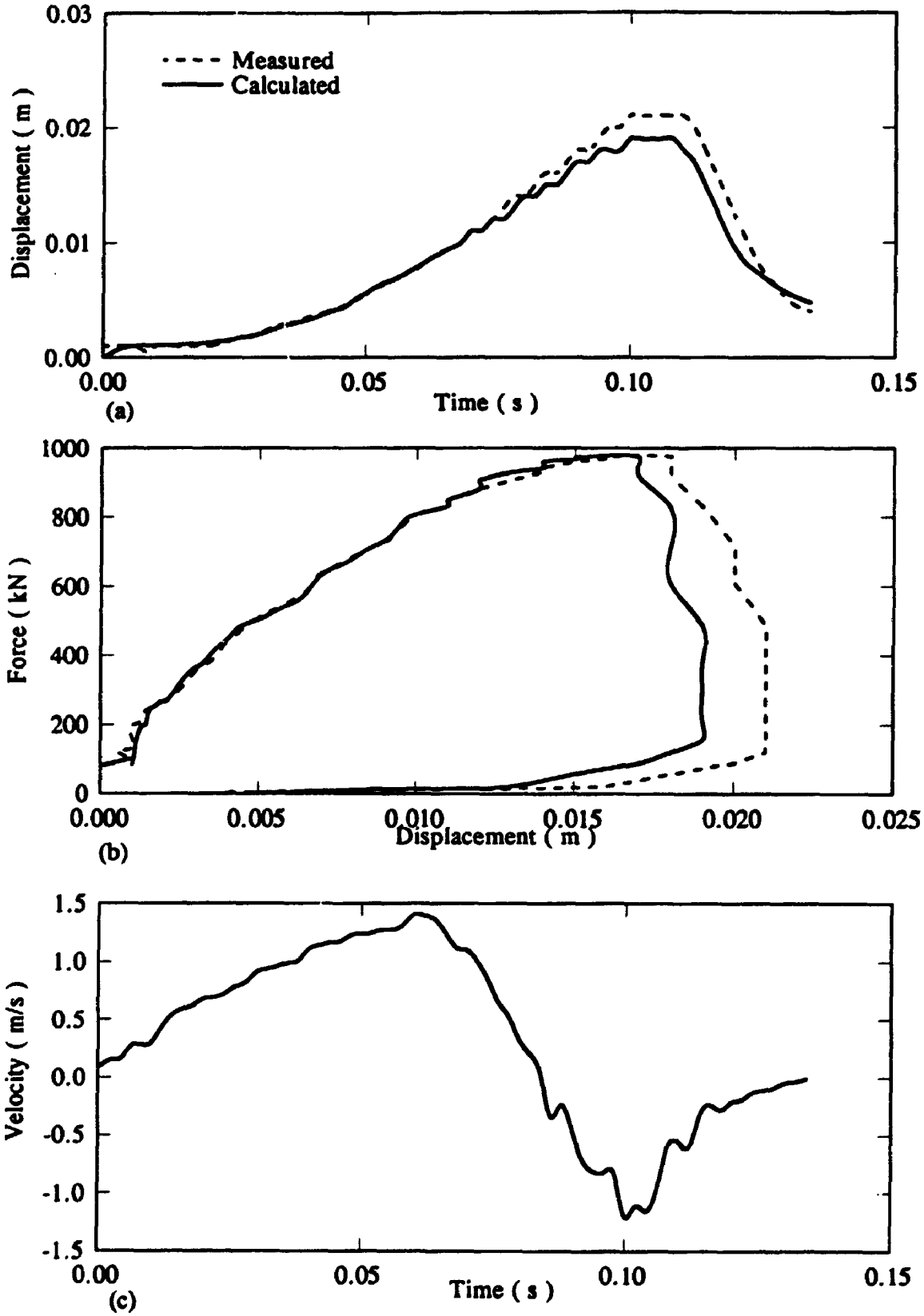

Figure 3.10 Measured and Predicted Response of Pile 9, Site 1 (a) Displacement vs. Time (b) Displacement vs. Force. (c) Predicted Velocity-Time History

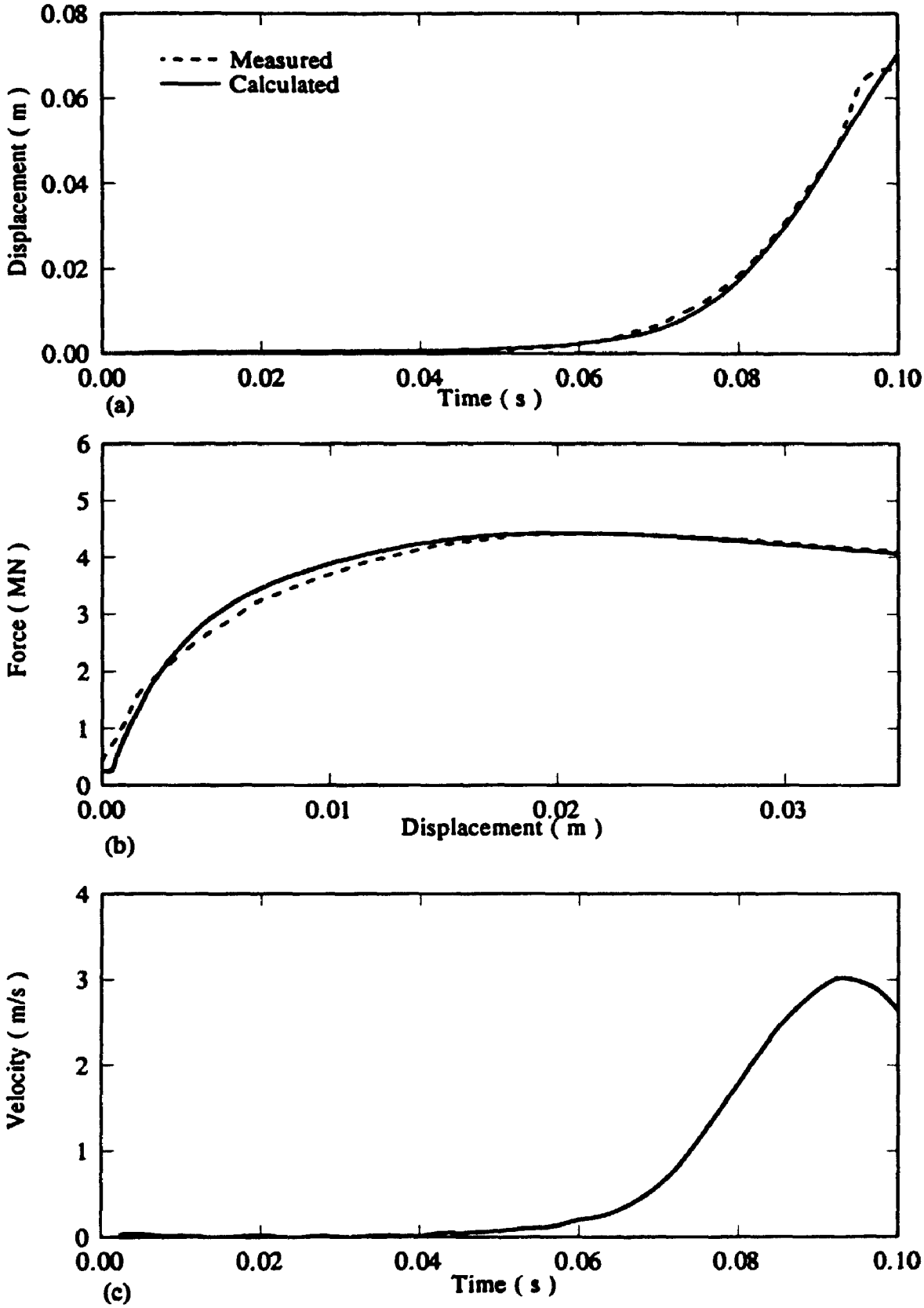

Figure 3.11 Measured and Predicted Response of Pile 2, Site 3 (a) Displacement vs. Time (b) Displacement vs. Force. (c) Predicted Velocity-Time History.

most part, just as good as in Fig. 3.9. The model parameters used in the theoretical analysis, for all the piles tested, are given in Table 1 as a contribution to the data bank needed for further refinement of the method.

Bearing Capacity

Table 2 summarizes the pile data, the bearing capacities measured and the bearing capacities predicted using the new test method and the analysis proposed. These results show very favourable predictions of the bearing capacity of the piles compared with the capacities established using conventional static load tests. This, along wi. the very good agreement between the measured response and the predicted one, shows the great capability of both the new test method and the proposed method of dynamic analysis for predicting pile bearing capacity. Also, it appears that the shaft resistance representation in this analytical model is close to reality as the radiation damping is accounted for in full before slippage and in part during it and the very important loading rate effects are also accounted for. As may be noticed, the predicted pile capacity does not need any modification to account for the remoulding effects because it is clear that the loading manner is very smooth with no oscillations and also that capacity is calculated as limiting resistance, i.e before failure occurs.

This approach can also be successful in the common pile driving analysis.

3.7. Pile Driving

The analytical model described may be used to analyze the pile driving problem provided that the force and displacement (or velocity) time histories are measured at

Table 3.1 Soil Parameters Used in Dynamic Analysis

Site[a]	Pile no.	Soil type	C_u (kPa)	ϕ' (deg)	G	α	K_s	N_q	G_m/G	r/b	J
1	6	Layered clay	30-240		$3.6x10^3$-$3.6x10^4$				0.15-0.60	0.5-0.6	0.78-0.5
	7	Layered clay	30-240		$3.6x10^3$-$3.6x10^4$	0.7			0.15-0.60	0.5-0.6	0.78-0.5
	8	Layered clay	25-200		$3x10^3$-$3x10^4$	1.0			0.15-0.60	0.5-0.6	0.78-0.5
	9	Layered clay	25-200		$3x10^3$-$3x10^4$	1.0			0.15-0.60	0.5-0.6	0.78-0.5
2	3	Clay and sand base	13.5		$4x10^3$	0.5		40	0.2-0.6	0.6-0.65	0.78-0.1
	4	Clay and sand	13.5	30	$4x10^3$	1.0	0.8	40	0.25-0.6	0.6-0.65	0.78-0.1
3	2	Sand		24-35	$6.2x10^3$-$1.8x10^4$		0.8	50	0.6	0.9	0.0-0.1
	4	Sand		24-35	$6.2x10^3$-$1.8x10^4$		1.85	90	0.6	0.9	0.0-0.1
	7	Clay	100-180		$1.2x10^4$-$5.3x10^4$	0.85			0.5	0.8	0.78-0.5

a1, McMaster University; 2, Lulu Island; 3, Texas A&M University.

Table 3.2 Pile Properties and Bearing Capacities

Site[a]	Pile no.	Length (m)	Diameter (m)	Measured bearing Capacity	Predicted Bearing Capacity	Deviation (%)	Notes[b]
1	6	18.3	0.178	586	526	10.2	D,C
	7	18.0	0.178	499	487	2.40	D,C
	8	17.7	0.178	342	318	7.00	D,C
	9	18.0	0.178	441	433	1.80	D,C
2	3	16.8	0.324	610	606	0.66	D,C
	4	23.2	0.324	1200	1166	2.80	D,O
3	2	10.1	0.909	1620	2458	34.0	R,C
	4	10.0	0.909	4050	4485	9.60	R,C
	7	9.83	0.909	3060	3150	2.86	R,C

[a]Sites as in Table 3.1.

[b]D, driven pile; R, drilled pile; C, closed end; O, open end.

the pile head. Employing the force time history as input force and using the displacement (or the velocity) time history as a guide, the matching process described in sections 3.5.1 and 3.5.2 is to be repeated until a satisfactory match with the measured data is achieved. In situations where neither the force nor the displacement time histories are measured, the hammer impact can be idealized as a pulse force at the pile head evaluated as (Clough and Penzien [64])

$$P(t) = k_c \frac{V_h}{\omega_d} e^{-\zeta \omega t} \sin \omega_d t \qquad (3.21)$$

where k_c is the cushion stiffness, V_h is the hammer impact velocity and ω_d is the damped natural frequency given by

$$\omega_d = \sqrt{\omega \left(1 - \zeta^2\right)} \qquad (3.22)$$

In Eq. 3.22, $\omega = \sqrt{(k_c / m)}$ is the undamped natural frequency, m is the hammer mass and ζ is a damping ratio calculated as

$$\zeta = k_c V_p / (2 \omega A E) \qquad (3.23)$$

where V_p is the primary wave velocity of the pile material and E and A are the Young's modulus of the pile and its cross-sectional area, respectively.

If the displacement (or velocity) time history is not available, the final set of the pile, which is routinely recorded while driving, may be used for the matching process.

For drivability assessment, this model may be also used. The driving hammer data may be used to produce a force-time history using Equation 3.21 to produce the

input force. This input force is to be applied to the pile embedded in the specific site and the proposed model is used to predict the final set per blow or the blow count. An example of pile driving analysis is shown in Fig. 3.12. The figure shows the force time history produced by Eq. 3.21 and both the displacement and velocity time histories.

3.8. Conclusion

1)The new pile test method is fast, easy to conduct, non-destructive and appears to give very good estimation for the pile behaviour especially in the working load range.

2)The analytical model presented is able to simulate not only the new test event but also the usual pile driving analysis.

3)As conventional soil mechanics parameters are used for this model and for the prediction of the bearing capacity of the piles, the method proves to be general and not dependent on the soil type.

4)The successful estimation of bearing capacity of all the piles on the different sites using the Statnamic test and the proposed method of analysis promise to be useful in other cases also.

5)The Statnamic test and its analysis offer an alternative to the costly and cumbersome conventional static loading test.

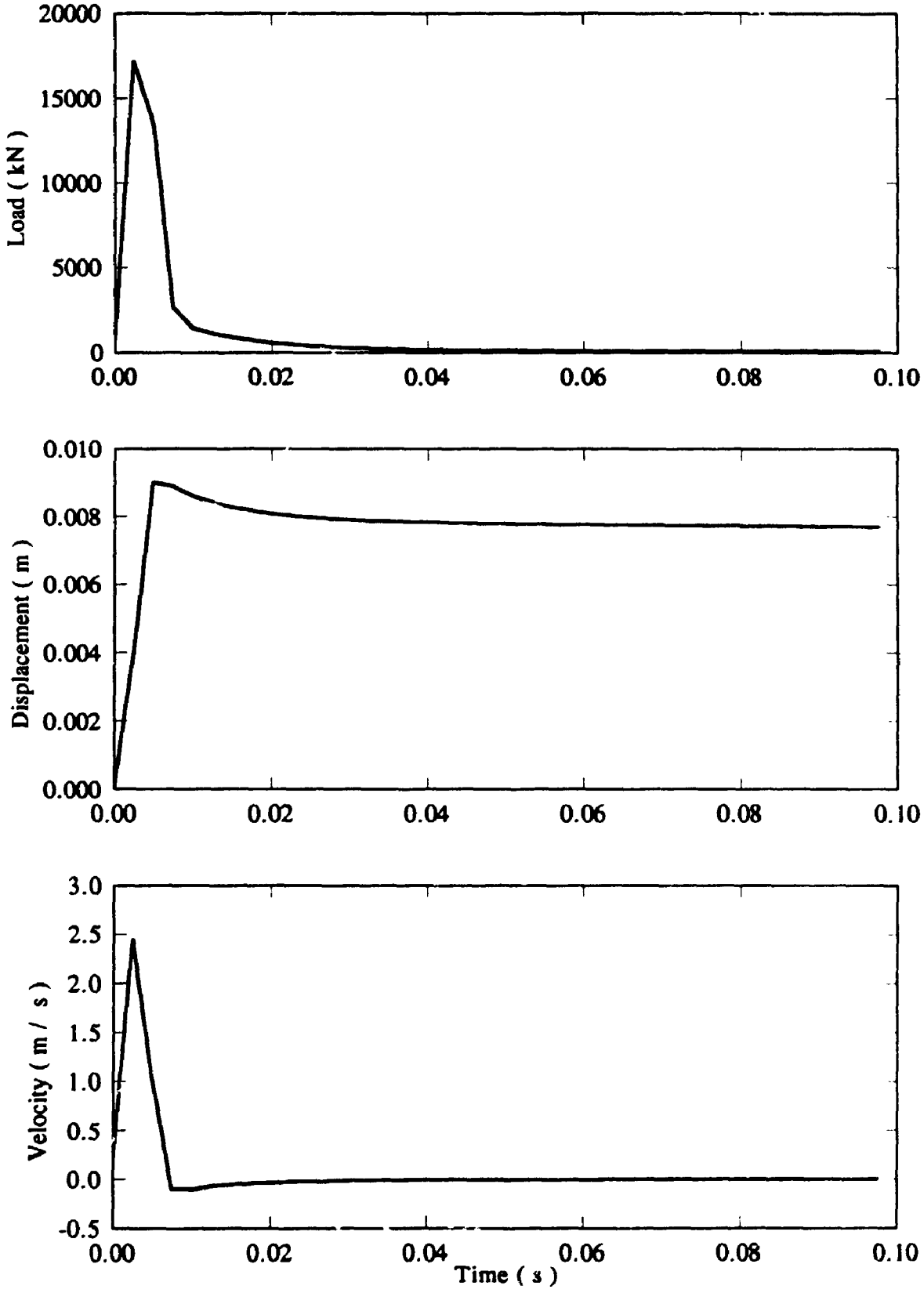

Figure 3.12 Pile Driving Analysis Using the Proposed Model

CHAPTER FOUR
NONLINEAR ANALYSIS OF AXIAL RESPONSE OF SINGLE PILES AND PILE GROUPS

4.1. Introduction

Many studies have been devoted to dynamic behaviour of piles, and in most of them the assumption of linearity was adopted. However, for high level of strain that exceeds the linear limit of the soil medium, a nonlinear analysis is called for. Studies of axial nonlinear response, to which this chapter is limited, were conducted by many researchers, e.g. [47,48,61,65,66]. In these studies, various shaft models as well as Finite Element techniques were implemented considering elasto-plastic springs in combination with the plane strain constants taken as frequency independent, and different types of damping and slippage elements. Mitwally and Novak [49] accounted approximately for the nonlinear behaviour of the soil adjacent to the pile by incorporating an annular weak zone with reduced soil shear modulus and a slippage element. Nogami and his colleagues [26,27,34] developed a time domain analysis based on the plane strain solution to model the elastic soil medium away from the pile and for the near field, incorporated a nonlinear element with constants derived from t-z curves. Holeyman [66,67] modified the Randolph and Wroth [68] solution to account for the nonlinear behaviour near the pile, but these solutions yield an infinite soil displacement at the pile unless the medium is fixed at an empirically chosen distance. Trochanis et al. [69] proposed a nonlinear shaft model using some constants which are not standard geotechnical parameters and have to be estimated empirically.

All these studies indicate that soil nonlinearity and relative movement at the soil-pile interface strongly affect pile behaviour and that the pile response further depends on the variation of soil properties with depth, energy dissipation through radiation, hysteretic damping, and, also, on the loading rate and the loss of soil strength after the ultimate

strength is exceeded. In this chapter an analysis is formulated based on a shaft model, that incorporates the above mentioned factors, and whose properties are specified using standard geotechnical parameters rather than being empirical. The applicability and efficiency of the approach are demonstrated using the cases of pile driving, Statnamic testing and t-z curve generation are demonstrated. This analysis differs from that described in Chapter 3 as the soil reactions to the pile motion are adjusted automatically according to the load level, thus the model input is not experience dependent. Also, the model described here allows for the group effects to be accounted for. Some equations used in Chapter 3 are repeated here for the continuity of reading.

4.2. Shaft Model

For three-dimensional nonlinear dynamic analysis the Finite Element Method, although powerful, is computationally expensive and not very suitable for common pile analysis; and analytical solutions are extremely complex. The Winkler foundation is the most versatile and economical model that can account for various complicated conditions in a simple manner and is therefore the model adopted here.

4.2.1. Soil Side Reactions

When a pile is subjected to high-level loading, the soil around the pile may exhibit strong nonlinearity in the region close to the pile and, a relative movement between the soil and pile may occur at the soil-pile interface. The soil outside this region behaves more or less elastically. Therefore, the soil around the pile is divided into two regions, the inner nonlinear field and the outer elastic region. Interface elements are also added to this model to account for the relative movements at the soil-pile interface. The elements of this model, shown in Fig.4.1, are discussed in the following sections.

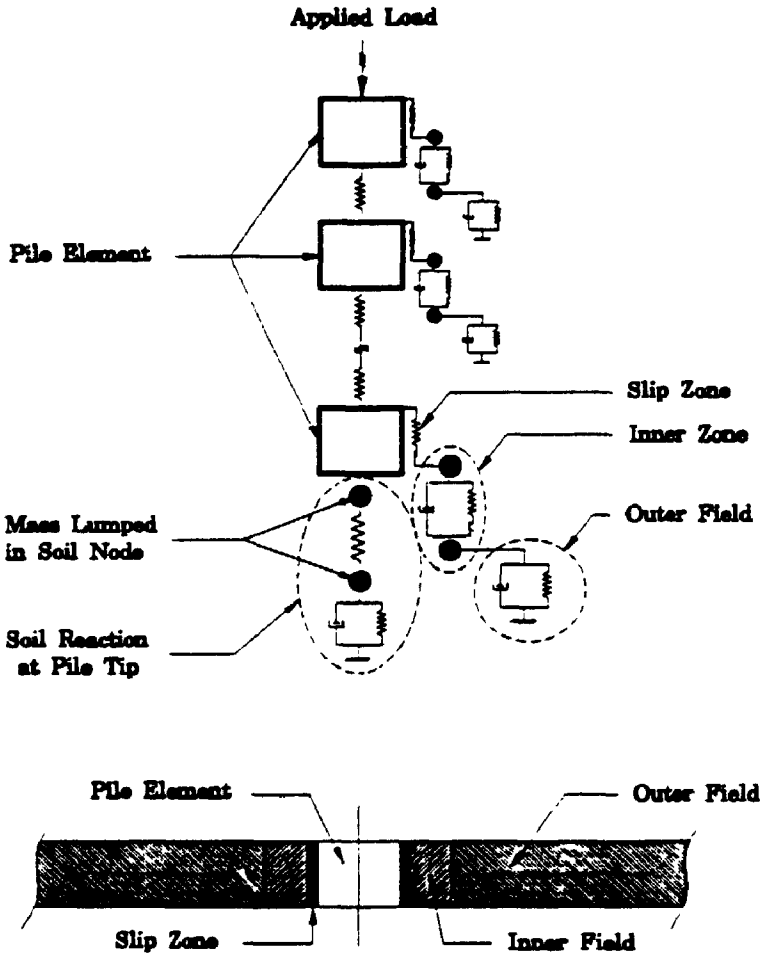

Figure 4.1 Elements of Proposed Model for Nonlinear Dynamic Analysis of Single Piles

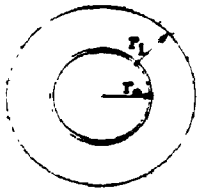

Figure 4.2 Plan View of a Single Pile in an Elastic Medium Under Plane Strain Conditions

Inner Field Element: Fig. 4.2 shows a plan view of a single pile in an elastic medium under plane strain conditions. The radius r_0 defines the pile surface and the radius r_1 defines the extent of the inner cylindrical zone to which the nonlinear behavior is confined. Under these conditions the displacement is infinite under static vertical loading, although the stresses and strains are finite. Randolph and Wroth [68] suggested a solution for this problem by assuming that the soil medium is limited by a cylindrical boundary at some radius R_m. By integrating the angular distortion from the radius R_m to the radius of the pile, r_0, a finite solution may be obtained. When the pile is strongly excited, nonlinear behavior occurs in the soil region adjacent to the pile. A few stress-strain relationships can be used to model this non-linearity. One relationship, Kondner [70], relates the shear stress, τ, to the shear deformation, γ, as

$$\frac{\gamma}{\gamma_r} = \frac{\eta}{1-\eta} \tag{4.1}$$

where $\eta = \tau/\tau_f$ in which τ_f = ultimate shear strength, $\gamma_r = \tau_f/G_s$ is the reference shear strain and G_s = initial tangent shear modulus. For the plane strain conditions assumed, and the infinitely long incompressible cylindrical pile, the displacement at pile surface, w_0, is obtained by direct integration of the angular distortion from the radius of the inner field r_1 to the radius of the pile r_o, i.e.

$$w_o = \int_{r_o}^{r_1} \gamma \, dr = \int_{r_o}^{r_1} \frac{dr}{\left(\frac{G_s r}{\tau_o r_o} - \frac{1}{\gamma_r} \right)} \tag{4.2}$$

Eq. 4.2 yields

$$w_o = \frac{\tau_o r_o}{G_s} \ln \left(\frac{\frac{r_1}{r_o} - \eta_o}{1 - \eta_o} \right) \tag{4.3}$$

where w_0 is the displacement at the pile shaft due to the stress in the inner field $\tau_o = \tau$ at $r = r_o$ and $\eta_0 = \tau_0/\tau_f$. From Eq. 4.3 the stress at $r = r_o$ is

$$\tau_o = \left[\frac{G_s}{r_o} \Big/ \ln\left(\frac{\frac{r_1}{r_o} - \eta_o}{1 - \eta_o} \right) \right] w_o \tag{4.4}$$

and the force per unit length at the pile shaft is

$$P_o = \left[2\pi G_s \Big/ \ln\left(\frac{\frac{r_1}{r_o} - \eta_o}{1 - \eta_o} \right) \right] w_o \tag{4.5}$$

From Eq. 4.5 the stiffness of the inner field K_{ni} may be written for a unit of the shaft length as

$$K_{ni} = 2\pi G_s \Big/ \ln\left(\frac{\frac{r_1}{r_o} - \eta_o}{1 - \eta_o} \right) \tag{4.6}$$

The shaft force produced by Eq. 4.5 is plotted versus the normalized displacement, $w_0 G_s / \tau_0 r_0$, in Fig. 4.3. This load-displacement relation indicates a smooth transition from linear to nonlinear behavior, and pure plastic behavior when the shear stress exceeds the ultimate soil strength, as the stiffness vanishes and the soil offers constant resistance to the pile movement.

To model the hysteretic behaviour of the soil it is assumed that the stiffness K_{ni} in the unloading phase is completely elastic and given by

$$K_{ni} = 2\pi G_s \Big/ \ln\left(\frac{r_1}{r_o} \right) \tag{4.7}$$

To account for the effect of the loading rate the ultimate soil resistance is modified as follows

$$R_{ud} = R_{us} \left(1 + J\, V^N \right) \tag{4.8}$$

where R_{us} is the ultimate soil resistance at a reference velocity, J = a factor depending on the soil type, N is an exponent reflecting the non-linearity of this effect and V = the loading velocity in the inner field. Finally, if material damping is to be considered, it

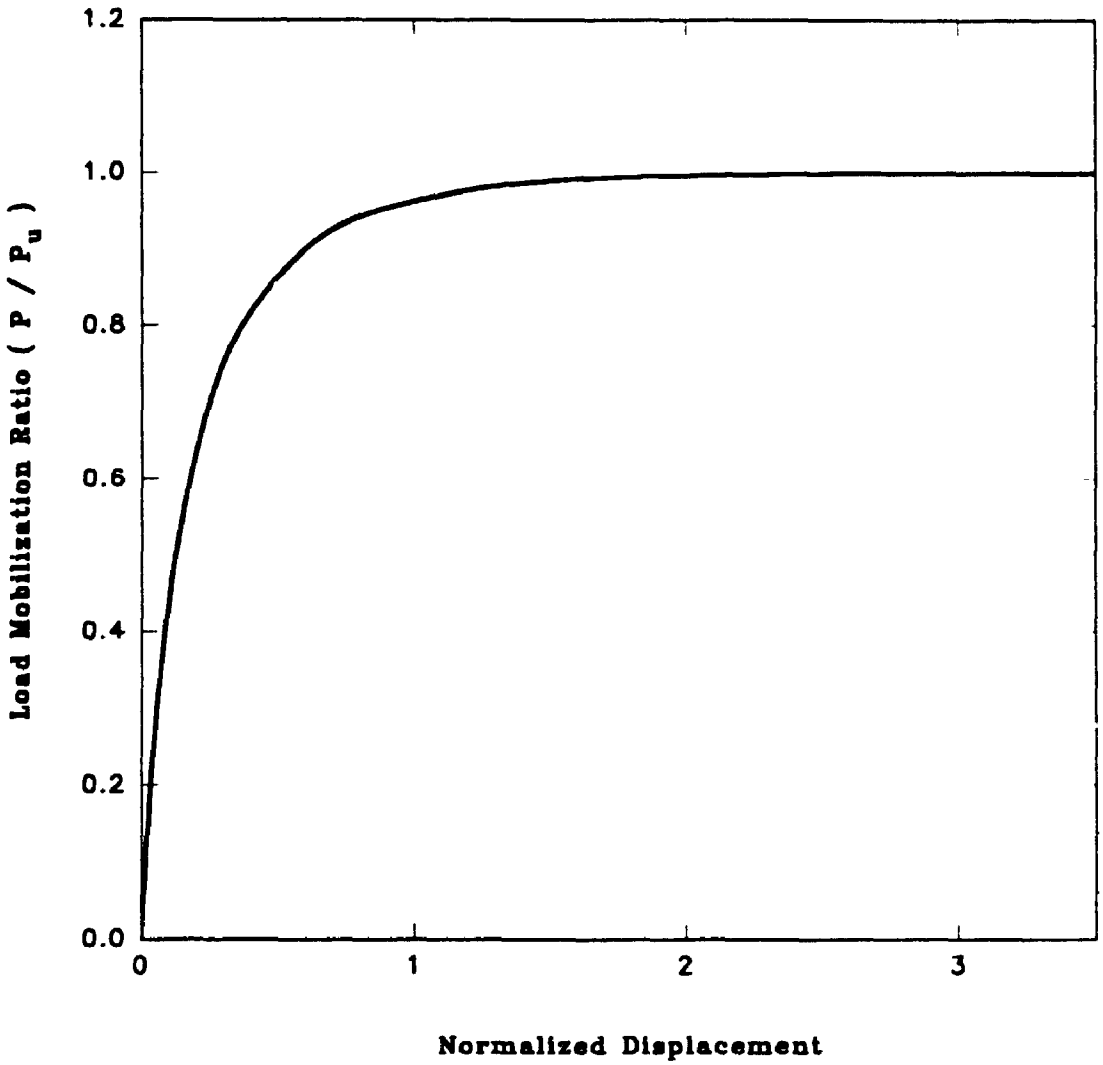

Figure 4.3 Nonlinear Soil Resistance to Pile Movement

may be added as a parallel dashpot with a constant, c_m, suitably chosen. There is a rigid plastic slider between the pile node and the inner field element. When the force in this slider exceeds the ultimate soil resistance included in Eq. 4.8, the slider is disconnected and slippage occurs.

Outer Field Element: For vertical vibration, the plane strain solution for an infinitely long massless cylinder vibrating in an infinite elastic medium is given by Novak et al. [21]

$$w(a_o,r) = \frac{1}{2\pi G_s} \frac{K_o(a_o^*,r)}{a_o^* \; K_1(a_o^*)} P_v(a_o) \tag{4.9}$$

where $w(a_o,r)$ = displacement amplitude at a distance r from the centre of the cylinder, $a_0=\omega r_0/V_s$, and $a^*_0=ia_0$ in which ω is the circular frequency; V_s is the shear wave velocity, $P_v(a_o)$ is the vertical exciting force and $i=\sqrt{-1}$.

Eq. 4.9 yields the complex stiffness of the outer medium as

$$K = 2\pi G_s \frac{a_o^* \; K_1(a_o^*)}{K_o(a_o^*)} \tag{4.10}$$

where K_1 and K_0 are the modified Bessel functions of the second kind of order one and zero respectively. The complex stiffness may be rewritten as

$$K = G_s(S_{v1} + iS_{v2}) \tag{4.11}$$

The variation of both the real and imaginary parts, S_{v1} and S_{v2} with frequency is shown in Fig. 3.4a. The real part, S_{v1}, is almost constant for $a_o > 0.3$. S_{v2} increases monotonically, almost linearly, with the frequency. This suggests that the outer field element can be modeled by a spring and dashpot whose constants are frequency independent and defined as

$$K_l = G_s \; S_{v1}$$

$$c = \frac{G_s r_o}{V_s} S_{v2}(a_0=1) \tag{4.12}$$

where S_{v1} and $S_{v2}(a_0=1)$ are frequency independent constants with S_{v1} chosen according to the dominant dimensionless frequency a_0. These frequency independent stiffness and damping parameters are needed for the dynamic analysis in the time domain.

4.2.2. Soil Reactions at Pile Base

Soil resistance at the pile tip is usually modeled by the reaction of a homogeneous elastic half-space to a rigid massless disk undergoing harmonic vibration and represented by a linear spring and a linear dashpot. The constants of this spring and dashpot are given as (Lysmer and Richart [53])

$$K_t = \frac{4 G_s R}{(1 - \nu_s)} \tag{4.13}$$

$$c_t = \frac{3.4 R \sqrt{G_s \rho_s}}{(1 - \nu_s)} \tag{4.14}$$

where R is the pile radius at the tip and ν_s is the soil Poisson's ratio.

Heterogeneity and nonlinearity cannot be modelled directly using this model. To account for these factors, the local soil properties at the pile base have to be modified. Holeyman [67] introduced a cone of modified properties underneath the pile tip to reproduce the half-space reactions. This solution, although very good at representing a half-space, is unable to dissipate energy in directions other than downward; furthermore, the lateral confinement is not effectively modeled. Therefore, another approximate model is adopted, which allows for radial wave propagation and lateral confinement.

The model replaces the homogeneous elastic half-space (Fig. 4.4a) by a soil layer underlain by half-space (Fig. 4.4b), with the layer represented by a nonlinear soil column

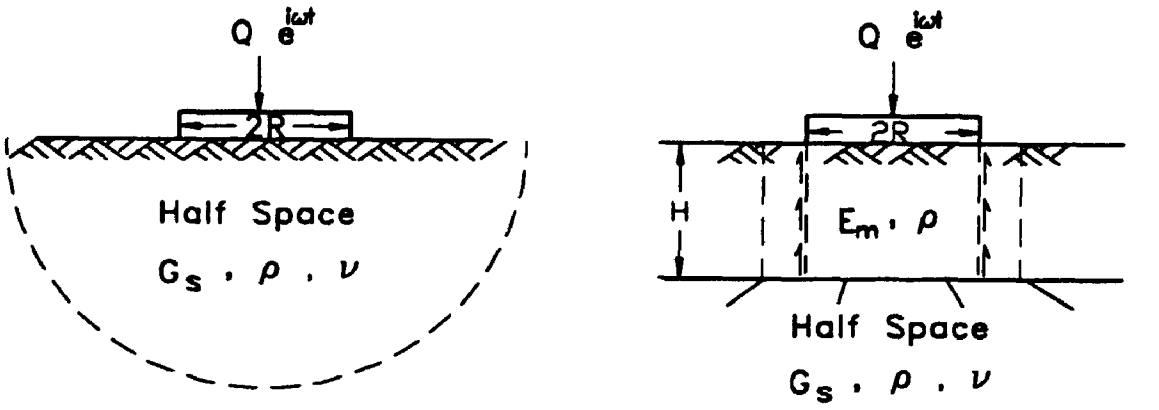

(a) Half Space (b) Equivalent System

Figure 4.4 Pile Base Modelling

under the pile base and plane strain soil reactions for the outer region. The thickness and properties of this soil layer are evaluated so that the dynamic behavior of both systems is the same. To this end, two conditions have to be satisfied. First, the static deflection should be equal for both systems. Second, the harmonic behavior should be the same.

Consideration of the plane strain reactions for an embedded foundation developed by Novak and Beredugo [71] and the compressibility of the soil column underneath the foundation yield the layer depth evaluated as

$$H = \frac{R}{2}[(1.84 - 6.41\,\nu_s) + \sqrt{(1.84 - 6.41\,\nu_s)^2 + 4(6.64 - 11.86\,\nu_s)}] \tag{4.15}$$

For linear conditions, the agreement between the two approaches was found to be excellent as shown in Fig. 4.5a. To account for soil layering under the pile, soil properties may vary with depth.

Nonlinearity: It is assumed that nonlinear behavior and plastic deformations are confined to the soil column and the inner field surrounding it; and the outer field and the half-space are assumed to behave elastically because the stress level is low enough in these regions. A nonlinear stress-strain relationship analogous to Eq. 4.1 is used for the soil column under the pile tip. The hyperbolic law, Kondner [70], for direct strains is adopted here as follows

$$\frac{\varepsilon}{\varepsilon_0} = \frac{\eta}{1-\eta} \tag{4.16}$$

where η is the mobilization ratio= Q/Q_r, where Q_r is the ultimate strength, and ε_0 is the reference direct strain = Q_r/E_i, where E_i is the initial modulus. For load reversal, it is assumed that the elastic behavior with the initial modulus is retained and the soil assumes no tension. The soil layer offers side reactions to the soil column. These reactions allow for nonlinearity and are calculated in the same way as the pile shaft. For harmonic loading, Fig. 4.5b shows the soil reaction-displacement relationship for a rigid

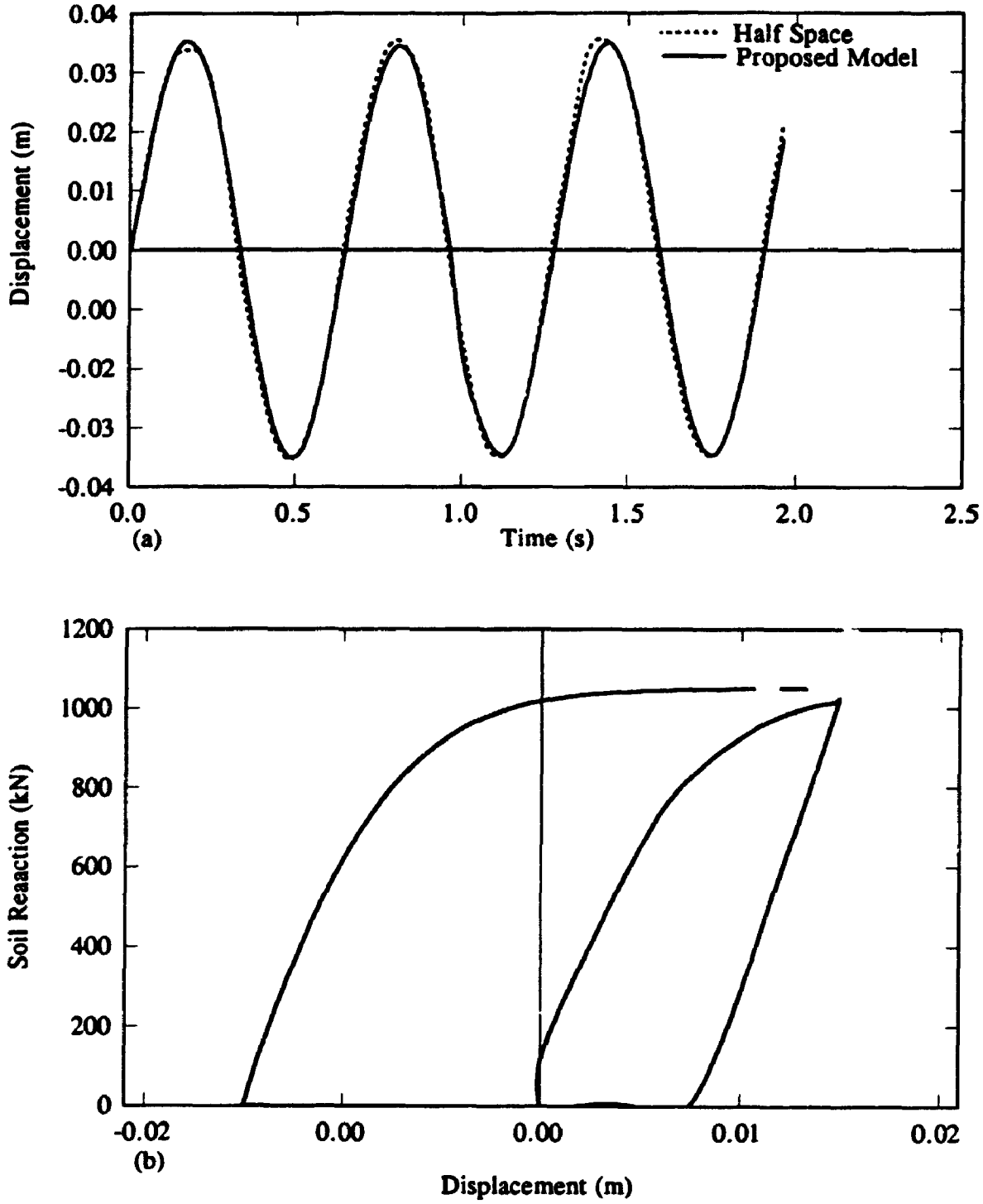

Figure 4.5 (a) Response of Circular Footing on Top of Homogeneous Elastic Half-Space Under Harmonic Loading (b) Soil Reactions for a Rigid Footing Undergoing Harmonic Vibration Employing the Proposed Nonlinear Model

footing base as represented by the proposed model. Modelling of the soil reactions in that manner provides energy dissipation through both radiation damping and hysteretic damping, and the soil mass is accounted for

4.3. Group Effect

When piles are used in a group, the displacement of each pile is affected by the presence of the other piles. This effect is incorporated in the analysis as follows. Under the assumption of wave propagation in the horizontal direction only and a Winkler soil model, the displacement at any point in the elastic soil domain may be given, in general, as

$$w(a_0,r) = w_0 \quad \psi_v(r,a_0) \tag{4.17}$$

in which w_0 is the amplitude of the disturbance at the source, and ψ_v is an attenuation function accounting for the wave propagation away from the source and the radiation damping. Eq. 4.17 may be rewritten in an approximate way as

$$w(a_0,r) = \frac{1}{K_1 + ica_0} \left(\sqrt{\frac{r_0}{r}} e^{-ia_0 \frac{r-r_0}{r_0}} \right) P_v(a_0) \tag{4.18}$$

where K_1 and c are frequency independent spring and dashpot constants appropriately chosen for the range of frequencies encountered. Eq. 4.18 is subjected to an inverse Fourier transform to obtain the unit impulse response function required for time domain analysis. This impulse function is given as

$$w(t,r) = \sqrt{\frac{r_0}{r}} \, A \, e^{-B(t-t_0)} \qquad t > t_0 \tag{4.19}$$

where $A = 1/c$, $B = K_1/c$ and $t_0 = (r-r_0)/V_s$.

Assuming linear variation of the interaction effect through each time step Δt, the soil displacement at the axis of the m^{th} pile due to a disturbance at the l^{th} pile is given by

$$w_m(t_i,r_{ml}) = P_i(t_i - t_{ml-1})\, H_1(t_i,r_{ml}) + P_i(t_i)\, H_2(t_i,r_{ml}) \tag{4.20}$$

where i is the label of the time step, r_{ml} is the distance between the piles m and l, t_{ml-1} is the travel time between them minus one time step; H_1 and H_2 are convolution integrals over the period Δt given as

$$H_1 = \int_0^{\Delta t} w(t-\tau,r)\left(1-\frac{\tau}{\Delta T}\right) d\tau$$

$$= \sqrt{\frac{r_0}{r}}\frac{A}{B}\left[\frac{1}{B\Delta t}e^{B\Delta t} - \left(1-\frac{1}{B\Delta t}\right)\right]e^{-B(t-t_0)} \qquad t \geq t_0 + \Delta t \tag{4.21}$$

$$H_2 = \int_0^{\Delta t} w(t-\tau,r)\frac{\tau}{\Delta T} d\tau$$

$$= \sqrt{\frac{r_0}{r}}\frac{A}{B}\left[\left(1-\frac{1}{B\Delta t}\right)e^{B\Delta t} + \frac{1}{B\Delta t}\right]e^{-B(t-t_0)} \qquad t \geq t_0 + \Delta t \tag{4.22}$$

Eq. 4.20 implies that H_2 is the inverse of the time domain stiffness of the medium if r equals to r_0, yielding the interaction force as

$$P = -[\, H_2(r=r_0)\,]^{-1}\, w_m \qquad l \neq m$$

$$= -K_v\, w_m \tag{4.23}$$

This force is to be considered in the analysis as discussed in the next section.

Fig. 4.6 shows a slice of the soil-piles system containing the elements of the model implemented in the group analysis. The mass of the inner field, m_s, is lumped at two nodes: one half, m_1, at the node adjacent to the pile, node 1, and the other half, m_2, at the node adjacent to the outer field, node 2. The visco-elastic spring, K_v, connects the two piles through the far field.

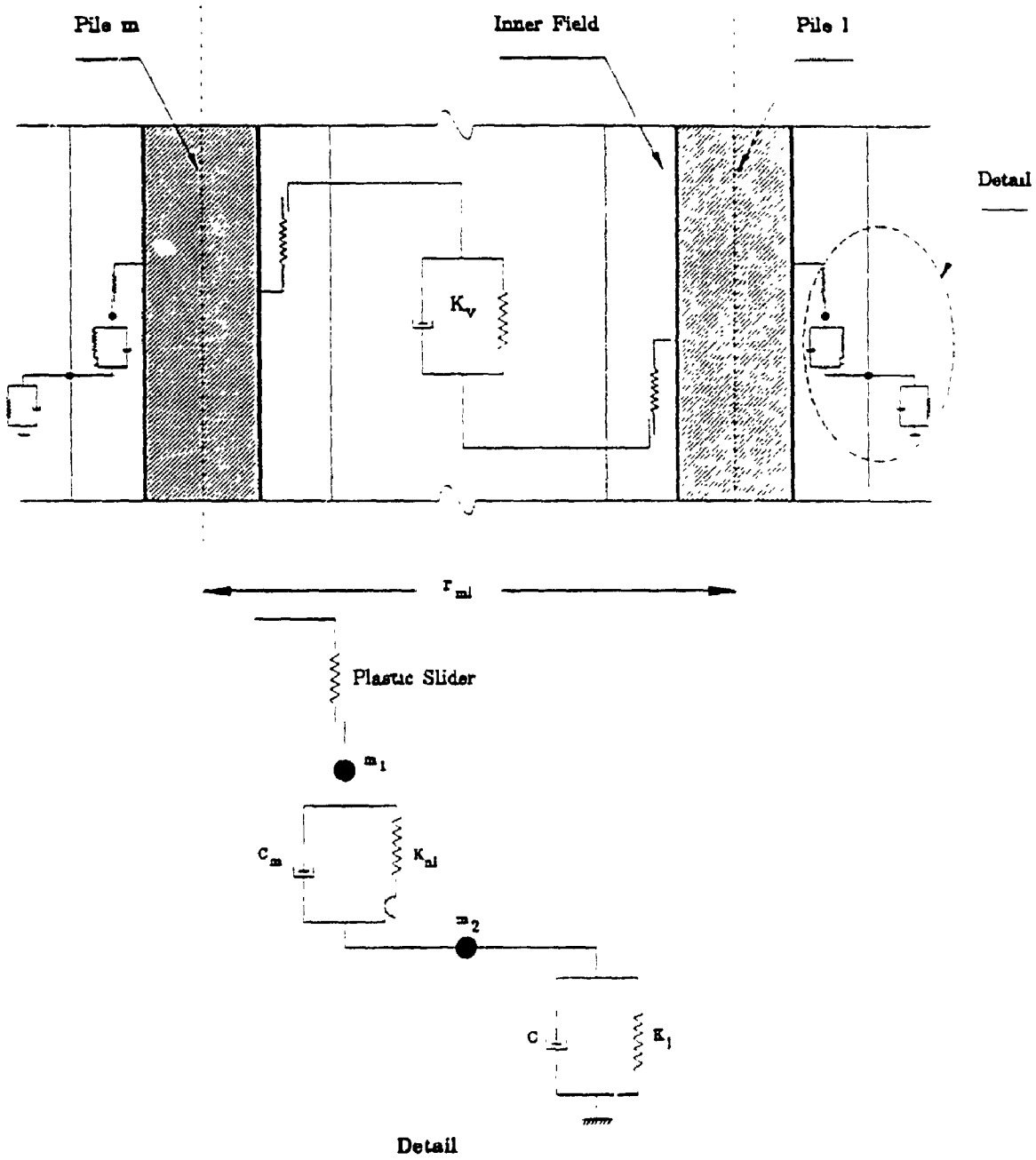

Figure 4.6 Elements of the Pile Group Model

4.4. Equations of Motion

The equations of motion for the inner field expressing the equilibrium of masses m_1 and m_2 are

$$\begin{aligned} m_1 \ddot{w}_1 + c_m(\dot{w}_1 - \dot{w}_2) + K_{nl}(w_1 - w_2) &= P_1 \\ m_2 \ddot{w}_2 - c_m(\dot{w}_1 - \dot{w}_2) - K_{nl}(w_1 - w_2) &= P_2 \end{aligned} \tag{4.24}$$

A dot means differentiation with respect to time; w_1 and w_2 are the displacements of nodes 1 and 2, and P_1 is the force in the rigid plastic slider and P_2 is the soil resistance at node 2; finally, c_m is the material damping in the inner field.

The equation of motion for the outer field may be written as

$$c\dot{w}_2 + K_l w = -P_2 + P \tag{4.25}$$

where P is the interactive force transmitted through the soil from pile to pile. Introducing compatibility and equilibrium between the inner field and the outer field yields

$$\begin{Bmatrix} P_1 \\ 0 \end{Bmatrix} = \begin{bmatrix} A_m m_1 + A_c c_m + K_{nl} & -K_{nl} - A_c c_m \\ -K_{nl} - A_c c_m & K_{nl} + A_m m_2 + A_c c_t + K_l \end{bmatrix} \begin{Bmatrix} w_1 \\ w_2 \end{Bmatrix} + \begin{Bmatrix} \delta_1 \\ \delta_2 - P \end{Bmatrix} \tag{4.26}$$

where $c_t = c + c_m$ is the total damping.

From Eq. 4.26 it can be deduced that

$$w_2 = \frac{K_{nl} + A_c c_m}{(K_{nl} + K_l + A_m m_2 + A_c c_t)} w_1 + \frac{P - \delta_2}{(K_{nl} + K_l + A_m m_2 + A_c c_t)} \tag{4.27}$$

$$P_1 = \left[K_{nl} + A_m m_1 + A_c c_m - \frac{(K_{nl} + A_c c_m)^2}{(K_{nl} + K_l + A_m m_2 + A_c c_t)} \right] w_1 - \frac{K_{nl}(P - \delta_2)}{(K_{nl} + K_l + A_m m_2 + A_c c_t)} + \delta_1 \tag{4.28}$$

where A_m and A_c are numerical integration constants for inertia and damping , respectively. Finally

$$\delta_1 = K_{nl}^{i-1} (w_1 - w_2)^{i-1} + c_m (\dot{w}_1 - \dot{w}_2)^{i-1} + m_1 \ddot{w}_1^{i-1} \quad (4.29)$$

$$\delta_2 = -K_{nl}^{i-1} (w_1 - w_2)^{i-1} - c_m (\dot{w}_1 - \dot{w}_2) + m_2 \ddot{w}_2^{i-1} + K_l w_2^{i-1} + c \dot{w}_2^{i-1} \quad (4.30)$$

When P_1 reaches the maximum soil resistance, K_{nl} assumes the value of zero. As the load increases, P_1 will vary according to the variation of the loading rate as Eq. 4.8 suggests; the rigid slider is disconnected and the pile and soil nodes move independently. At this point, for some soil types, the ultimate static resistance of the soil may be reduced to display a post peak resistance which has been observed for some soils such as dense sand and stiff clay. Reconnection of the pile-soil nodes occurs again when the relative velocity between the pile and soil nodes is equal to zero. The stiffness of the spring K_{nl} is assumed to be linear in the unloading phase.

4.4.1. Solution of Equations of Motion

For single piles and pile groups, the pile and soil displacements are evaluated in the time domain using the linear acceleration assumption and the Newmark β method for direct time integration of the equations of motion. The modified Newton-Raphson iteration scheme is used to derive and solve the governing equilibrium equations [60].

4.5. Bearing Capacity Prediction

For each soil layer, the parameters affecting the behavior of the aforementioned model can be subdivided into two groups. The first group comprises parameters that can be established through experiments; these are undrained shear strength, c_u, angle of internal friction, ϕ, the shear modulus, G_s (which can be correlated with c_u or ϕ empirically), and soil density (which includes the effect of the water table level). The

second group comprises some parameters that cannot be determined in the laboratory, such as the adhesion coefficient, α, the earth pressure coefficient, K_0, and the point resistance coefficient, N_c, for clay and N_q, for sand. These parameters may be chosen within the range recommended in the literature and then adjusted using the comparison with the measured displacement or velocity and analyzing the pile response employing the described model for the given load.

A good match with the measured pile response may be obtained by iteratively adjusting the parameter values of the second group. When a satisfactory match is obtained, the measured values of c_u and ϕ along with the fine tuned parameters for the second group are used to determine the bearing capacity of the pile using Eqs. 3.19 and 3.20.

4.6. Residual Driving Stresses

Installing piles by driving or jacking results in residual stresses along the pile. To incorporate this effect in the proposed model, a series of single blows is applied leading to a state of residual stresses at the end of driving; then, the analysis continues to model the dynamic response to any subsequent loading. The residual stresses often reach a significant level, however, their effect on the dynamic component of the response, particularly to harmonic load, is usually not very strong. Fig. 4.7 shows the residual driving stress distribution along a 20.0 m in length and 0.5 m diameter pile embedded in a homogeneous soil with $G_s = 2 \times 10^7$ N/m^2 and $c_u = 1 \times 10^5$ N/m^2 for the last 4 hammer blows. It may be observed from Fig. 4.7b that residual stresses do not affect the dynamic impedance function of the pile as the stiffness (slope of the hysteretic loop) and the damping (area of the hysteretic loop) are not affected by the inclusion of residual stresses in the analysis.

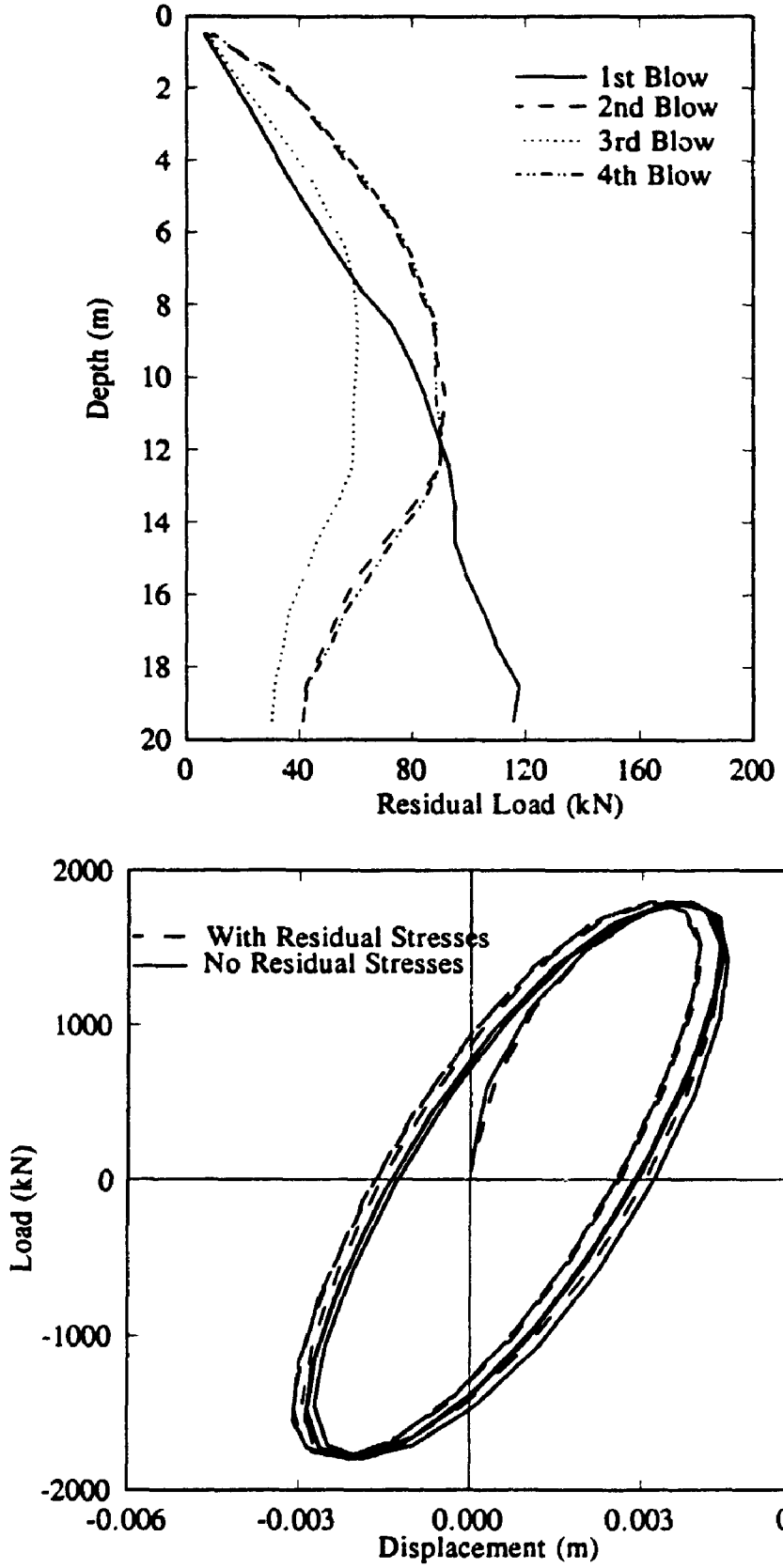

Figure 4.7 Effect of Driving Residual Stresses on the Pile Response to Harmonic Load

4.7. Validation of the Model

The analytical model described is applied to analyze the pile response to different dynamic loads in order to demonstrate the capacities of the approach. These loads represent typical loading conditions, under which piles may be examined. Such loading conditions include the driving process using hammers, Statnamic loading test, and harmonic load applied at the single pile head or to piles in a group.

4.7.1. Pile Driving

A steel pipe of outer diameter 1.68 m and wall thickness 37.5 mm was driven as a part of an offshore oil production platform in Brazil, at the de Pargo 1A site. This site consists of a 13.0 m layer of fine silty sand to quartz sand whose angle of internal friction $\phi = 34^0$, underlain by a 90.0 m layer of calcareous sand mixed with marine deposits with angle of internal friction ϕ, varying from 26^0 to 33^0. Force-time histories were measured at the pile head. Further soil, pile and hammer details can be found in Danziger [72], where the driving records are also available. Two hammer blows at two different embedment depths are analyzed, one for a 33.0 m embedded pile and the other for a 44.5 m embedded pile. Fig. 4.8 shows the computed velocity at the pile head as compared to the measured velocity time history for the two cases. The computed velocities agree very well with the measured ones in the first 0.05 s of the records, the most important part. The peak displacement at the pile head was computed for each blow as 19.1 mm and 38.5 mm respectively. The measured values for the displacement are 19.8 and 39.0 respectively. Pile capacities at both depths were calculated as 11.2 MN and 26.4 MN; the measured capacity at the 44.5 m embedment is 26.0 MN. A few other piles on the same site were also analyzed and equally favorable agreement was obtained in all cases.

This shows the applicability of the approach to the pile driving analysis and the determination of the bearing capacity of piles using either the proposed approach or the

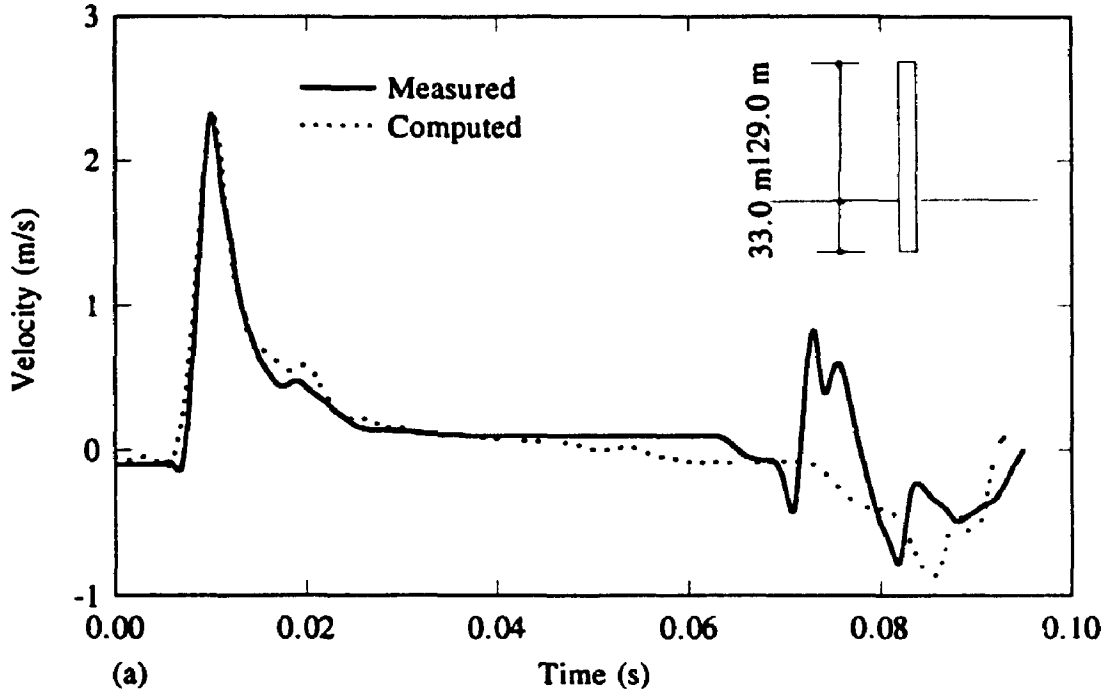

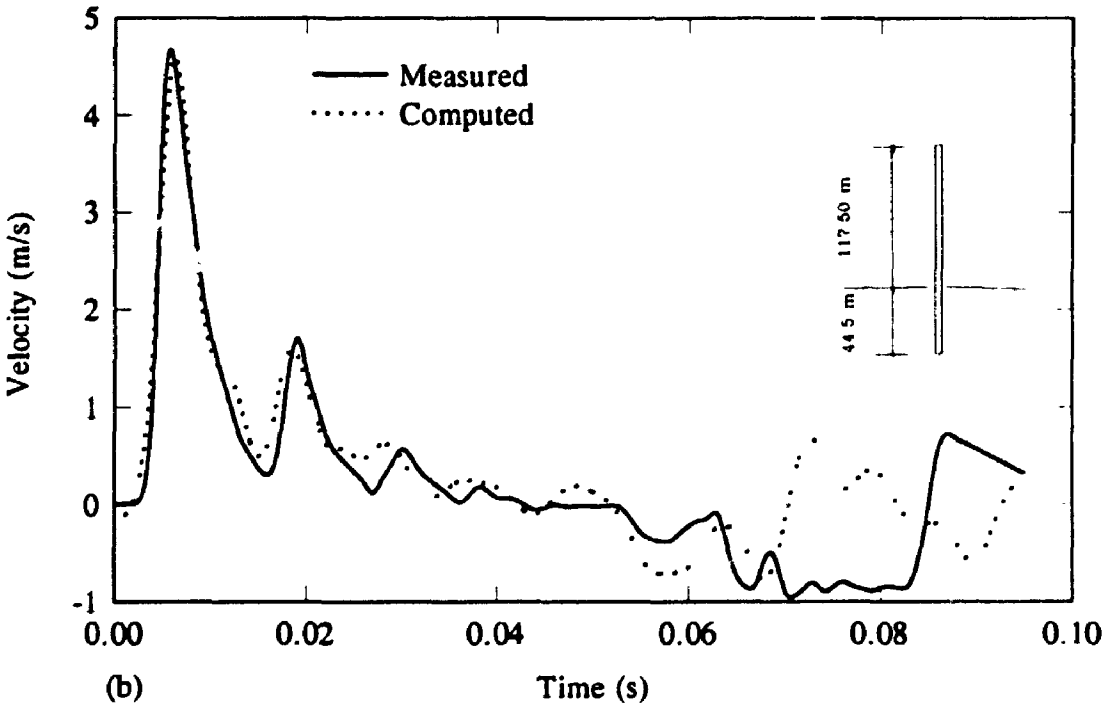

Figure 4.8 Velocity-Time History of Pile A1, de Pargo Site, Brazil: (a) Signal A13300 (b) Signal A14450 [Pile Driving Data from Danziger (1991)]

Case Western University Method which requires the first peak values for both pile head force and velocity.

4.7.2. Statnamic Pile Testing

Some of the Statnamic loading tests are reanalyzed using the developed nonlinear model, namely the piles on the Riverside campus at the Texas A&M University. Fig. 4.9a shows an example of both the measured and calculated displacement-time curves. Fig. 4.9b displays the quasi static load-displacement curve, obtained by plotting only the static component of the soil reactions versus the displacements, and its comparison with the measured data. The agreement is satisfactory. Pile capacities predicted using the proposed dynamic analysis and Eqs. 3.19 and 3.20 are 1.8, 4.4 and 3.1 MN; the measured capacities are 1.62, 4.05 and 3.06 MN for piles number 2, 4 and 7, respectively.

4.7.3. Harmonic Loading

The proposed approach was used to analyze some of the harmonic axial loading tests conducted on a 273 mm diameter steel pipe pile driven 13.4 m into a layered deposit of overconsolidated clay. A linear inertial mass vibrator was used to produce harmonic loading. Further details may be found in Muster et al. [73]. Fig. 4.10 shows the calculated and measured vertical displacements per unit load applied to the pile cap (vertical flexibility) as functions of frequency. The calculated resonance frequency and amplitude for the system agree quite well with the measured values as may be seen from Fig. 4.10. The slight irregularities of the theoretical curve result from nonlinearity, which results from the soil-pile interface failure in the topmost soil layers even at small load amplitudes.

To further illustrate the capacities of the model, a harmonic load is applied at the head of a pile 0.4 m in diameter and 20.0 m in length fully embedded in homogeneous

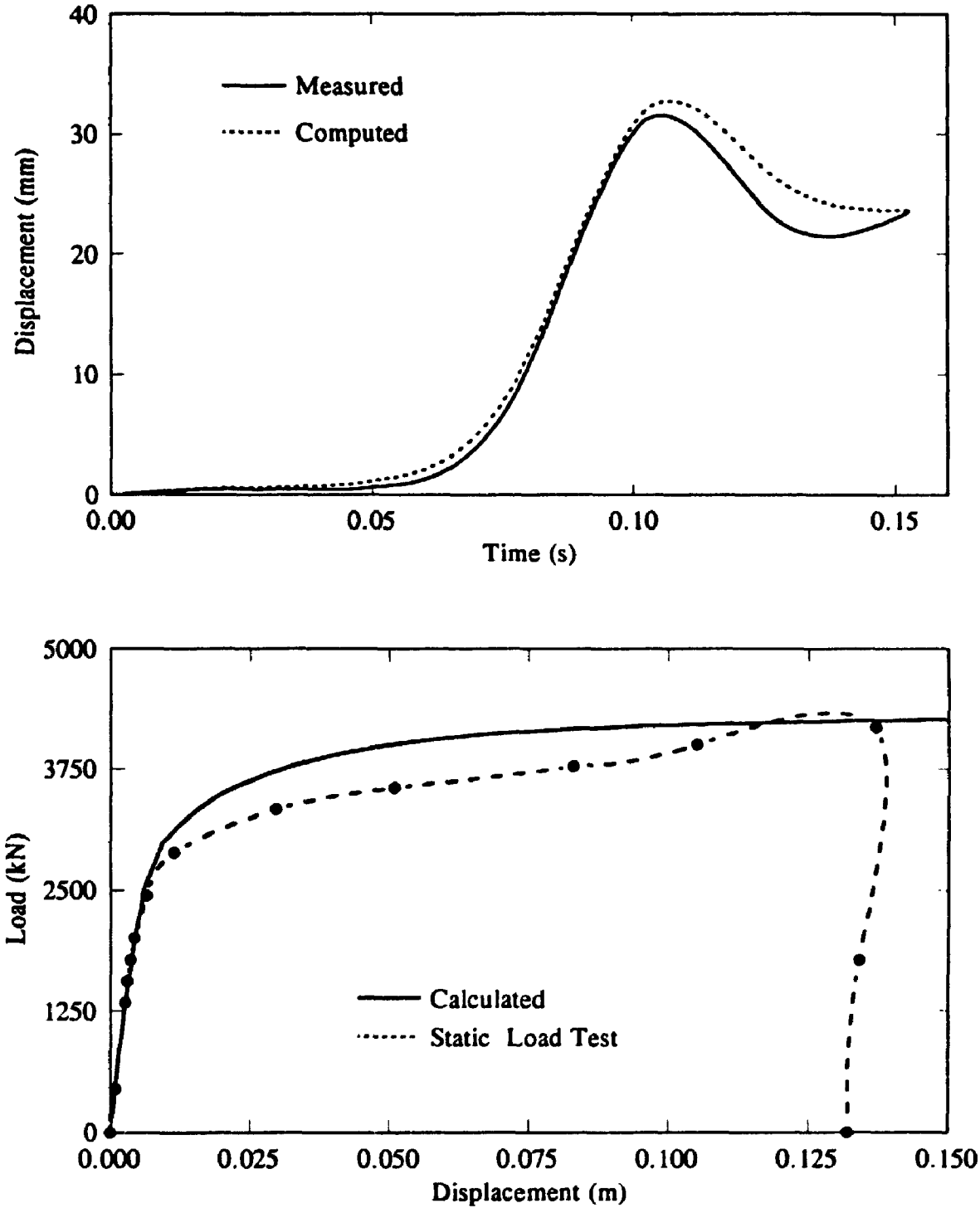

Figure 4.9 Response Curves for Pile 4 on Texas A&M University Site: (a) Displacement -Time History; (b) Load-Displacement Curve (Measured Data from M. Janes, Berminghammer Inc.)

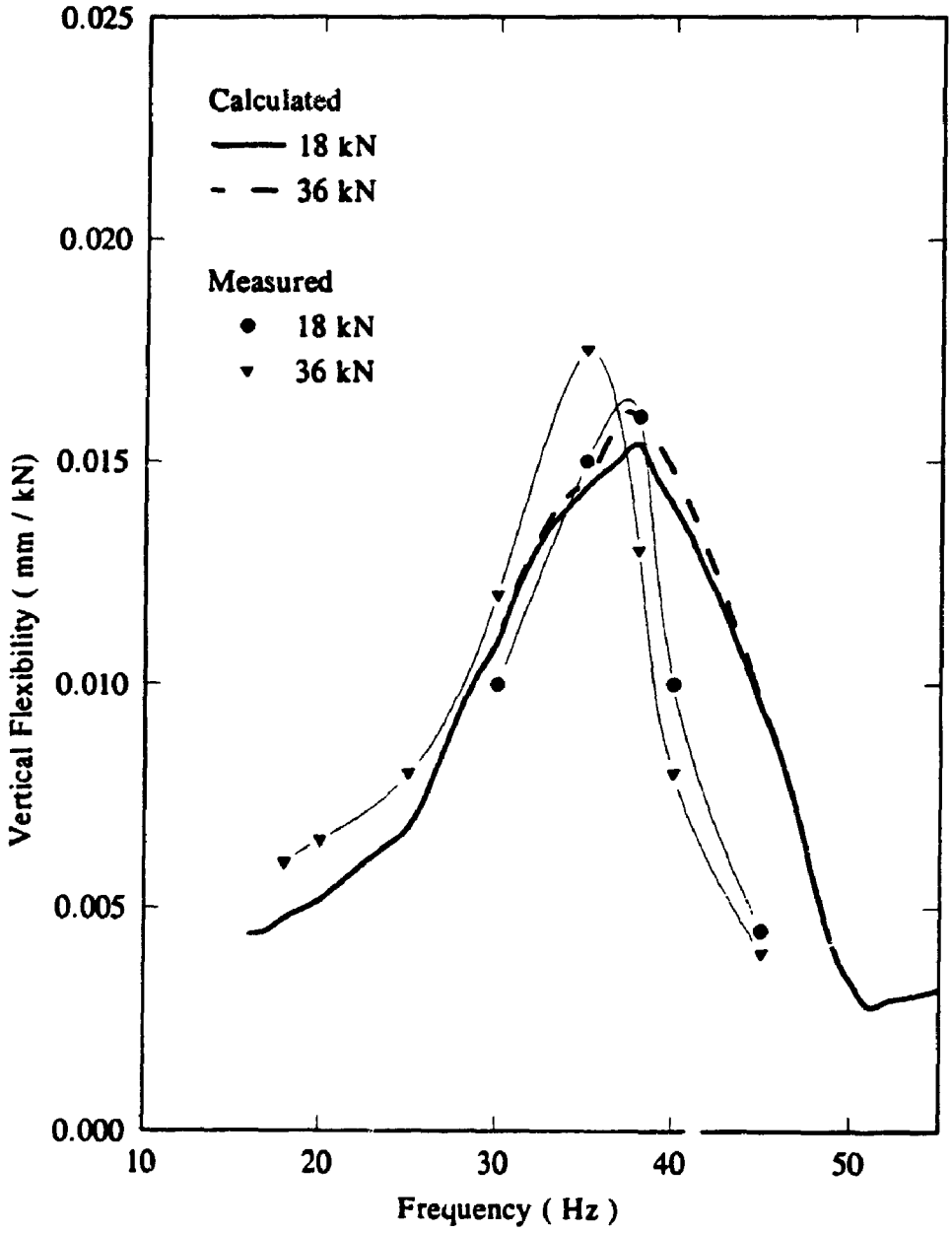

Figure 4.10 Measured and Computed Vertical Flexibilies [Experimental Data of Muster et al. (1986)]

clayey soil whose undrained shear strength C_u = 100.0 kPa and shear modulus G_s = 20.0 MPa. The pile is first loaded as a single pile and then as a pile in a group of two or three identical piles, 2.0, 3.0, and 5.0 diameters apart, with only one of them loaded. Fig. 4.11a presents a hysteretic loop generated by a cyclic load of constant amplitude. It may be observed that the nonlinear behavior is more pronounced for the higher load levels. Fig. 4.11b shows three hysteretic loops generated by cyclic loads of different peak amplitudes. It may be seen that as the load level increases the energy dissipation, manifested by the area of the hysteretic loop, increases and the equivalent stiffness decreases. Fig. 4.12 shows the displacement time histories of a single pile and of two identical piles in a group with two different spacing to diameter ratios, s/d, with only one of them loaded. It may be observed from Fig. 4.12 that the presence of the load-free pile near the loaded one increases the apparent pile resistance and reduces the pile displacement. These effects are more pronounced for closer piles. Accordingly, the pile velocity may be affected and thus also the prediction of the pile bearing capacity using the Case Western Method. Fig. 4.13 shows nonlinear response curves of the same pile, but with an added mass on top of it taken as 1000 times the pile mass needed to reduce the damping ratio. The variation of the resonance frequency with the load level, and, accordingly, the nonlinearity, may be noticed. Also, more than one response peak occurs as the load level increases.

4.8. Approximate Nonlinear Analysis for Pile Group Response

The proposed analytical model may be applied to analyze the response of the entire pile group, accounting directly for the nonlinearity and the interaction between all piles at the same time. An alternative approach is to solve just two piles at a time, with the results to be superimposed to assemble the global flexibility matrix of the entire group. The second approach, which is developed by Poulos [74] for the static analysis of pile groups and then extended by Kaynia and Kausel [11] to dynamic analysis, may

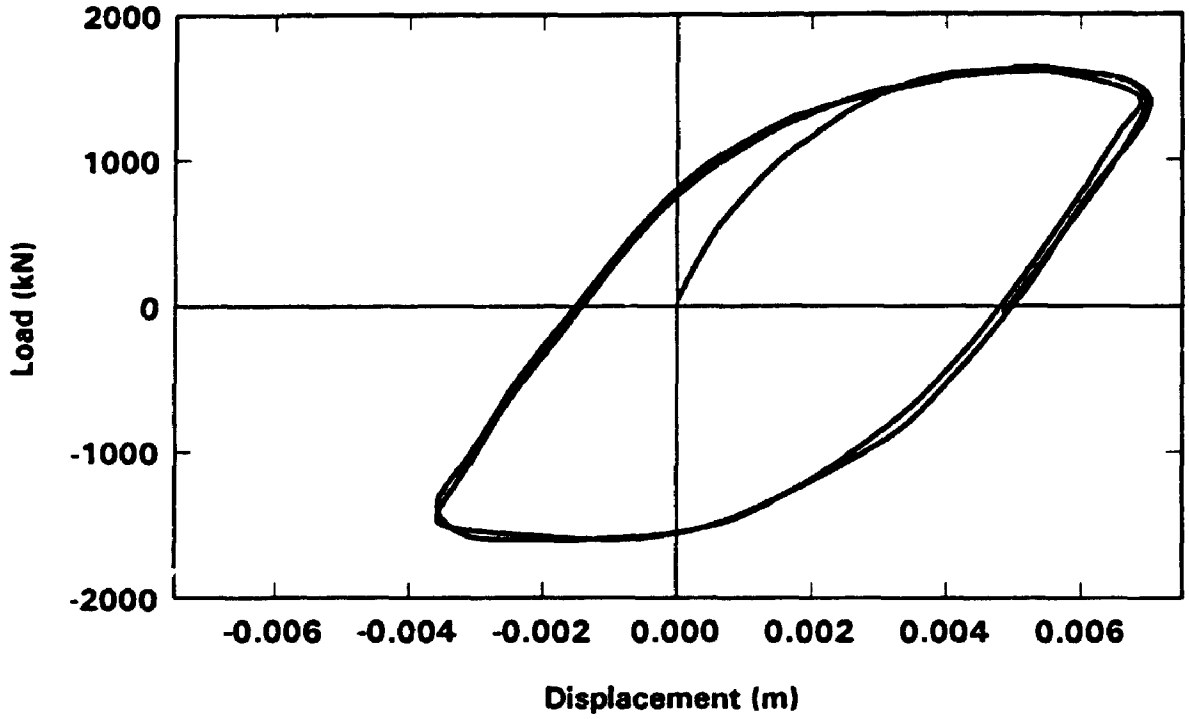

Figure 4.11a Hysteretic Loop for Pile Undregoing Harmonic Vibration Employing Proposed Nonlinear Model

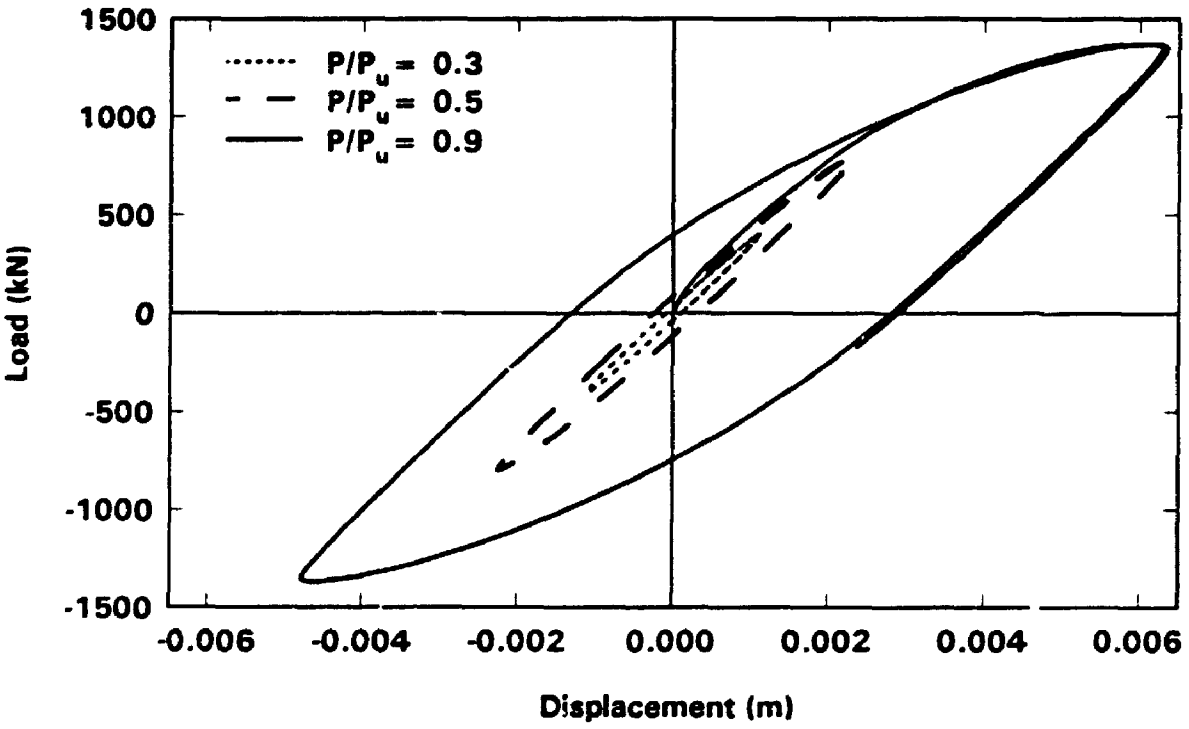

Figure 4.11b Hysteretic Loops Generated by Cyclic Loads of Differennt Amplitudes as Ratios of Pile Capacity

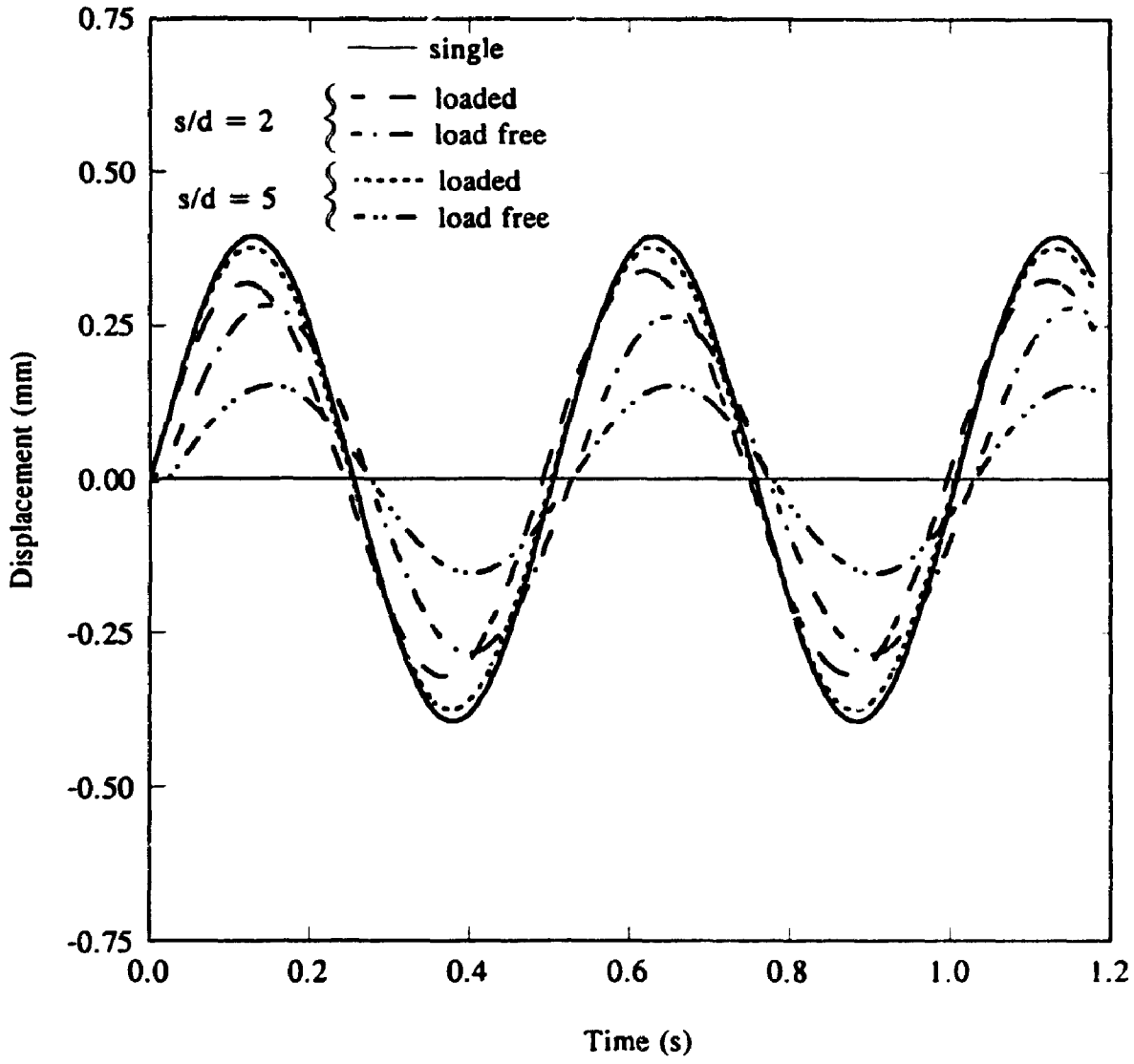

Figure 4.12 Comparison between Response Time Histories of Single Pile and Group of 2 Identical Piles with Only One of Them Loaded

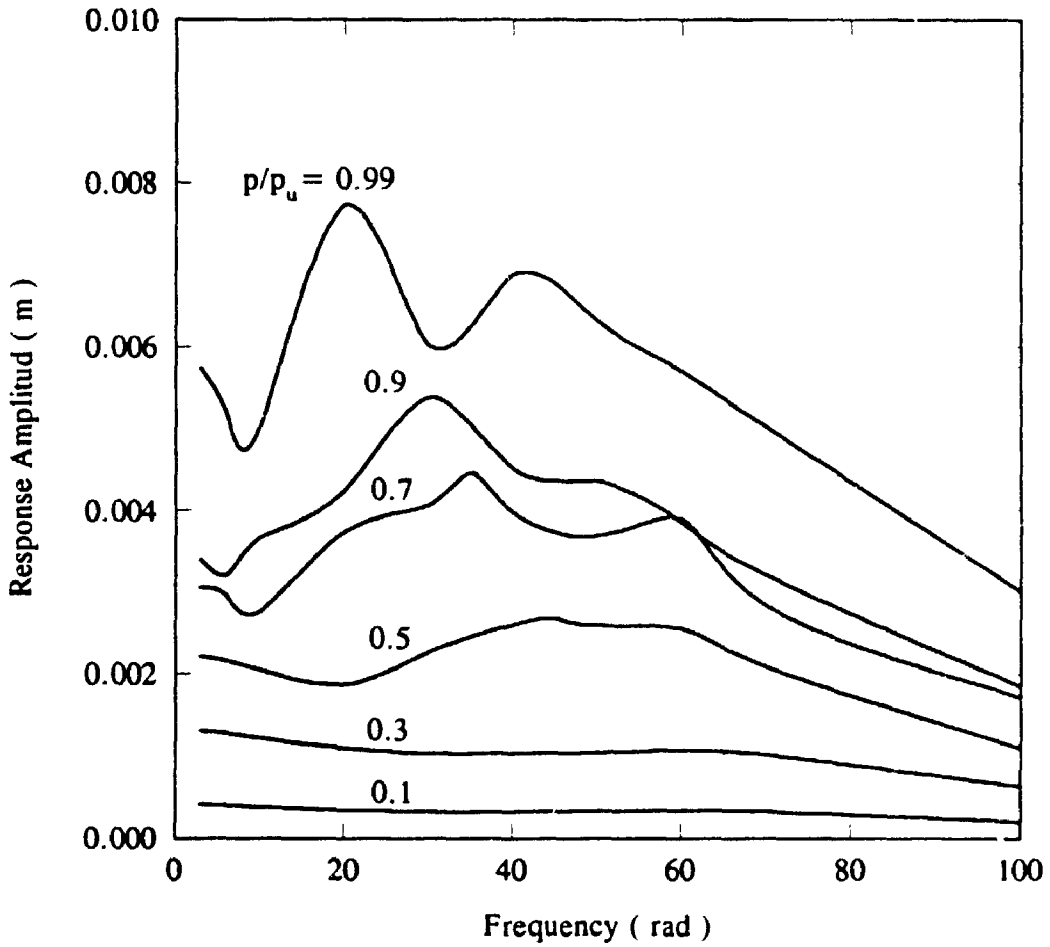

Figure 4.13 Nonlinear Pile Response Curve Versus Frequency for Pile Loaded by Harmonic Load with Different Intensities

be very advantageous if it is implemented in conjunction with pile-soil-pile interaction factors, along with single pile solutions. To approximately account for group nonlinearity in the analysis, the equivalent linear single pile parameters as well as interaction factors have to be established depending on the P/P_U ratio, where P_U is the ultimate bearing capacity of the pile defined by Eqs. 3.19 and 3.20.

4.8.1. Single Piles

The stiffness and damping parameters of a single pile are required, in conjunction with the interaction factors, for the application of the superposition method to pile groups. Data on the single pile parameters are available in the literature for linear elastic conditions only. In figures that follow, P is the amplitude of the dynamic load assumed to be harmonic and P_U is the pile ultimate capacity.

The charts given here show the variation of the equivalent linear stiffness and damping parameters F_1 and F_2 with the loading ratio P/P_U. The stiffness is approximated by the slope of the backbone of the hysteretic loop and the damping is approximated by its area. Utilizing the dimensionless parameters F_1 and F_2, the equivalent linear stiffness and damping of a single pile may be computed as

$$K = \frac{E_P A}{R} F_1$$

$$C = \frac{E_P A}{V_s} F_2 \qquad (4.31)$$

where E_P is the pile Young's modulus, R and A are its radius and cross sectional area, respectively and V_s is the initial shear wave velocity of the soil.

Fig. 4.14 shows the parameters F_1 and F_2 for floating piles in a homogeneous soil medium with pile to soil initial stiffness ratio, E_P/G_s, equal to 1500 and a range of slenderness ratios L/d, where L and d are the pile length and diameter, respectively. It may be noticed from Fig. 4.14 that F_1 decreases as the loading ratio increases while

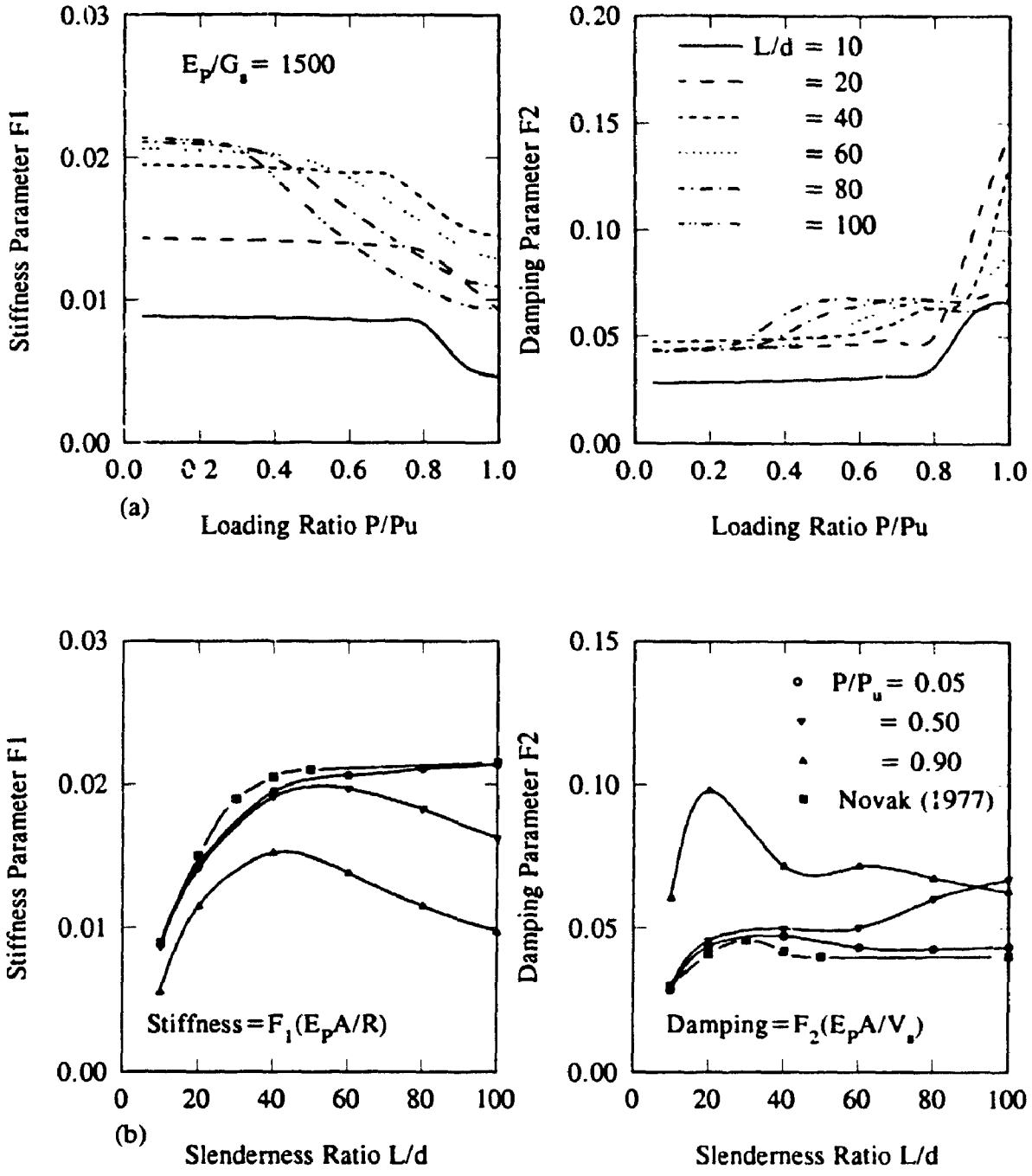

Figure 4.14 Stiffness and Damping Parameters of Vertical Response for Floating Single Piles in Homogeneous Half-Space (E_p/ G_s = 1500)

F_2 increases, especially for higher L/d ratios. In Fig. 4.14b, F_1 and F_2 are plotted versus L/d for three loading ratios and the results are compared with those given by Novak [19], who used a more rigorous frequency domain solution. For $P/P_U = 0.05$, where the conditions are almost linear, a good agreement with Novak's results may be noticed. For $P/P_U = 0.5$, the effect of nonlinearity becomes pronounced only for the L/d ratio exceeding 40, a typical value in many applications (eg. for offshore piles). As P/P_U approaches 0.9 a dramatic change is observed in Fig. 4.14 for all L/d ratios. This change is very important for the limit state analysis of both the foundation and the supported structure. Fig. 4.15 shows F_1 and F_2 for E_p/G_s equal to 300 corresponding to softer piles or stiffer soils. It may be noticed from this figure that the nonlinearity effect is stronger and that F_1 and F_2 change dramatically even for $P/P_U = 0.5$. Figs. 4.16 and 4.17 present F_1 and F_2 for end bearing piles in homogeneous soil. As expected, the nonlinearity effect is less pronounced than in the case of floating piles, especially for shorter piles. Figs. 4.18 to 4.21 show F_1 and F_2 for parabolic soil medium. From these figures, it may be observed that the nonlinearity effect is slightly less for the parabolic profile than for homogeneous soil.

4.8.2. Interaction Factors

To facilitate an approximate nonlinear dynamic analysis of pile groups, equivalent linear interaction factors are established and presented here for a range of soil and pile parameters.

The equivalent linear interaction factor may be defined in two different ways. First, the displacement of a load-free pile is normalized by the displacement of the loaded contiguous pile when no other piles are present. This definition has its merits especially for strictly linear analysis. Second, the interaction factor can be defined as the difference between the displacement of a pile in a group of two equally loaded piles and the displacement of an equally loaded single pile, normalized by the displacement of the

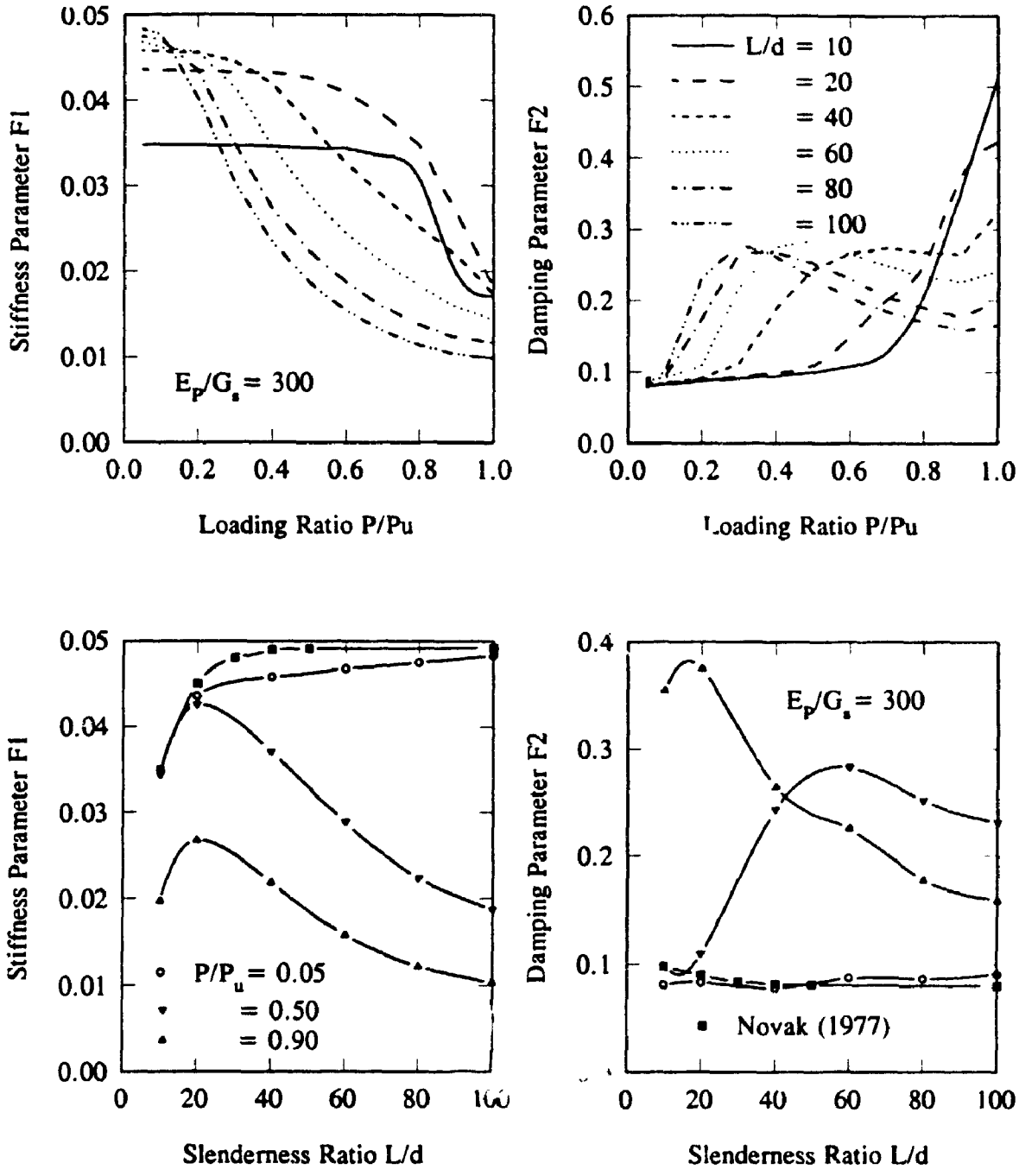

Figure 4.15 Stiffness and Damping Parameters of Vertical Response for Floating Silngle Piles in Homogeneous Half-Space (E_p/G_s = 300)

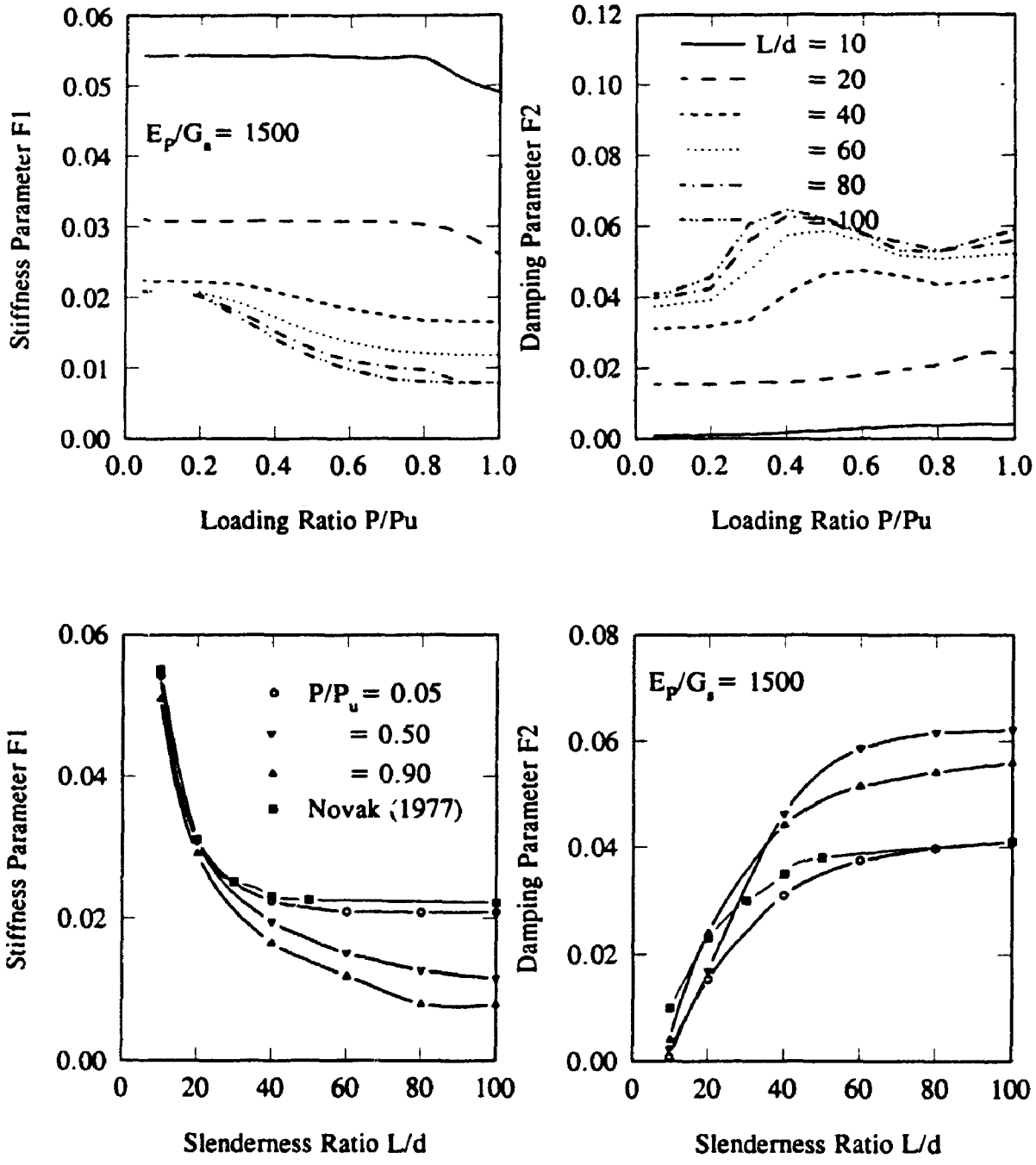

Figure 4.16 Stiffness and Damping Parameters of Vertical Response for End-Bearing Single Piles in Homogeneous Soil (E_p/G_s = 1500)

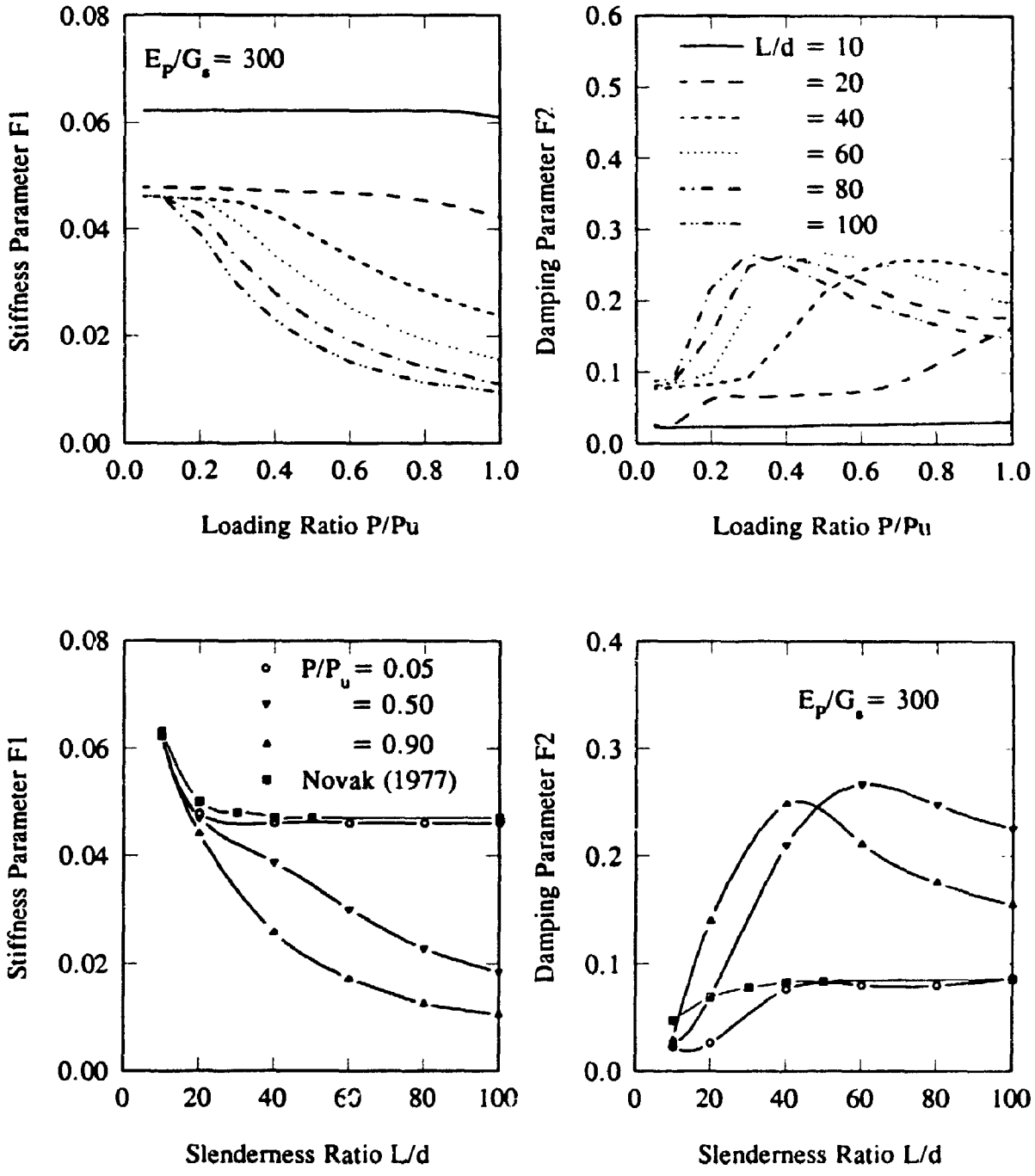

Figure 4.17 Stiffness and Damping Parameters of Vertical Response for End-Bearing Single Piles in Homogeneous Soil (E_p/G_s = 300)

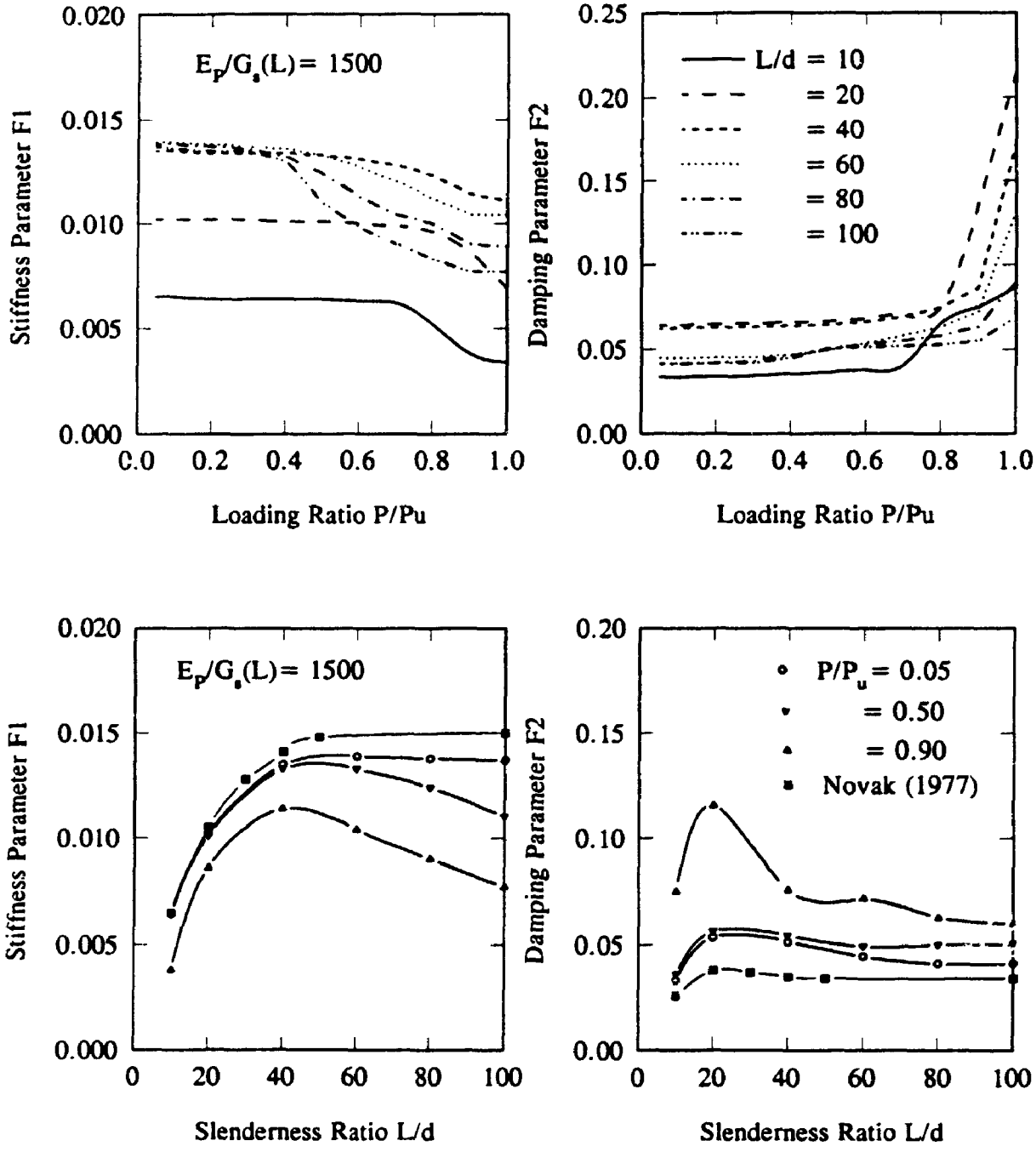

Figure 4.18 Stiffness and Damping Parameters of Vertical Response for Floating Single Piles in Parabolic Soil ($E_p/G_s(L) = 1500$)

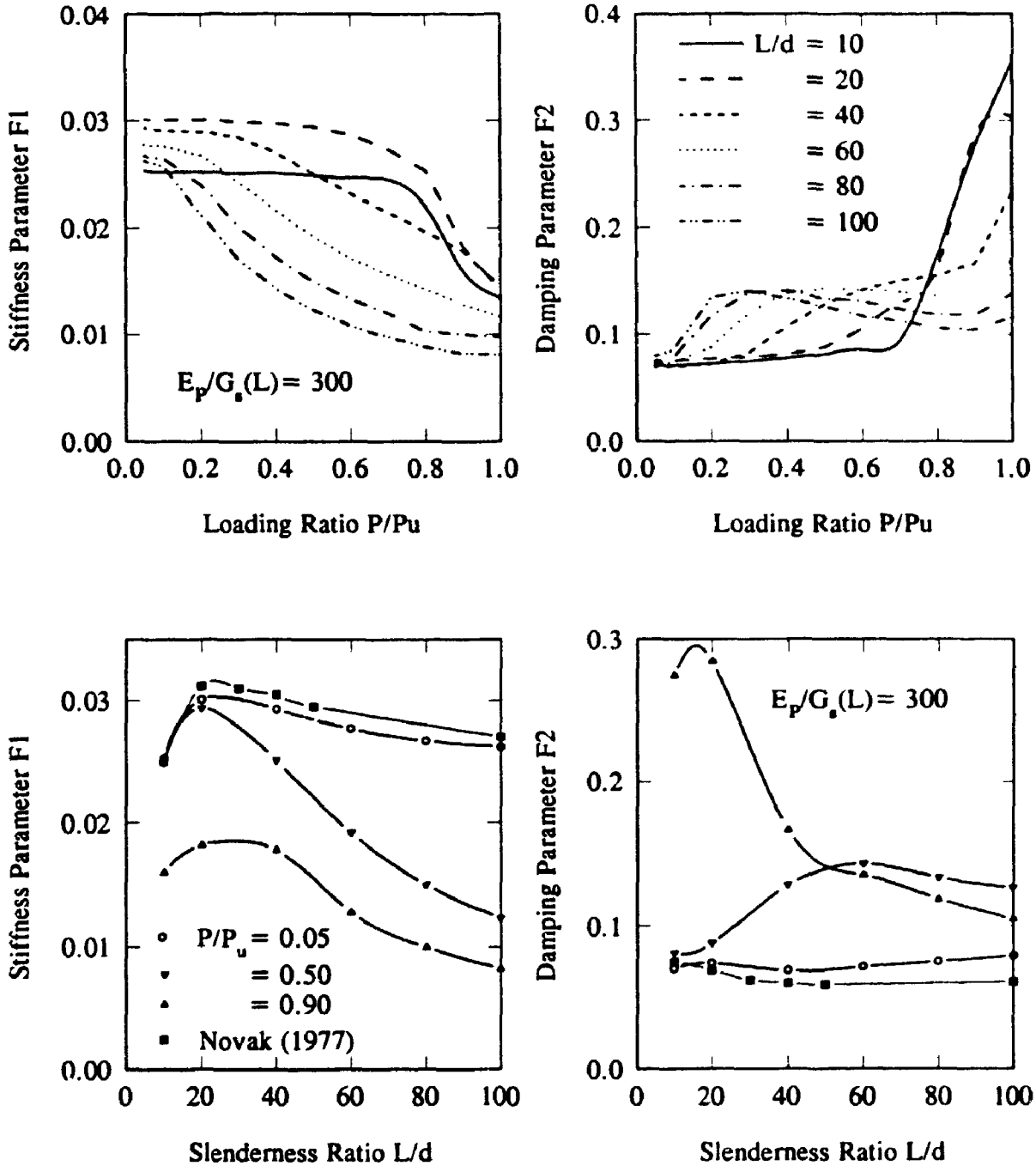

Figure 4.19 Stiffness and Damping Parameters of Vertical Response for Floating Single Piles in Parabolic Soil ($E_p/G_s = 300$)

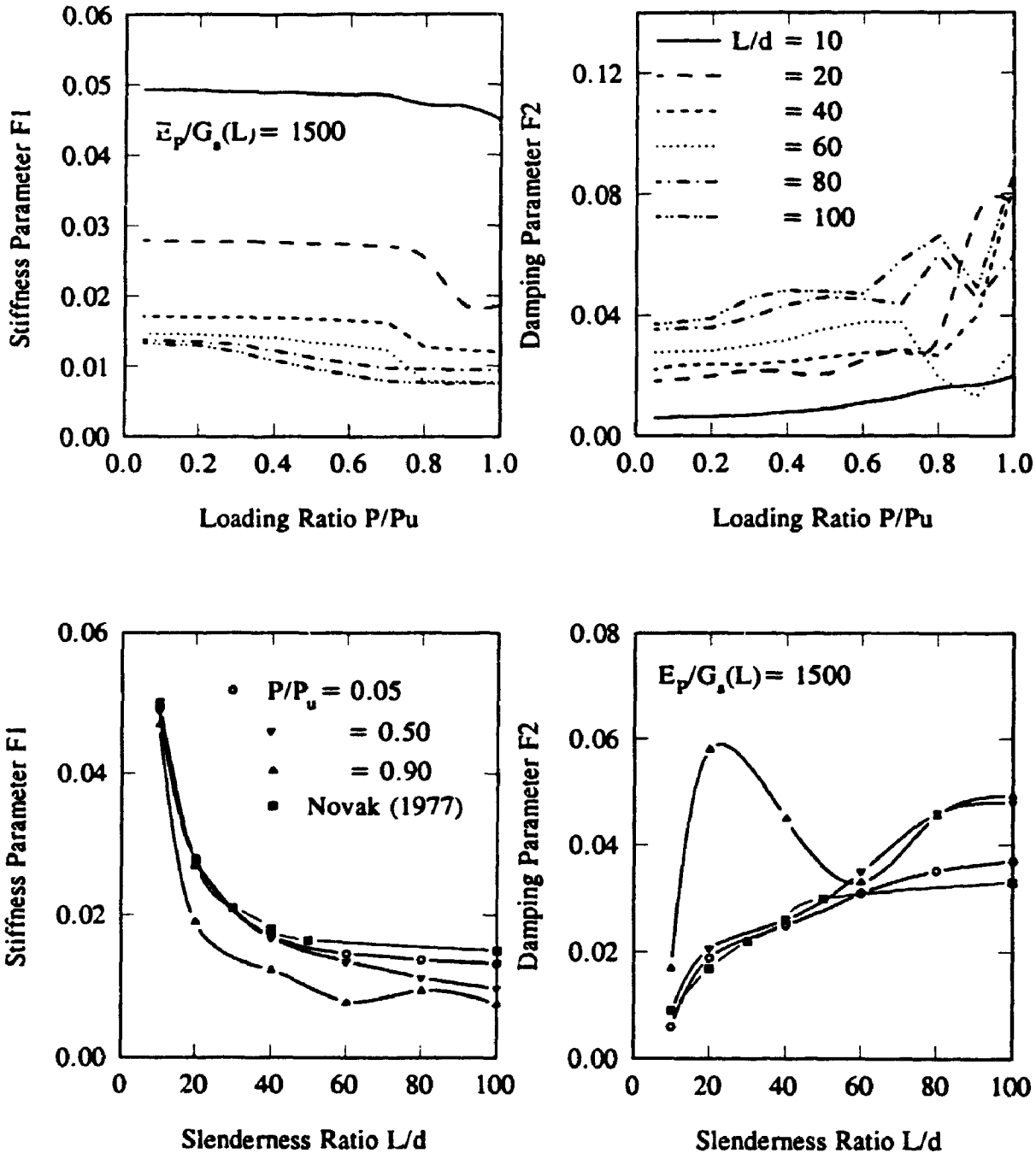

Figure 4.20 Stiffness and Damping Parameters of Vertical Response for End-Bearing Single Piles in Parabolic Soil (E_p/G_s = 1500)

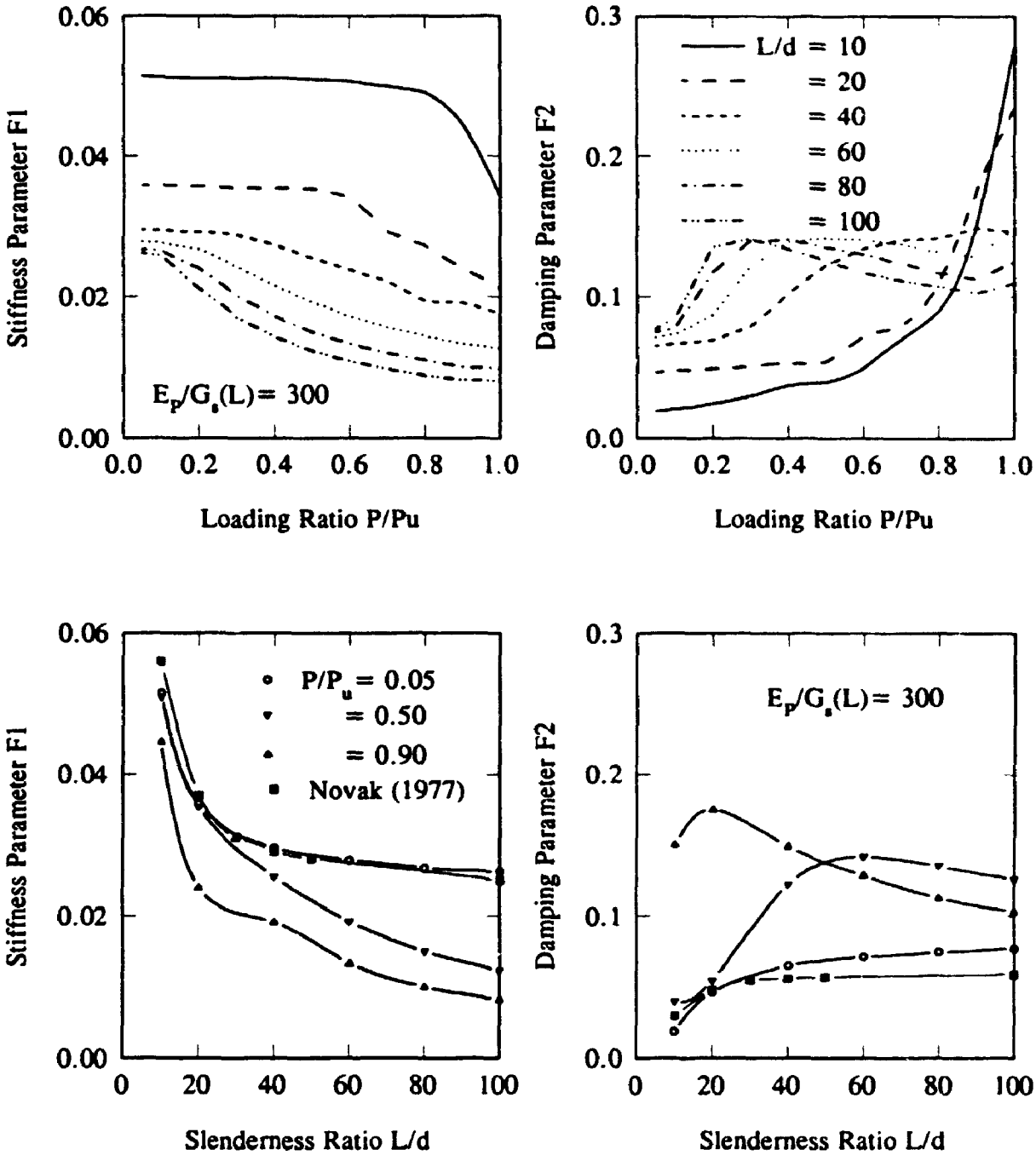

Figure 4.21 Stiffness and Damping Parameters of Vertical Response for End-Bearing Single Piles in Parabolic Soil (E_p/G_s = 300)

single pile. The advantage of this definition is that the nonlinearity is accounted for at both piles. However, the difference between the interaction factors computed using the two methods was found to be insignificant for loading ratios P/P_U less than about 0.8. To establish the equivalent linear interaction factors, three loading cases are considered in the analysis separately: a pile loaded individually, a group of two identical piles with only one of them loaded and finally both piles in the group are loaded. The resulting displacement at the pile head is

$$w_m(t) = |w_m| e^{i\phi_m} \tag{4.32}$$

where $|w_m|$ is the amplitude, approximated by the peak displacement, and ϕ_m is the phase shift, approximated by the time lag between the peaks of both the displacement and load. The subscript m takes values 0, 1 and 2 for the three loading cases, respectively. The loading starts from zero and the amplitude and phase shift are established after 5 loading cycles, as the response was found to stabilize almost completely after this number of cycles. According to the first definition, the interaction factor is

$$\alpha = \frac{w_1(t)}{w_0(t)} \tag{4.33}$$

and according to the second definition, the interaction factor is

$$\alpha = \frac{u_2(t) - u_0(t)}{u_0(t)} \tag{4.34}$$

The dynamic interaction factor is a complex quantity which can be described either by its real and imaginary parts α_1 and α_2 or in terms of its absolute value, $|\alpha|$, and phase shift, ϕ. Thus the interaction factor, α, may be written as

$$\alpha = \alpha_1 + i\,\alpha_2 = |\alpha| e^{i\phi} \tag{4.35}$$

The amplitude, $|\alpha|$, and the phase shift, ϕ, of the interaction factor resulting from Eq.

4.33 may be approximated by

$$|\alpha| = \frac{|w_1|}{|w_0|} \qquad (4.36)$$

$$\phi = \phi_1 - \phi_0$$

adopting the approach given by Eq. 4.34, the real and imaginary parts, α_1 and α_2 may be approximated by

$$\alpha_1 = \frac{|w_2|}{|w_0|}\cos(\phi_2 - \phi_0) - 1.0 \qquad (4.37)$$

$$\alpha_2 = \frac{|w_2|}{|w_0|}\sin(\phi_2 - \phi_0)$$

in the above relations

$$|\alpha| = \sqrt{\alpha_1^2 + \alpha_2^2} \qquad (4.38)$$

$$\phi = \tan^{-1}\left(\frac{\alpha_2}{\alpha_1}\right)$$

The equivalent linear dynamic interaction factors described by Eqs. 4.37 and 4.38, are plotted for a range of soil and pile parameters in Figs. 4.22-4.29. Fig. 4.22 shows the interaction factors for a pile embedded in homogeneous soil with L/d=20, for different pile to pile spacing to diameter ratios, s/d, different pile to soil initial stiffness ratios, E_p/E_s, and different dimensionless frequencies $a_0=\omega r_0/V_s$ where ω is circular frequency. It may be observed from these figures that a moderate decrease occurs in the amplitude as P/P_U starts increasing, but as P/P_U exceeds 0.7, a dramatic decrease occurs especially for the lower frequency range. As for the phase shift, it may be considered almost constant except for some oscillations. Figs. 4.23 and 4.24 display the interaction factors for L/d=60 and 100, respectively. It may be observed from these figures that the decrease in the amplitude starts from lower P/P_U ratios in this case, especially for

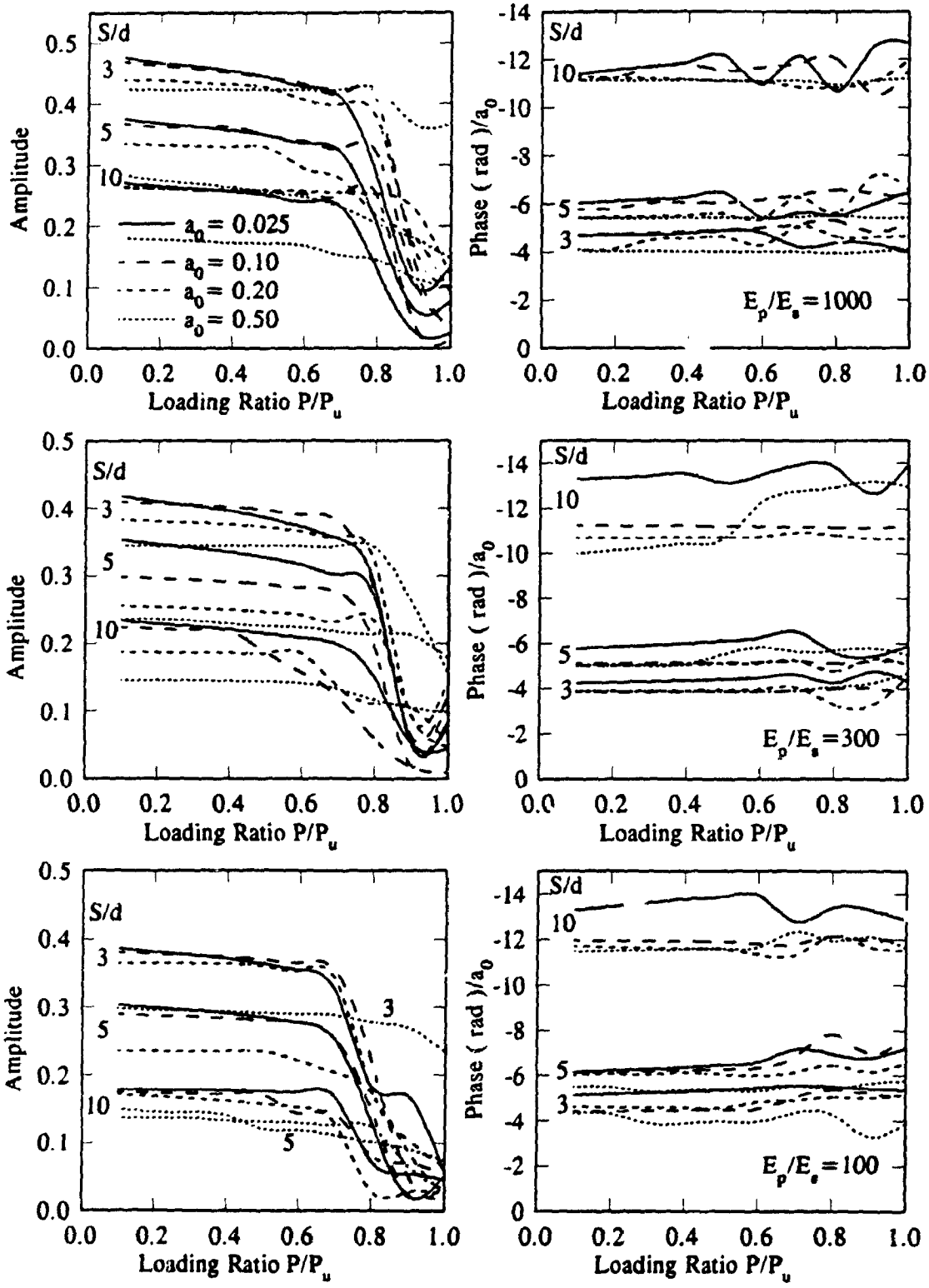

Figure 4.22 Vertical Dynamic Interaction Factors for Approximate Nonlinear Analysis for Floating Piles in Homogeneous Soil (L/d = 20, E_p/E_s = 100, 300, 1000)

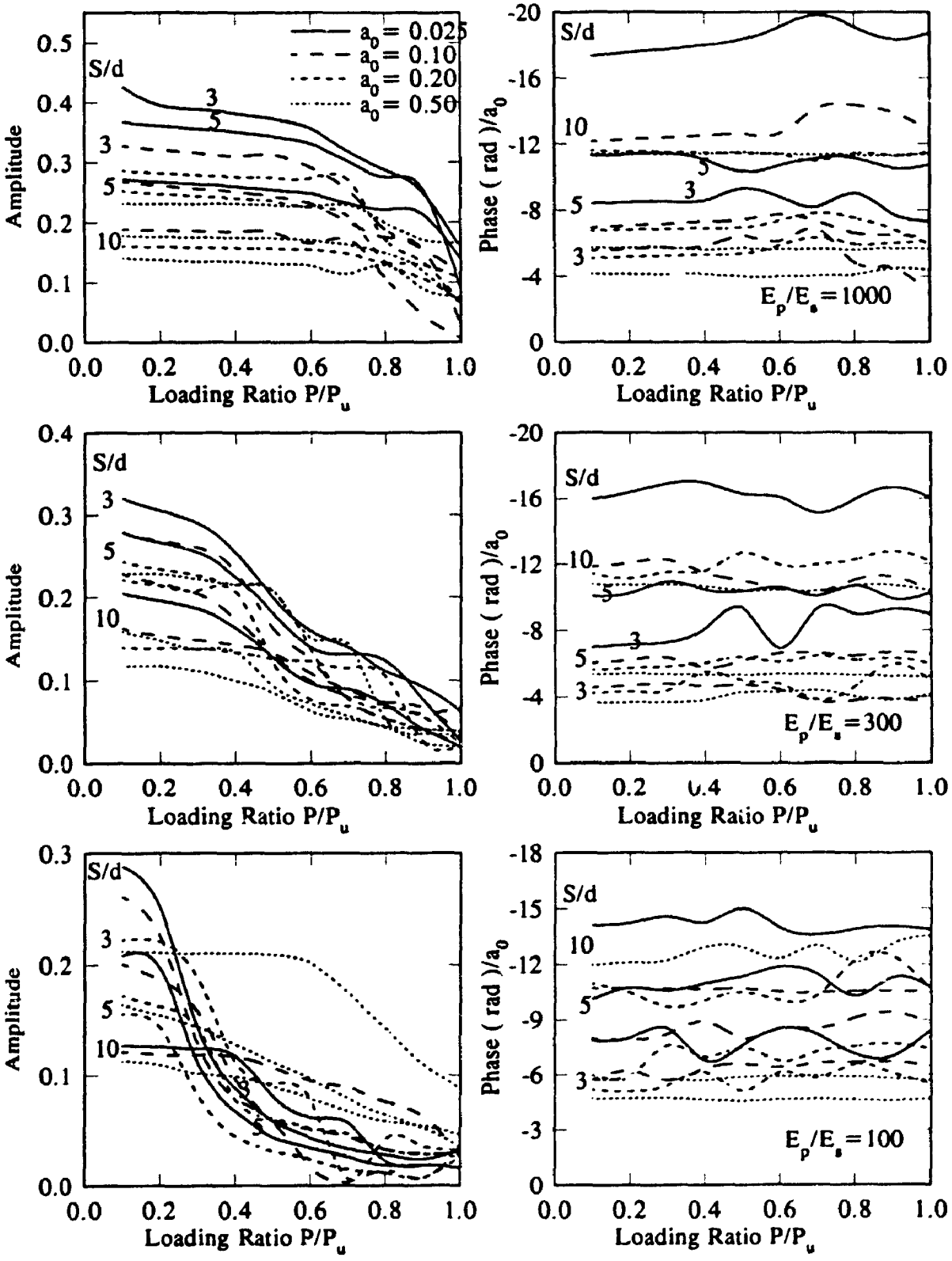

Figure 4.23 Vertical Dynamic Interaction Factors for Approximate Nonlinear Analysis for Floating Piles in Homogeneous Soil (L/d = 60, E_p/E_s = 100, 300, 1000)

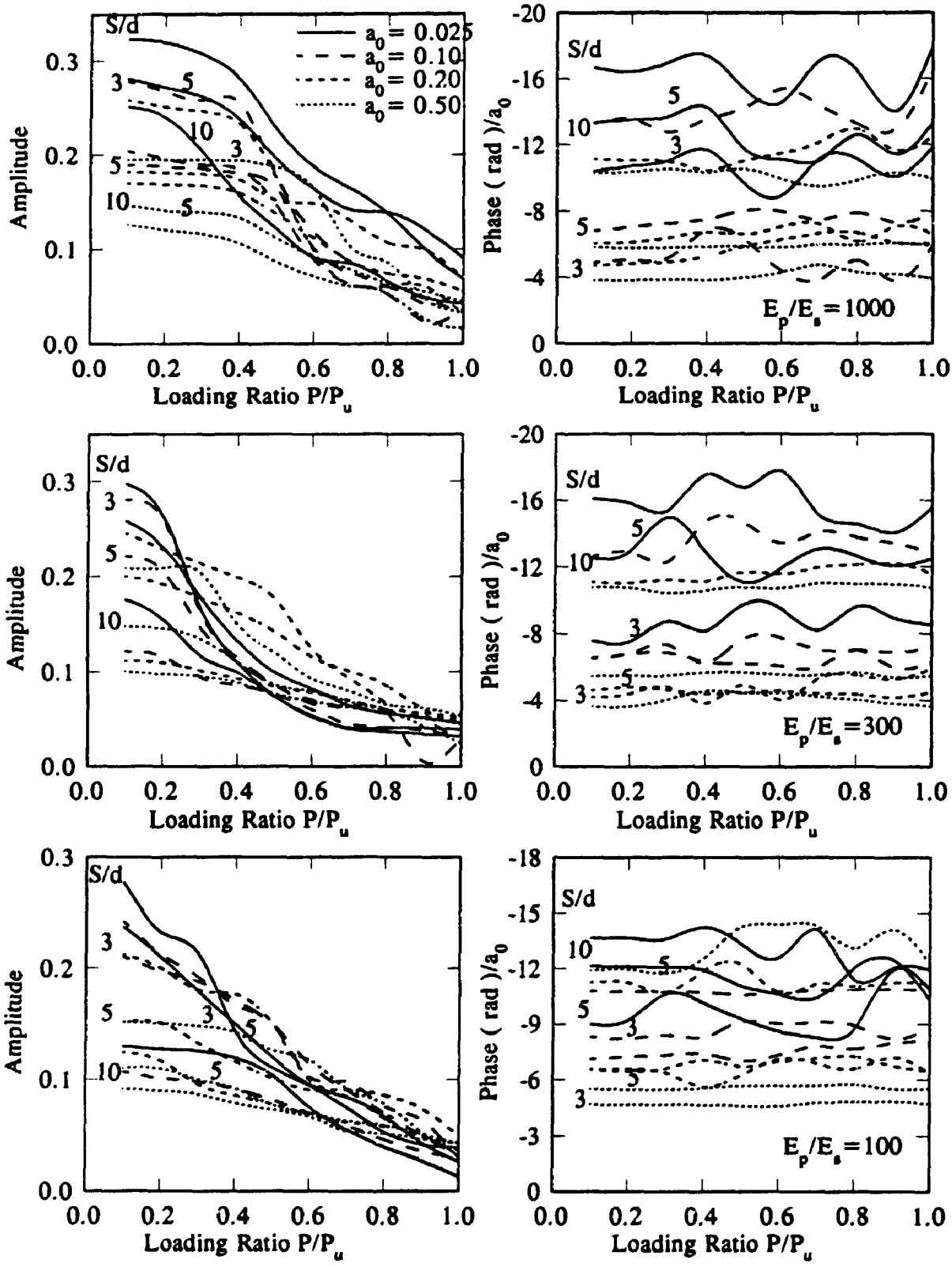

Figure 4.24 Vertical Dynamic Interaction Factors for Approximate Nonlinear Analysis for Floating Piles in Homogeneous Soil (L/d = 100, E_p/E_s = 100, 300, 1000)

stiffer soils, furthermore, the oscillations in the phase shift are more pronounced; nevertheless it may still be considered constant.

Figs. 4.25-4.27 present the equivalent linear interaction factors for parabolic soil profiles. These figures show that the same nonlinearity effects take place in the parabolic soil medium but to a lesser degree compared to the homogeneous case.

Figs. 4.28 and 4.29 show the variation of the interaction factors with a_0 for L/d=40 for homogeneous and parabolic soil media, respectively. For comparison, the results obtained by El-Marsafawi et al [75], using a more rigorous frequency domain BEM solution are also plotted. The agreement between the two results is good for P/P_U=0.1, a nearly linear case. It may also be noticed that the nonlinearity effect on the phase shift is quite negligible.

These observations suggest that the amplitude of the interaction factors may be reduced according to the given charts when large strains are encountered, while the phase shifts may be taken as equal to those available for linear conditions.

4.8.3. Examples

To evaluate the performance of the superposition method and to compare it with the more accurate direct analysis approach, two example problems are solved using both approaches. The pile group configuration used as a test case is a 2×2 group of four piles with s/d=5 and 10 where s is the center to center spacing between the nearest two piles. The complex stiffness, K_G, of a pile group connected by a rigid cap may be expressed as

$$K_G = k_G + i\,\omega\,c_G = k_G + i\,a_0\,\overline{c_G} \qquad (4.39)$$

where k_G is the stiffness, c_G is the constant of equivalent viscous damping, i is the imaginary unit and $\overline{c_G} = \frac{c_G V_s}{d}$, for a parabolic soil V_s is replaced by $V_s(L)$.

The stiffness and damping of the 2×2 pile group embedded in homogeneous soil

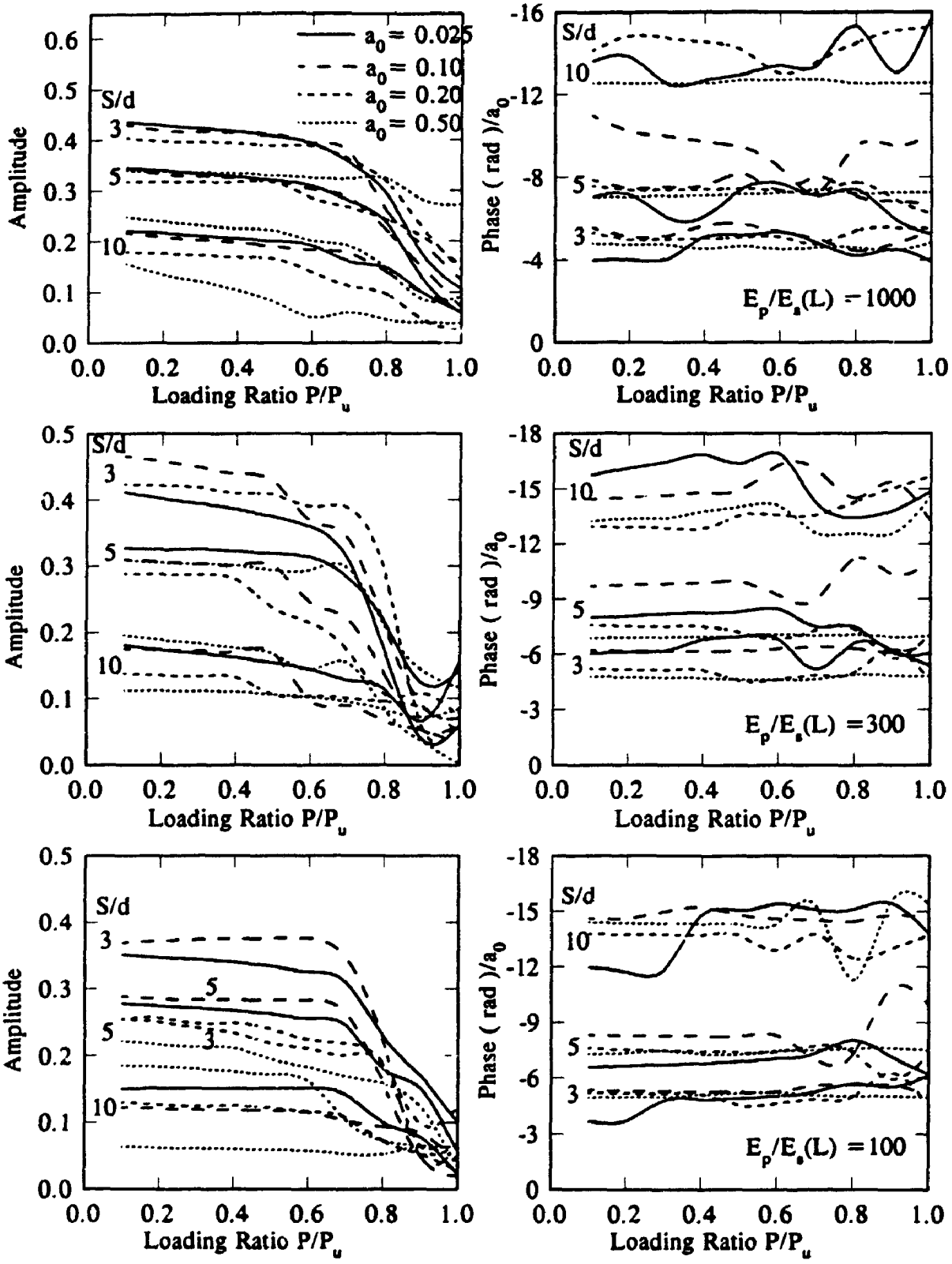

Figure 4.25 Vertical Dynamic Interaction Factors for Approximate Nonlinear Analysis for Floating Piles in Parabolics Soil (L/d = 20, $E/E_s(L)$ = 100, 300, 1000)

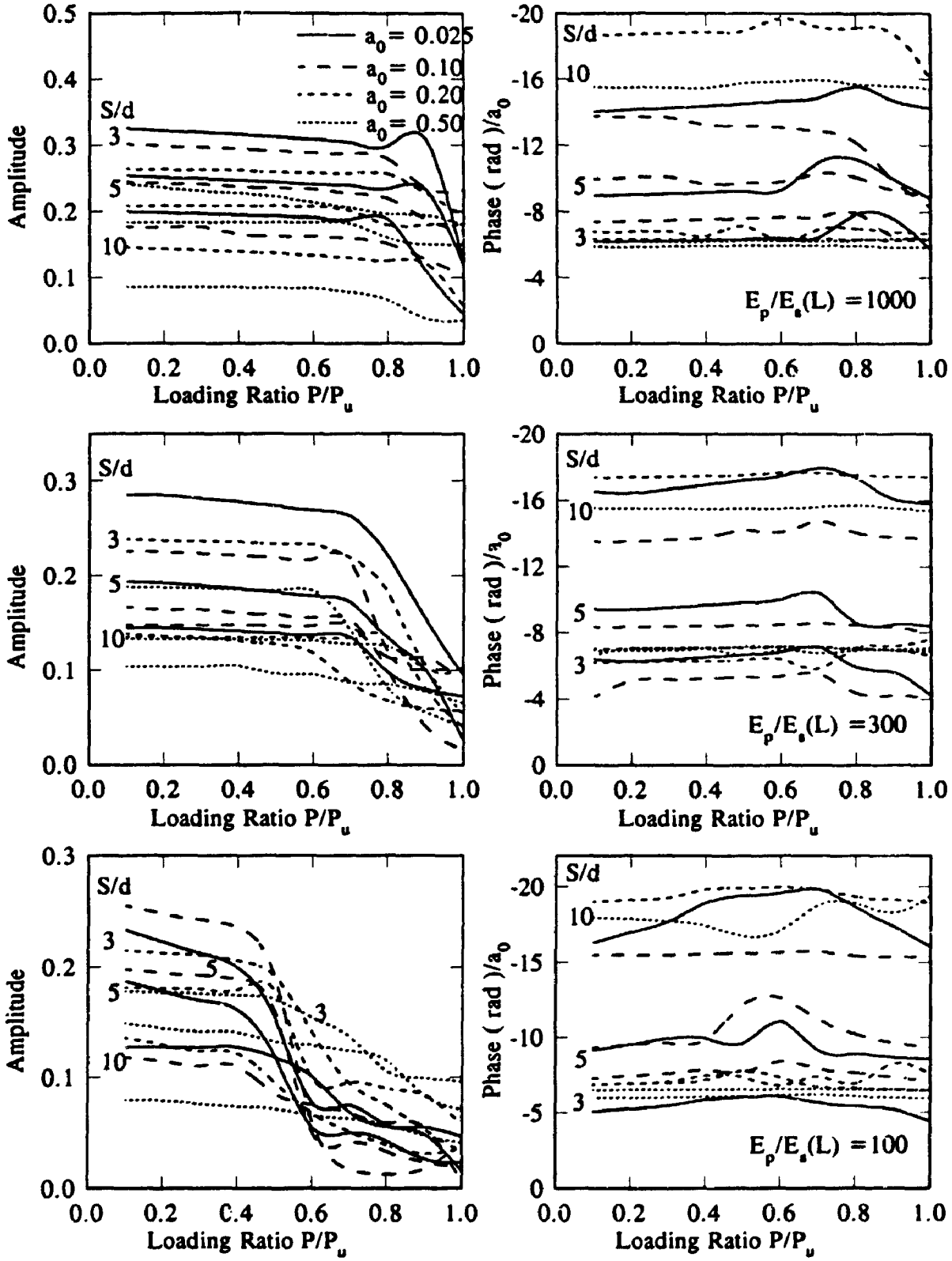

Figure 4.26 Vertical Dynamic Interaction Factors for Approximate Nonlinear Analysis for Floating Piles in Parabolics Soil (L/d = 60, $E/E_s(L)$ = 100, 300, 1000)

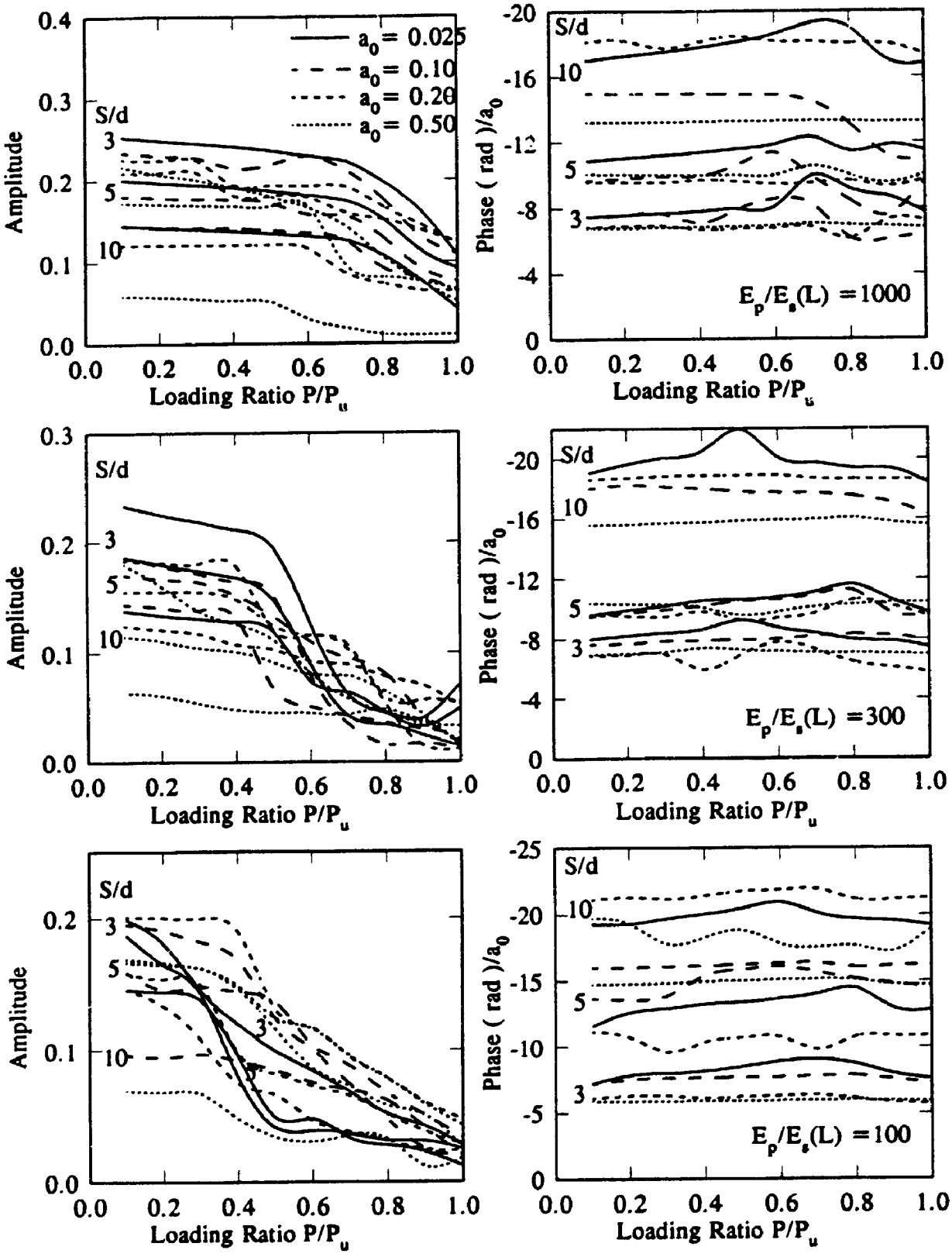

Figure 4.27 Vertical Dynamic Interaction Factors for Approximate Nonlinear Analysis for Floating Piles in Parabolics Soil (L/d = 100, $E/E_s(L)$ = 100, 300, 1000)

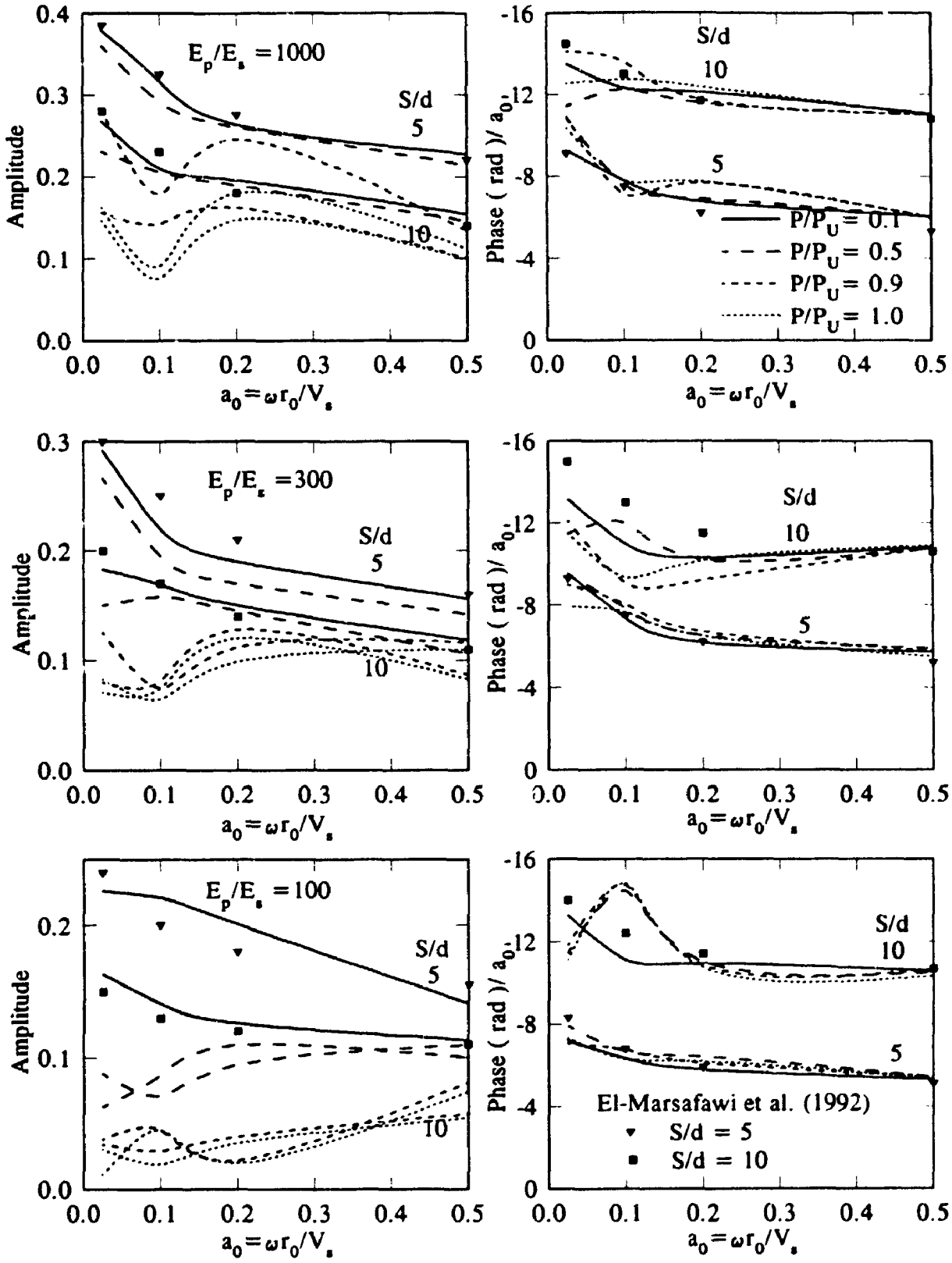

Figure 4.28 Vertival Dynamic Interaction Factors for Floating Piles in Homogeneous Soil Medium Versus Dimensionless Frequency a_0 (L/d = 40)

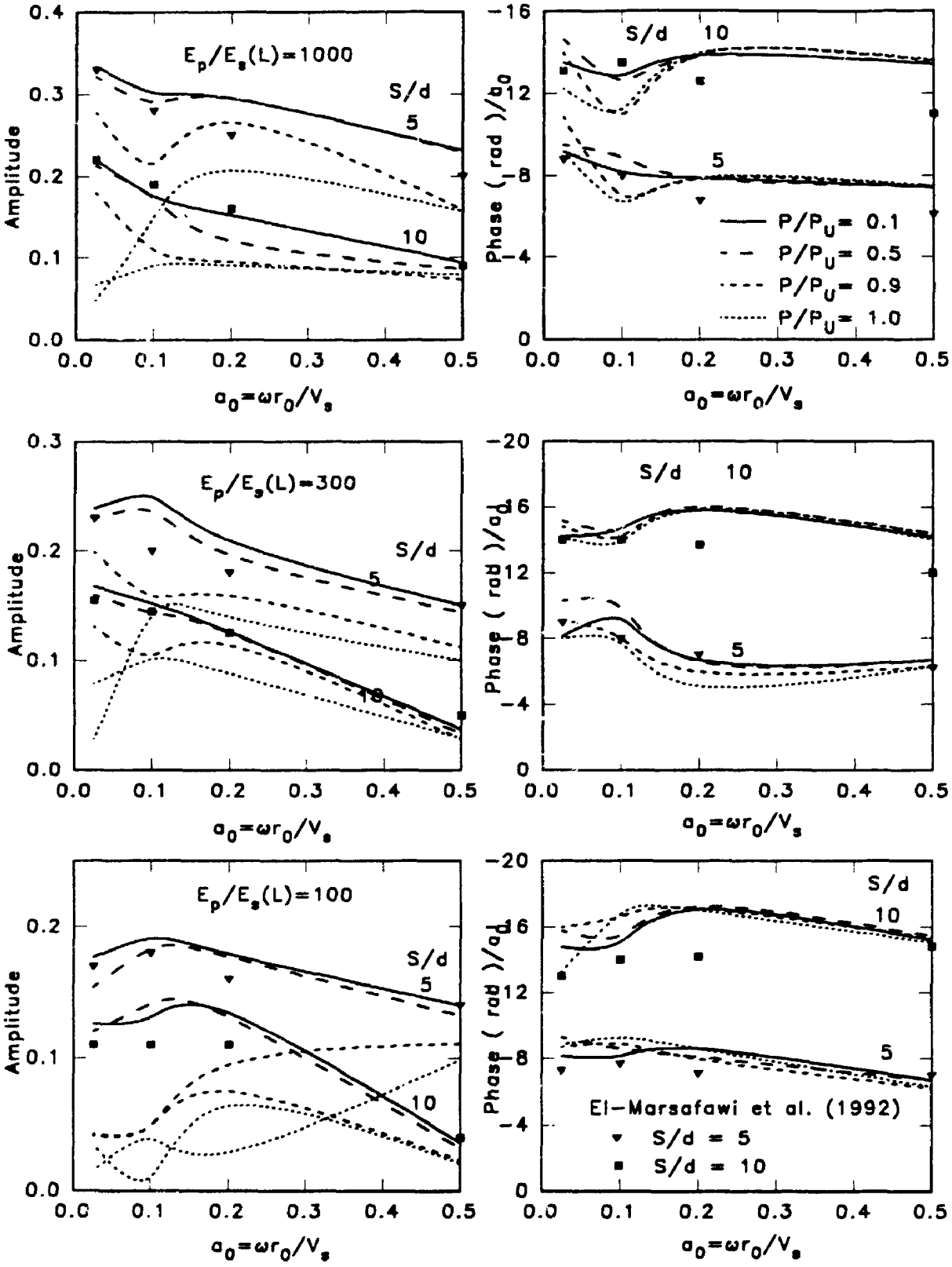

Figure 4.29 Vertical Dynamic Interaction Factors for Floating Piles in Parabolic Soil Medium Versus Dimensionless Frequency a_0 (L/d = 40)

medium are obtained using both the direct analysis and the superposition approach. The results are compared in Fig. 4.30. The stiffness and damping are normalized by the nonlinear static stiffness of a single pile evaluated for the same level of loading. It may be noticed from Fig. 4.30 that the agreement between the two approaches is excellent for the linear loading conditions as was expected. Also, a rather good agreement may be observed for the nonlinear loading conditions, especially for the stiffness. The damping obtained through the superposition approach appears to be overpredicted. For the parabolic soil medium, similar agreement may be observed in Fig. 4.31 and the maximum discrepancy is within 20% for the stiffness, while the damping is overpredicted as in the homogeneous case.

4.9. Conclusion

1-The displacement and velocity time histories, as well as pile capacities computed using the proposed model, compare favourably with field-measured data. The model uses only conventional soil mechanics parameters or parameters directly correlated to them.

2-The different applications presented here show the suitability of the model for pile-driving analysis, the production of equivalent stiffness and damping parameters which are to be implemented in superstructure response to vertical loading and the generation of the dynamic t-z curves which are widely used for offshore pile analysis.

3-It may be concluded that single piles stiffness and damping parameters as well as interaction between piles are greatly affected by the level of loading. Such an effect should be included in the analysis of the dynamic axial response of pile groups.

4-The effect of nonlinearity is that it reduces single pile and pile group stiffness and increase the damping. In addition, nonlinearity reduces the amplitude of interaction factors between piles, while the phase shift is only slightly affected. These effects are more pronounced for slender and flexible piles such as those typical of offshore structures. Moreover, the nonlinearity effects are more pronounced for lower range of

frequencies and homogeneous soil profile.

5-Finally, the model facilitates direct analysis of pile group response to dynamic vertical loading with little computing effort and allows one to generate interaction factors for different loading ratios, different pile spacings and different soil profiles. For a basic range of parameters the nonlinear interaction factors are provided.

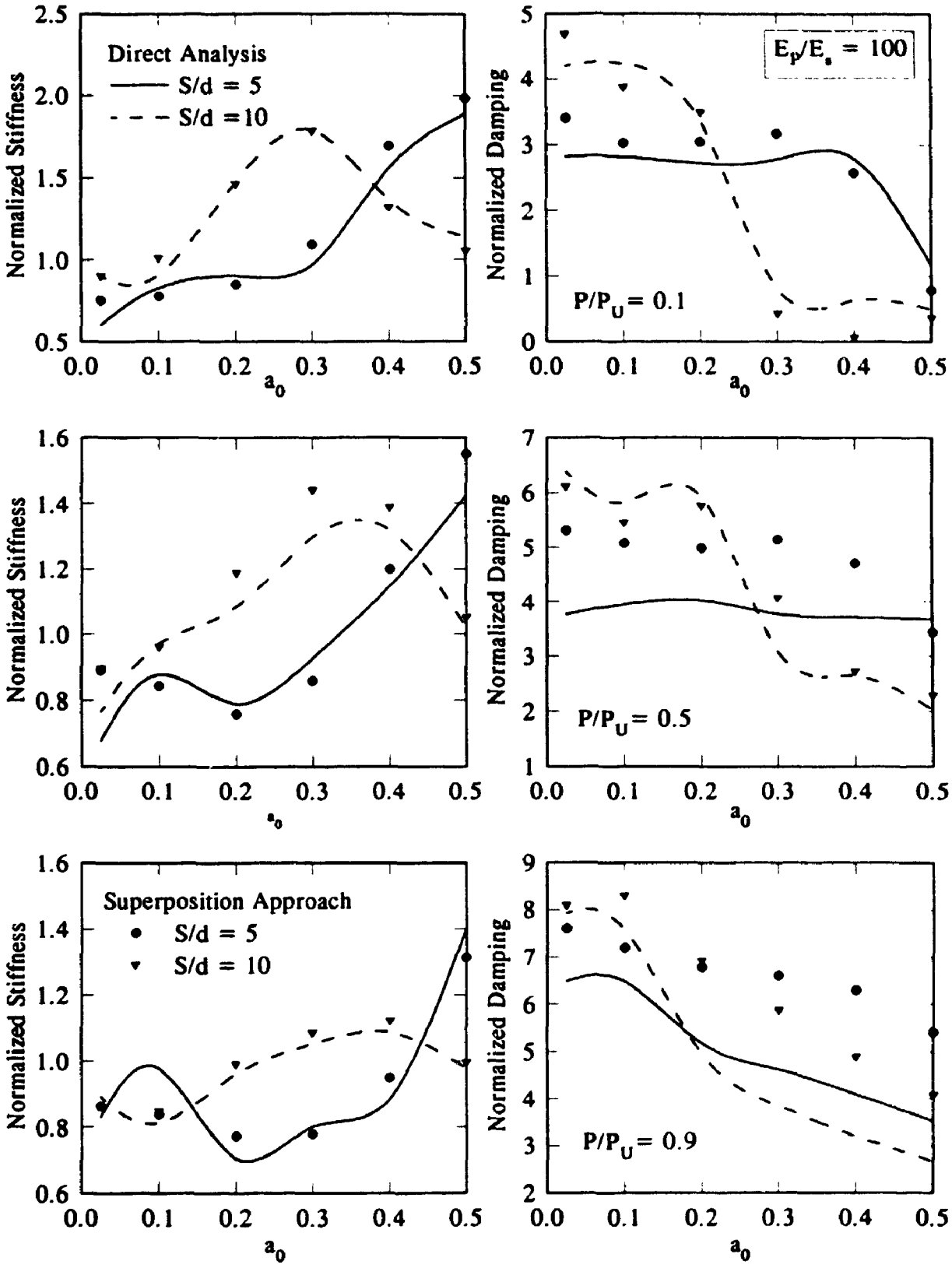

Figure 4.30 Vertical Normalized Dynamic Stiffness of a 2 X 2 Floating Pile Group in Homogeneous Soil Using Direct Analysis and the Superposition Method

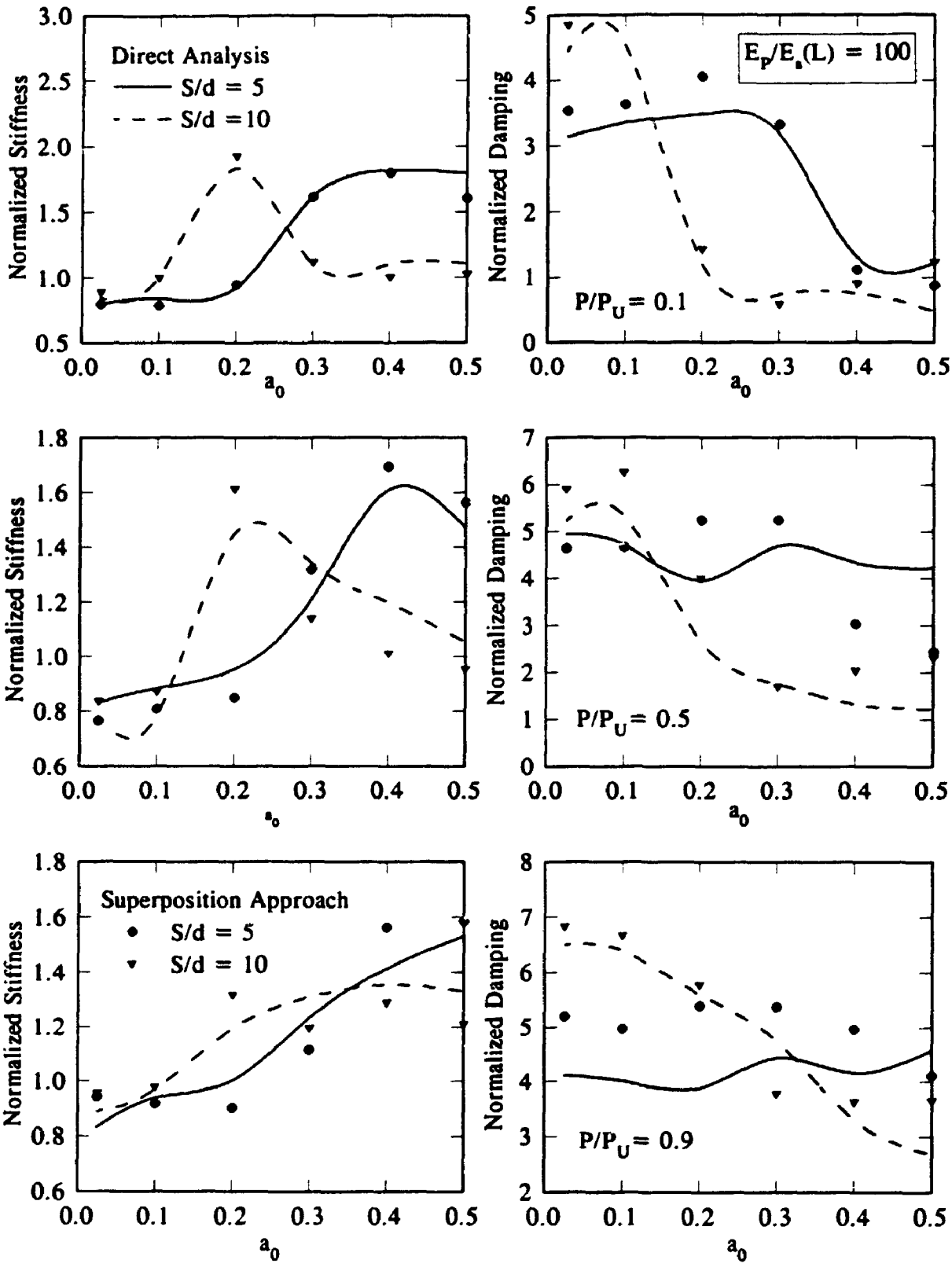

Figure 4.31 Vertical Normalized Dynamic Stiffness of a 2 X 2 Floating Pile Group in Parabolics Soil Using Direct Analysis and the Superposition Method

CHAPTER FIVE
NONLINEAR ANALYSIS OF LATERAL RESPONSE OF SINGLE PILES AND PILE GROUPS

5.1. Introduction

Piles are frequently subjected to lateral forces that result from loading on supported structures such as buildings, quay walls and offshore structures.

Various approaches have been developed for the static and dynamic lateral response of piles such as finite element analysis [35,37,39], but this approach requires large computational efforts. The boundary element approach is also used [10,11,12,13,14], but the inclusion of the soil nonlinear behavior in this approach is difficult. The Winkler model, although approximate, seems to be a powerful technique to model the response of single piles and pile groups to lateral dynamic loads. Matlock et. al [25] developed a unit load transfer curves approach, also known as p-y curves, for the time domain nonlinear analysis. Nogami and Konagai [27] have developed a time domain analysis method for flexural response of single piles based on the frequency domain solution developed by Novak et al. [21], and included the group effect as well as nonlinear behavior of the soil.

In this study, a computationally efficient model for lateral response of single piles and pile groups is developed. The model developed accounts for the nonlinear behavior of the soil adjacent to the pile, and slippage and gapping at the soil-pile interface in a rational manner. The energy dissipation in the soil through different types of damping is also included in the analysis. For the most part, the parameters of the model are standard geotechnical parameters.

5.2. Single Pile Model

The piles are assumed to be vertical with a circular cross section embedded in a

horizontally nonlinear layered soil. Based on the Winkler hypothesis, the soil is divided into a number of layers. Piles are also divided into segments with the same number and length as the soil layers (Fig. 5.1). The analysis is formulated in the time domain to facilitate the modelling of the nonlinear behavior and discontinuity conditions. The elements of this model are shown in Fig. 5.2 and are discussed in detail in the following sections.

5.2.1. Soil Reactions Modelling

In each layer the soil model is divided into two parts as shown in Fig. 5.3. The first part is an inner field model to which nonlinearity is confined. The second part is a far field model which accounts for wave propagation away from the pile. This model is similar to the one developed for the axial response in chapter 4 except that the soil reactions at both sides of the pile are modelled separately to account for the state of stress and discontinuity conditions at both sides as the load direction changes.

Inner Field Element: The soil reaction of the inner field is modelled by a nonlinear spring the stiffness of which is calculated with the assumption that plane strain conditions hold, the inner field is a homogeneous isotropic viscoelastic medium, the pile is rigid and circular, there is no separation at the soil-pile interface, and the displacements are small. The stiffness solution under these conditions was obtained by Novak and Sheta [8] as

$$k_{nl} = \frac{8\pi G_m (1-\nu)(3-4\nu)[(r_0/r_1)^2+1]}{(r_0/r_1)^2 + (3-4\nu)^2\,[(r_0/r_1)^2+1]\ln(r_1/r_0) - 1} \qquad (5.1)$$

where r_0 and r_1 are the inner and outer radii of the inner field, respectively and ν is the Poisson's ratio of the soil stratum. G_m is the modified shear modulus calculated according to the strain level, assuming that Poisson's ratio is constant, as

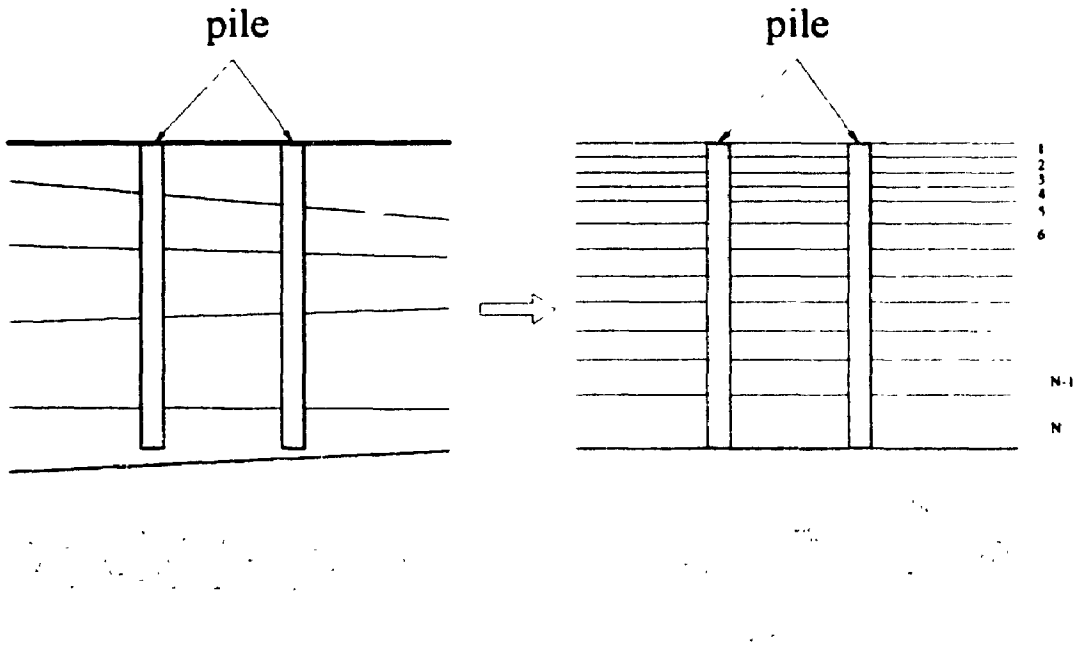

Figure 5.1 Discretization of the Soil-Pile System

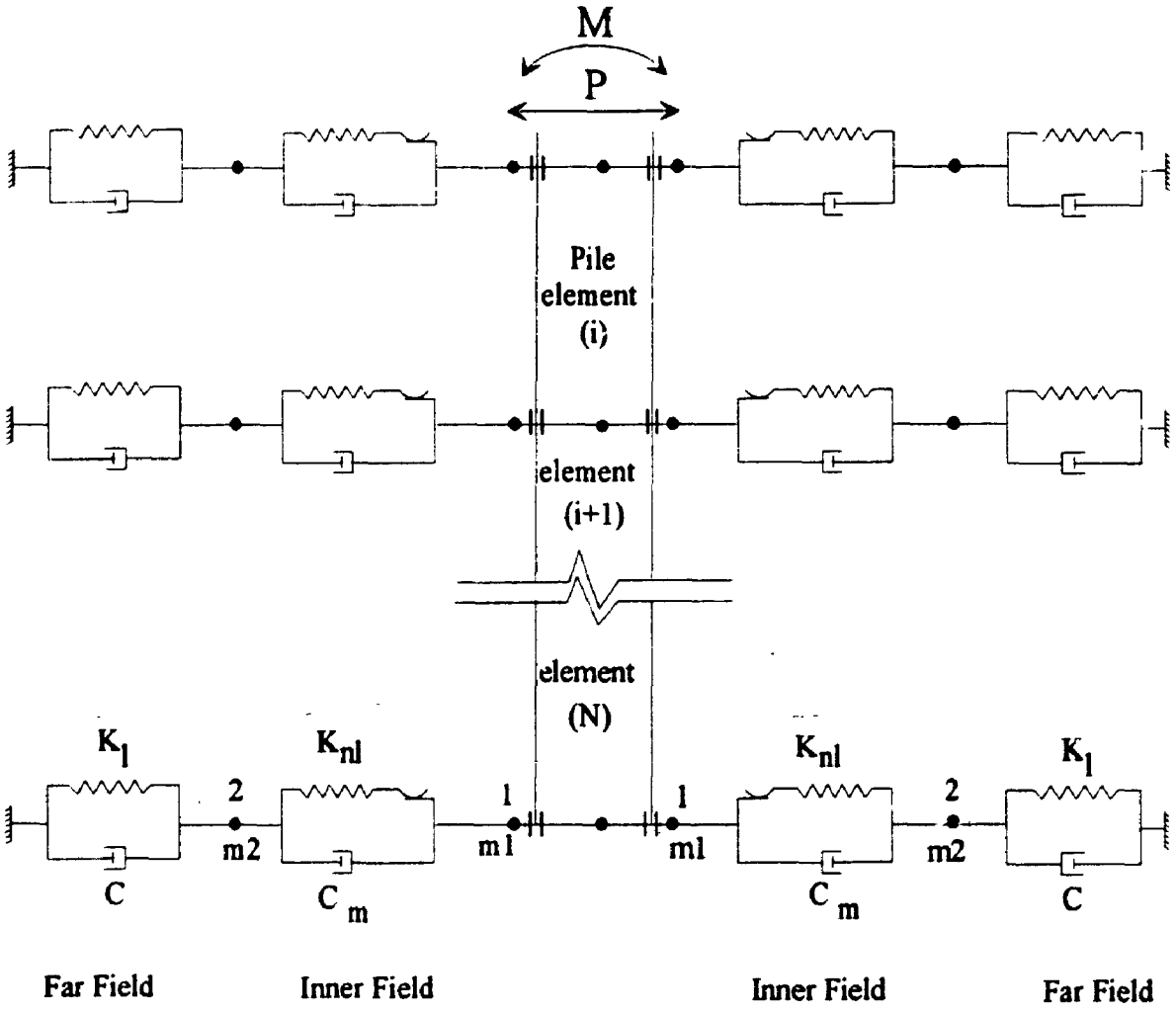

Figure 5.2 Elements of the Proposed Model for Nonlinear Dynamic Analysis of Lateral Response of Single Piles

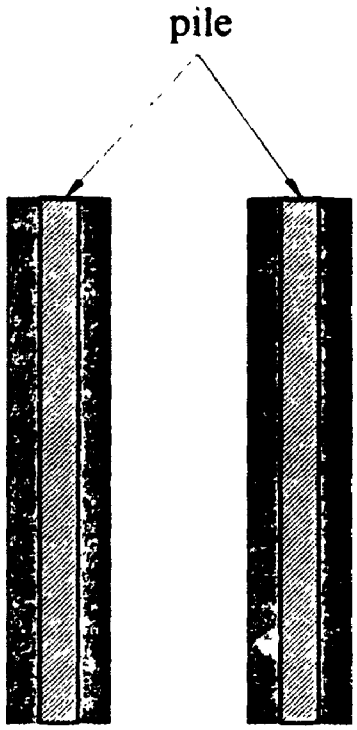

ELEVATION

far field model

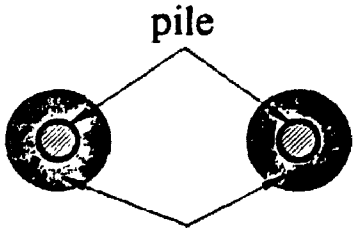

inner field model

PLAN

Figure 5.3 Proposed Soil Model in Plane Strain Condition

$$G_m = G_{max} (1 - \eta) \tag{5.2}$$

G_{max} is the initial shear modulus of the soil layer, η is the mobilization ratio defined as $\eta = P / P_U$ where P is the horizontal load at the spring and P_U is the ultimate resistance of the spring calculated using the standard relations given by the API [76]. For clay, the resistance is given as a strength per unit length of the soil layer by

$$P_U = 3 c_u d + \gamma X d + J c_u X \qquad X \le X_R \tag{5.3}$$

$$P_U = 9 c_u d \qquad X > X_R \tag{5.4}$$

where c_u = undrained shear strength , d = pile diameter, γ is the effective unit weight of soil, J = empirical coefficient ranging from 0.25 to 0.5, X = depth below the surface and X_R = depth of the reduced resistance zone, which can be calculated by solving eqs. 5.3 and 5.4 simultaneously.

The corresponding criteria for the lateral resistance of sands at shallow depths P_{U1} or at large depth P_{U2} are

$$P_{U1} = A \{ \gamma X [\frac{K_0 X \tan\phi \sin\beta}{\tan(\beta - \phi)\cos\alpha} + \frac{\tan\beta}{\tan(\beta - \phi)} (d + X \tan\beta \tan\alpha) + K_0 X \tan\beta (\tan\phi \sin\beta - \tan\alpha) - K_a d] \} \tag{5.5}$$

$$P_{U2} = A \gamma X d [K_a (\tan^8\beta - 1) + K_0 \tan\phi \tan^4\beta] \tag{5.6}$$

In these equations A is an empirical adjustment factor dependent on the depth from the soil surface and can be found in [76], K_0 is the earth pressure coefficient at rest (0.4), ϕ is the effective friction angle of the sand, $\beta = \phi/2 + 45^0$, $\alpha = \phi/2$, K_a is the Rankin minimum active earth pressure coefficient defined as $K_a = \tan^2(45^0 - \phi/2)$.

Far Field Element : Novak et al.[21] solved the problem of the horizontal vibration of

piles. In their solution, the plane strain conditions are assumed to hold. An explicit solution for the soil horizontal complex stiffness of a unit length of a cylinder embedded in a linear viscoelastic medium is given as

$$K = \pi\, G\, a_0^2\, T \tag{5.7}$$

In this equation $G = G_{max}$ is the initial shear modulus of the soil layer, $a_0 = \omega r_0/V_s$ is a dimensionless frequency and T is a dimensionless factor given by

$$T = -\frac{4K_1(b_0^*)K_1(a_0^*) + a_0^* K_1(b_0^*)K_0(a_0^*) + b_0^* K_0(b_0^*)K_1(a_0^*)}{b_0^* K_0(b_0^*)K_1(a_0^*) + a_0^* K_1(b_0^*)K_0(a_0^*) + b_0^* a_0^* K_0(b_0^*)K_0(a_0^*)} \tag{5.8}$$

where a_0^* and b_0^* are complex dimensionless frequencies defined as

$$a_0^* = \frac{i\, a_0}{\sqrt{1+i\, D_s}} \quad , \quad b_0^* = \frac{i\, a_0}{\xi\, \sqrt{1+i\, D_l}} \tag{5.9}$$

in which ξ is the ratio between the longitudinal and shear wave velocities of the soil layer, D_s and D_l are the material damping constants, usually assumed to be both equal to D, associated with shear and longitudinal waves, respectively, and finally, K_0 and K_1 are the modified Bessel functions of the second kind of orders 0 and 1, respectively . This solution is not suitable for the time domain analysis because it is frequency dependent. However, the real and imaginary parts may be separated and Eq. 5.7 can be rewritten as

$$K = G\,[S_{u1}(a_0, \nu, D) + i\, S_{u2}(a_0, \nu, D)] \tag{5.10}$$

in which S_{u1} and S_{u2} are real. Fig. 5.4 shows the variations of S_{u1} and S_{u2} with the dimensionless frequency a_0, and ν. It may be observed from the figure that for the frequency range between 0.05 and 0.5, typical of offshore loading and many other applications, S_{u1} may be considered constant, while S_{u2} increases monotonically with a_0.

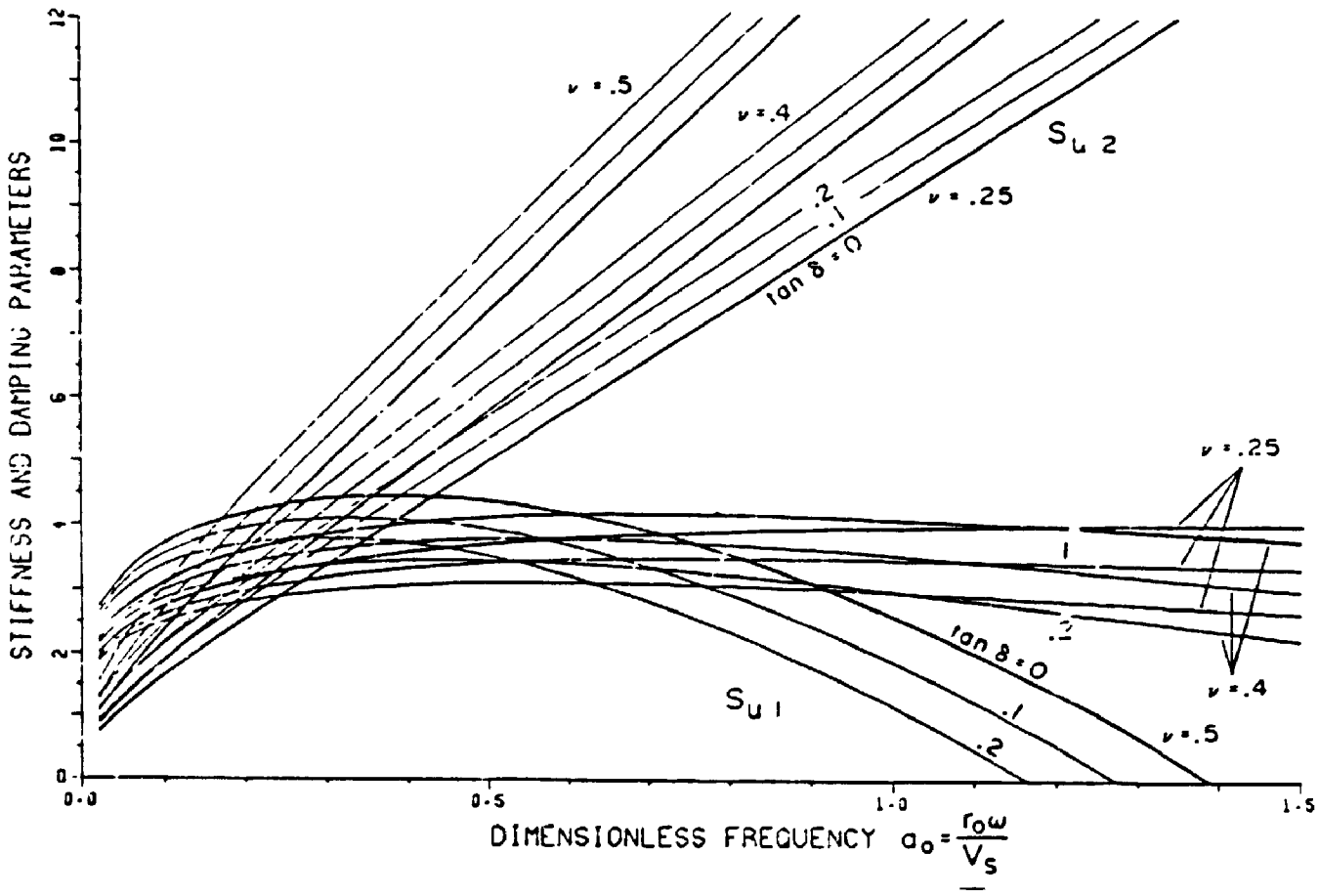

Figure 5.4 Variations of Horizontal Stiffness and Damping Parameters, S_{u1} and S_{u2}, with Dimensionless Frequency a_0 and Soil Poisson's Ratio

The effect of Poisson's ratio is that as it increases, both of S_{u1} and S_{u2} increase in the specified range of frequency. These observations suggest that the outer field element can be modelled by a spring and dashpot whose constants depend on Poisson's ratio, but they are frequency independent and defined as

$$K_1 = G\, S_{u1}\,(\nu)$$
$$c = \frac{2\,G\,r_0}{V_s}\, S_{u2}(a_0 = 0.5, \nu) \qquad (5.11)$$

where S_{u1} and S_{u2} are frequency independent with their values chosen according to Poisson's ratio of the soil layer and the dominant dimensionless frequency a_0. These frequency independent stiffness and damping parameters are used in the dynamic analysis in the time domain.

5.2.2. Discontinuity Conditions

Discontinuity conditions of the motion between pile and soil are caused by the slippage and gapping at the soil-pile interface. To model these conditions logically the soil reactions to the pile motion at both sides are modelled separately as shown in Fig. 5.2. The load-deflection curve for a pile node at the topmost part of the pile, where soil-pile separation takes place, is shown in Fig. 5.5 as well as the corresponding horizontal displacements of the soil nodes on both sides of the pile. For the pile initially loaded rightward, the soil node at the left is separated from the pile as the force in the near field element reaches zero assuming that soil does not resist tension. The soil node on the right is pushed with the pile to the right and K_{u1} decreases as the load increases. In the unloading phase the pile separates from the soil on its right also. When the pile is loaded more leftward, it comes into contact again with the soil node on its left and pushes it until unloading occurs again, separation takes place and the pile returns to its original position. The result of this is that soil nodes are left in a displaced position and a

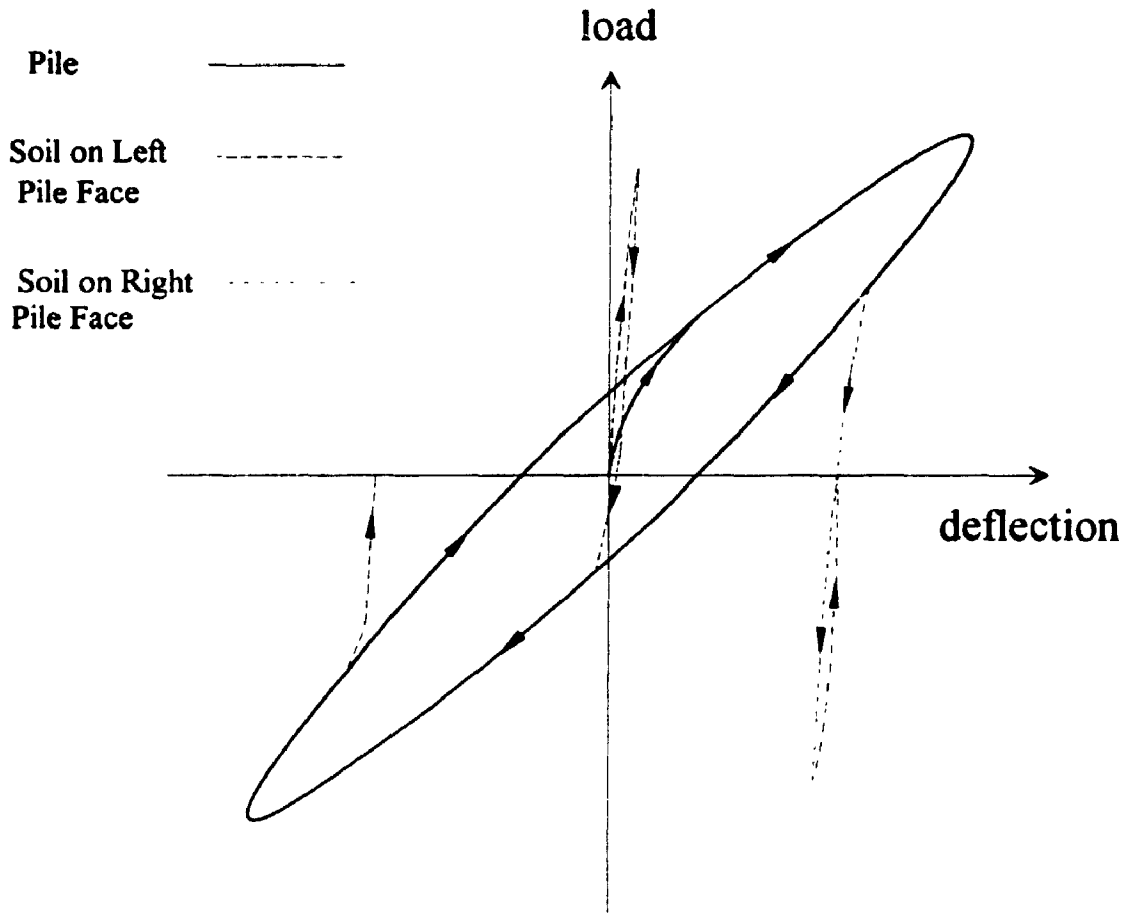

Figure 5.5 Pile and Soil Displacements for a Case with Pile-Soil Separation

permanent gap develops. The development of such gaps is a phenomenon observed in offshore piles especially after storm conditions, however, afterward healing occurs and gaps are closed. Development of these gaps greatly affects the pile response to any subsequent loading as will be discussed later.

5.2.3. Pile Modelling

The pile shaft is assumed to be elastic, vertical and has a circular cross section. It is subdivided into a number of elements and every element is assumed to have a constant cross section. The structural stiffness matrix of each individual element is defined by the standard four by four bending stiffness matrix relating the translation u and rotation θ to load P and moment M and is given as

$$E_p I_p \begin{bmatrix} 12/l^3 & -12/l^3 & 6/l^2 & 6/l^2 \\ -12/l^3 & 12/l^3 & -6/l^2 & -6/l^2 \\ 6/l^2 & -6/l^2 & 4/l & 2/l \\ 6/l^2 & -6/l^2 & 2/l & 4/l \end{bmatrix} \begin{Bmatrix} u_1 \\ u_2 \\ \theta_1 \\ \theta_2 \end{Bmatrix} = \begin{Bmatrix} P_1 \\ P_2 \\ M_1 \\ M_2 \end{Bmatrix} \qquad (5.12)$$

where E_p and I_p are Young's modulus and second moment of area of the pile, respectively, and l is the element length. The pile structural stiffness matrix may then be constructed by superposition of the sub-matrices of the individual elements.

The number of elements has a great effect on the accuracy of the results. Poulos [77] found that the greater the number of the elements the greater the accuracy of the results. Evangelista and Viggiani [78] found that using smaller elements for the upper part of the pile and increasing the element length with the depth resulted in maintaining the accuracy while using fewer number of elements. El Sharnouby and Novak [79] found that using twelve pile elements increasing in length with depth, with the top elements 1/4 of the average element length gave accurate results with a minimum of computational efforts. However, for dynamic analysis it is somewhat different. A

sensitivity study was done and 20 elements increasing in length with depth were found to give accurate results.

To reduce the computational efforts, only degrees of freedom of interest are maintained and the rest are eliminated through a static condensation process. Thus, only the transitional degrees of freedom along the pile and the rotational degree of freedom at the pile head are maintained.

5.3. Group Effect

Since each pile is affected not only by its own load but also by the load and deflection of other piles in the group, the dynamic stiffness of a group of piles is greatly affected by the interaction between piles. This effect is incorporated in the analysis as follows. For the lateral vibration, interaction between piles depends on the angle, θ, between the lines of the two piles and the direction of the horizontal applied force, as well as the spacing between them. Gazetas and Dobry [33] found that the 90^0-passive pile m (Fig. 5.6) is affected essentially only by S-waves which emanate from active pile l and which have a phase velocity V_s. They also found that the 0^0-passive pile is affected by compression-extension waves coming from the active pile and propagating with an apparent phase velocity which is equal to the so-called Lysmer's analog velocity, V_{La} given by

$$V_{La} = \frac{3.4\ V_s}{\pi\,(1-\nu)} \tag{5.13}$$

Assuming that waves propagate in the horizontal direction only and also assuming a Winkler soil model, the displacement at any point in the elastic soil domain may be given (Makris and Gazetas [80]), in general, as

$$u(a_0, r, \theta) = u_0\ \psi_u(a_0, r, \theta) \tag{5.14}$$

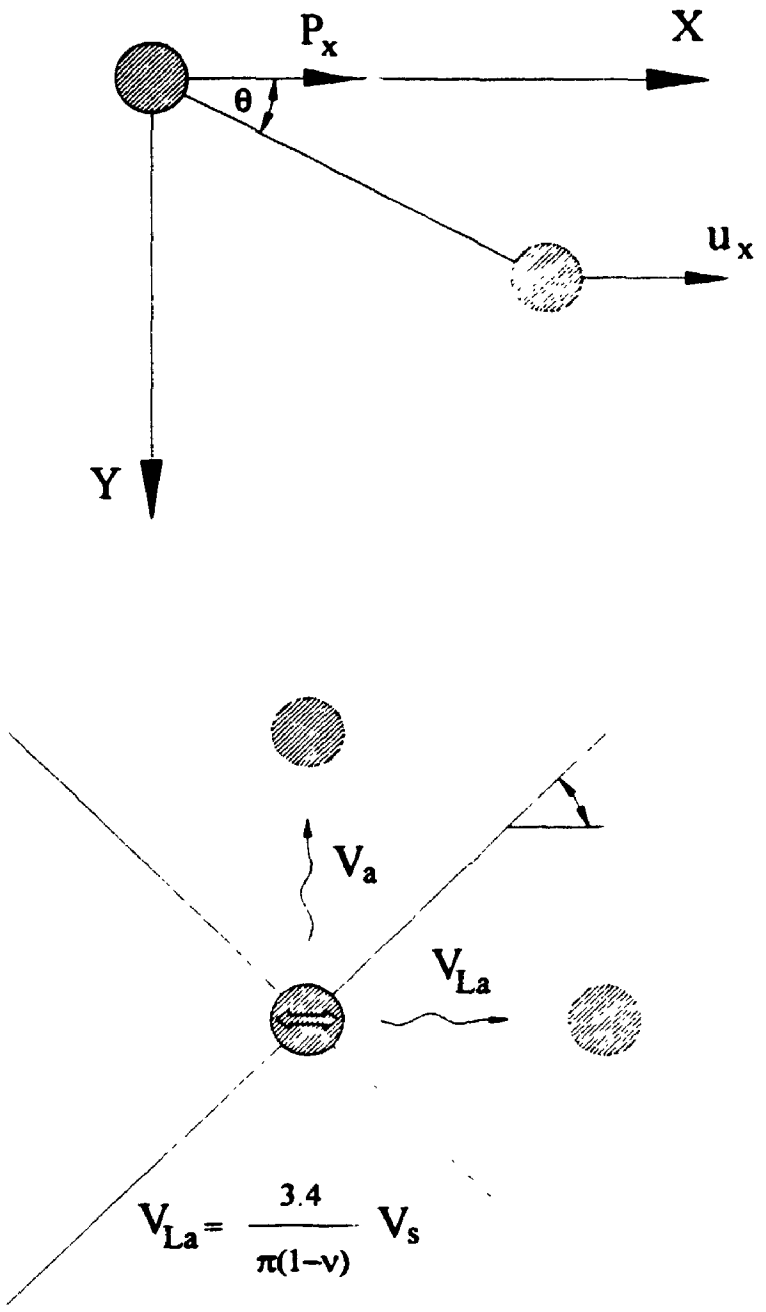

Figure 5.6 (a) Plan View of Two Piles at Angle θ (b) Assumed Apparent Velocities of Waves Emanating from a Laterally Oscillating Pile

In Eq. 5.14 u_0 is the amplitude of the disturbance at the source, and ψ_u is an attenuation function accounting for the wave propagation away from the source and the radiation damping. It is sufficient to compute ψ_u only for $\theta = 0^0$ and $\theta = 90^0$ and the approximation by Poulos [81] and Kaynia and Kausel [11] may be used to evaluate ψ_u at any angle θ as

$$\psi_u(a_0, r, \theta) = \psi_u(a_0, r, 0^0)\cos^2\theta + \psi_u(a_0, r, 90^0)\sin^2\theta \tag{5.15}$$

in which

$$\psi_u(a_0, r, 0^0) = \sqrt{\frac{r_0}{r}}e^{-ia_0\frac{\pi(1-\nu)(r-r_0)}{3.4r_0}}$$
$$\psi_u(a_0, r, 90^0) = \sqrt{\frac{r_0}{r}}e^{-ia_0\frac{(r-r_0)}{r_0}} \tag{5.16}$$

Using this approximation for the attenuation function, Eq. 5.14 may be rewritten as

$$u(a_0, r, 0^0) = \frac{1}{K_1 + ica_0}\sqrt{\frac{r_0}{r}}e^{-ia_0\frac{\pi(1-\nu)(r-r_0)}{3.4r_0}}P_h(a_0)$$
$$u(a_0, r, 90^0) = \frac{1}{K_1 + ica_0}\sqrt{\frac{r_0}{r}}e^{-ia_0\frac{(r-r_0)}{r_0}}P_h(a_0) \tag{5.17}$$

where K_1 and c are the frequency independent spring and dashpot constants defined in Eq. 5.11. Subjecting Eq. 5.17 to an inverse Fourier transform, the unit impulse response function required for time domain analysis is obtained as

$$u(t,r) = \sqrt{\frac{r_0}{r}}A\,e^{-B(t-t_0)} \qquad t > t_0 \tag{5.18}$$

where $A = 1 / c$, $B = K_1 / c$ and t_0 is given by

$$t_0 = \frac{\pi (1-\nu)(r-r_0)}{3.4\ V_s} \qquad \theta = 0^0$$
$$t_o = \frac{(r-r_0)}{V_s} \qquad \theta = 90^0 \tag{5.19}$$

The interaction effect is assumed to vary linearly through each time step Δt. The soil displacement at the axis of the mth pile due to a disturbance at the lth pile is given by

$$u_m(t_i, r_{ml}) = P_l(t_i - t_{ml-1})\, H_1(t_i, r_{ml}) + P_l(t_i)\, H_2(t_i, r_{ml}) \tag{5.20}$$

where i is the number of the time step, r_{ml} is the distance between the piles m and l, t_{ml-1} is the travel time between them minus one time step; H_1 and H_2 are convolution integrals over the period Δt given as

$$H_1 = \int_0^{\Delta t} u(t-\tau, r)\left(1 - \frac{\tau}{\Delta T}\right) d\tau$$
$$= \sqrt{\frac{r_0}{r}}\frac{A}{B}\left[\frac{1}{B\Delta t} e^{B\Delta t} - \left(1 - \frac{1}{B\Delta t}\right)\right] e^{-B(t-t_0)} \qquad t \geq t_0 + \Delta t \tag{5.21}$$

$$H_2 = \int_0^{\Delta t} u(t-\tau, r)\frac{\tau}{\Delta T} d\tau$$
$$= \sqrt{\frac{r_0}{r}}\frac{A}{B}\left[\left(1 - \frac{1}{B\Delta t}\right) e^{B\Delta t} + \frac{1}{B\Delta t}\right] e^{-B(t-t_0)} \qquad t \geq t_0 + \Delta t \tag{5.22}$$

Equation 5.20 implies that H_2 is the inverse of the time domain stiffness of the medium if r equals to r_0, yielding the interaction force as

$$P = -[\ H_2(r=r_0)\ ]^{-1}\ u_m \qquad l \neq m$$
$$= -K_\mu\ u_m \tag{5.23}$$

For $\theta = 0^0$ or 90^0 relevant values of t_0 from Eq. 5.19 are to be substituted in Eqs. 5.21 and 5.22. For any value of θ Eq. 5.15 can be used to obtain the interaction force, P.

This force is to be considered in the analysis as discussed in the subsequent section. Fig. 5.7 shows a slice of the soil-pile system containing the elements of the model implemented in the group analysis. The visco-elastic spring, K_u, connects the two piles through the far field.

5.4. Equations of Motion

The mass of the inner field, m_s, is lumped at two nodes: one half, m_1 , at the node adjacent to the pile, node 1, and the other one, m_2, at the node adjacent to the outer field, node 2 as shown in Fig. 5.2. If the material damping is to be added, a parallel dashpot may be considered with a constant c_m to be suitably chosen.

The equations of motion for the inner field expressing the equilibrium of masses m_1 and m_2 are

$$\begin{aligned} m_1 \ddot{u}_1 + c_m(\dot{u}_1 - \dot{u}_2) + K_{nl}(u_1 - u_2) &= P_1 \\ m_2 \ddot{u}_2 - c_m(\dot{u}_1 - \dot{u}_2) - K_{nl}(u_1 - u_2) &= P_2 \end{aligned} \qquad (5.24)$$

where u_1 and u_2 are displacements of nodes 1 and 2, and P_1 is the force in the nonlinear spring which includes the confining pressure also, P_2 is the soil resistance at node 2; finally, c_m is the material damping in the inner field.

The equation of motion for the outer field may be written as

$$c\dot{u}_2 + K_l u = -P_2 + P \qquad (5.25)$$

where P is the interactive force transmitted through the soil from pile to pile. Introducing compatibility and equilibrium between the inner field and the outer field results in

$$\begin{Bmatrix} P_1 \\ 0 \end{Bmatrix} = \begin{bmatrix} A_m m_1 + A_c c_m + K_{nl} & -K_{nl} - A_c c_m \\ -K_{nl} - A_c c_m & K_{nl} + A_m m_2 + A_c c_t + K_l \end{bmatrix} \begin{Bmatrix} u_1 \\ u_2 \end{Bmatrix} + \begin{Bmatrix} \delta_1 \\ \delta_2 - P \end{Bmatrix} \qquad (5.26)$$

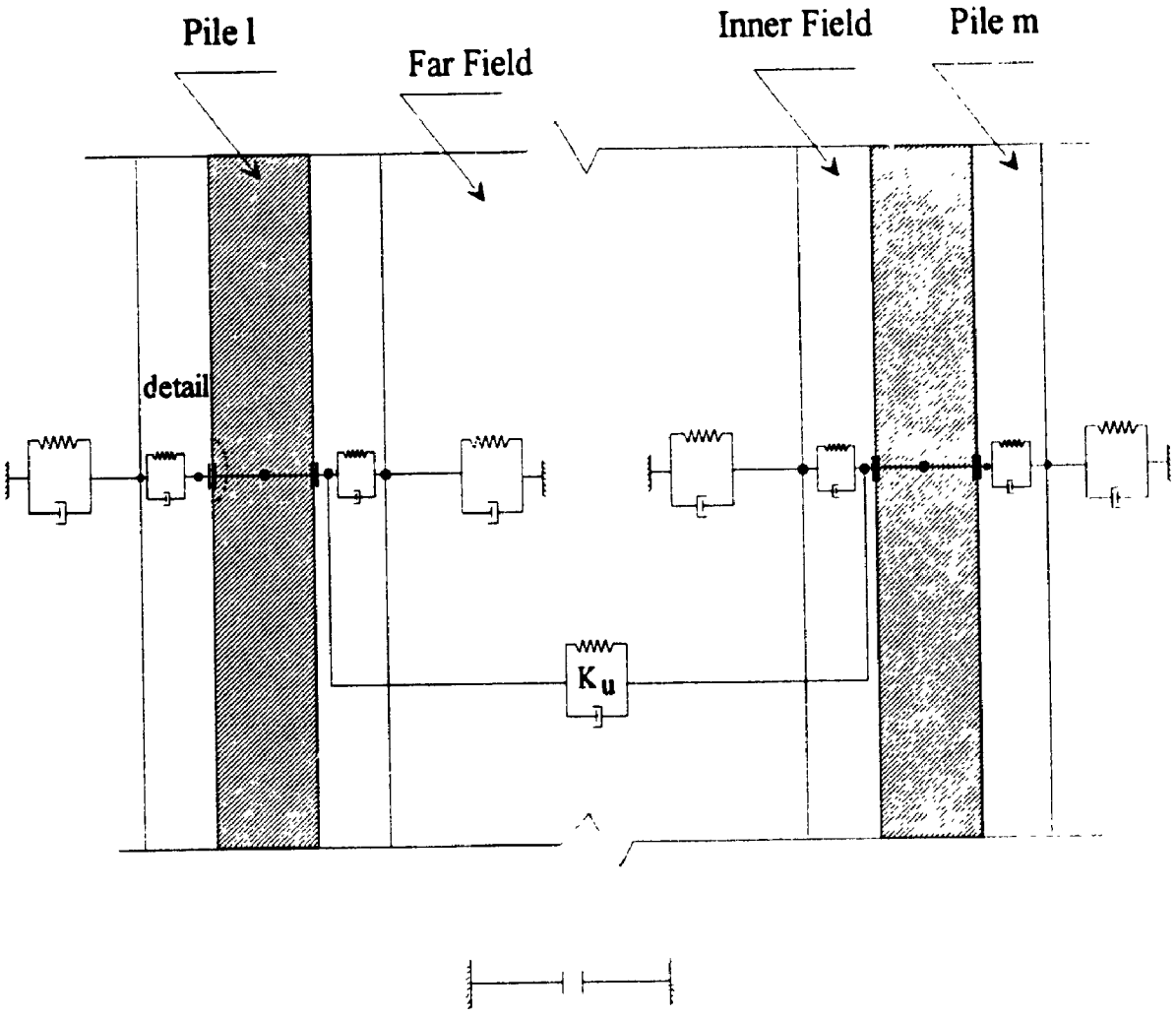

Figure 5.7 Elements of the Model Implemented in the Nonlinear analysis of Lateral Response of Pile Group

where $c_t = c + c_m$ is the total damping. From Eq. 5.26 it can be deduced that

$$u_2 = \frac{K_{nl} + A_c c_m}{(K_{nl} + K_l + A_m m_2 + A_c c_t)} u_1 + \frac{P - \delta_2}{(K_{nl} + K_l + A_m m_2 + A_c c_t)} \tag{5.27}$$

$$P_1 = \left[K_{nl} + A_m m_1 + A_c c_m - \frac{(K_{nl} + A_c c_m)^2}{(K_{nl} + K_l + A_m m_2 + A_c c_t)} \right] w_1 - \frac{K_{nl}(P - \delta_2)}{(K_{nl} + K_l + A_m m_2 + A_c c_t)} + \delta_1 \tag{5.28}$$

where A_m and A_c are constants of numerical integration for inertia and damping, respectively. Finally

$$\delta_1 = K_{nl}^{i-1} (u_1 - u_2)^{i-1} + c_m (\dot{u}_1 - \dot{u}_2)^{i-1} + m_1 \ddot{u}_1^{i-1} \tag{5.29}$$

$$\delta_2 = -K_{nl}^{i-1} (u_1 - u_2)^{i-1} - c_m (\dot{u}_1 - \dot{u}_2) + m_2 \ddot{u}_2^{i-1} + K_l u_2^{i-1} + c \dot{u}_2^{i-1} \tag{5.30}$$

Eqs. 5.24 through 5.30 are valid for soil nodes on both sides of the pile.

When the pile is moving away from the soil node, P_1 decreases until it reaches zero. If loading continues in the same direction, the resistance offered by that element will stay at zero (no tension is allowed) and the soil node on this side is disconnected from the pile node accommodating for the gap opening. On the other hand, when the pile is moving towards the soil node, P_1 increases until it reaches the maximum soil resistance and K_{nl} decreases until it reaches the value of zero; the near field spring on this side offers constant resistance to the pile motion. At this point, for some soil types, the ultimate static resistance of the soil may be reduced to display a post peak resistance as it has been observed for some soils such as dense sand and stiff clay. Reconnection of the soil-pile nodes occurs again when the pile returns to the displaced position of the soil node and continues to move in the direction of the soil node. The stiffness of the spring K_{nl} is assumed to be linear in the unloading phase.

5.4.1. Solution of Equations of Motion

For single piles and pile groups, the pile and soil displacements are evaluated in

the time domain using the linear acceleration assumption and the Newmark β method for direct time integration of the equations of motion. The modified Newton-Raphson iteration scheme is used to derive and solve the governing equilibrium equations [60].

5.5. Validation of the Model

The validity of the proposed nonlinear dynamic analysis is assessed through comparison with the results of some actual field tests as well as other analytical solutions in the literature.

5.5.1. Comparison with Field tests

Full-scale field tests on single piles were conducted at the University of Houston. Piles were loaded with a static cyclic load (O'Niel and Dunnavant [82]) and a dynamic load (Blaney and O'Niel [83]). The soil profile at the site is shown in Fig. 5.8. Piles used in the tests are steel pipe piles with an outside diameter of 0.274 m. and a wall thickness of 0.009 m. Fig. 5.9 shows the piles and settings for both cyclic and dynamic tests. The proposed model was used to compute the response for both cases. The results from the analytical model and the field measurements are plotted in Fig. 5.10 for the cyclic load test and in Fig. 5.11 for the dynamic load test. The cyclic pile response was computed for a monotonically increasing load. The correlation between the computed and measured responses for both the cyclic and dynamic load test is very good and may be observed in Figs. 5.10 and 5.11.

5.5.2. Comparison with Other Analytical Approaches

To further examine the proposed model, the results obtained using the model are compared with those obtained using a more rigorous frequency domain solution due to Nogami [29]. The stiffness and damping parameters for a single pile and a group of two piles embedded in a homogeneous soil stratum underlain by a bed rock (Fig. 5.12) are

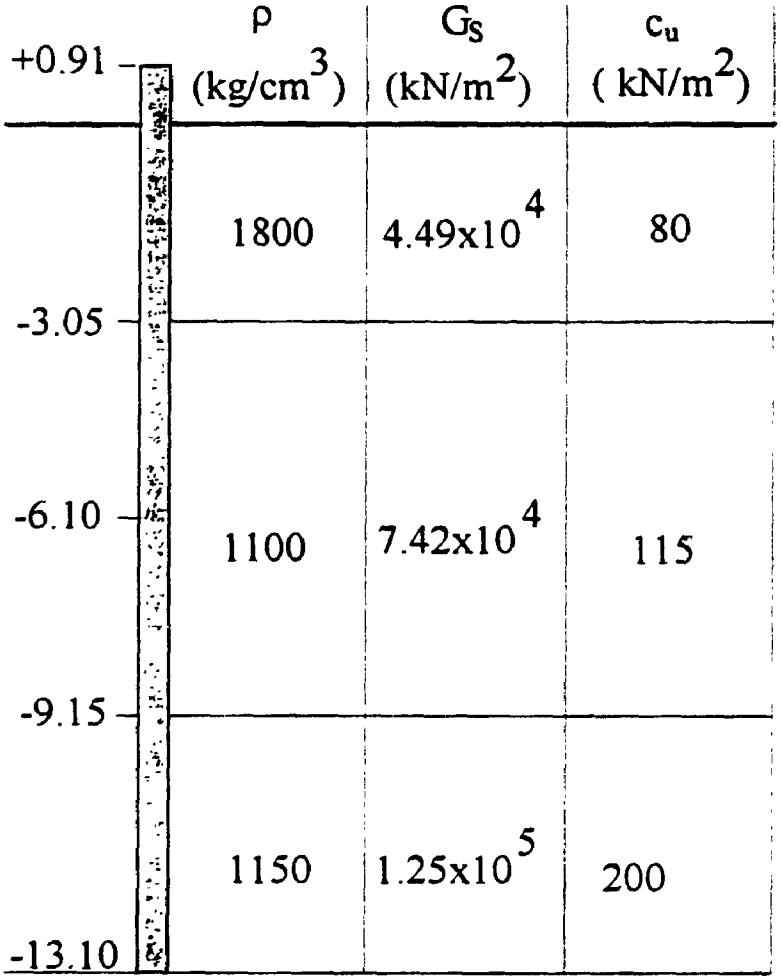

Figure 5.8 Soil Profile for University of Houston Site

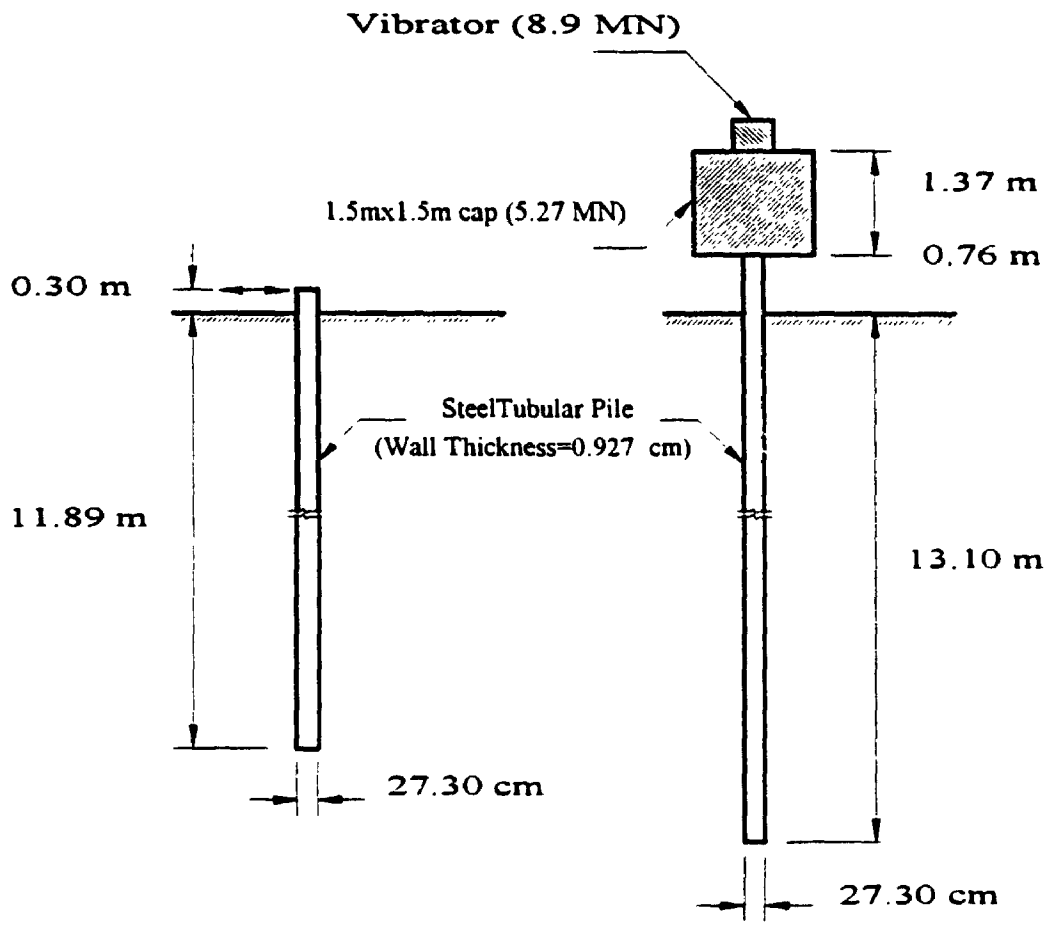

a- Cyclic Pile Load Test b- Dynamic Pile Load Test

Figure 5.9 Pile Properties and Test Settings for (a) Cyclic Pile Load Test and (b) Dynamic Pile Load Test

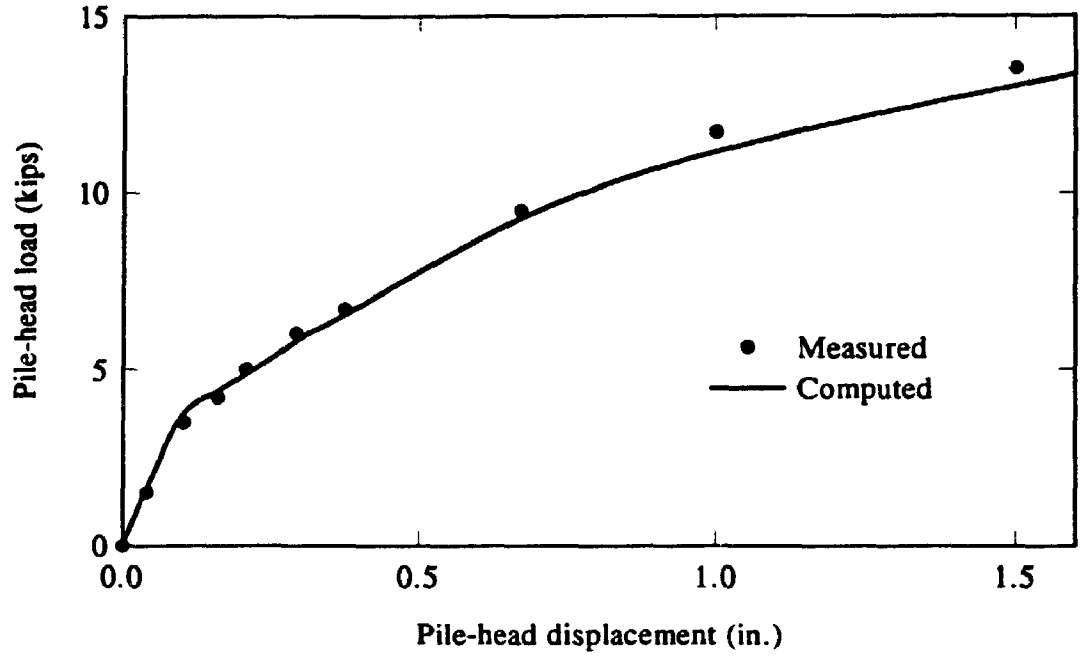

Figure 5.10 Computed and Measured Cyclic Pile Response

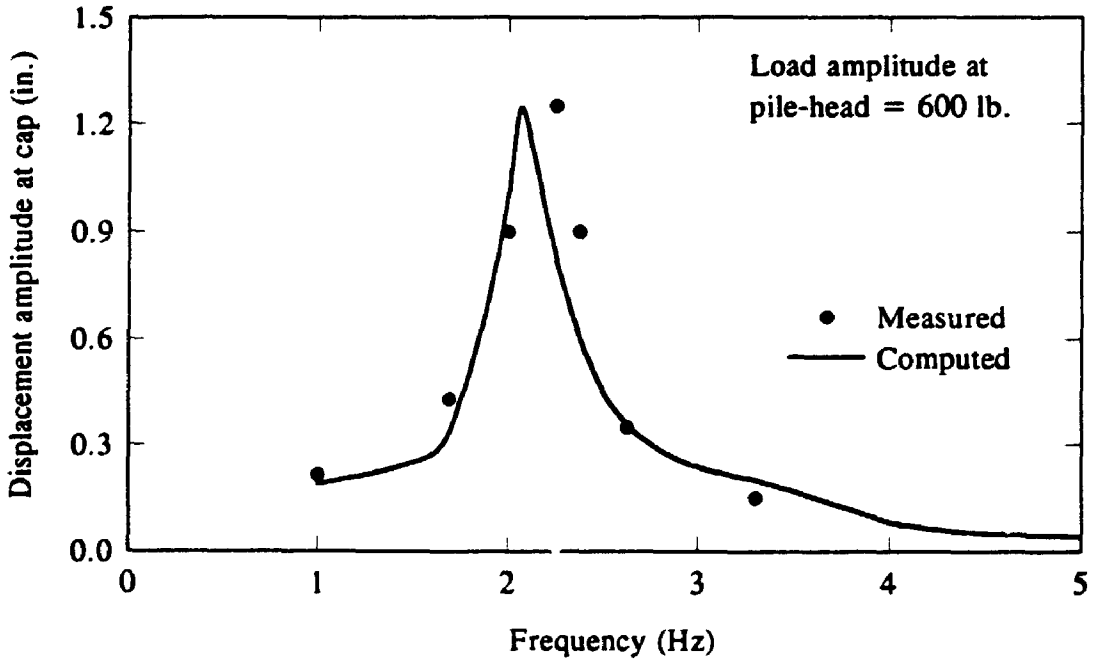

Figure 5.11 Computed and Measured Dynamic Pile Response

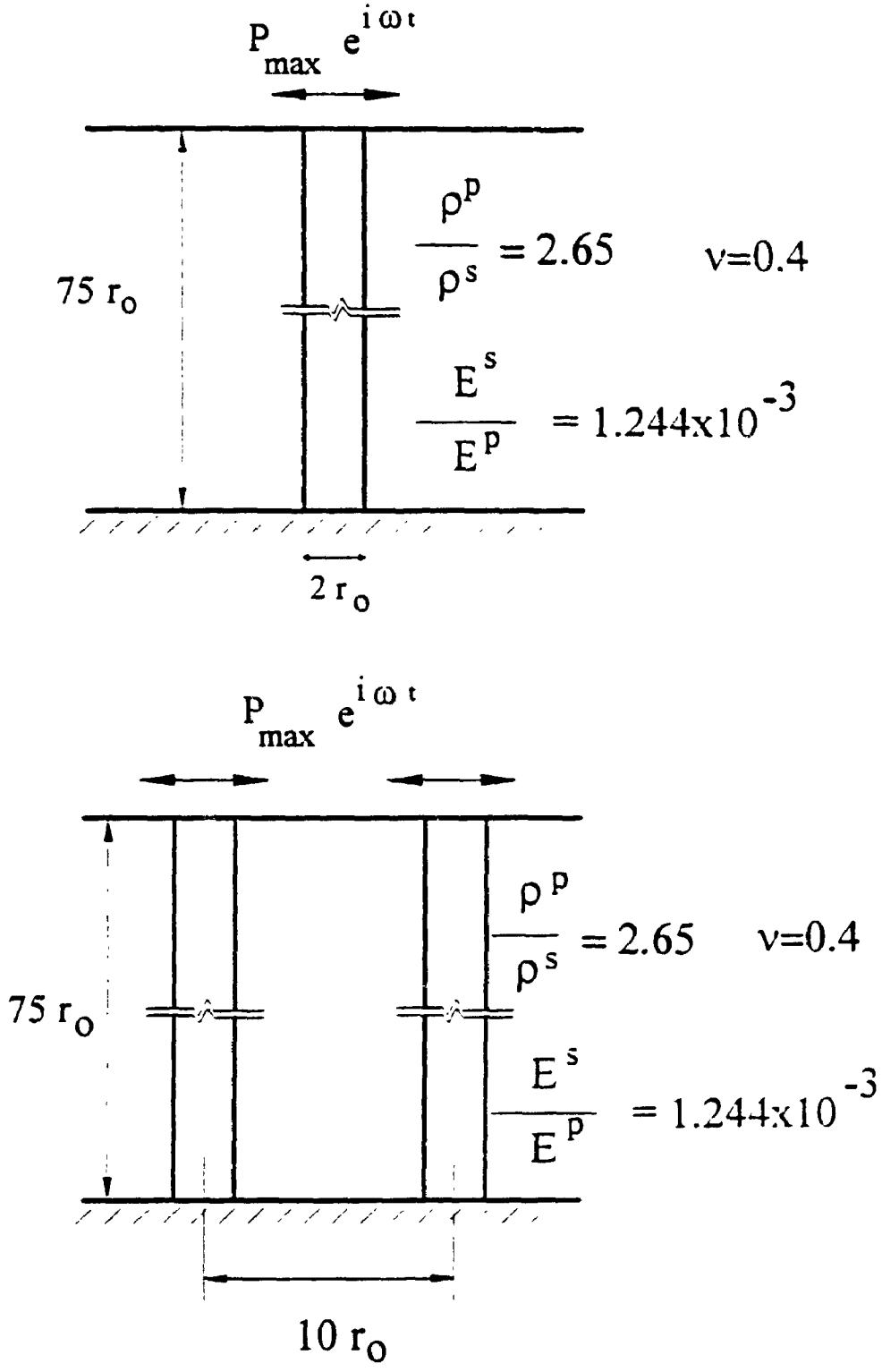

Figure 5.12 Soil Profile for the Example Used in the Comparison with More Rigorous Frequency Domain Solution (a) Single Pile (b) Group of 2 Identical Piles

computed using both approaches and plotted in Fig. 5.13 for the single pile case and Fig. 5.14 for the two-pile group. A very good agreement between the two results may be observed from the figures, especially for the single pile case.

5.6. Approximate Nonlinear Analysis for Pile Group Response

The proposed analytical model may be applied to analyze the response of the entire pile group, accounting directly for the non-linearity and the interaction between all piles simultaneously. Alternatively, the superposition approach may be used to approximate the group response. To approximately account for group nonlinearity in the analysis, the equivalent linear single pile parameters, as well as interaction factors, have to be established depending on the P/P_U ratio, where P_U is the ultimate bearing capacity of the pile as defined by Eqs. 5.3 through 5.6 and P is the amplitude of the applied harmonic load at the pile head. Definitions for the single pile flexibilities, to be used to get the relevant stiffnesses, and interaction factors for the lateral response case are shown in Fig. 5.15.

5.6.1. Single Piles

The stiffness and damping parameters of a single pile are computed for a steel pipe pile having an outer diameter of 1.45 m, a wall thickness of 0.05 m and a penetration depth of 50 m. Piles are assumed to be embedded in different soil profiles as shown in Fig. 5.16.

Because of the coupling effect between the horizontal and rotational stiffnesses of the pile, the complex flexibilities for the horizontal, coupling, and rotational cases are calculated first and then the 2 by 2 complex flexibility matrix is inverted to obtain the complex stiffness matrix of the pile. The real part of the complex stiffness matrix represents the stiffness and the imaginary part represents the damping.

The flexibility terms are defined, as depicted in Fig. 5.15, using a unit horizontal

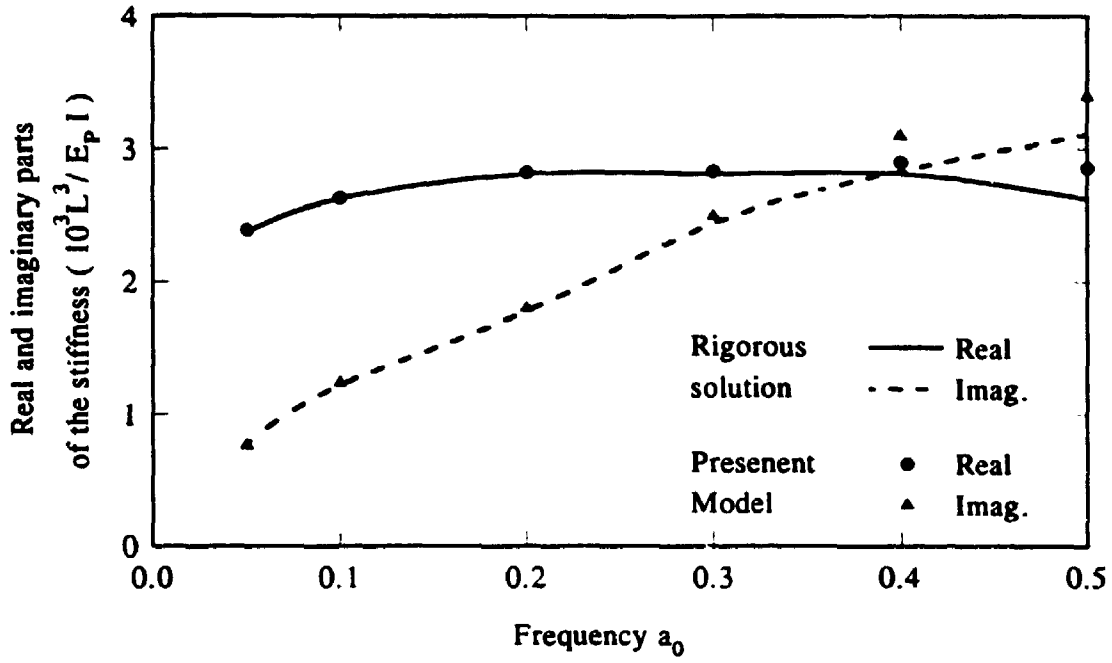

Figure 5.13 Complex Stiffness for a Single Pile

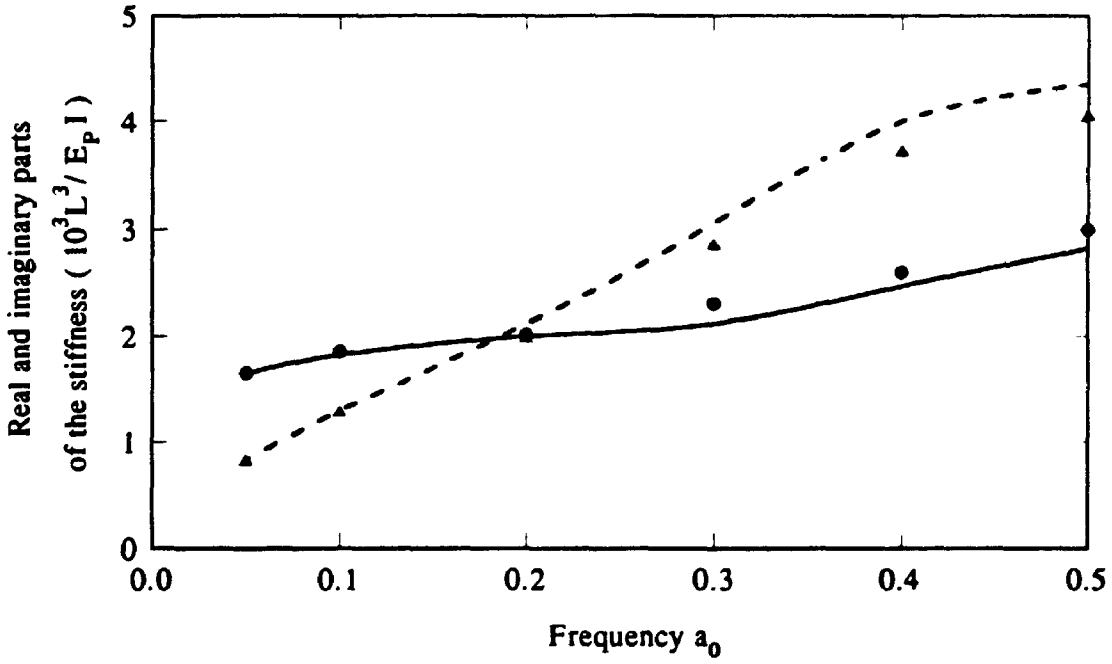

Figure 5.14 Comlex Stiffness for Two-Pile Group ($\theta = 0$)

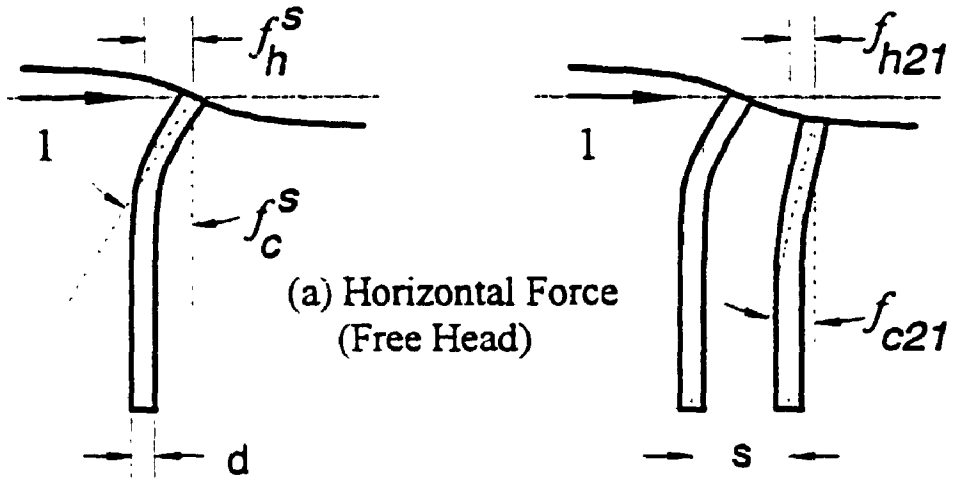

$$\alpha_h = \frac{f_{h21}}{f_h^s} \qquad \alpha_c = \frac{f_{c21}}{f_c^s}$$

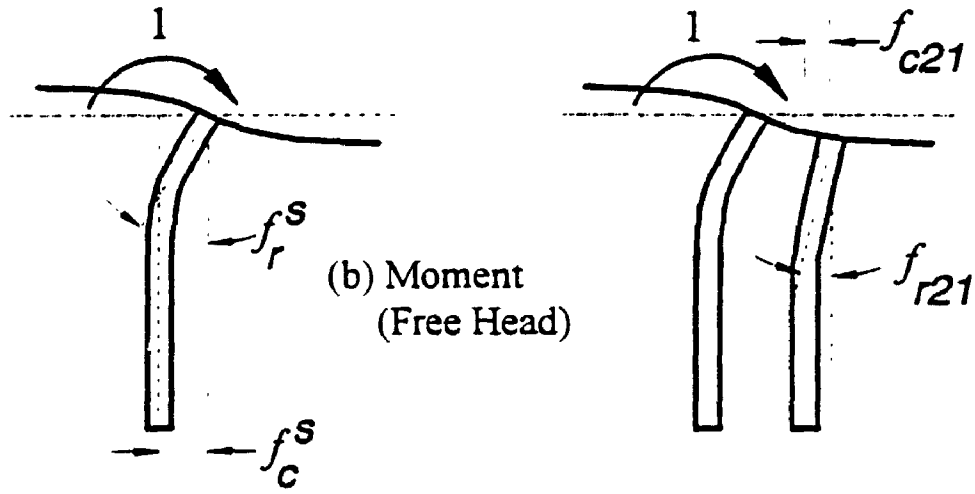

$$\alpha_r = \frac{f_{r21}}{f_r^s} \qquad \alpha_c = \frac{f_{c21}}{f_c^s}$$

Figure 5.15 Definition of Single Pile Flexibility Terms and Interaction Factors

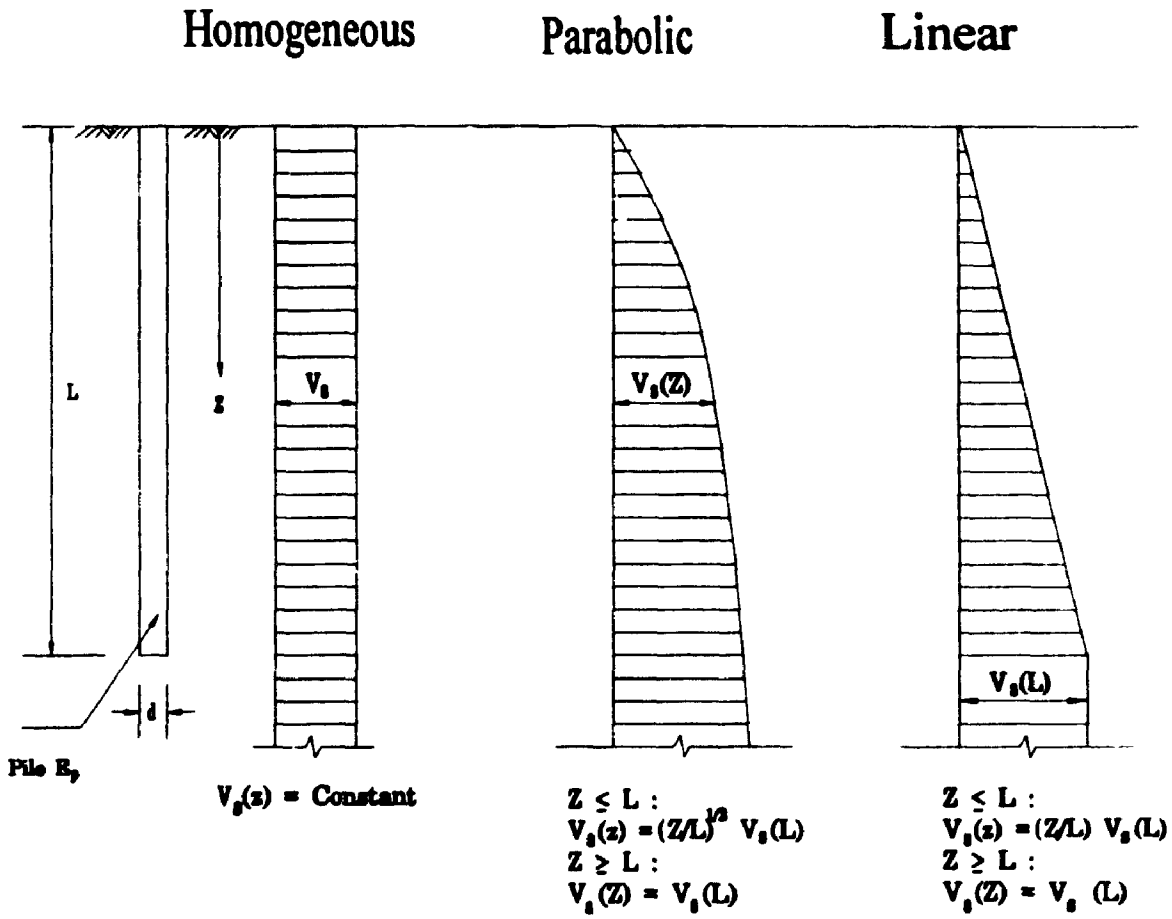

Figure 5.16 Definition of Soil Shear Wave Velocity Variation for Various Soil Profiles Considered in the Analysis

load or a unit moment at the pile head and then calculating the corresponding deflections at the pile head. The horizontal flexibility is the horizontal translation due to horizontal load, the rotational flexibility is the rotation due to moment, and the coupling flexibility is the rotation due to a horizontal load or a horizontal translation due to moment. To compute these flexibilities approximately accounting for the nonlinearity, a harmonic load, or moment, with amplitude P, or M, starting from zero is applied at the pile head and the response is then computed for a number of cycles until it stabilizes. The amplitude of the flexibility term, $|f_l|$, is approximated by the peak displacement divided by the amplitude of the applied load. The phase shift, ϕ_l, is approximated by the time lag between the peaks of both the displacement and load. The subscript l assumes different values for different flexibilities, i.e., h for horizontal, c for coupling and r for rotational. The figures displayed below show the variations of the equivalent linear stiffness and damping parameters for the horizontal, coupling and rotational cases with the loading ratio P/P_U.

Fig. 5.17 shows the stiffness and damping constants for the pile embedded in a homogeneous soil medium whose V_s = 100 m/s and excited with two different frequencies. The figure shows that as the loading ratio P/P_U increases, the horizontal and coupling stiffness constants decrease with mild slope until P/P_U =0.6; at this loading ratio the stiffness constants decrease dramatically until they reach one third of the linear case (P/P_U = 0.05). The damping constants also display the same behavior but they start decreasing at lower loading ratios. The decrease in the rotational stiffness is negligible up to P/P_U = 0.8 but the decrease in the damping is significant even at lower P/P_U ratios, especially for the higher frequency. To study the influence of the soil profile on the results, Figs. 5.18 and 5.19 show stiffness and damping constants for parabolic and linear soil profiles, respectively, each with a shear wave velocity $V_s(L)$ = 100 m/s. It may be observed from the two figures that as P/P_U increases, the horizontal and coupling stiffness constants decrease slowly , but as P/P_U exceeds 0.4, a dramatic

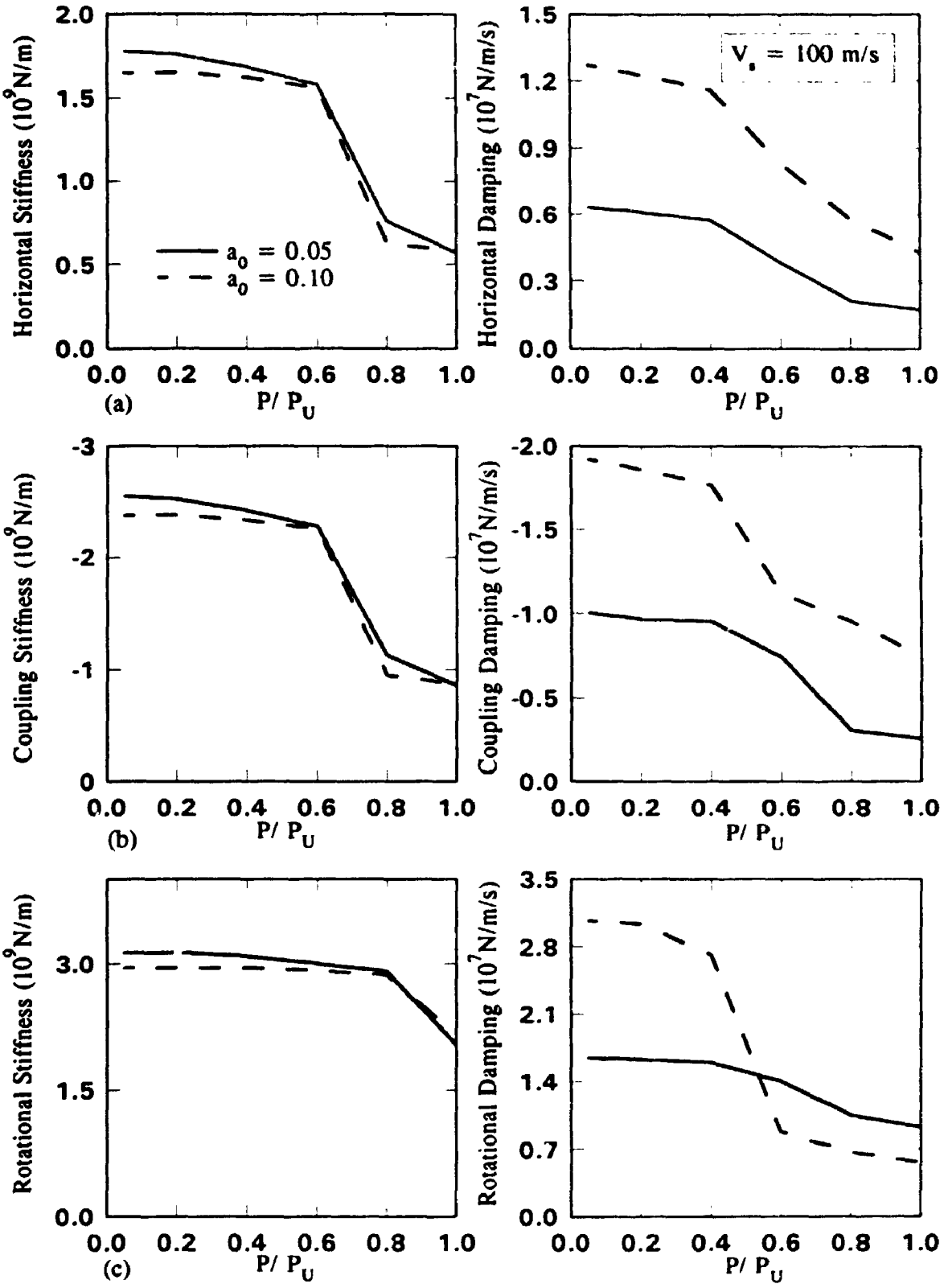

Figure 5.17 Equivalent Linear Stiffness and Damping for Single Piles in Homogeneous Soil Profile (a) Horizontal (b) Coupling (c) Rotational

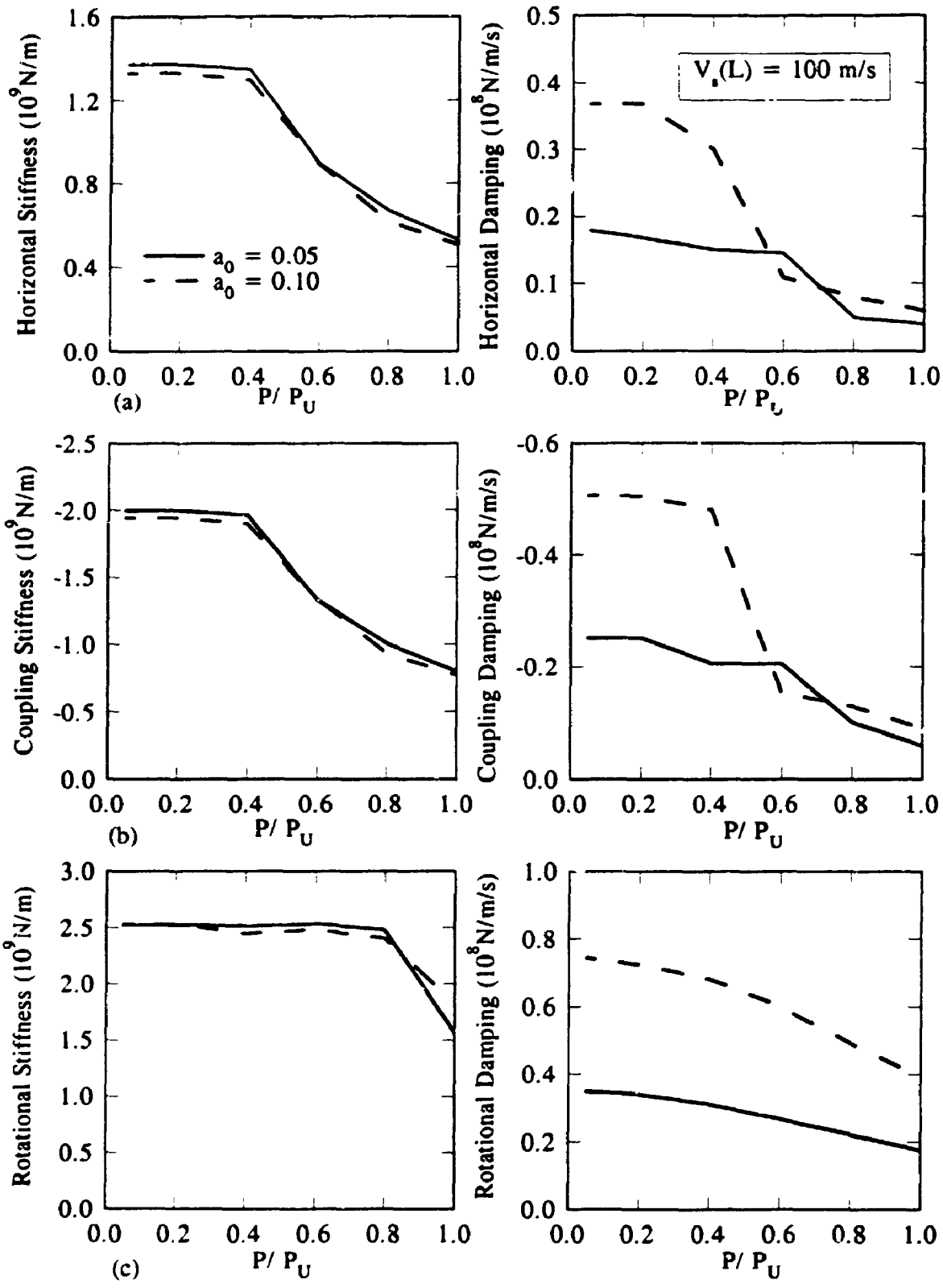

Figure 5.18 Equivalent Linear Stiffness and Damping for Single Piles in Parabolic Soil Profile (a) Horizontal (b) Coupling (c) Rotational

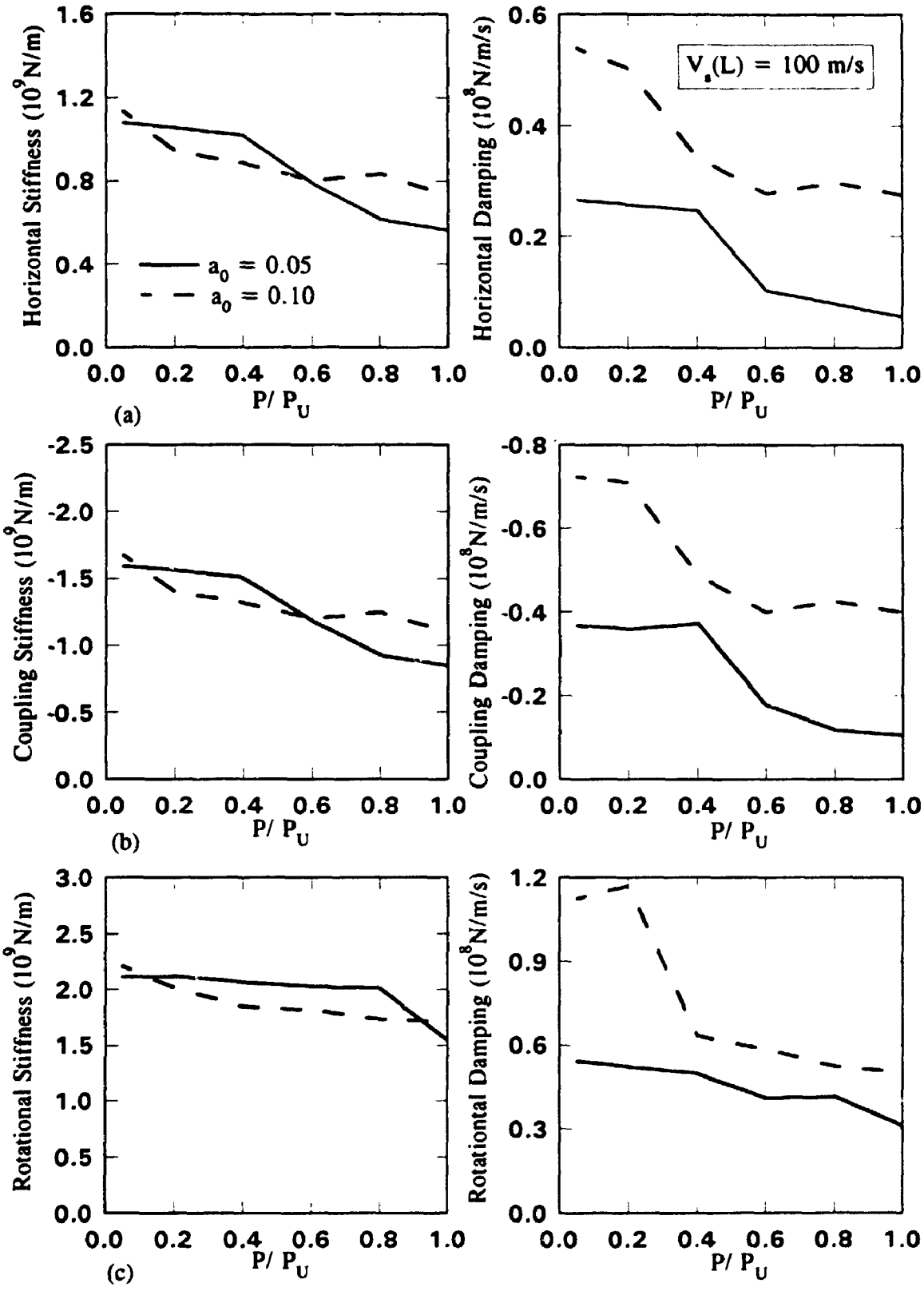

Figure 5.19 Equivalent Linear Stiffness and Damping for Single Piles in Linear Soil Profile (a) Horizontal (b) Coupling (c) Rotational

reduction in the stiffness occurs with no significant difference between the frequencies considered here. The drop in the damping is more pronounced at the higher frequency. This drop may be attributed to the diminishment of the radiation damping as a result of gapping. This radiation damping forms a larger portion of the total damping as the frequency increases. The decrease in the rotational constants is moderate. In Fig. 5.20 stiffness and damping constants for a parabolic soil profile with $V_s(L) = 200$ m/s are given to examine the effect of the shear wave velocity on the nonlinear behavior. It may be observed from the figure that a dramatic drop in the horizontal and coupling constants starts at P/P_U as low as 0.2. Stiffness constants become almost 40% of the linear case at $P/P_U = 0.4$, then the rate of the decrease becomes milder and the stiffness becomes as low as 28% of the linear case. Similar behavior is observed for damping, with a more pronounced drop in the damping for the higher frequency case. Also, the stiffness and damping of the rotational case have more pronounced nonlinear effects than the case of softer soil.

5.7.2. Interaction Factors

The interaction coefficients are needed to perform the group analysis using the superposition approach. To account approximately for the nonlinear effects in the lateral group analysis, the interaction factors should be established taking the load level and nonlinear conditions into consideration.

The equivalent linear interaction factor is defined as the displacement of a load-free pile normalized by the displacement of the loaded contiguous pile when no other piles are present (Fig. 5.15). To establish the equivalent linear interaction factors, two loading cases are considered separately: a pile loaded individually and a group of two identical piles with only one of them loaded. The resulting deflection at the pile head is

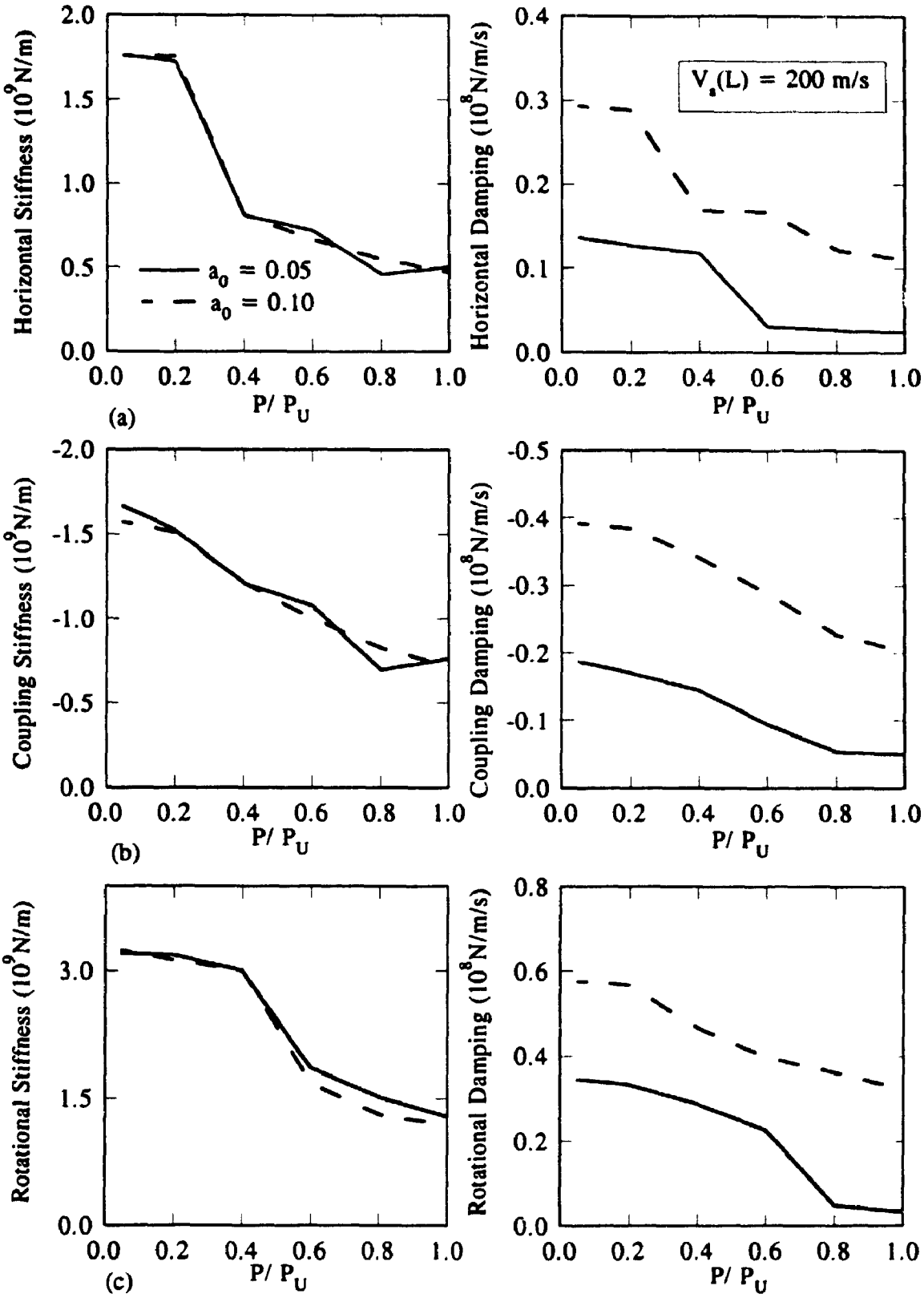

Figure 5.20 Equivalent Linear Stiffness and Damping for Single Piles in Parabolic Soil Profile (a) Horizontal (b) Coupling (c) Rotational

$$u_{lm}(t) = |u_{lm}|\, e^{i\phi_{lm}} \tag{5.31}$$

In eq. 5.31, $|u_l|$ is the amplitude, either in horizontal translation or rotation, approximated by the peak deflection, and ϕ_l is the phase shift, approximated by the time lag between the peaks of both the deflection and force. The subscript m takes the values 0 for the case of single pile loading and 1 for the load-free pile in the second case of loading. The loading starts from zero and the amplitude and phase shift are established after 5 loading cycles. The response was found to stabilize almost completely after this number of cycles. The interaction factor is defined as

$$\alpha_l = \frac{u_{ll}(t)}{u_{l0}(t)} \tag{5.32}$$

The dynamic interaction factor is a complex quantity which can be described either by its real and imaginary parts, α_1 and α_2, or in terms of its absolute value, $|\alpha|$, and phase shift, ϕ. Thus the interaction factor, α, may be written as

$$\alpha = \alpha_1 + i\,\alpha_2 = |\alpha|\, e^{i\phi} \tag{5.33}$$

The amplitude, $|\alpha_l|$, and the phase shift, ϕ_l, of the interaction factor resulting from Eq. 5.32 may be approximated by

$$|\alpha_l| = \frac{|u_{ll}|}{|u_{l0}|} \tag{5.34}$$

$$\phi_l = \phi_{ll} - \phi_{l0}$$

The equivalent linear dynamic interaction factors described by Eqs. 5.34 are plotted for a range of soil parameters in Figs. 5.21-5.28. Figs. 5.21 and 5.22 show the interaction factors for a pile embedded in homogeneous soil with shear wave velocity V_s = 100 m/s, for two pile to pile spacing to diameter ratios, s/d = 5 and 10, and two

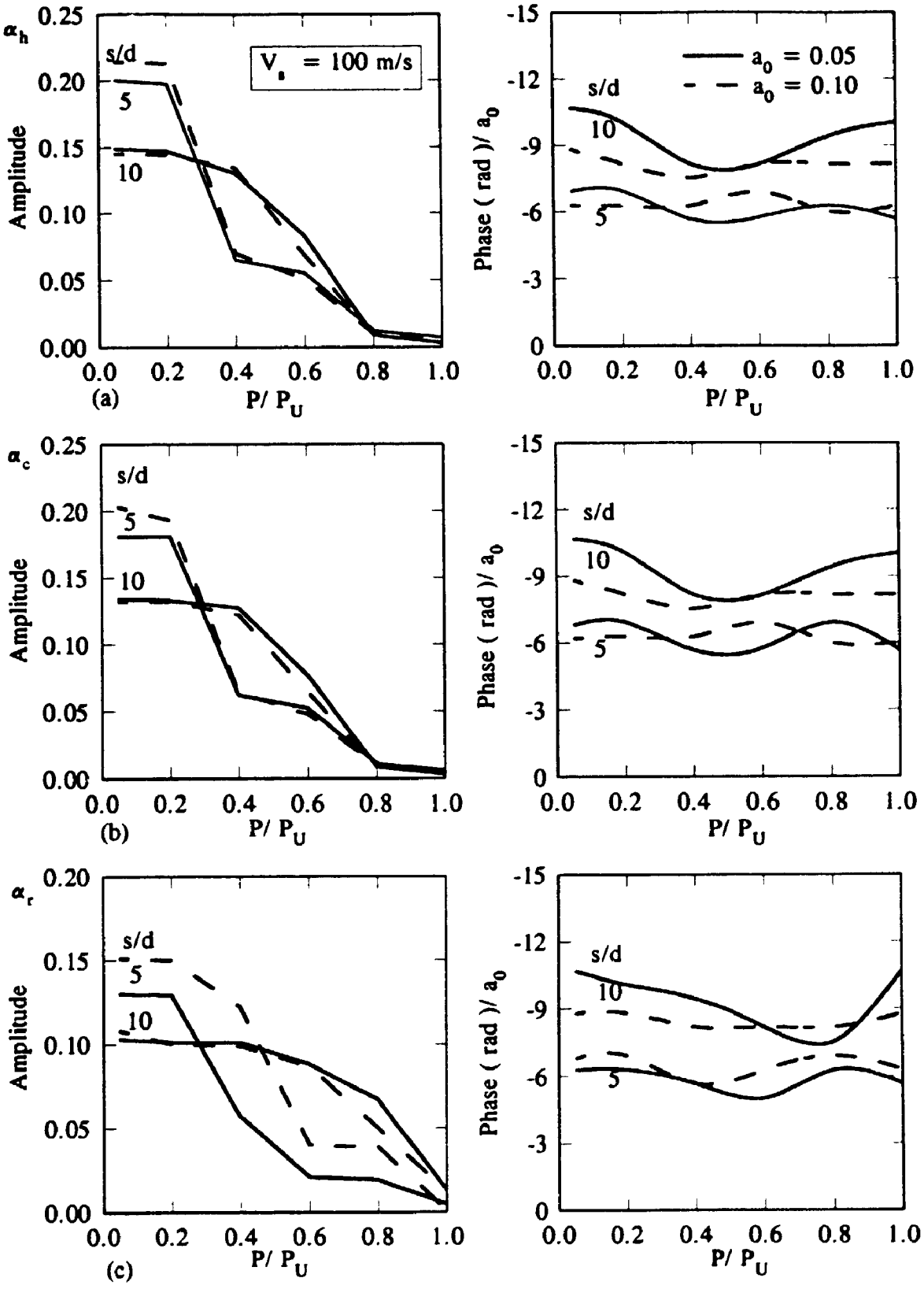

Figure 5.21 Dynamic Interaction Factors for Approximate Nonlinear Analysis for Piles in Homogeneous Soil (θ = 0) (a) Horizontal (b) Coupling (c) Rotational

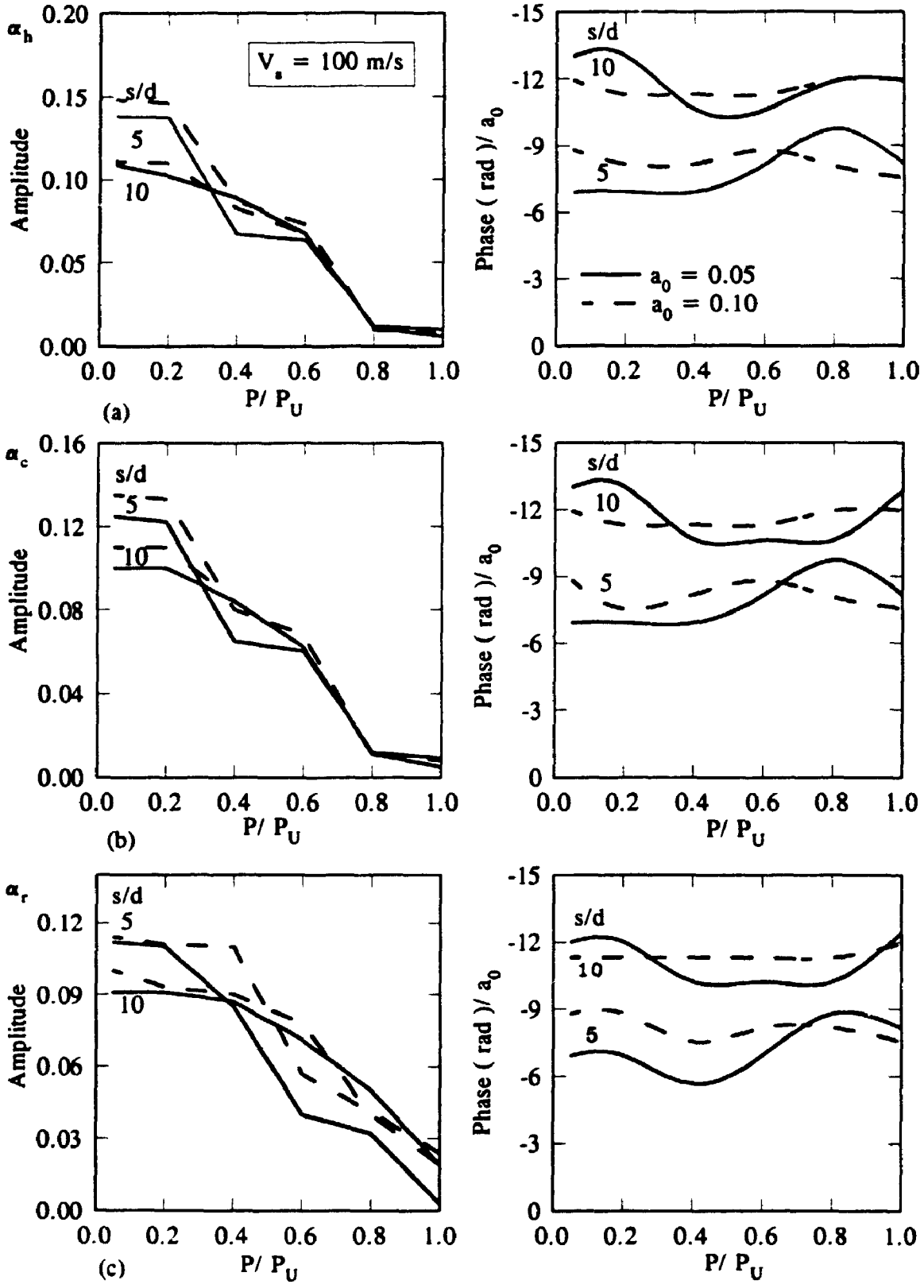

Figure 5.22 Dynamic Interaction Factors for Approximate Nonlinear Analysis for Piles in Homogeneous Soil (θ = 90) (a) Horizontal (b) Coupling (c) Rotaional

different frequencies for the angles $\theta = 0^0$ and 90^0, respectively. It may be observed from the figures that a dramatic decrease occurs in the amplitude as P/P_u starts increasing, for the horizontal, coupling and rotational cases. The phase shift oscillates, yet still could be considered constant.

To explore the nonlinear effects for different soil profiles, Figs. 5.23 and 5.24 present the equivalent linear interaction factors for a parabolic soil profile case and Figs. 5.25 and 5.26 for the linear soil profile case. These figures show that similar non-linearity effects take place in parabolic and linear soil media with the same observation regarding the phase shift.

To investigate the effect of the shear wave velocity on the nonlinear characteristics of interaction factors, Figs. 5.27 and 5.28 show the variation of interaction factors for a parabolic profile with $V_s(L) = 200$ m/s . Again, the same dramatic drop in the amplitude may be observed, while the phase shift oscillates about the initial linear value.

5.7. Conclusions

1- The lateral dynamic response computed using the proposed model compares favourably with field-measured data as well as the more rigorous frequency domain approach. The model uses only conventional soil mechanics parameters or parameters directly correlated to them.

2- Single pile stiffness and damping parameters as well as interaction between piles are greatly affected by the level of loading. Such an effect should be included in the analysis of the dynamic lateral response of pile groups particularly for strongly nonhomogeneous soil profiles and limit state considerations.

3- The effect of nonlinearity is that it reduces single pile and pile group stiffness as well as damping. Also, nonlinearity reduces the amplitude of interaction factors between piles, while the phase shift oscillates but still may be considered constant. These effects

are more pronounced for stiffer soils or softer piles such as those typical of offshore structures.

4- Finally, the model facilitates direct analysis of a pile group lateral response to dynamic loading with little computing effort and allows the generation of interaction factors for different loading ratios, different pile spacing to diameter ratios and different soil profiles. For a basic range of parameters, the nonlinear interaction factors are provided.

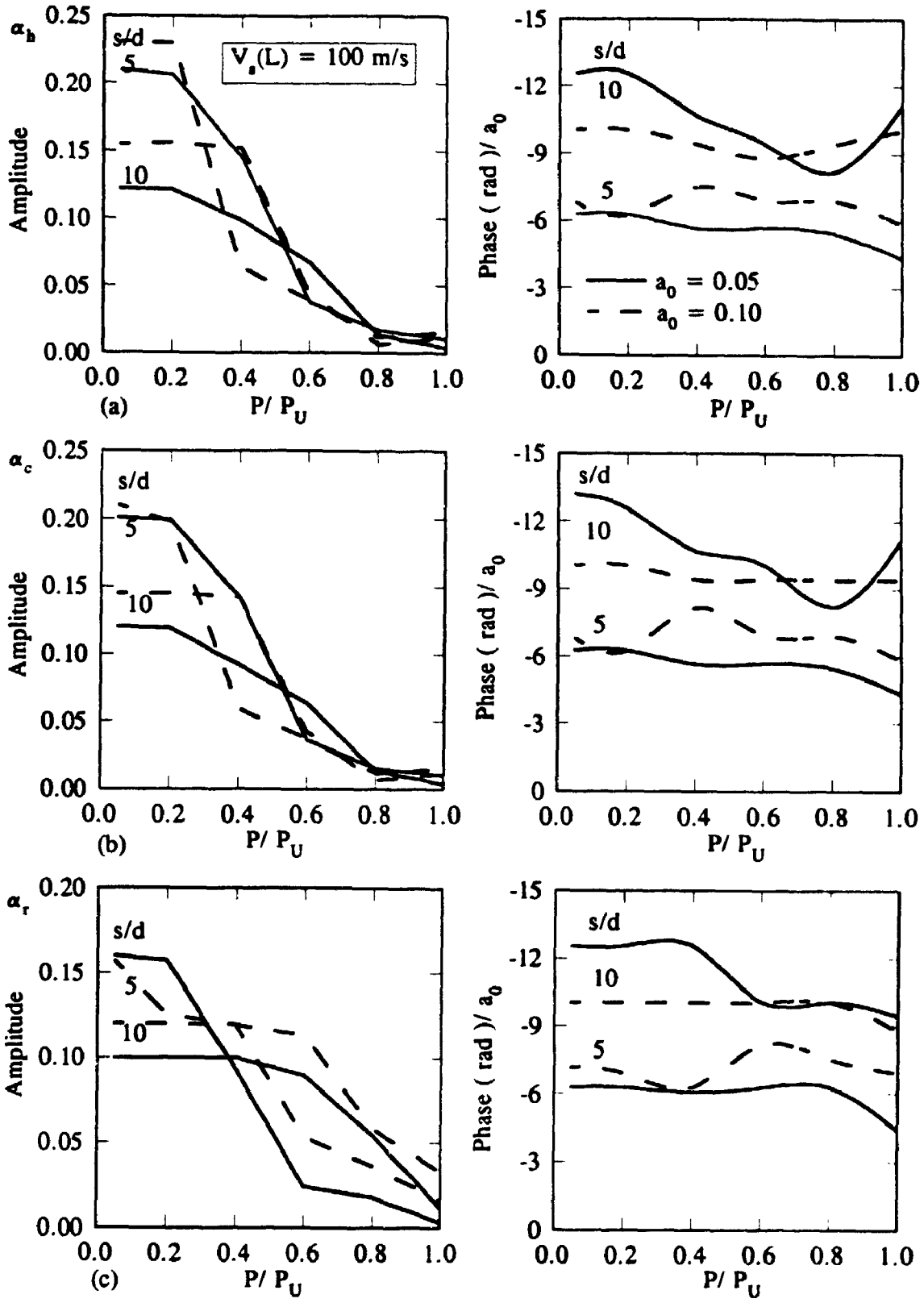

Figure 5.23 Dynamic Interaction Factors for Approximate Nonlinear Analysis for Piles in Parabolic Soil (θ = 0) (a) Horizontal (b) Coupling (c) Rotational

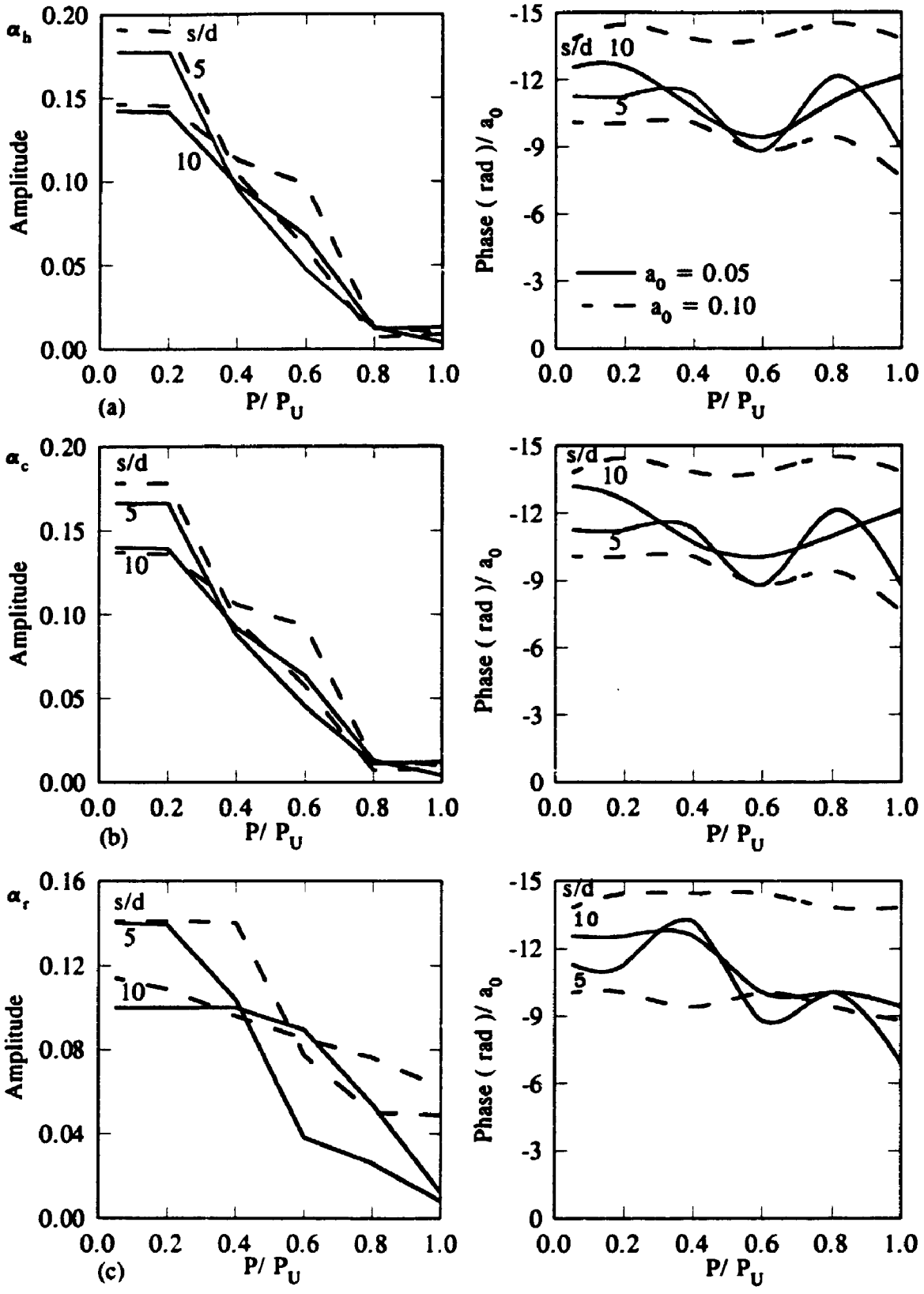

Figure 5.24 Dynamic Interaction Factors for Approximate Nonlinear Analysis for Piles in Parabolic Soil (θ =90) (a) Horizontal (b) Coupling (c) Rotational

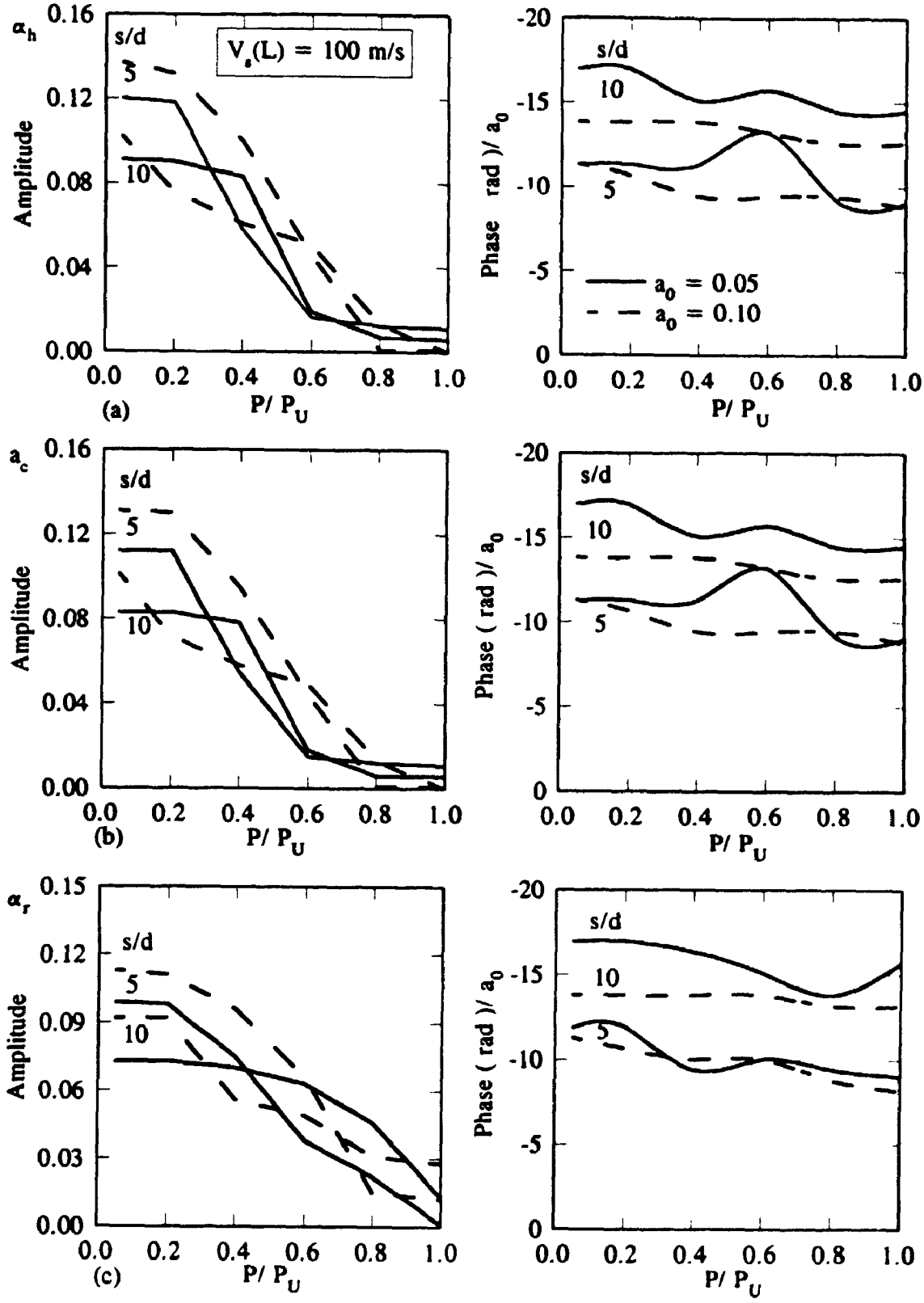

Figure 5.25 Dynamic Interaction Factors for Approximate Nonlinear Analysis for Piles in Linear Soil (θ = 0) (a) Horizontal (b) Coupling (c) Rotational

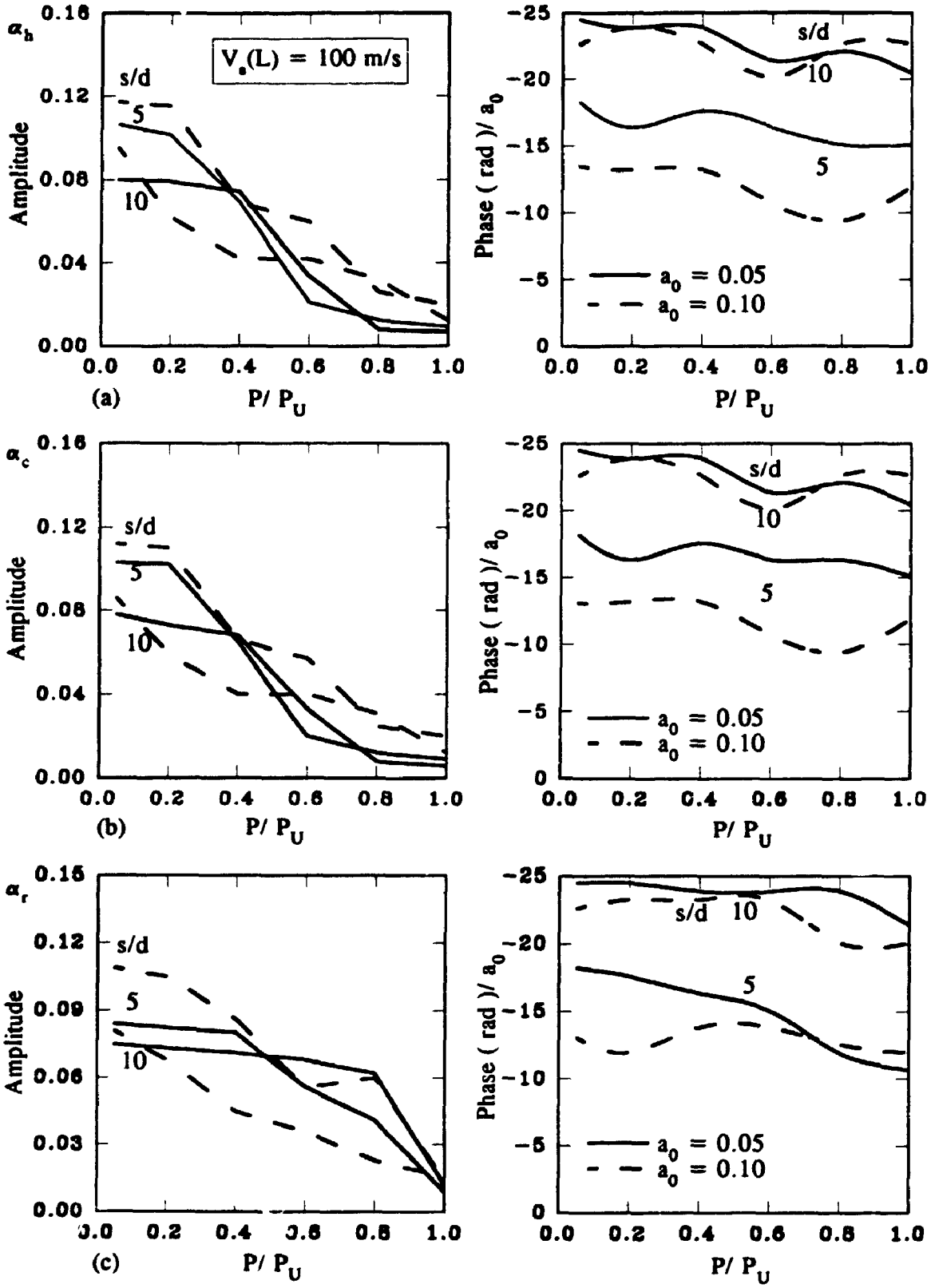

Figure 5.26 Dynamic Interaction Factors for Approximate Nonlinear Analysis for Piles in Linear Soil (θ = 90) (a) Horizontal (b) Coupling (c) Rotational

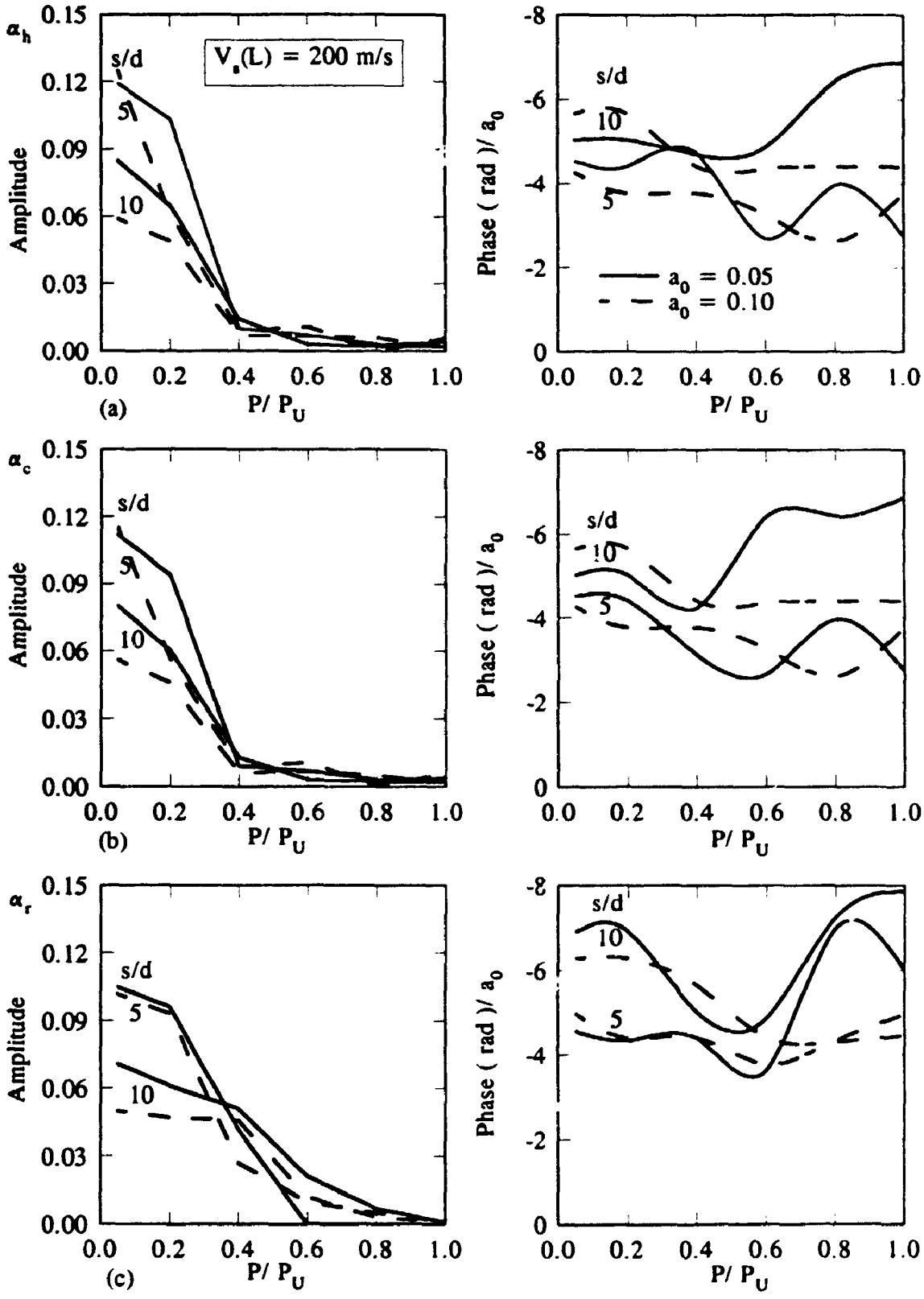

Figure 5.27 Dynamic Interaction Factors for Aproximate Nonlinear Analysis for Piles in Parabolic Soil (θ = 0) (a) Horizontal (b) Coupling (c) Rotational

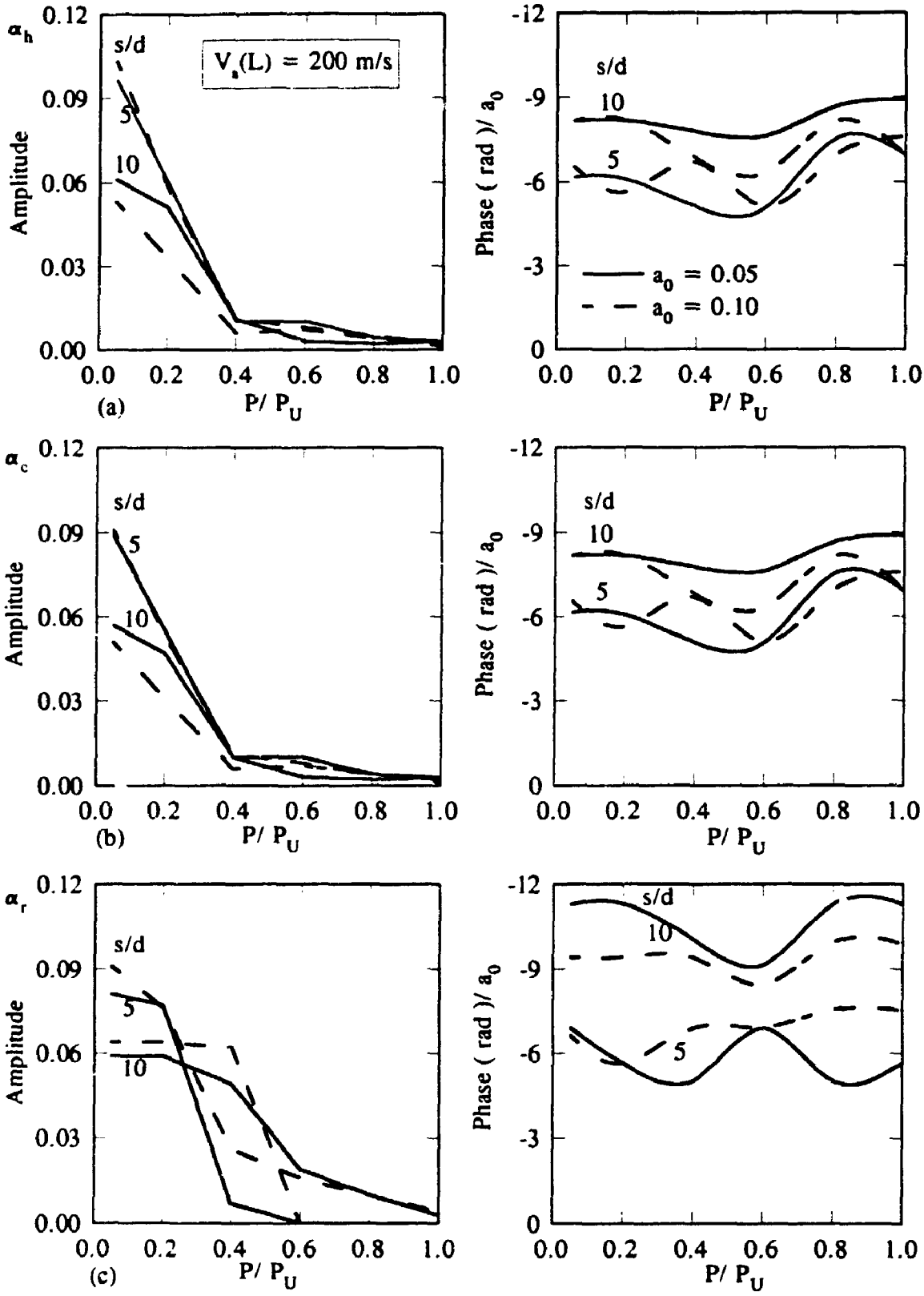

Figure 5.28 Dynamic Interaction Factors for Approximate Nonlinear Analysis for Piles in Parabolic Soil (θ = 90) (a) Horizontal (b) Coupling (c) Rotational

CHAPTER SIX
WAVE FORCES ON OFFSHORE STRUCTURES

6.1. Introduction

Ocean waves exhibit notably random behavior and as such, the resulting loads on offshore structures are random in nature. For that reason, prediction of the response of an offshore structure subjected to random waves forms an integral part of usual design procedure.

Water particle kinematics have to be evaluated in order to evaluate wave loads on a specific structure. In early attempts, wave kinematics were calculated adopting a regular wave concept. In this concept, for a given water depth,the flow is completely defined by wave height and period. This approach is inadequate to describe real ocean waves. Two other approaches are available; a time dependent deterministic model which is complex and has many boundary specifications, or stochastic model which considers statistical properties of the problem. The latter approach is more feasible and is implemented by treating the sea surface elevation as a random variable.

Wave forces exerted on bodies depend on the size of the body relative to the wave length. Morison's Equation is used to calculate wave loads on small bodies, while for large bodies diffraction theory is used to calculate wave loads.

In this chapter, a review of wave loading on offshore structures and the important parameters affecting it are given. Two approaches for modelling the wave directionality are discussed. These are the directional spectrum model and the coherence function model.

6.2. Review of Wave Loading

Regular wave theories describe waves which are periodic in time and space, and have a symmetric rigid profile. The linear theory (Airy theory) is a simple approach that

overcomes the problem of the nonlinear free surface boundary condition by assuming waves of infinitesimal steepness. The resulting wave is a simple harmonic progressive wave with a closed elliptical water particle path. The wave phase speed v_c is related to the spatial, κ, and temporal, ω, frequencies as

$$\omega^2 = g\kappa \tanh(\kappa D)$$
$$v_c = \frac{g}{\kappa} \tanh(\kappa D) \qquad (6.1)$$

where g is the acceleration due to gravity and D is the water depth, Fig. 6.1. The linear wave theory is very important in offshore engineering because it is simple and is valid for all water depths as opposed to other wave theories. It is also essential for the statistical treatment of random waves. Nonlinear approximations have also been adopted and may be found in detail in Philips [84]. Nonlinear wave theories are important for pseudo-deterministic analysis of extreme loading conditions.

Irregular wave theories describe waves which are not periodic in time or space. Sub-surface kinematics are related to the completely prescribed surface profile. Linear irregular waves are based mainly on a Fourier analysis of the prescribed surface profile to determine amplitudes and phases of harmonic components followed by a linear superposition of a number of linear Airy waves [85].

Wave forces on bodies depend on the body size. The presence of a cylinder causes wave scattering and disturbance of the flow field. For $d/\lambda > 0.2$ (λ = wave length), the velocity and acceleration of the flow can not be considered constant over a distance equal to the cylinder diameter, d. Diffraction analysis in this case is important and the total force is determined by integrating the pressure evaluated from the superposition of the undisturbed pressure field and the pulsating pressure resulting from the disturbance of the flow field.

Morison's Equation [86] applies to cylinders of $d/\lambda < 0.2$ assuming that velocities and accelerations are constant over distances equal to the member diameter.

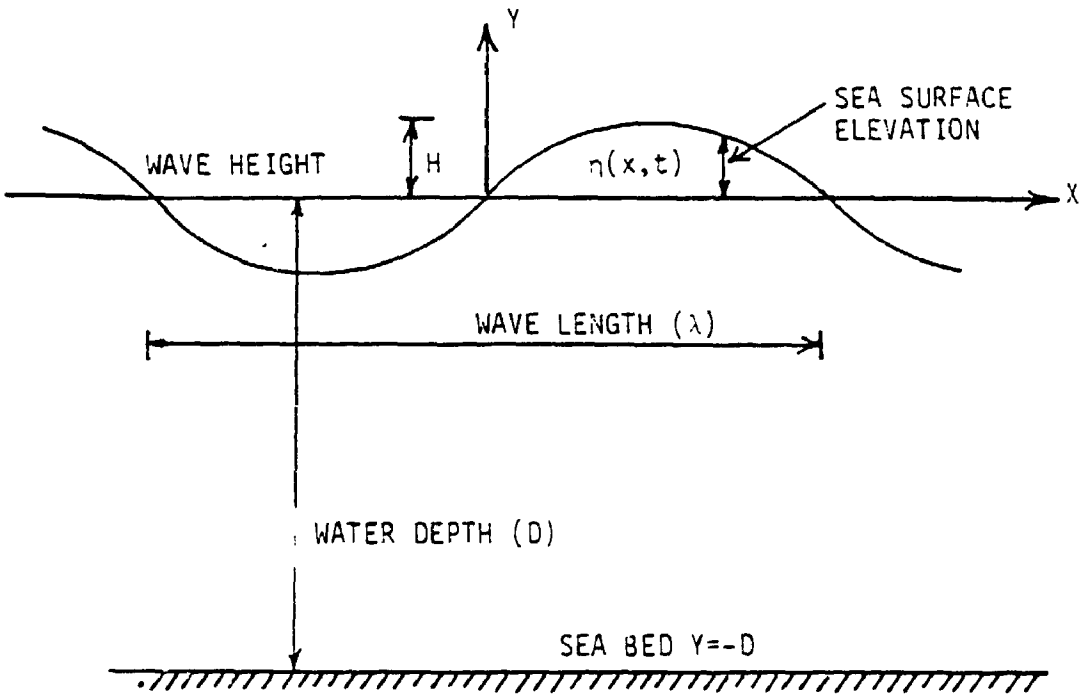

Figure 6.1 Definition Diagram for Wave Parameters

In such cases, both drag and inertia effects are important and the total horizontal fluid force, F, acting on a unit length of a fixed rigid cylinder is given by

$$F = \frac{1}{2}\rho C_D d\, \dot{v}|\dot{v}| + \rho \pi \frac{d^2}{4} C_M \ddot{v} \tag{6.2}$$

where ρ = fluid density, $\dot{v}$ and $\ddot{v}$ are the fluid velocity and acceleration components perpendicular to the cylinder axis, respectively. C_D and C_M are drag and inertia coefficients. A wide scatter of experimentally obtained C_D and C_M values have been reported by most investigators [87].

The drag term in Morison's Equation is nonlinear and has to be linearized to allow for statistical representation of random wave forces. An equivalent linearization technique is used to linearize it [88].

The directional spectrum model is used to describe the sea surface elevation resulting in the reduction of the along wave forces and the prediction of lateral forces [89]. Another approach may be used to model the spatial incoherence of waves. This model, called coherence function model, allows for the reduction of the along wave forces through a coherence function [90].

In the current study, the linear wave theory is employed to enable the statistical representation of random waves. Wave forces are evaluated using the modified Morison's Equation which takes into account the motion of the cylinder [91], by the equation

$$F = \frac{1}{2}\rho C_D d\,|\dot{v} - \dot{u}|(\dot{v} - \dot{u}) + \rho \pi \frac{d^2}{4}[C_M \ddot{v} - (C_M - 1)\ddot{u}] \tag{6.3}$$

where $\ddot{u}$ and $\dot{u}$ are the acceleration and velocity of the cylinder, respectively. The linearized form of the drag force based on the linearization technique is used in this study. For a flexible cylinder, the linearized drag force is given by

$$(\dot{v} - \dot{u})\,|\dot{v} - \dot{u}| = \sqrt{8/\pi}\ \sigma_{\dot{r}}\,(\dot{v} - \dot{u}) \tag{6.4}$$

where $\dot{r} = \dot{v} - \dot{u}$ is the relative velocity between the water particle and the cylinder, and $\sigma_{\dot{r}}$ is the standard deviation of this relative velocity.

6.3. Spectral Density of Water Particle Kinematics

In the current study, random waves are represented as a stationary Gaussian process. In this model, the sea surface elevation above mean sea level h(x,t) is represented as a sum of many sinusoidal components with different amplitudes and phase angles. For a unidirectional wave system propagating in the X direction, h(x,t) is given by [92]

$$h(x,t) = \sum_{n=1}^{N} c_n \cos(\kappa_n x - \omega_n t + \varepsilon_n) \tag{6.5}$$

where a_n is the amplitude of the n^{th} harmonic component whose frequency and wave number are ω_n and κ_n , respectively, and ϵ_n is a statistically independent random phase angle associated with the n^{th} wave. The mean square value of the n^{th} harmonic component is $a^2_n/2$ and is equal to $S_{hh}(\omega_n)\,\Delta\omega$, where $S_{hh}(\omega_n)$ is the one sided power spectral density of sea surface elevation. Accordingly

$$a_n = \sqrt{2\,S_{hh}(\omega_n)\,\Delta\omega} \tag{6.6}$$

If the number of harmonic terms N approaches ∞, $\Delta\omega \to \omega_n$, $\omega_n \to \omega$ and $S_{hh}(\omega_n)$ is replaced by the continuous spectrum $S_{hh}(\omega)$. Eq. 6.5 becomes

$$h(x,t) = \int_0^{\infty} \cos(\kappa x - \omega t + \varepsilon)\sqrt{2S_{hh}(\omega)\,d\omega} \tag{6.7}$$

Eq. 6.7 represents unidirectional long crested random waves which is suitable for modelling a swell travelling at some distance from a storm. For a storm generating area,

a more confused sea with short crested waves is more likely to occur and other model has to be used to include the wave directionality.

6.3.1 Power Spectrum of Sea Surface Elevation

Waves grow due to wind, from regular long crested waves to irregular short crested ones. This growth continues with time or fetch until a fully developed sea is attained. The wave spectrum also grows and the spectral peak frequency shifts towards successively lower frequency with an increase in spectral energy.

6.3.1.1. Unidirectional Spectrum (Frequency Spectrum)

There are many spectra specified for either fully or partially developed seas. Spectra for fully developed seas are expressed in terms of a reference mean wind speed, at 19.5 m above the mean sea level, $\bar{U}$, as the only parameter. The spectrum used in this study is from this category. This spectrum, known as Pierson-Moskowitz Spectrum [93], is written as

$$S_{hh}(\omega) = \frac{\alpha g^2}{\omega^5} e^{-0.74(\bar{\omega}/\omega)^4} \tag{6.8}$$

where $\alpha = 8.1 \times 10^{-3}$, g is the acceleration due to gravity and $\bar{\omega} = g / \bar{U}$. This spectrum is shown in Fig. 6.2. Spectra for partially developed seas account for fetch or fetch and duration.

6.3.1.2. Directional Spectrum

The directional spectrum may be expressed in the form

$$S_{hh}(\omega, \theta) = S_{hh}(\omega) G(\omega, \theta) \tag{6.9}$$

where $G(\omega,\theta)$ is a directional spread function which represents the distribution of wave

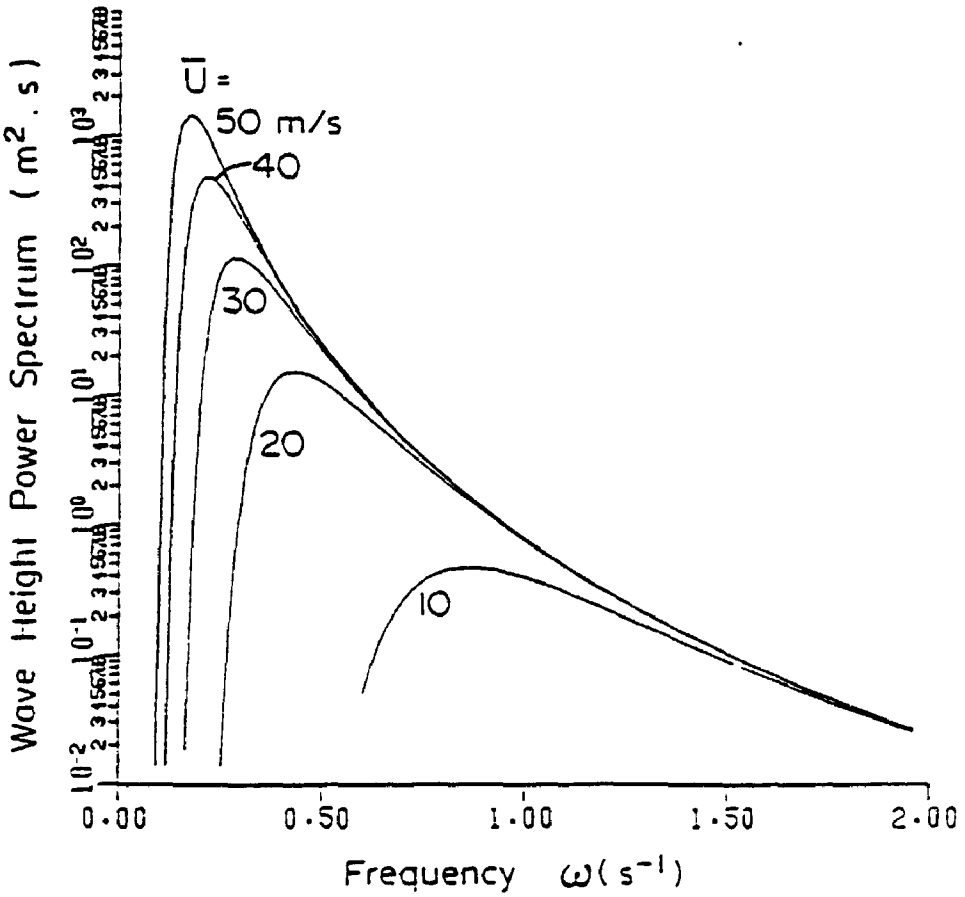

Figure 6.2 Pierson-Moskowitz Spectrum of Sea Surface Elevation

energy among waves progressing in different directions. The directional spread function is always positive and is symmetric about the mean direction of wave advance $\overline{\theta}$. There are many spread functions, one of them is the circular normal directional spreading function given by Borgman [94] as

$$G(\theta) = \frac{1}{2\pi I_0(a)} e^{a\cos(\theta - \overline{\theta})} \qquad (6.10)$$

where I_0 is the modified Bessel function of the first kind of order zero and a expresses the degree of spread; higher values of the parameter a indicate higher concentration about $\overline{\theta}$.

6.3.2. Water Particle Kinematics Spectra

Spectra of water particles kinematics are derived based on the stationary Gaussian model of random waves. A general expression for the cross spectrum of water particles velocities in a directional wave system is presented. Also the spectrum of a unidirectional wave system is given. An alternative representation of the water particle kinematics based on the use of a coherence function is then introduced. This latter model is employed to evaluate wave forces on cylindrical members of offshore towers.

6.3.2.1. Directional Spectrum Model

At each frequency, the surface elevation consists of a number of harmonic waves progressing in different directions. Each one of these waves contributes to sea surface elevation. Using Airy wave theory, the horizontal velocity of water particles at any depth is related to the sea surface elevation. The cross spectrum of water particle velocities at any two points is obtained from their cross correlation function by subjecting it to Fourier transform. The general expression for the cross spectrum of a directional wave system as derived by Berge [95] is

$$S_{\dot{v}_1\dot{v}_2} = \omega^2 \frac{\bar{S}_{hh}(\omega)}{\sinh^2 \kappa D} HYP1[\kappa(y1 + D)]\, HYP2[\kappa(y2 + D)]$$
$$\int_{\pi}^{-\pi} G(\omega,\theta)\, C1(\theta)\, C2(\theta) e^{i\kappa[(x1-x2)\cos\theta + (z1-z2)\sin\theta]}\, d\theta \tag{6.11}$$

where

$$C1(\theta) = \begin{cases} \cos\theta & for\ \ 1 \mathbin{/\!/} X \\ \sin\theta & for\ \ 1 \mathbin{/\!/} Z \\ 1 & for\ \ 1 \mathbin{/\!/} Y \end{cases} \tag{6.12}$$

in which $1 /\!/ X$ indicates velocity component at point 1 to be in the X direction. $C2(\theta)$ is similarly defined for the velocity component at point 2. Finally,

$$HYP1[\kappa(y1 + D)] = \begin{cases} \cosh[\kappa(y1 + D)] & for\ 1 \mathbin{/\!/} X\ or\ Z \\ -i \sinh[\kappa(y1 + D)] & for\ 1 \mathbin{/\!/} Y \end{cases} \tag{6.13}$$

and

$$HYP2[\kappa(y2 + D)] = \begin{cases} \cosh[\kappa(y2 + D)] & for\ 2 \mathbin{/\!/} X\ or\ Z \\ -i \sinh[\kappa(y2 + D)] & for\ 2 \mathbin{/\!/} Y \end{cases} \tag{6.14}$$

Cross spectral densities of water particle accelerations can be obtained from those of velocities, i.e.

$$S_{\dot{v}_1\dot{v}_2}(\omega) = i\,\omega\, S_{\dot{v}_1\dot{v}_2}(\omega) = S^*_{\dot{v}_1\dot{v}_2}(\omega) \tag{6.15}$$

and

$$S_{\dot{v}_1\dot{v}_2}(\omega) = \omega^2 S_{\dot{v}_1\dot{v}_2}(\omega) \tag{6.16}$$

in which the asterisk means the complex conjugate.

The general expression for cross spectra of water particle velocities of a

unidirectional fully correlated wave system progressing in a mean direction that makes an angle $\bar{\theta}$ with the X axis is

$$S_{v_1 v_2} = \omega^2 \frac{\bar{S}_{hh}(\omega)}{\sinh^2 \kappa D} HYP1[\kappa(y1 + D)]\, HYP2[\kappa(y2 + D)]$$
$$C1(\bar{\theta})\, C2(\bar{\theta}) \exp\{i\kappa[(x1 - x2)\cos\bar{\theta} + (z1 - z2)\sin\bar{\theta}]\} \qquad (6.17)$$

In Eq. 6.17, C1(θ) and C2(θ) are given by Eq. 6.12 with θ substituted by $\bar{\theta}$, and HYP1[κ (y1 + D)] and HYP2[κ(y2 + D)] are given by Eqs. 6.13 and 6.14, respectively.

6.3.2.2 Coherence Function Model

The main feature of the directional model is that the along wave force on any member of the tower is less than that of a unidirectional wave system having the same total energy because a portion of this total energy produces lateral forces. Another reason for the reduction in the along wave forces is that the wave forces are not in phase along the entire length of the member. This second factor is termed the lack of spatial correlation and has been briefly discussed by Malhorta and Penzien [88].

The cross spectra of water particle velocity of the unidirectional fully correlated model, is widely used and is expressed by Eq. 6.17. For example, in the X direction, Eq. 6.17 takes on the form

$$S_{v_{x1} v_{x2}} = \omega^2 \frac{\bar{S}_{hh}(\omega)}{\sinh^2 \kappa D} \cosh\kappa(y1 + D) \cosh\kappa(y2 + D)$$
$$\cos^2\bar{\theta} \exp\{i\kappa[(x1 - x2)\cos\bar{\theta} + (z1 - z2)\sin\bar{\theta}]\} \qquad (6.18)$$

For short crested waves, the amplitude of the cross spectrum of wave forces attenuates with increased separation. Novak and Mitwally [96] accounted for this attenuation through a coherence function to model the lack of spatial correlation. The cross spectrum of water particle velocity is then given by

$$S_{v_1 v_2}(\omega) = \left\{ S_{v_1 v_2}(\omega)_{\text{fully correlated}} \right\} R \tag{6.19}$$

where R is the square root of the coherence function and is given by

$$R = e^{-c\frac{\Delta r}{\lambda}} \tag{6.20}$$

in which, c is an exponential decay factor and Δr is the absolute value of the distance between the 2 points. The exponential decay factor may be determined from laboratory experiments or from full scale measurements.

6.4. Wave Forces on Members of Offshore Towers

The spectra of wave forces on a typical joint of an offshore structure can be computed from cross spectral densities of water particle velocities and accelerations.

Fig. 6.3 shows an offshore tower idealized as a space frame. The coordinate system is also shown in the figure, where X, Y and Z are the global axes and x,y and z are the global coordinates. The rotational degrees of freedom are eliminated using static condensation, and only 3 translational d.o.f. are retained at each joint. Let d.o.f. i be positioned at node n at which N_n members meet. The modified Morison's Equation, Eq. 6.3, is used to evaluate the wave force $W_i(t)$ acting on the structure corresponding to d.o.f. i. The drag and inertia coefficients are assumed to be constant. Also velocities and accelerations are taken to be constant along the tributary length and equal to their values at the nodes. Finally, the drag term is linearized using Eq. 6.4. With these assumptions, $W_i(t)$ is given as

$$\begin{aligned} W_i(t) = \sum_{k=1}^{N_n} \Gamma_k \Bigg[\int_0^{L_k} \left\{ \rho \pi \frac{d_k^2}{4} C_M \dot{v}(S_k,t) + \frac{1}{2} \rho d_k C_D \sqrt{8/\pi}\, \sigma_{\dot{r}_i}\, \dot{v}(S_k,t) \right\} dS_k \\ - \rho \pi \frac{d_k^2}{4} (C_M - 1) L_k \ddot{u}_i(t) - \frac{1}{2} \rho d_k C_D \sqrt{8/\pi}\, \sigma_{\dot{r}_i} L_k \dot{u}_i(t) \end{aligned} \tag{6.21}$$

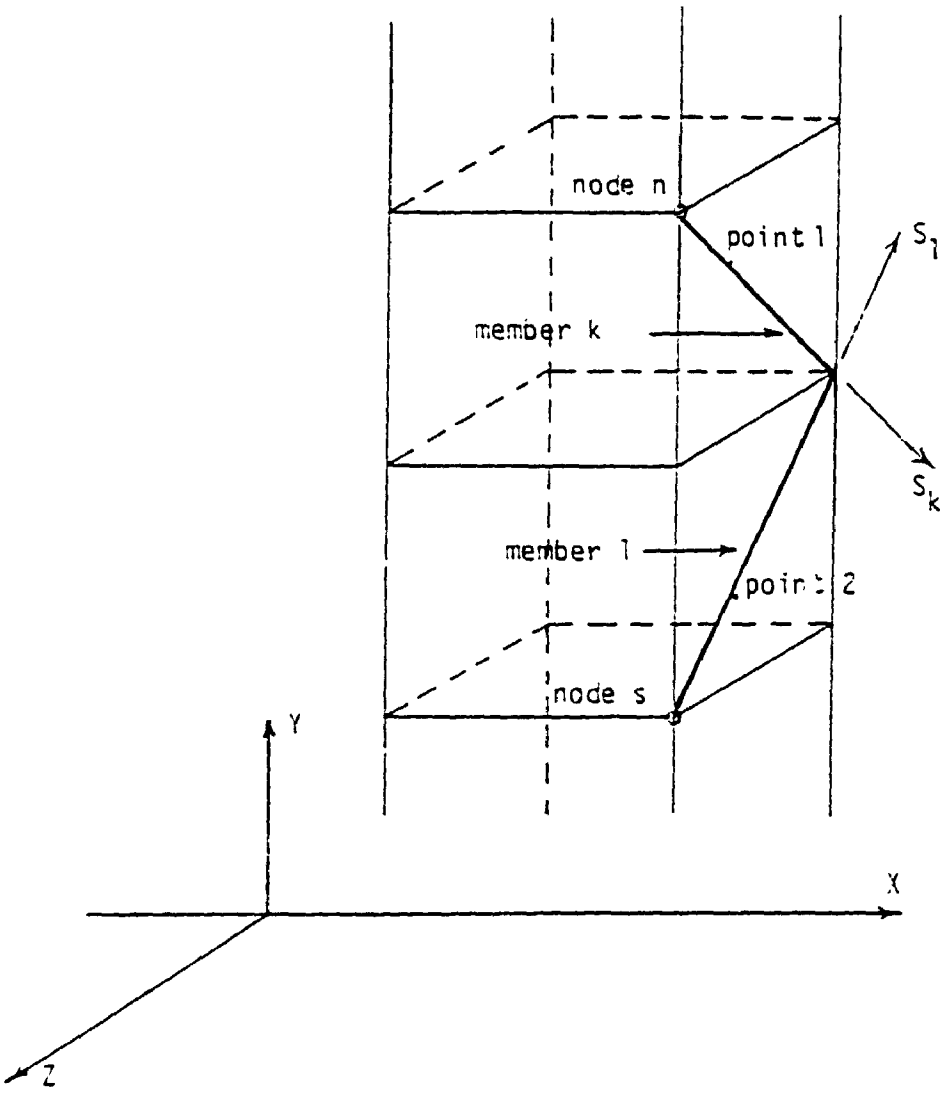

Figure 6.3 Coordinate System for Offshore Tower

In Eq. 6.21, $\sigma_{\dot{z}_i}$ is the standard deviation of the relative velocity, associated with d.o.f. i, between the water particle and the structure. L_k and d_k are the tributary length and diameter of member k, respectively. S_k is its element coordinate and Γ_k is given as

$$\Gamma_k = \begin{cases} \sqrt{q_k^2 + r_k^2} & \text{for } i \parallel X \\ \sqrt{p_k^2 + r_k^2} & \text{for } i \parallel Y \\ \sqrt{p_k^2 + q_k^2} & \text{for } i \parallel Z \end{cases} \tag{6.22}$$

where p_k, q_k and r_k are the direction cosines of the k^{th} member with axes X, Y and Z, and given by

$$\begin{aligned} p_k &= (x - x_n)/S_k \\ q_k &= (y - y_n)/S_k \\ r_k &= (z - z_n)/S_k \end{aligned} \tag{6.23}$$

in which x_n, y_n and z_n are global coordinates of node n.

The third and fourth terms in Eq. 6.21 are the added mass and hydrodynamic damping, respectively. Transferring these terms to the other side of the equation of motion, the effective force associated with d.o.f. i, $P_i(t)$, is

$$P_i(t) = \sum_{k=1}^{N_e} \Gamma_k \left[\int_0^{L_k} \left\{ \alpha_k \ddot{v}(S_k,t) + \beta_k \sigma_{\dot{r}_i} \dot{v}(S_k,t) \right\} dS_k \right. \tag{6.24}$$

where

$$\begin{aligned} \alpha_k &= C_M(\rho \pi d_k^2) / 4 \\ \beta_k &= 1/2 \, \rho d_k C_D \sqrt{8/\pi} \end{aligned} \tag{6.25}$$

The cross spectrum of nodal loads associated with d.o.f. i and m, $S_{P_i P_m}(\omega)$, is evaluated as the Fourier transform of their cross correlation function and is obtained as

$$S_{P_iP_m}(\omega) = \sum_{k=1}^{N_s}\sum_{l=1}^{N_s}\Gamma_k\Gamma_l\int_0^{L_k}\int_0^{L_l}\{\alpha_k\alpha_l S_{\dot{v}_1\dot{v}_2}(S_k,S_l,\omega) + \alpha_k\beta_l\sigma_{\dot{r}_m}S_{\dot{v}_1\dot{v}_2}(S_k,S_l,\omega) + \alpha_l\beta_k\sigma_{\dot{r}_i}S_{\dot{v}_1\dot{v}_2}(S_k,S_l,\omega) + \beta_k\beta_l\sigma_{\dot{r}_i}\sigma_{\dot{r}_m}S_{\dot{v}_1\dot{v}_2}(S_k,S_l,\omega)\}dS_l\,dS_k \quad (6.26)$$

In Eq. 6.26, the subscripts 1 and 2 refer to any two point falling on members k and l, respectively. L_l and S_l are the tributary length and element coordinate, respectively, of the l^{th} member attached to joint s, at which N_s members meet.

Substituting from Eqs. 6.15 and 6.16 and rearranging, the cross spectrum of nodal loads can be written as

$$S_{P_iP_m}(\omega) = \sum_{k=1}^{N_s}\sum_{l=1}^{N_s}\Gamma_k\Gamma_l\{G_{kl}(\omega)\,I_{kl} + \alpha_k\beta_l\sigma_{\dot{r}_m}[i\,\omega\,I_{kl}]^*\} \quad (6.27)$$

where

$$G_{kl}(\omega) = \alpha_k\alpha_l\omega^2 + i\,\omega\,\beta_{kl}\alpha_l\sigma_{\dot{r}_i} + \beta_k\beta_l\sigma_{\dot{r}_i}\sigma_{\dot{r}_m} \quad (6.28)$$

and

$$I_{kl} = \int_0^{L_k}\int_0^{l_l} S_{\dot{v}_1\dot{v}_2}(S_k,S_l,\omega)\,dS_l\,dS_k \quad (6.29)$$

Standard deviations of relative velocities, $\sigma_{\dot{r}_i}$ and $\sigma_{\dot{r}_m}$ are evaluated in an iterative procedure as their values depend on the structure response. In the first iteration relative velocities are assumed to be equal to water particle velocities .

6.4.1. Wave Forces Using the Directional Spectrum Model

To evaluate cross spectra of nodal loads, integrals of water particle velocities cross spectra, I_{kl}, have to be evaluated. The expression for $S_{\dot{v}_1\dot{v}_2}(\omega)$ needs to be written in terms of the elements coordinates S_k and S_l. The coordinates x1, y1, z1 and x2, y2, z2 are related to S_k and S_l by

$$\begin{aligned} x1 &= x_n + p_k S_k \qquad x2 = x_s + p_l S_l \\ y1 &= y_n + q_k S_k \qquad y2 = y_s + q_l S_l \\ z1 &= z_n + r_k S_k \qquad z2 = z_s + r_l S_l \end{aligned} \tag{6.30}$$

The expression for I_{kl} is given here for the case of velocities in the X direction and is termed $I_{k_x l_x}$, i.e.

$$I_{k_x l_x} = I_{kl} \quad for \quad i \,//\, X \quad and \quad m \,//\, X \tag{6.31}$$

After substituting by Eqs. 6.30 and 6.11 into Eq. 6.29 and carrying out the integrations with respect to S_k and S_l, Eq. 6.29 becomes

$$\begin{aligned} I_{k_x l_x} = \frac{\omega^2 \bar{S}_{hh}(\omega)}{4\kappa^2 \sinh^2 \kappa D} \int_{-\pi}^{\pi} G(\omega,\theta)\cos^2\theta\, \Lambda_{ns} \Big[\frac{e^{\Lambda_n}}{R_{ak}}(e^{\bar{\kappa} R_{ak}} - 1) \\ + \frac{e^{-\Lambda_n}}{R_{bk}}(e^{\bar{\kappa} R_{bk}} - 1) + \frac{e^{\Lambda_s}}{R_{al}}(e^{\bar{\kappa} R_{al} L_r} - 1) + \frac{e^{-\Lambda_s}}{R_{bl}}(e^{\bar{\kappa} R_{bl} L_r} - 1) \Big] d\theta \end{aligned} \tag{6.32}$$

where

$$\Lambda_n = \kappa(y_n + D) \quad and \quad \Lambda_s = \kappa(y_s + D) \tag{6.33}$$

$$\Lambda_{ns} = e^{i\kappa[(x_n - x_s)\cos\theta + (z_n - z_s)\sin\theta]} \tag{6.34}$$

and

$$\begin{aligned} R_{ak} &= [q_k + i(p_k \cos\theta + r_k \sin\theta)] \quad , \quad R_{bk} = [-q_k + i(p_k \cos\theta + r_k \sin\theta)] \\ R_{al} &= [q_l - i(p_l \cos\theta + r_l \sin\theta)] \quad , \quad R_{bl} = [-q_l - i(p_l \cos\theta + r_l \sin\theta)] \end{aligned} \tag{6.35}$$

Finally $L_r = L_l/L_k$ and the dimensionless wave number $\kappa = \kappa L_k$.

6.4.2. Wave Forces Using the Coherence Function Model

The coherence function expressed by Eq. 6.20 is plotted in Fig. 6.4 for different values of the exponential decay parameter c. The figure shows that the coherence decays faster as the value of c increases. The value of c may vary with types of waves or

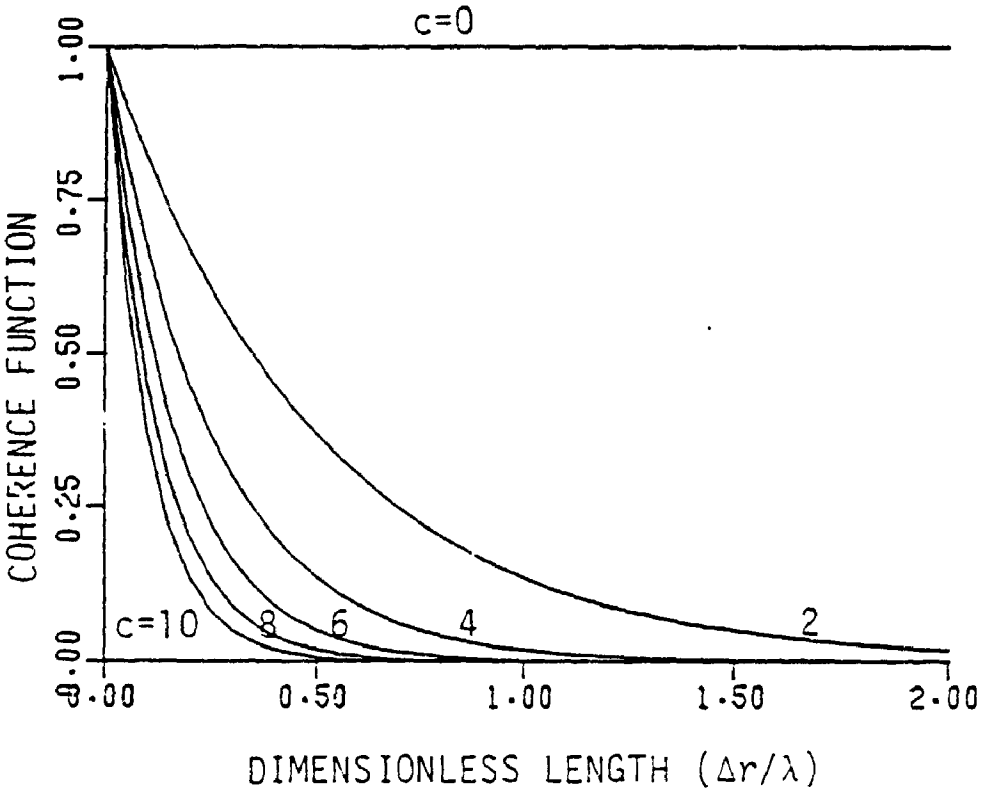

Figure 6.4 Exponential Decay Coherence Function

direction of separation, but it is assumed to be constant here.

When points 1 and 2 are in general positions, the coherence function is given by

$$R = e^{\frac{-c}{\lambda}\sqrt{\Delta x^2 + \Delta y^2 + \Delta z^2}} \tag{6.37}$$

where Δx, Δy and Δz are absolute values of the separation between the two points in directions X, Y and Z. However, a linearized form of the coherence function is required to decouple the integrations upon substitution to evaluate integrals I_{kl}. Davenport [97] suggested a linearized coherence function given by

$$R = e^{-\gamma\frac{c}{\lambda}(\Delta x + \Delta y + \Delta z)} \tag{6.38}$$

where γ is a correction factor that depends on the orientation of the line joining the two points. If $\Delta x = \Delta y = \Delta z$ then $\gamma = 0.5772$ while if the line joining the two points is parallel to any of the three global axes then $\gamma = 1$. For all other orientations γ takes on a value between 0.5772 and 1.

In the coherence function model, the wave system is assumed to advance in a direction that makes an angle $\bar{\theta}$ with the X direction and the spatial coherence is accounted for in Eqs. 6.19 and 6.38. Taking Eq. 6.17 and substituting $\bar{\theta}$ for θ, the cross spectral density of water particle velocities is as follows,

$$\begin{aligned} S_{\dot{v}_1\dot{v}_2}(\omega) = {} & \frac{\omega^2 \bar{S}_{hh}(\omega)}{4\sinh^2\kappa D}\Lambda_{ns}\exp\{i\kappa[(p_k\cos\bar{\theta}+r_k\sin\bar{\theta})S_k-(p_l\cos\bar{\theta}+r_l\sin\bar{\theta})S_l]\} \\ & .HYP1\,[\Lambda_n+\kappa q_k S_k]\;HYP2[\Lambda_s+\kappa q_{lS_l}]\exp\{-c\frac{\kappa\gamma}{2\pi}\,|p_kS_k-p_{lS_l}+x_n-x_s\,|\} \\ & .\exp\{-c\frac{\kappa\gamma}{2\pi}\,|q_kS_k-q_{lS_l}+y_n-y_s\,|\}\;.\;\exp\{-c\frac{\kappa\gamma}{2\pi}\,|r_kS_k-r_{lS_l}+z_n-z_s\,|\} \end{aligned} \tag{6.39}$$

On substituting Eq. 6.39 into Eq. 6.29 and carrying out the integrations, the integral I_{kl} is obtained. This integral is substituted into Eq. 6.27 and the cross spectrum of nodal loads is obtained. Closed form solutions for different member orientations are rather

lengthy and are given in [90].

6.4.3. Examples

Wave forces obtained using either the directional spectrum model or the coherence function model display a reduction in the along wave force spectrum compared to the wave force spectrum obtained from the fully correlated unidirectional spectrum. The reduction in the wave force spectrum can be measured by the reduction factor $\bar{R}_x(\bar{\kappa})$ defined as

$$\bar{R}_x(\kappa) = |S_{P_xP_x}(\bar{\kappa}) / \bar{S}_{P_xP_x}(\bar{\kappa})| \tag{6.40}$$

where $S_{P_xP_x}(\kappa)$ is given by either of the two models and $\bar{S}_{P_xP_x}(\bar{\kappa})$ is obtained using the fully correlated unidirectional model. The reduction factor evaluated at $\bar{\theta} = 0^0$ represents the reduction in along wave forces.

Fig. 6. 5 shows the real part of the wave force spectrum obtained using three different approaches. It may be noticed from the figure that no attenuation of the spectral amplitudes occur for the fully correlated unidirectional model. Also, it may be noticed that the spectral amplitudes evaluated using the directional spectrum model attenuate almost linearly. On the other hand, the attenuation of the spectral amplitudes obtained using the coherence function model is almost exponential and is sensitive to the value of the constant c. The variation in the reduction of the along wave force spectrum, obtained using the directional spectrum model, with the angular spread parameter is shown in Fig. 6.6. It may be noticed from the figure that $\bar{R}_x(\bar{\kappa})$ increases as the angular spread parameter increases. In Fig. 6.7, the variation in the reduction of the along wave force spectrum shown for the coherence function model with the exponential decay constant c. The figure shows that $\bar{R}_x(\bar{\kappa})$ decreases as c increases accommodating the spatial incoherence effects.

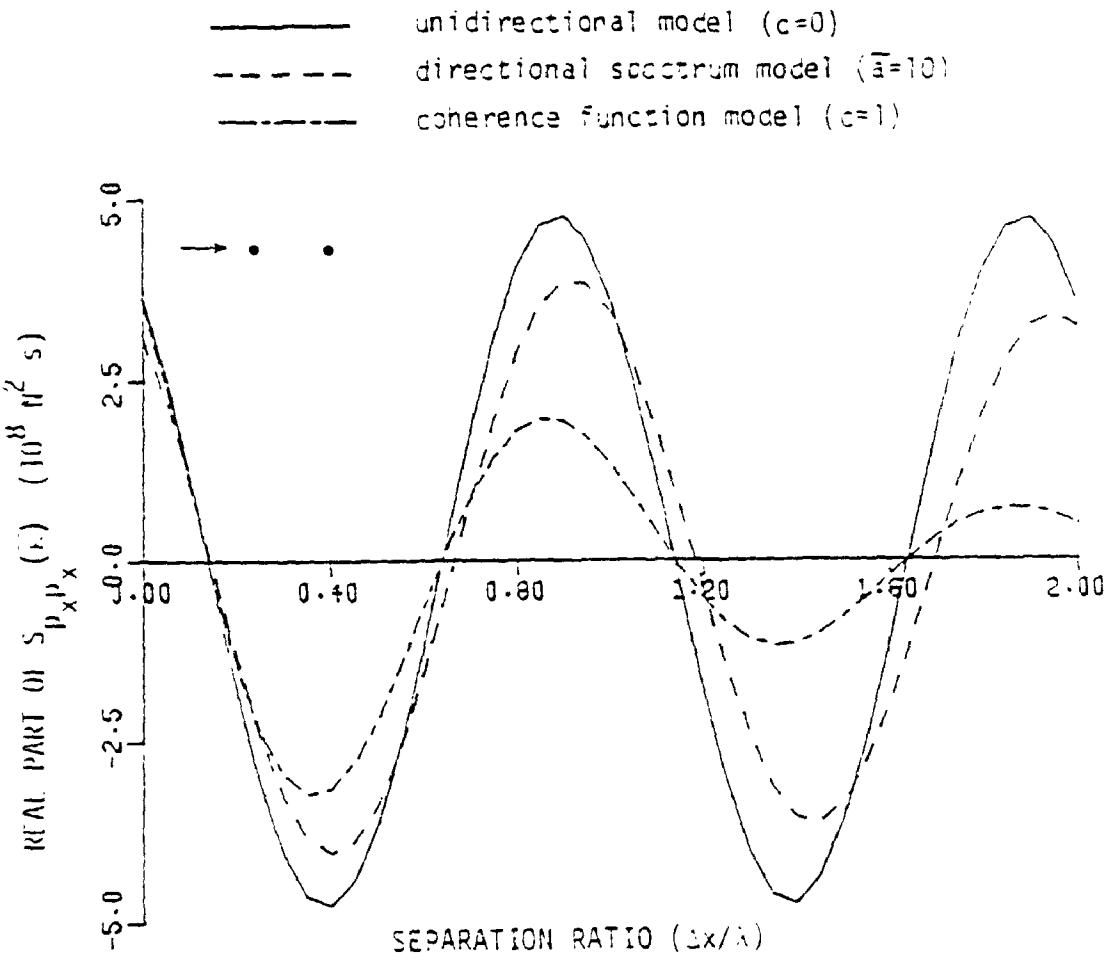

Figure 6.5 Variation in the Real Part of Along Wave Force Spectrum with Separation to Wave Length Ratio (Comparison between Three Models)

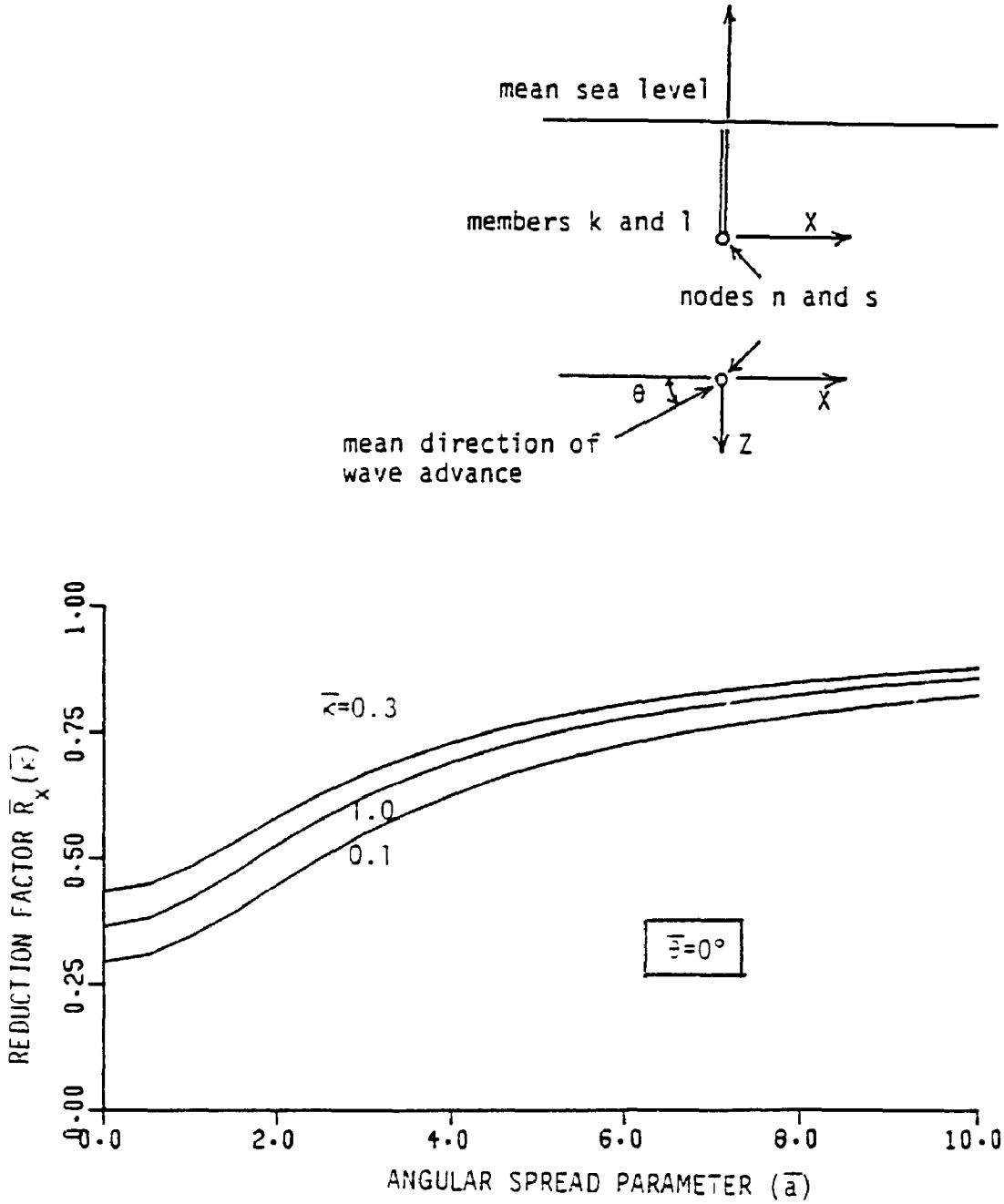

Figure 6.6 Variation in the Reduction Factor of Along Wave Force Spectrum with Directional Spread (Directional Spectrum Model)

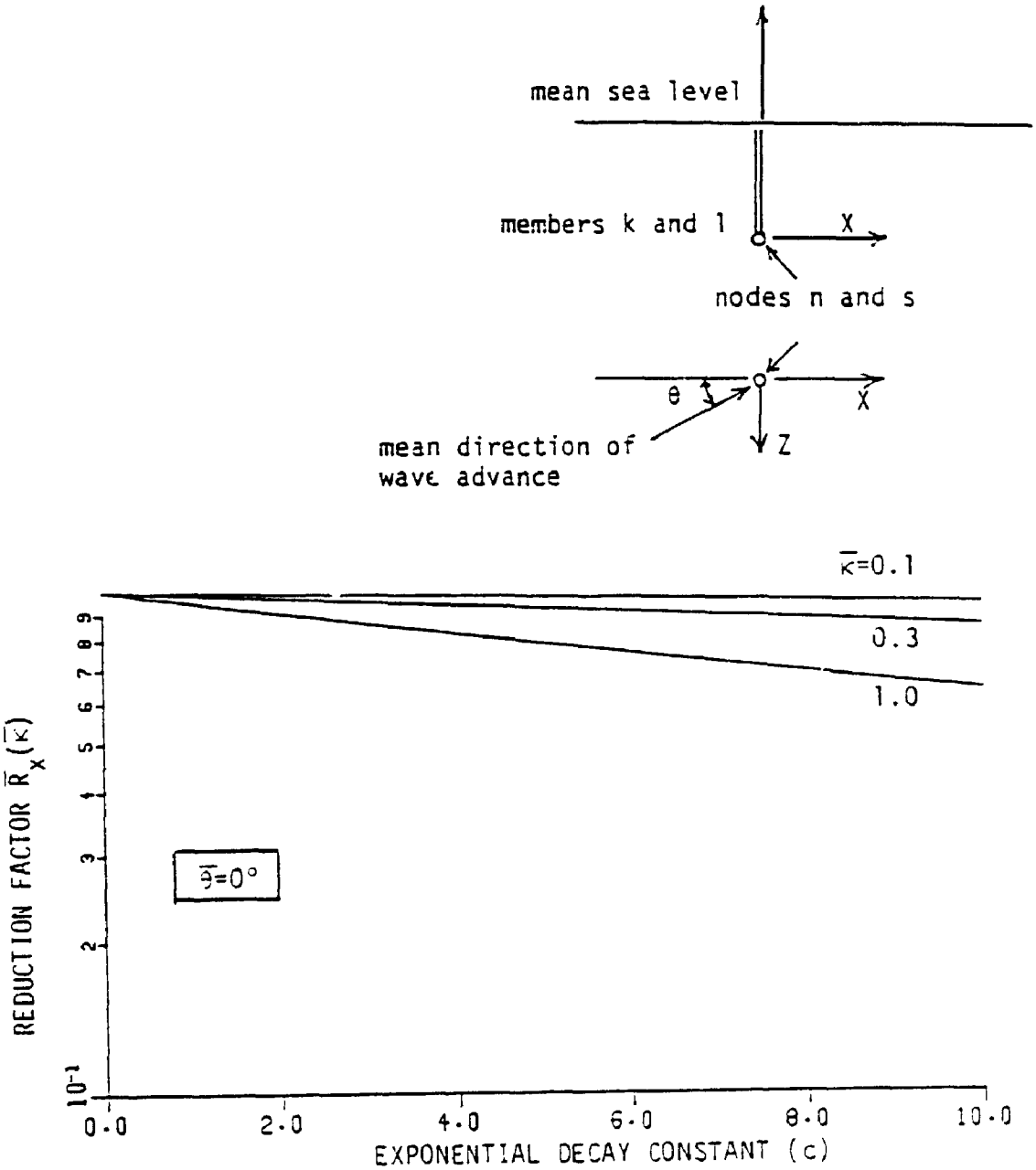

Figure 6.7 Variation in the Reduction Factor of Along Wave Force Spectrum with Exponential Decay Constant (Coherence Function Model)

CHAPTER SEVEN

STRUCTURAL RESPONSE OF OFFSHORE TOWERS WITH PILE INTERACTION

7.1. Introduction

The dynamic characteristics of offshore structures are very important for both operational and safety reasons. These dynamic characteristics include natural frequencies, damping ratios and response amplitudes due to different environmental loads. To predict these characteristics, all the parameters affecting them should be known and their influence should be well understood.

The accuracy of the prediction of these characteristics depends on several factors. These factors include the parameters used in the analysis, the modelling of the structure and the foundation, as well as environmental loads, and the method employed to solve the governing equations of motion. However, large uncertainties are associated with the above mentioned factors and good approximations are accepted.

The formulation of the governing equations of motion and the solution procedure employed are described in this chapter. The superstructure is idealized as a space frame, masses are lumped at the structural nodes and structural damping is modeled by equivalent viscous damping. Natural frequencies, damping ratios and mode shapes are obtained by solving the equations of motion of free vibration using the complex eigenvalue analysis. Power spectra of the structural response to wave forces are evaluated using the modal superposition method. The response evaluation is carried out in an iterative procedure in order to account for the nonlinear behavior of the supporting

piles as well as the hydrodynamic damping which depends on the structural displacements.

7.2. Structural Model

Offshore structures are subjected to severe environmental loads from time to time. The effect of such severe conditions should be studied to avoid unnecessarily high safety factors. Structural members of an offshore tower behave linearly within a certain deformation range beyond which they behave nonlinearly.

Bea [98] performed a series of "static, push-over" analyses to determine at what loadings and displacements, and where the major nonlinear developments might be expected in an offshore platform He found that the first nonlinear action would develop in the piles supporting the structure. The first 9 nonlinear events were all concentrated in the foundation piles.

For small offshore structures, it is easy to idealize the tower as a space frame. For large offshore towers, installed in deep water, some simplifications are brought about. These simplifications include the idealization of the offshore tower as a combination of equivalent beam elements replacing the actual vertical segments of the structure. Berge [95] assumed a rigid diaphragm at each horizontal level, thus the number of nodes was limited to one at each level. Penzien et al. [99] used an equivalent one dimensional model and assigned stiffness coefficients that are typical to real design values. However, one of the drawbacks of the one dimensional models is that the soil structure interaction is not included in a realistic way. Improvements in the one dimensional models are required to account for the complicated pile-soil-pile interaction

under different loading conditions.

In this current study, a space frame idealization is used to model the offshore tower as shown in Fig. 7.1. Members of the offshore tower are modeled by space frame elements that have two nodes, one at each end, and each node has six degrees of freedom, 3 translations and 3 rotations. These degrees of freedom are associated with the global Cartesian axes X,Y and Z and the positive directions are shown in Fig. 7.2.

7.2.1. Formation of the Structure Global Matrices

The global structural stiffness matrix is constructed from the stiffness matrices of the individual elements following the standard displacement method. To account for the inertia forces of the tower either a lumped mass matrix or a consistent mass matrix could be used. The lumped mass matrix is formed by lumping the masses of the individual members at the nodes and their rotatory inertias are ignored. The lumped mass approach yields lower natural frequencies as the mass is pushed to the extremities of the members. On the other hand, the consistent mass matrix is based on using the same shape functions as those used for the stiffness matrix evaluation. However, both methods were found to yield errors of about the same magnitude in beam problems [100]. Another way to account for the inertia forces in a rigorous way is the dynamic stiffness method which considers the correct deformed shape under dynamic conditions. However, this method is not suitable for the eigenvalue analysis.

The number of degrees of freedom considered in the analysis is a key factor for the computational effort and cost to compute the natural frequencies and mode shapes. For an economic and efficient analysis to be performed, only the degrees of freedom of

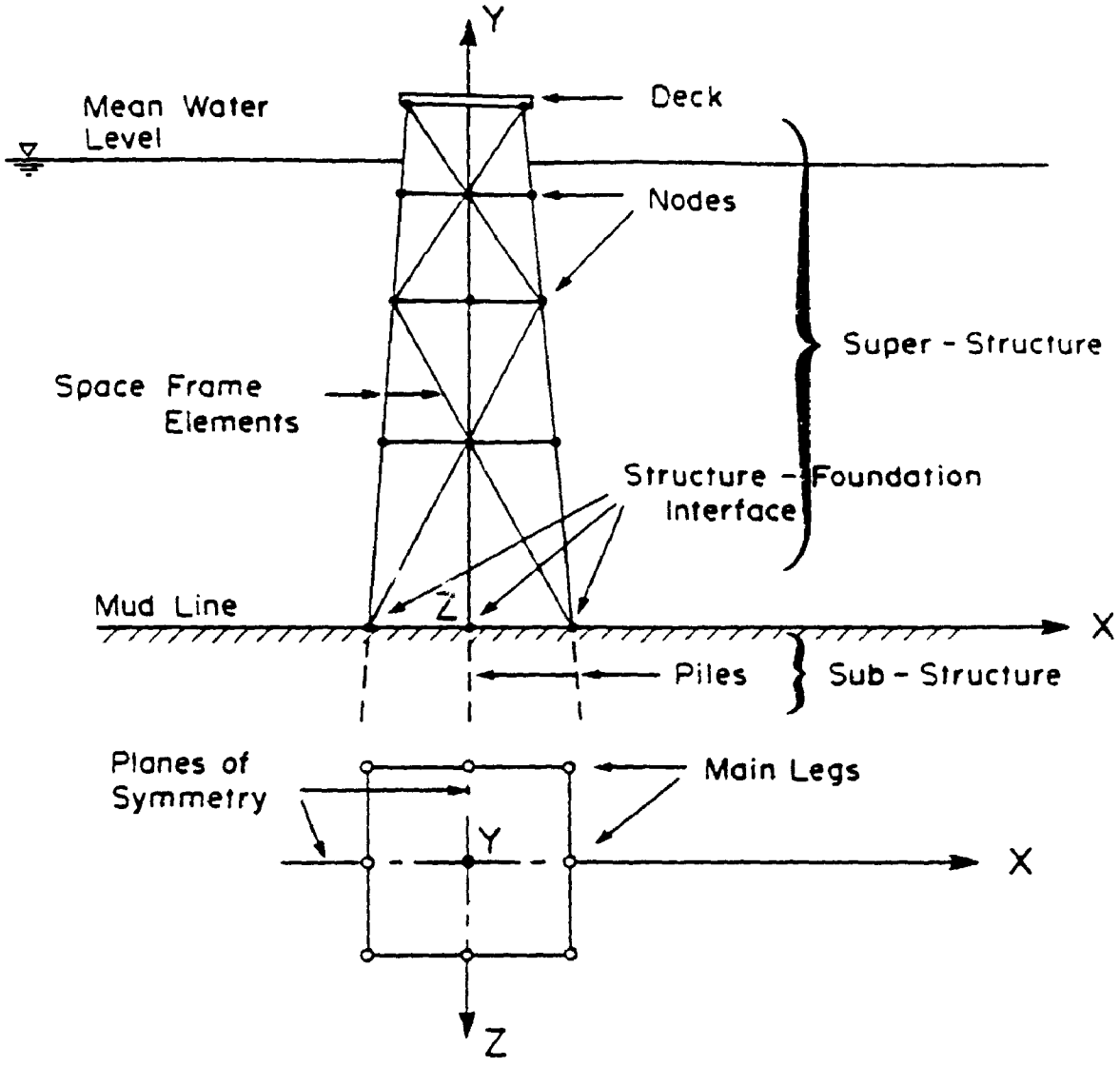

Figure 7.1 Offshore Tower Idealization

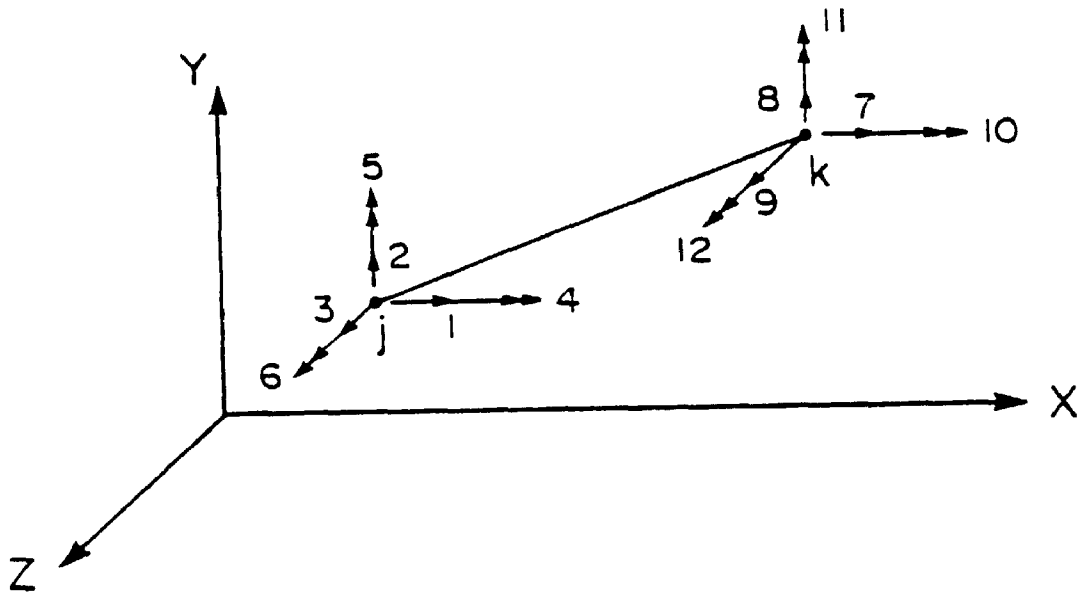

Figure 7.2 Cartesian Coordinate System and Global Degrees of Freedom

interest are retained and the rest of degrees of freedom may be eliminated or condensed. If the choice of degrees of freedom to be retained is right, the accuracy of the solution would not be affected as only the first few modes are important for the response evaluation. The master degrees of freedom to be retained are those associated with high mass to stiffness ratios and distributed throughout the structure.

In this study, the lumped mass approach is followed and the rotatory inertia of individual elements is neglected. The mass matrix obtained is diagonal and pertains to the translational degrees of freedom. In the global stiffness matrix, only the translational degrees of freedom are retained. The rotational degrees of freedom are condensed except those at the structure-foundation interface because they are important as a significant part of the overall flexibility and damping of the foundation is associated with these degrees of freedom. The static condensation technique is used to attain the global stiffness matrix pertaining to the degrees of freedom of interest.

The structural damping incorporated in the analysis is the material damping and is hysteretic in nature. Structural damping is expressed as equivalent viscous damping and the damping matrix of the offshore tower [C_s] is obtained as

$$[C_s] = \frac{2\beta [K_s]}{\omega} \tag{7.1}$$

where [K_s] is the condensed stiffness matrix of the offshore tower, β is the material damping ratio and ω is the frequency.

7.2.3. Piled Foundation Stiffness Matrix

The nonlinear analyses for axial and lateral piles response described in Chapter

4 and Chapter 5, respectively, are used to obtain the equivalent linear single piles stiffness and damping, as well as equivalent linear interaction factors. These parameters are obtained according to the displacement level at pile heads.

The complex foundation stiffness matrix $[K_f]^*$ is obtained as the inverse of the complex foundation flexibility matrix $[F_f]$, i.e.

$$[K_f]^* = [F_f]^{-1} \tag{7.2}$$

For a group of n piles, the foundation flexibility matrix is a symmetric 6n × 6n matrix, i.e

$$[F_f] = \begin{bmatrix} [f]_{11} & \cdot & [f]_{1i} & \cdot & [f]_{1n} \\ \cdot & \cdot & \cdot & \cdot & \cdot \\ [f]_{i1} & \cdot & [f]_{ii} & & [f]_{in} \\ \cdot & \cdot & \cdot & \cdot & \cdot \\ [f]_{n1} & \cdot & [f]_{ni} & \cdot & [f]_{nn} \end{bmatrix} \tag{7.3}$$

where each of the diagonal submatrices $[f]_{ii}$ is the inverse of the single pile 6 × 6 complex stiffness matrix. The off diagonal submatrices $[f]_{ij}$ represent the interaction between the degrees of freedom at the heads of piles i and j, i.e.

$$[f] = \begin{bmatrix} \alpha_h f_h & & & & & & \alpha_c f_c \\ & \alpha_v f_v & & & & & \\ & & \alpha_h f_h & \alpha_c f_c & & & \\ & & \alpha_c f_c & \alpha_r f_r & & & \\ & & & & \alpha_\eta f_\eta & & \\ \alpha_c f_c & & & & & & \alpha_r f_r \end{bmatrix} \tag{7.4}$$

In Eq. 7.4, f_i-s are the equivalent linear flexibility terms, and α_i-s are the complex equivalent linear interaction factors obtained in Chapters 4 and 5. The subscripts h, c, r and η are for horizontal, coupling, rotational and torsional terms, respectively. The torsional flexibility is obtained using Novak and Howell solution [101] and the interaction factor α_η is neglected because it is usually very small.

The foundation stiffness matrix, $[K_f]$, is then calculated as the real part of the complex stiffness matrix $[K_f]^*$. The foundation damping matrix, $[C_f]$, is computed as the equivalent viscous damping, i.e

$$[C_f] = Im\{[K]^*\}/\omega \tag{7.5}$$

The foundation stiffness and damping matrices are to be added to the tower stiffness and damping matrices at the pertinent degrees of freedom.

7.2.3. Exploiting Symmetry

The response analysis of offshore towers requires large memory storage and computation costs. Exploiting symmetry for the analysis of towers which possess a symmetric configuration with regard to one or more vertical planes may reduce the computation requirements significantly. For symmetrical structures, only one part of the structure is assembled and the analysis is carried out for this part only. For example, if the structure is symmetric with regard to 2 vertical planes, only one quarter is assembled. Four cases of vibration modes of this quarter yield all the vibration modes for the original structure; two cases are for the structure vibrating either symmetrically or antisymmetrically with respect to both planes and two cases are for the structure

vibrating symmetrically with regard to one plane and antisymmetrically with regard to the other [102]. This idealization is valid even when the loading pattern is not symmetric, because any unsymmetrical loading can be decomposed into a symmetric and an antisymmetric loading.

For the tower, exploiting symmetry is achieved by introducing artificial appropriate restraints at joints located on planes of symmetry. For symmetric vibration, joints on a plane of symmetry must be prevented from translation normal to the symmetry plane and rotations in the plane. For antisymmetric vibration, joints on a plane of symmetry must be prevented from translations in the plane and rotation normal to the plane. In addition, the properties of members that lie in those planes must be altered. The rigidities and masses of members lying in a plane of symmetry must be halved. In the event that a member lies in two planes of symmetry, its rigidities and mass must be divided by four. If a member is normal to and bisected by a plane of symmetry, a new joint is introduced at midlength and restrained as described above. These changes may be incorporated into the structural data and do not necessitate any additional programming.

For the foundation, symmetry is taken into account by equating the appropriate degrees of freedom of the foundation flexibility matrix according to the vibration mode under consideration. If one of the piles falls on a plane of symmetry, its rigidity is halved. In a flexibility formulation this corresponds to doubling its flexibility.

7.3. Governing Equations of Motion

The equations of motion of an offshore tower subjected to wave forces are written

as

$$[M_s]\{\ddot{u}\} + [C_b]\{\dot{u}\} + [K]\{u\} = \{W(t)\} \tag{7.6}$$

In Eq. 7.6, [K] is the sum of the stiffness matrices of the structure [K_s] and the foundation [K_f], [C_b] is the sum of damping matrices of the structure [C_s] and the foundation [C_f], and [M_s] is the structural lumped mass matrix. $\{u\}$, $\{\dot{u}\}$ and $\{\ddot{u}\}$ are the vectors of structural displacements, velocities and accelerations, respectively. Finally, the vector { W(t) } is the vector of wave forces the elements of which are defined by Eq. 6.21, i.e.

$$W_i(t) = \sum_{k=1}^{N_n} \Gamma_k \left[\int_0^{L_k} \left\{ \rho \pi \frac{d_k^2}{4} C_M \dot{v}(S_k,t) + \frac{1}{2} \rho d_k C_D \sqrt{8/\pi}\, \sigma_{f_i} v(S_k,t) \right\} dS_k \right. \\ \left. - \rho \pi \frac{d_k^2}{4} (C_M - 1) L_k \ddot{u}_i(t) - \frac{1}{2} \rho d_k C_D \sqrt{8/\pi}\, \sigma_{f_i} L_k \dot{u}_i(t) \right] \tag{7.7}$$

where d_k, L_k and S_k are the diameter, tributary length and element coordinate of member k, respectively, and N_n is the number of members attached to joint n at which d.o.f. i is located. The drag and inertia coefficients C_D and C_M are assumed to be constant with the respective values 1.4 and 2. The linearized form of the drag component is used in the analysis. Eq. 7.6 can be solved in its nonlinear form using the numerical integration in the time domain. Godeau and Deleuil [103] solved the equations of motion in the time domain, however; in addition to the high computational costs involved, there is some difficulty associated with interpreting the resulting response time histories.

Using the linearized form of the drag term and transferring both the added mass

and the hydrodynamic damping to the left hand side of the equations of motion, Eq. 7.6 is rewritten as

$$[M]\{\ddot{u}\} + [C]\{\dot{u}\} + [K]\{u\} = \{P(t)\} \tag{7.8}$$

The total damping matrix is given by

$$[C] = [C_s] + [C_f] + [C_H] \tag{7.9}$$

in which the hydrodynamic damping matrix, $[C_H]$, is a diagonal matrix with elements

$$(C_H)_{ii} = \sum_{k=1}^{N_s} \frac{1}{2} \rho C_D d_k \sqrt{8/\pi}\, \sigma_{f_i} \Gamma_k L_k \tag{7.10}$$

where σ_{f_i} is the standard deviation of the relative velocity between the structure and water particles at the position and direction of d.o.f. i. The total mass matrix [M] is the sum of the structural diagonal mass matrix and the added mass matrix which is also diagonal and defined as

$$(M_a)_{ii} = \sum_{k=1}^{N_s} \rho (C_m - 1) \pi \frac{d_k^2}{4} \Gamma_k L_k \tag{7.11}$$

Eq. 7.8 can be solved in the frequency domain, e.g. [6[illegible] this approach, the time dependent force is Fourier transformed into a set of discrete harmonic components. The response to each of these components, which is also harmonic, is obtained by solving the resulting set of linear simultaneous algebraic equations giving the frequency response of different degrees of freedom. Time histories of the responses are obtained as the Fourier transforms of the frequency response amplitudes of each degree of freedom and the

power spectral density of the response is obtained from the standard relationship with the Fourier transform. The frequency response method is suitable for systems with frequency dependent properties. However, this method is computationally expensive for the analysis of structures with large number of degrees of freedom. In such situations, the modal analysis is preferred especially when the response is dominated by the first few modes.

In modal analysis approach, the structural response is obtained using the superposition technique which is valid for linear systems only. However, for real offshore towers the response is dominated by the first mode only and the error due to the application of the modal analysis is small. The analysis starts with the solution of the free vibration problem to compute the natural frequencies, mode shapes and the modal damping ratios. For the case of nonproportional damping, as it is herein, classical normal modes do not uncouple the damping matrix. Foster [104] used the nonclassical complex eigen valued modal superposition to uncouple the equations of motion. In this study, the modal superposition is adopted and the complex eigen value approach is used to solve the equations of free vibration. Foundation stiffness and damping matrices are evaluated at the first natural frequency which is obtained by iteration starting with undamped system and classical analysis.

7.4. Free Vibration Analysis

Setting the force vector { P(t) } in Eq. 7.8 to zero, the equations of motion of the free vibration are obtained, i.e.

$$[M]\{\ddot{u}\} + [C]\{\dot{u}\} + [K]\{u\} = \{0\} \tag{7.12}$$

The complementary function of this equation is sought in the form

$$\{u\} = \{\phi\} e^{\lambda t} \tag{7.13}$$

where $\{\phi\}$ is a vector of constants and λ should satisfy the characteristic equation obtained by substituting Eq. 7.13 into Eq. 7.12, i.e.

$$(\lambda^2[M] + \lambda[C] + [K])\{\phi\} = \{0\} \tag{7.14}$$

The resulting equation, Eq. 7.14, is a set of algebraic equations of order N in λ^2 , the solution of which in this form is not amenable to the algorithms developed for solving either the standard or the generalized eigen value problems.

This set of N second order linear differential equations (L.D.E.) can be transformed into a set of 2 N first order L.D.E. [105]

$$[A]\{\dot{q}\} + [B]\{q\} = \{0\} \tag{7.15}$$

where the Vector { q } is defined as

$$\{q\} = \begin{Bmatrix} \{\dot{u}\} \\ \{u\} \end{Bmatrix} \tag{7.16}$$

and the matrices [A] and [B] are given by

$$[A] = \begin{bmatrix} [0] & [M] \\ [M] & [C] \end{bmatrix} \tag{7.17}$$

and

$$[B] = \begin{bmatrix} -[M] & [0] \\ [0] & [K] \end{bmatrix} \tag{7.18}$$

The solution to Eq. 7.15 is sought in the form

$$\{q\} = \{\Phi\} e^{\mu t} \tag{7.19}$$

Substituting Eq. 7.19 in Eq. 7.15 yields

$$\mu [A]\{\Phi\} + [B]\{\Phi\} = \{0\} \tag{7.20}$$

which is the generalized eigenvalue problem.

N pairs of complex conjugate eigenvalues and N pairs of complex eigenvectors are obtained upon solution of Eq. 7.20. The complex eigenvalues can be expressed in the form

$$(\mu_j)_{1,2} = -\zeta_j \omega'_j \pm i \omega_j \sqrt{1 - \zeta_j^2} \tag{7.21}$$

From Eq. 7.21, the damped frequency ω'_j can be obtained as

$$\omega'_j = Im[\mu_j] \tag{7.22}$$

and the modal damping ratio is given by

$$\zeta_j = \frac{-Re[\mu_j]}{|\mu_j|}$$

where Re and Im indicate the real and imaginary parts, respectively. This method has been used in soil structure interaction problems, e.g. [106] and is also used in this study in order to establish the damped natural frequencies and the modal damping ratios.

7.5. Response to Wave Forces

The actual coordinates can be related to the generalized coordinates using the mode shapes which have been evaluated from the free vibration analysis by the equation

$$u_i(t) = \sum_{j=1}^{N} \phi_{ij}\,\eta_j(t) \tag{7.24}$$

where ϕ_{ij} is the modal coordinate associated with d.o.f. i in mode j and $\eta_j(t)$ is the generalized coordinate of mode j. From the theory of random vibration, the spectral density of the response at d.o.f. i, $S_{u_i u_i}(\omega)$, is given as

$$S_{u_i u_i}(\omega) = \sum_{j=1}^{N}\sum_{r=1}^{N} \phi_{ij}\,\phi_{ir}\,S_{\eta_j \eta_r}(\omega) \tag{7.25}$$

where $S_{\eta_j \eta_r}(\omega)$ is the cross spectrum of the generalized coordinates $\eta_j(t)$ and $\eta_r(t)$, and is given by

$$S_{\eta_j \eta_r}(\omega) = H^*_j(i\omega)\,H_r(i\omega)\,S_{F_j F_r}(\omega) \tag{7.26}$$

In Eq. 7.26, $H_j(i\omega)$ and $H_r(i\omega)$ are the mechanical admittance functions of modes j and r respectively, and $S_{F_j F_r}(\omega)$ is the cross spectrum of the generalized forces $F_j(t)$ and $F_r(t)$, respectively. The generalized force in mode j, Fj(t), is given by

$$F_j(t) = \sum_{i=1}^{N} \phi_{ij} P_i(t) \tag{7.27}$$

Hence, the cross spectrum of the generalized forces is

$$S_{F_j F_r}(\omega) = \sum_{i=1}^{N} \sum_{m=1}^{N} \phi_{ij} \phi_{mr} S_{P_i P_m}(\omega) \tag{7.28}$$

in which $S_{P_i P_m}(\omega)$ is the cross spectrum of nodal loads $P_i(t)$ and $P_m(t)$ given by Eq. 6.26.

Mitwally [90] found that a stepwise approximation to the velocity field and lumping the areas and volumes of the members at the nodes have little effect for longer waves where most of the energy lies. Also, he found that the cancelling effect tends to reduce the error. These approximations are adopted here. Consequently, $S_{P_i P_m}(\omega)$ is obtained as

$$\begin{aligned} S_{P_i P_m}(\omega) = \sum_{k=1}^{N_s} \sum_{l=1}^{N_s} \Gamma_k \Gamma_l L_k L_l \{ & (\omega^2 \alpha_k \alpha_l + i\omega \alpha_l \beta_k \sigma_{t_l} \\ & + \beta_k \beta_l \sigma_{t_l} \sigma_{t_m}) S_{\dot{v}_1 \dot{v}_2}(\omega) + \alpha_k \beta_l \sigma_{t_m} [i\omega S_{\dot{v}_1 \dot{v}_2}(\omega)]^* \} \end{aligned} \tag{7.29}$$

Denote

$$\begin{aligned} A_k &= \sum_{k=1}^{N_s} \Gamma_k L_k \alpha_k \qquad & A_l &= \sum_{l=1}^{N_s} \Gamma_l L_l \alpha_l \\ B_k &= \sum_{k=1}^{N_s} \Gamma_k L_k \beta_k \qquad & B_l &= \sum_{l=1}^{N_s} \Gamma_l L_l \beta_l \end{aligned} \tag{7.30}$$

After substituting Eq. 7.30 into Eq. 7.29 and rearranging the terms, the cross spectrum of nodal loads is obtained as

$$S_{P_iP_m}(\omega) = S_{\dot{v}_i\dot{v}_m}(\omega)[\omega^2 A_k A_l + i\omega\sigma_{r_l} B_k A_l + \sigma_{r_l}\sigma_{r_m} B_k B_l] + \sigma_{r_m} A_k B_l [i\omega S_{\dot{v}_i v_m}(\omega)]^* \quad (7.31)$$

The variance of the relative velocity is obtained from its power spectrum, i.e.

$$\sigma^2_{\dot{r}_i} = \int_0^\infty S_{\dot{r}_i\dot{r}_i}(\omega)d\omega \quad (7.32)$$

As

$$\dot{r}_i(t) = \dot{v}_i(t) - \dot{u}_i(t) \quad (7.33)$$

the power spectral density $S_{\dot{r}_i\dot{r}_i}(\omega)$ is expressed as

$$S_{\dot{r}_i\dot{r}_i}(\omega) = S_{\dot{v}_i\dot{v}_i}(\omega) + S_{\dot{u}_i\dot{u}_i}(\omega) - S_{\dot{v}_i\dot{u}_i}(\omega) - S_{\dot{u}_i\dot{v}_i}(\omega) \quad (7.34)$$

Noting that

$$S_{\dot{v}_i\dot{u}}(\omega) = i\omega S_{\dot{v}_i u_i}(\omega) \qquad S_{\dot{u}_i\dot{v}}(\omega) = -i\omega S_{\dot{v}_i u_i}(\omega)$$
$$S_{\dot{u}_i\dot{u}}(\omega) = \omega^2 S_{u_i u_i}(\omega) \qquad S_{\dot{v}_i u}(\omega) = S^*_{u_i\dot{v}_i}(\omega) \quad (7.35)$$

Eq. 7.34 can be rewritten as

$$S_{\dot{r}_i\dot{r}_i}(\omega) = S_{\dot{v}_i\dot{v}_i}(\omega) + \omega^2 S_{u_i u_i}(\omega) - 2\omega\, Im[S_{u_i\dot{v}_i}(\omega)] \quad (7.36)$$

The cross spectrum of structural displacements and water particle velocity $S_{u_i\dot{v}_i}(\omega)$ is given by

$$S_{u_i\dot{v}_i}(\omega) = \sum_{j=1}^{N}\sum_{l=1}^{N} \phi_{ij}\phi_{lj} H^*_j(i\omega)\{C_M S_{\dot{v}_l\dot{v}_i}(\omega) + \sqrt{\frac{8}{\pi}} C_D \sigma_{\dot{r}_i} S_{\dot{v}_i\dot{v}_i}(\omega)\} \quad (7.37)$$

Then the variance of the relative velocity can be calculated as

$$\sigma^2_{f_i} = \sigma^2_{\dot{v}_l \dot{v}_m} + \sigma^2_{\dot{u}_l \dot{u}_l} - 2\omega \int_0^{\infty} Im[S_{\dot{u}_l \dot{v}_l}(\omega)]\, d\omega \qquad (7.38)$$

7.6. Solution Procedure

Stiffness, damping and mass matrices are assembled as described in Sec. 7.3. Solution of the free vibration problem is carried out using the complex eigen value analysis to establish the natural frequencies, mode shapes and modal damping ratios. For free vibration analysis in still water, water particle velocity v is assumed to be zero; then the drag term is proportional to the square of the structural velocity and due its quadratic nature can be neglected for small amplitudes. However, the hydrodynamic damping is included in the structure response analysis to certain sea states.

To examine the relative importance of different sources of damping, the foundation modal damping ratios, ζ_{fj}, and the structural modal damping ratios, ζ_{sj}, are evaluated separately in the free vibration analysis. This is done by considering only the pertinent damping matrix for each case in Eq. 7.9. The structural modal damping ratios, ζ'_{sj}, obtained in this manner are correct only for the first mode. For higher modes, the corrected structural damping ratios are obtained from

$$\zeta_{sj} = \zeta'_{sj}\, \omega_1 / \omega_j \qquad (7.39)$$

where ω_1 and ω_j are the natural frequencies of the structure at the first and j^{th} mode, respectively. Foundation damping ratios do not need this correction as the variation in stiffness and damping properties at low frequency is very mild. However, the response is usually dominated by the first mode for real structures.

The response analysis proceeds by specifying the sea state and is performed in an iterative procedure. In the first cycle, structural velocities are assumed to be zero; then the relative velocity is equal to the water particle velocity and the hydrodynamic damping matrix [C_H] can be evaluated. Also, The foundation stiffness and damping are computed assuming that displacement amplitudes are small (linear conditions). A free vibration analysis is carried out to determine the hydrodynamic modal damping ratios, ζ_{hj}. This is done by setting other damping matrices to zero. During each cycle the system is linear and superposition holds, thus the total modal damping ratio, ζ_j, is the sum of ζ_{sj}, ζ_{fj} and ζ_{hj}. Because of the iterative nature of the solution and to avoid excessive computational costs, the classical mode shapes are used in the evaluation of the response spectra. This is a reasonable approximation because the difference between classical and nonclassical mode shapes is significant only for systems with high damping ratios and for higher modes. After the response spectra are evaluated, new values of the variances of relative velocities are evaluated and another cycle of iteration is carried out. Only in the second cycle, the foundation stiffness and damping are adjusted to the level of displacements at pile heads to account for the nonlinear behavior of piles. These displacements are calculated as mean peak values, i.e.

$$u_{ip} = \gamma_m \sigma_{ui} \tag{7.40}$$

where σ_{ui} is the standard deviation of the response at the pile head and γ_m is the peak factor given by [107]

$$\gamma_m = \sqrt{2 \ln fT} + \frac{0.5772}{\sqrt{2 \ln fT}} \tag{7.41}$$

where T is the duration of the storm, and

$$f = \frac{\bar{\omega}}{2\pi} \tag{7.42}$$

The iteration procedure is terminated when convergence is achieved according to the following criterion

$$\frac{\| \sigma_i^{(k)} - \sigma_i^{(k-1)} \|_2}{\| \sigma_i^{(k)} \|_2} \leq \epsilon \tag{7.43}$$

where ϵ is a specified tolerance, k denotes the iteration number and the vector norm $\| \sigma_i \|_2$ is defined by

$$\| \sigma_i \|_2 = (\sum_{i=1}^{N} \sigma^2_i)^{0.5} \tag{7.44}$$

For a jacket type offshore tower, the results of this analysis are presented in detail in the next chapter.

CHAPTER EIGHT

EFFECT OF PILE FOUNDATION ON TOWER RESPONSE

8.1. Introduction

The response of a typical offshore tower to wave loads is analyzed using the procedures described in Chapters 4 through 7 to explore the effect of the pile foundation on the tower response. The tower , shown in Fig. 8.1, is supported by 10 piles, each having an outer diameter 1.45 m and a penetration depth of 50 m. Six main piles extend through the main legs all the way to the top of the tower and 4 skirt piles are cut off and welded at the level of the first bracing. The tower is 122 m high and stands in 104 m of water. The members of the tower deck section are not idealized individually but their mass and stiffness are lumped and accounted for by assigning high stiffness and mass values to the members at the tower top level.

The tower is symmetric about both axes X and Z, so taking advantage of symmetry, only one quarter of the structure is modeled. The nodes and member numbering details in the assembled quarter are shown in Figs. 8.2 and 8.3. The properties of the members and the supporting piles are shown in Table 8.1. Members 11, 28, 40, 51 and 52 are assigned high stiffness and mass values to account for the unmodeled deck section. Two sets of boundary conditions are applied which give the required mode shapes:

1. X is an axis of symmetry and Z is an axis of antisymmetry; these conditions yield the lowest natural frequency of the structure which is associated with the sway in the X direction.

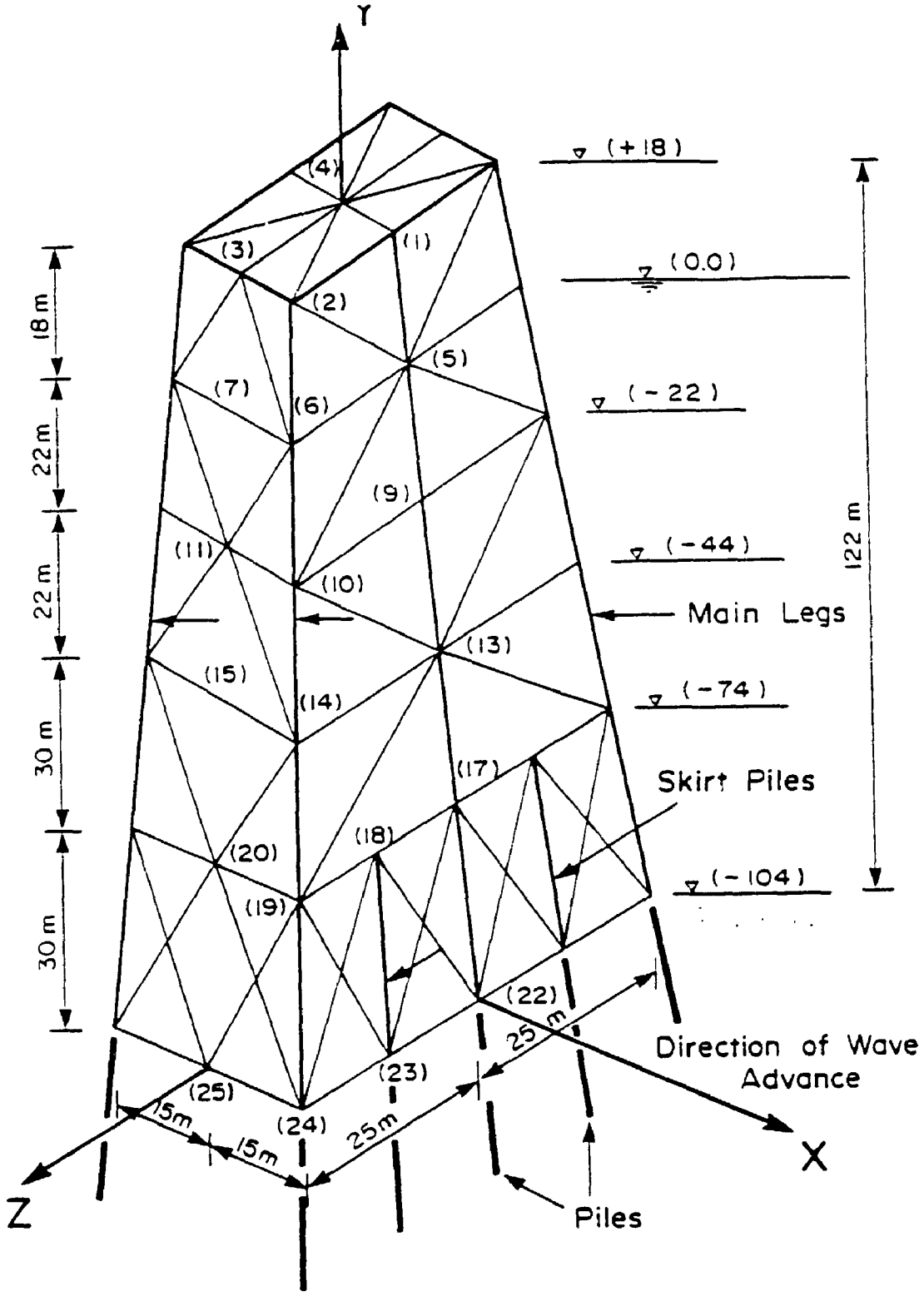

Figure 8.1 Fixed Offshore Tower Used in the Analysis

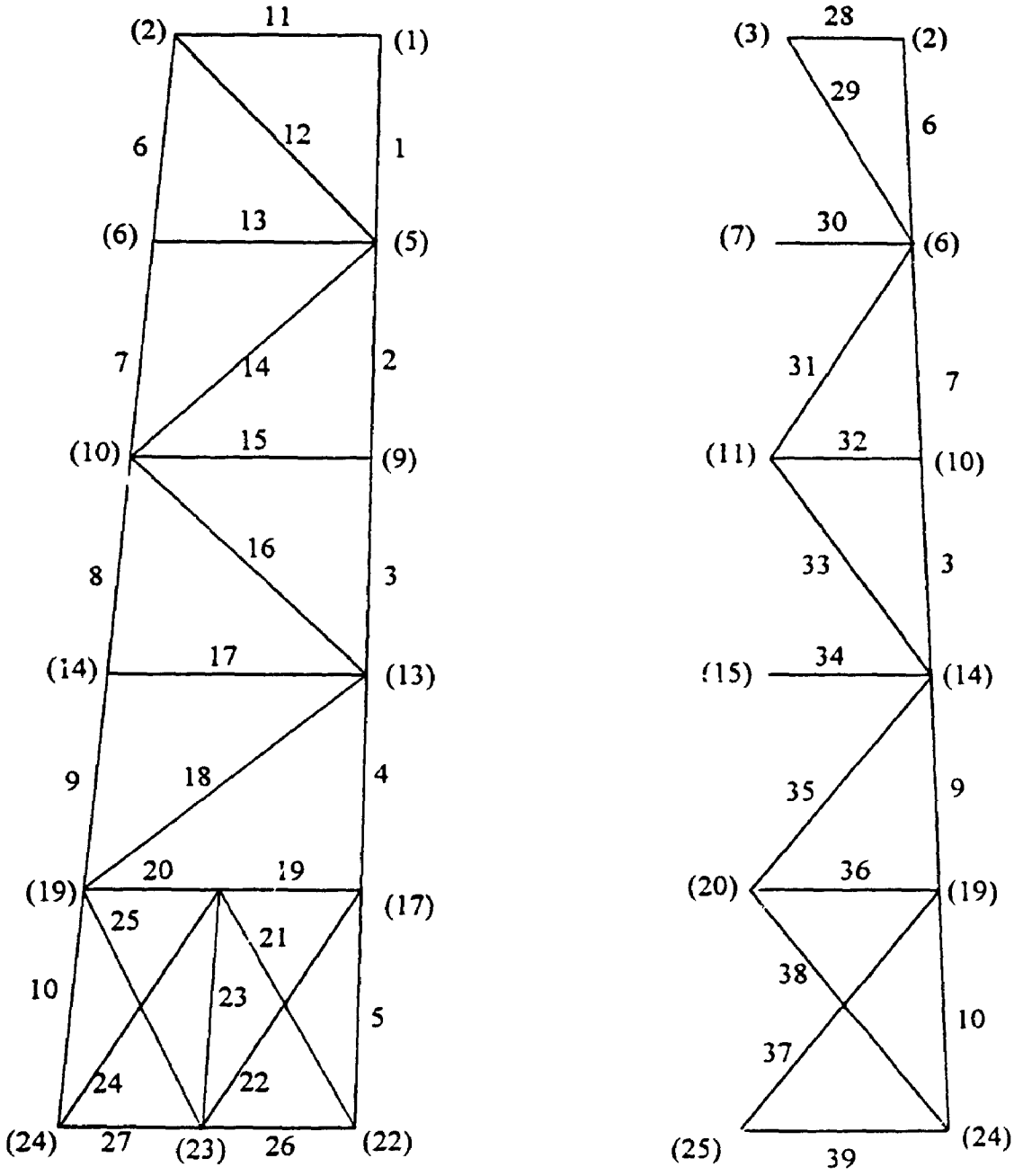

Figure 8.2 Member and Node Numbering of the Tower

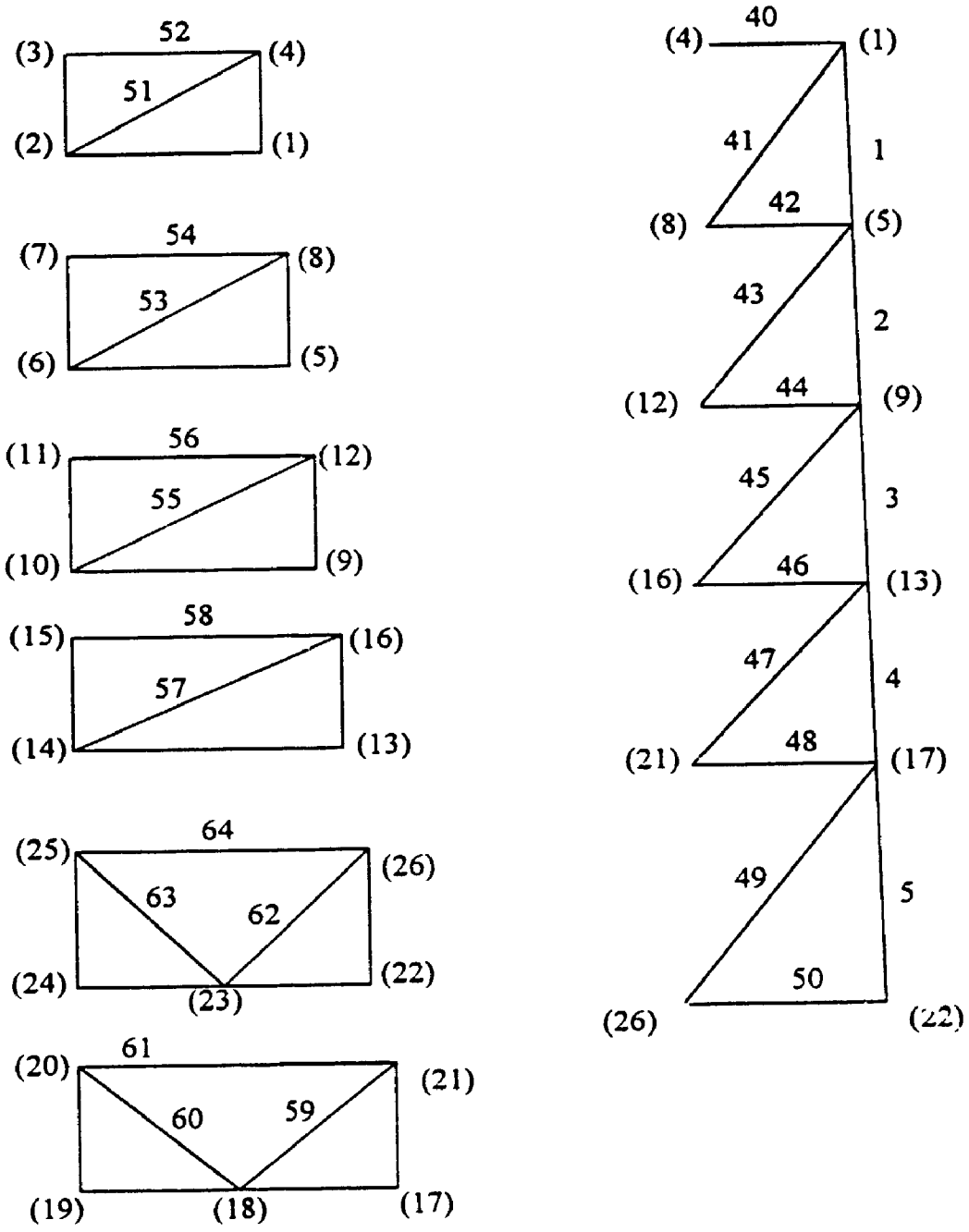

Figure 8.3 Member and Node Numbering of the Tower (Continued)

Table 8.1 Structural Properties of Tower Memebers

Member No.	Wall Thickness	Diameter
11-28-40-51-52	0.10	3.0
2-3-4-5-7-8-9-10-23	0.04	1.6
1-6	0.04	1.6
16-18-34-49-50-58-61-64	0.025	1.2
12-13-14-15-17-19-20-21-22-24-25-26-27-30-35-37-38-39-44-45-46-48-54-56-59-60-62-63	0.02	1.0
29-31-32-33-36-41-42-43-47-53-55-57	0.02	0.8
Piles	0.05	1.45

2. Both X and Z are axes of antisymmetry; these conditions yield the torsional mode.

Sway in the Z direction is obtained similarly by considering Z to be an axis of symmetry and X an axis of antisymmetry. However, sway in the Z direction is not considered since wave forces are calculated using the coherence function model described in Chapter 6 which is a unidirectional model and waves are assumed to progress in the X direction. The vertical vibration modes are obtained considering both X and Z as axes of symmetry. These modes, however, are very stiff and associated with high natural frequencies and are not considered in the analysis.

To illustrate the effect of the piled foundation on the tower response, a parametric study is conducted and the results are presented in this chapter. Four main factors defining the foundation system are considered, i.e. nonlinear soil behavior, soil profile, pile-soil-pile interaction and soil shear wave velocity. The nonlinear behavior of three different soil profiles is considered in this study. The effect of the characteristic wind speed $\bar{U}$ on the response is also considered. In addition to these parameters, the effect of the deck mass on the response quantities is examined. Structural and foundation damping ratios are evaluated separately in order to elucidate their variation with the foundation system parameters independently.

The drag and inertia coefficients are assigned the constant values of 1.4 and 2, respectively. Material damping ratio of the superstructure, β, is assumed to be 1 % which is suitable for materials with low internal damping such as steel. The deck mass varies depending on the type of platform, its production capacity, topside facilities and stage of completion of the platform [41]. A low value of the deck mass was first assigned when examining the variation of free vibration characteristics with the

foundation parameters. For examining the variation of the tower response with the system parameters, a higher value of the deck mass was assumed since this brings the natural frequencies closer to the wave energy spectrum peak. However, the variation of the free vibration characteristics with the deck mass, expressed as a ratio of the total mass of the superstructure, is also examined. The exponential decay parameter, c, in the coherence function model, is assumed to be constant in all directions and is equal to 1.

For all the results presented in this chapter, the term nonlinear analysis means nonlinear analysis for the foundation system whereby the tower members are assumed to behave linearly all the time. Moreover, the foundation itself is assumed to be linear in each individual case for the free vibration analysis and it is also assumed to be linear within each iteration in the tower response analysis. Equivalent linearization is used to determine the equivalent linear properties of the pile foundations for each level of loading.

8.2. Effect of Foundation Parameters on Free Vibration Characteristics

For all the results presented in this section, the deck mass is 760 tons, which represents 20.33 % of the total mass of the structure. Also, the interaction between piles is considered unless otherwise stated.

8.2.1. Effect of Foundation Nonlinearity

During a storm or due to the collision of a ship or an iceberg with the tower, large loads develop at pile heads causing large displacements of the piles. The soil reactions to the pile motion are nonlinear in nature and slippage and separation at the

soil-pile interface may occur due to these loads. To explore the effect of soil nonlinearity and slippage and separation at soil-pile interface, the foundation stiffness and damping constants are calculated for different loading levels at pile heads, P/P_U, as ratio of pile capacities. These stiffness and damping constants are then used in the free vibration analysis. Three soil profiles are considered in the analysis as it was found that the nonlinear effects vary according to the homogeneity of the soil. For all soil profiles, the shear wave velocity at the pile tip, $V_s(L)$, is taken equal to 100 m/s or 200 m/s.

Fig. 8.4 shows the variation in the first undamped and damped natural frequency, ω_1, with the loading level for homogeneous, parabolic and linear soil profiles. This first natural frequency pertains to the first sway mode. It may be observed from the figure that ω_1 decreases as P/P_U increases. This decrease is more pronounced for the nonhomogeneous soil with partial recovery for parabolic medium at $P/P_U = 0.8$. This recovery may be attributed to the drop of the interaction between piles at this loading level. Both the undamped and damped natural frequencies follow the same trend. Fig. 8.5 displays the variation in the second natural frequency, ω_2, which is associated with the first torsional mode. It can be seen from the figure that ω_2 also decreases as P/P_U increases but the difference between the damped and undamped natural frequencies is increasing for higher P/P_U ratios. In Fig. 8.6, the first two modal foundation damping ratios are plotted for the three soil profiles. It may be noticed from the figure that the general trend is the increase in the damping as the load increases with some oscillations particularly for nonhomogeneous soils. These oscillations may be attributed to the decrease of both the interaction between piles and single pile stiffness with different rates and they have opposite effect on the damping ratios. It may be observed from Fig. 8.7

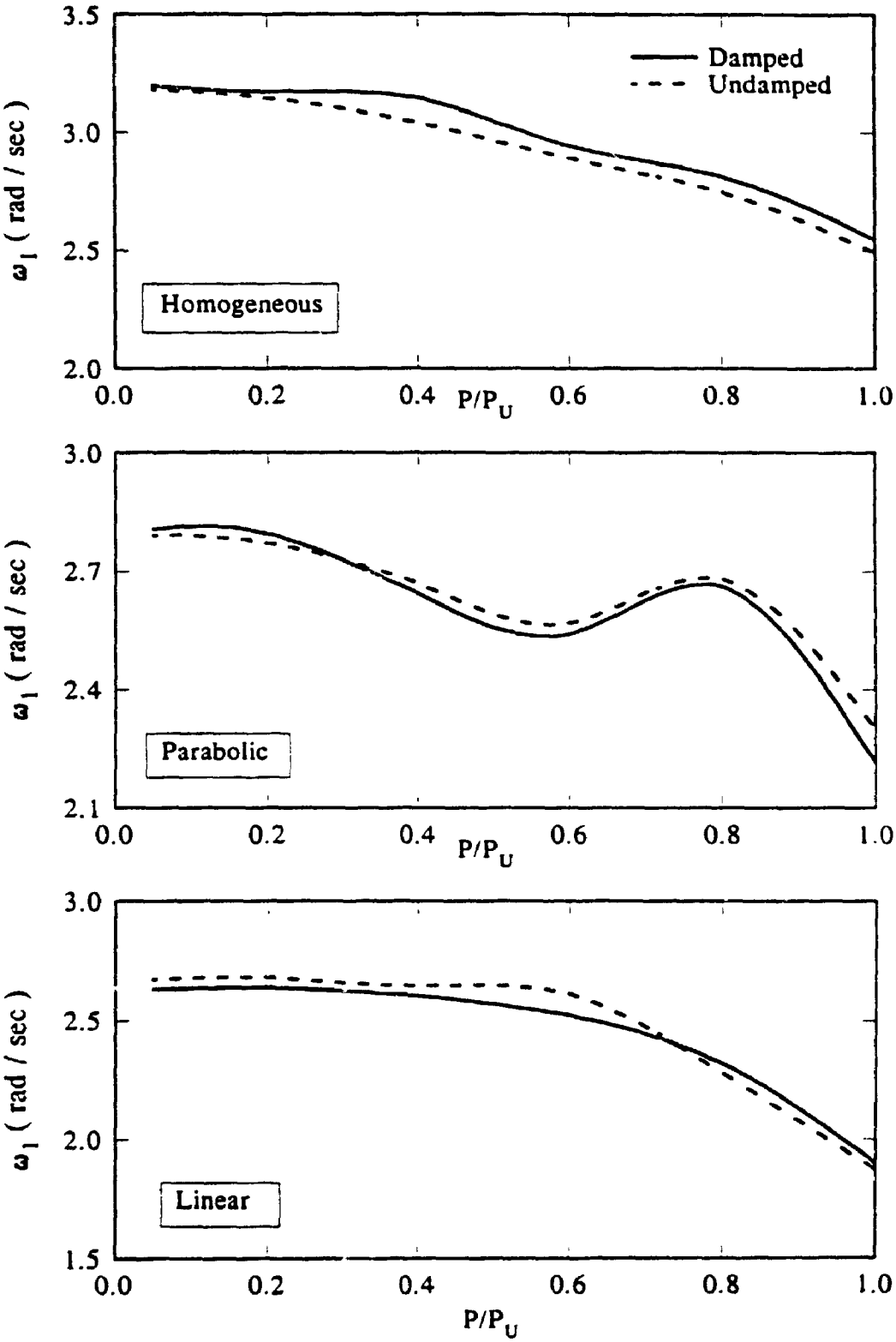

Figure 8.4 Variation in the First Natural Frequency of the Tower with Loading Ratio for Three Soil Profiles ($V_s(L)$ = 100 m/s, Interaction Considered)

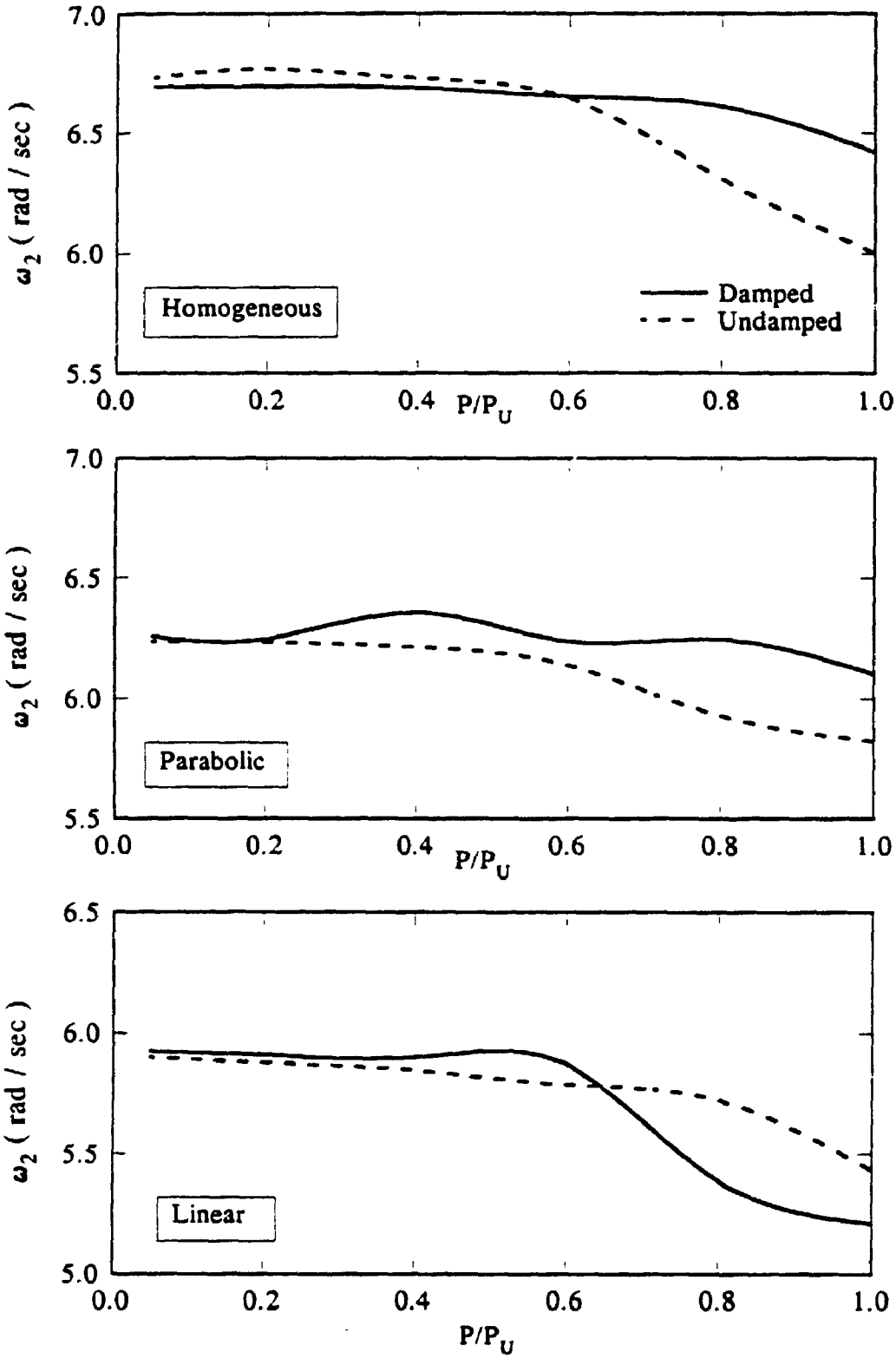

Figure 8.5 Variation in the Second Natural Frequency of the Tower with Loading Ratio for Three Soil Profiles (V_s(L) = 100 m/s, Interaction Considered)

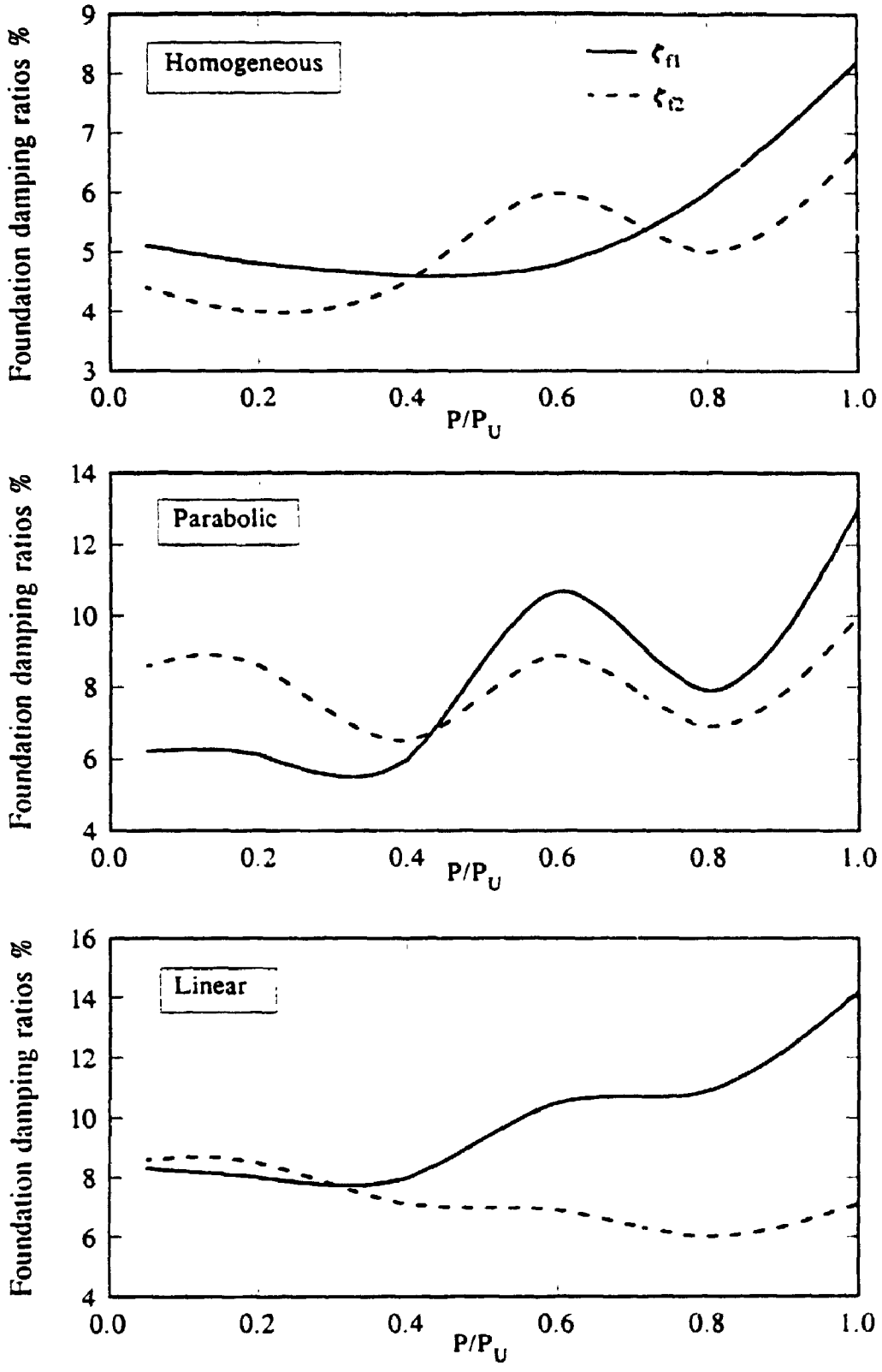

Figure 8.6 Variation in Foundation Damping Ratios of the Tower with Loading Ratio for Three Soil Profiles ($V_s(L)$ = 100 m/s, Interaction Considered)

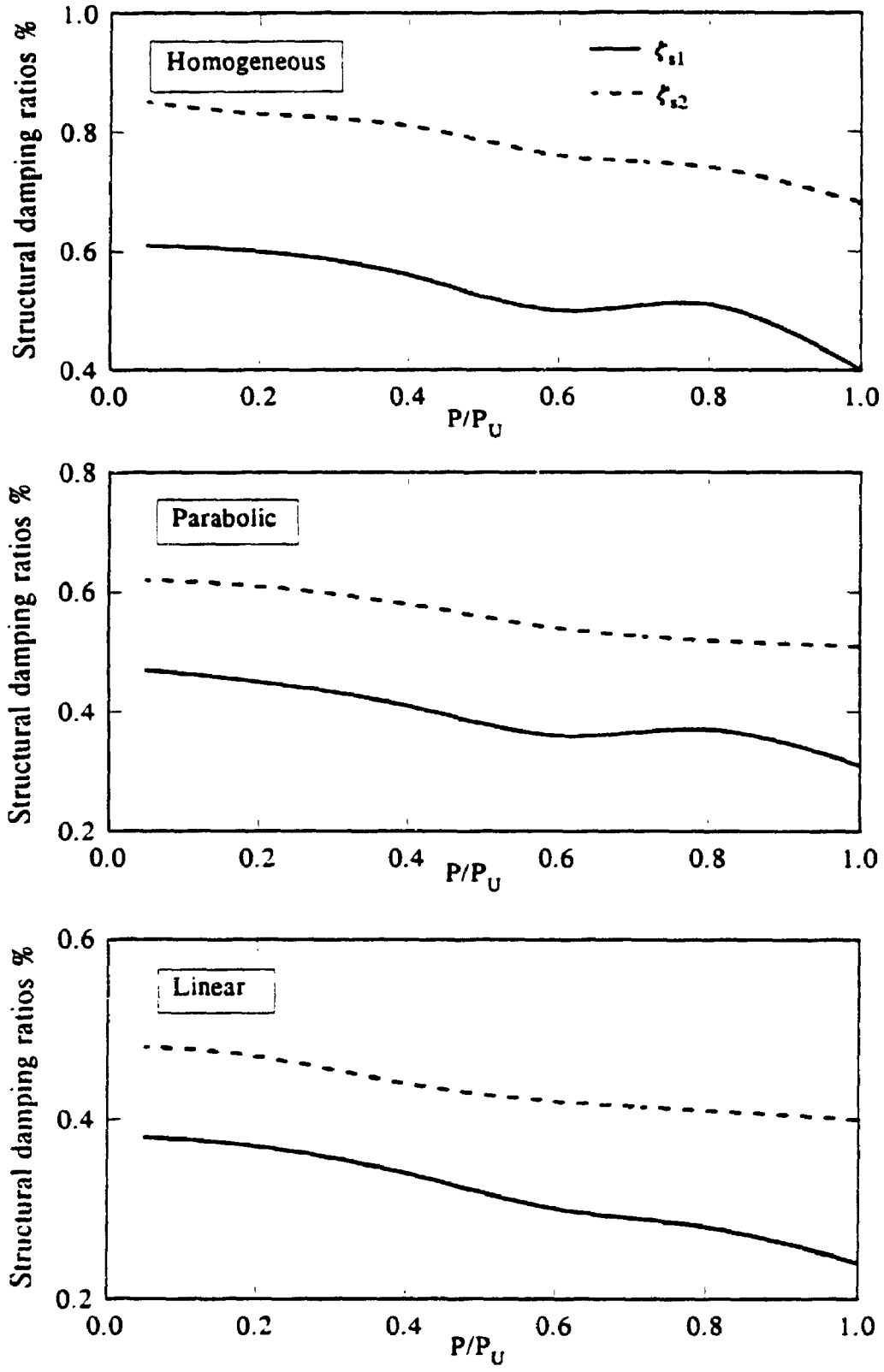

Figure 8.7 Variation in Structural Damping Ratios of the Tower with Loading Ratio for Three Soil Profiles ($V_s(L)$ = 100 m/s, Interaction Considered)

that the structural damping ratios decrease as the loading ratio P/P_U increases. This is due to the decrease in structural curvature with the increase in the foundation flexibility.

8.2.2. Effect of Soil Stiffness

The free vibration characteristics of the tower are calculated for a parabolic soil profile with two different shear wave velocities, $V_s(L)$ = 100 and 200 m /s. Fig. 8.8 shows the variation in the first two damped natural frequencies with the loading ratio P/P_U. It may be noticed from the figure that the nonlinearity effects are more pronounced for the stiffer soil case; the natural frequencies for the stiffer soil are higher but as the loading ratio increases, these frequencies decrease until they become even less than those of the softer soil. The variation of the first two foundation damping ratios with P/P_U is presented in Fig. 8.9. From the figure, it may be noticed that the damping ratios for the stiffer soil is less than for the softer one for lower P/P_U ratios. However, as P/P_U increases the damping ratios for the stiffer soil become almost equal to those for the softer soil. Structural damping was found to follow the usual trend of decreasing with the increase in the foundation flexibility.

8.2.3. Effect of Pile-Soil-Pile Interaction

Pile-soil-pile interaction has a significant effect on damping ratios and to a smaller extent on natural frequencies even for the relatively large s/d ratios for this particular tower. These effects are shown in Fig. 8.10 and 8.11 for the first and second natural frequencies for the three soil profiles considered in the analysis, respectively, and Fig. 8.12 for the first foundation damping ratios. The natural frequencies decrease when the

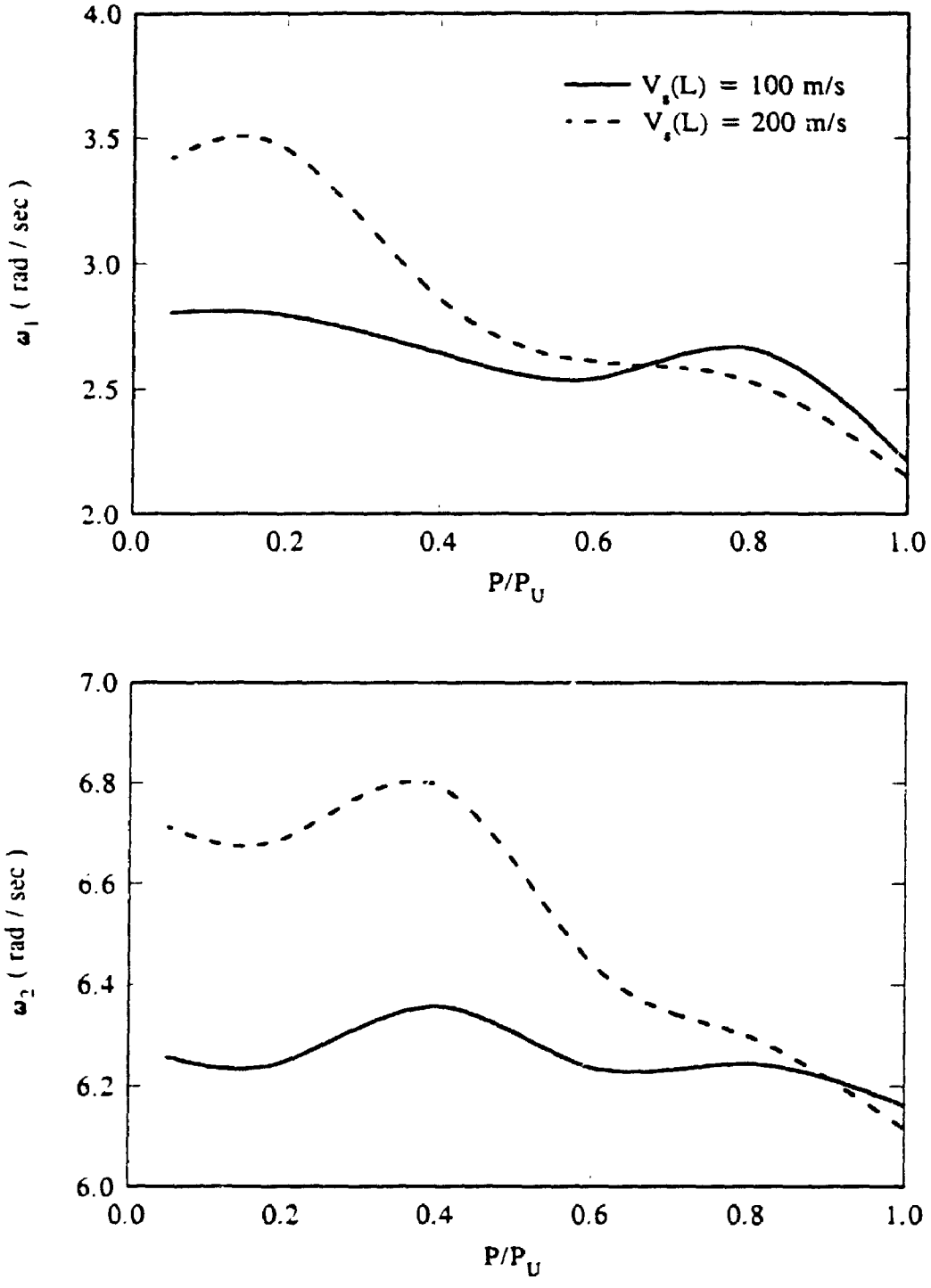

Figure 8.8 Variation in the Tower Natural Frequencies with Loading Ratio for Two Soil Shear Wave Velocities (Parabolic Profile, Interaction Considered)

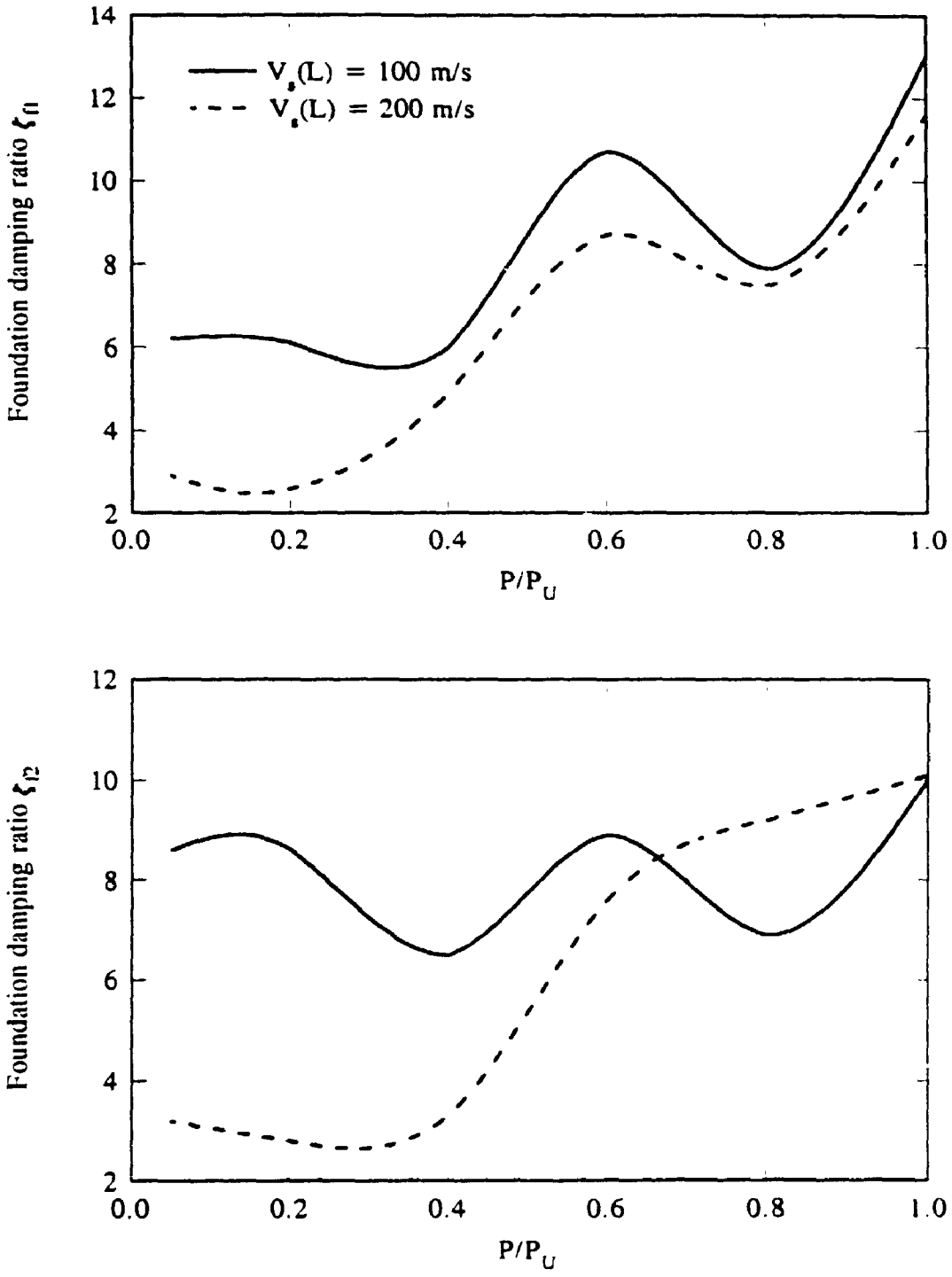

Figure 8.9 Effect of Soil Shear Wave Velocity on Foundation Damping Ratios
(Parabolic Profile, Interaction Considered)

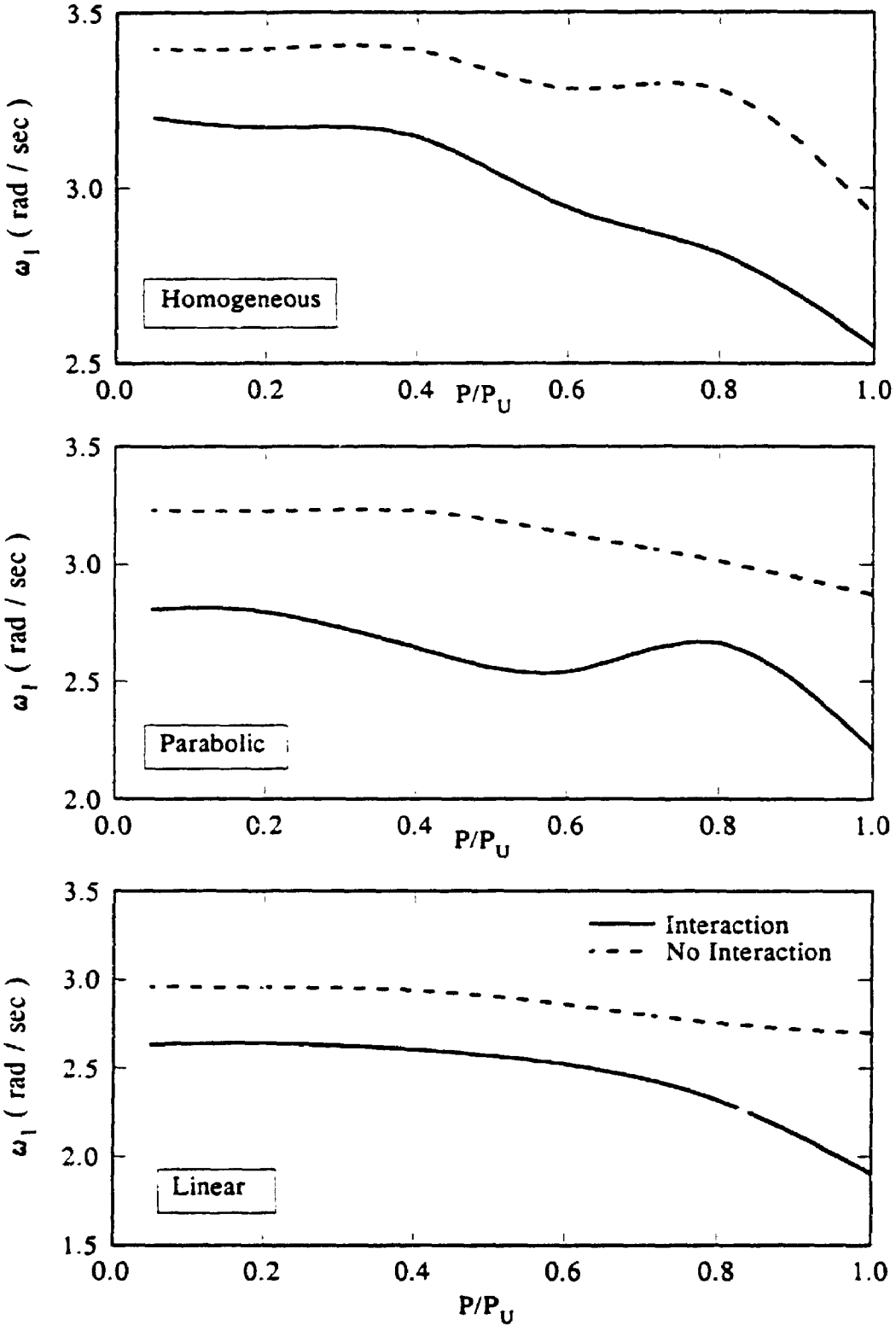

Figure 8.10 Effect of Pile-Soil-Pile Interaction on the First Natural Frequency of the Tower for Three Soil Profiles ($V_s(L)$ = 100 m/s)

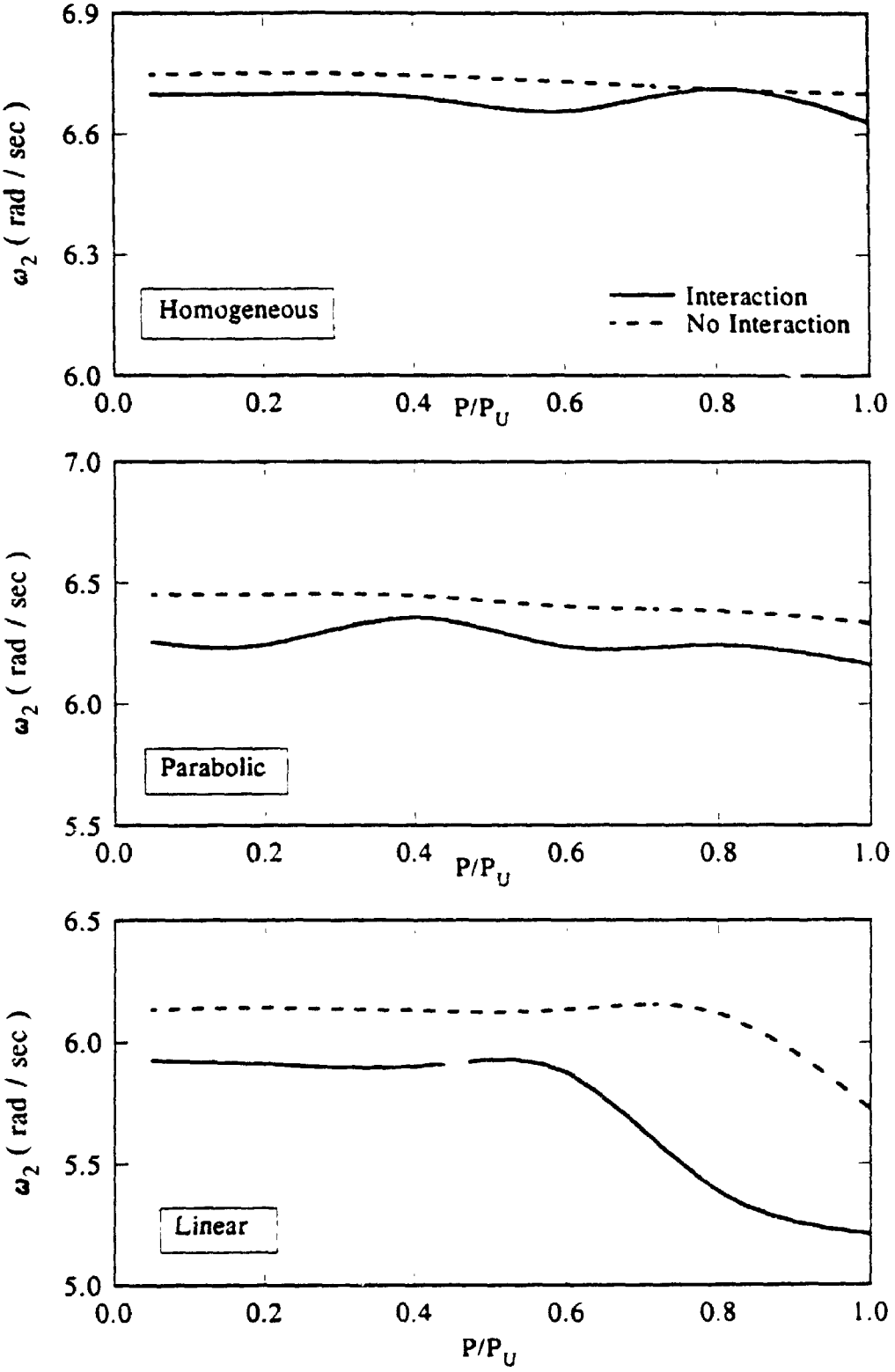

Figure 8.11 Effect of Pile-Soil-Pile Interaction on the Second Natural Frequency of the Tower ($V_s(L)$ = 100 m/s)

interaction is considered and the effect is more pronounced on the first natural frequency. The first foundation damping ratios increase significantly when the interaction is considered as may be observed from Fig. 8.12.

8.2.4. Effect of Deck Mass

The deck mass may vary during different operational processes and the variation may reach a factor of 2 [41]. The natural frequencies, damping ratios and the tower response are affected accordingly. To examine this effect on the free vibration characteristics of the tower, two different ratios of the deck mass to total mass of the tower, 20.33 % and 59.21 %, are assumed in the analysis of the tower. Variation in the first and second undamped natural frequencies of the tower is shown in Figs. 8.13 and 8.14, respectively. It may be observed from the figures that the natural frequencies drop significantly as the deck mass ratio increases for all soil profiles and different loading levels. Also, it was found that modal damping as percentage of the critical damping decreases as the deck mass ratio increases. The drop of the natural frequency due to the increase in deck mass ratio is very important because it brings the resonant frequencies closer to the wave energy spectral frequency, $\bar{\omega}$, leading to dynamic amplification of the response.

8.3. Variation in Hydrodynamic Damping with the Different Parameters

The hydrodynamic damping is a major source of damping especially with higher sea states. It is derived from the motion of the tower in the water and it is affected by this motion and as such, the behavior of the tower foundation affects the hydrodynamic damping. For all the results presented in this section, the deck mass is assumed to be

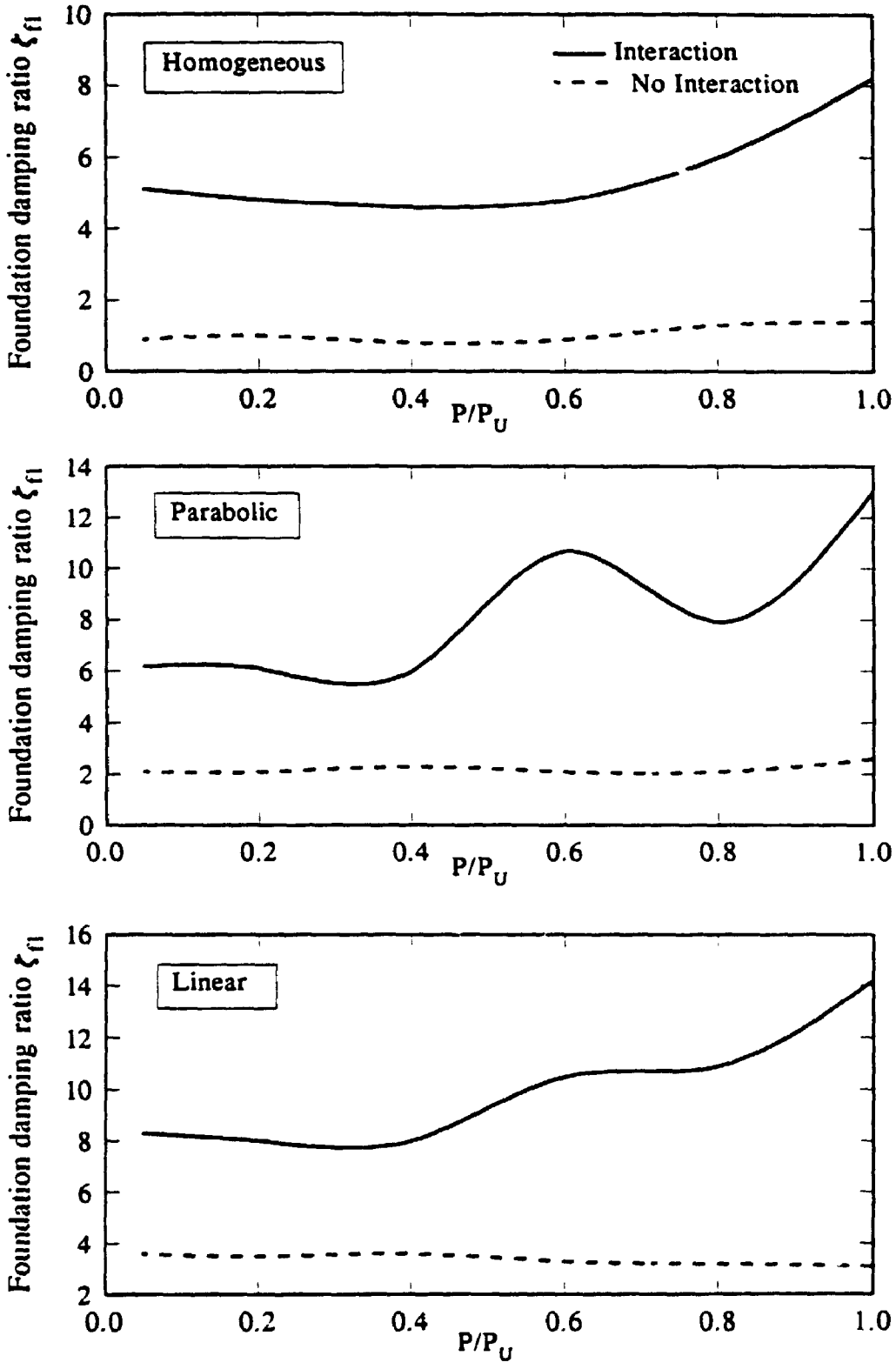

Figure 8.12 Effect of Pile-Soil-Pile Interaction on the First Foundation Damping Ratio for Three Soil Profiles ($V_s(L)$ = 100 m/s)

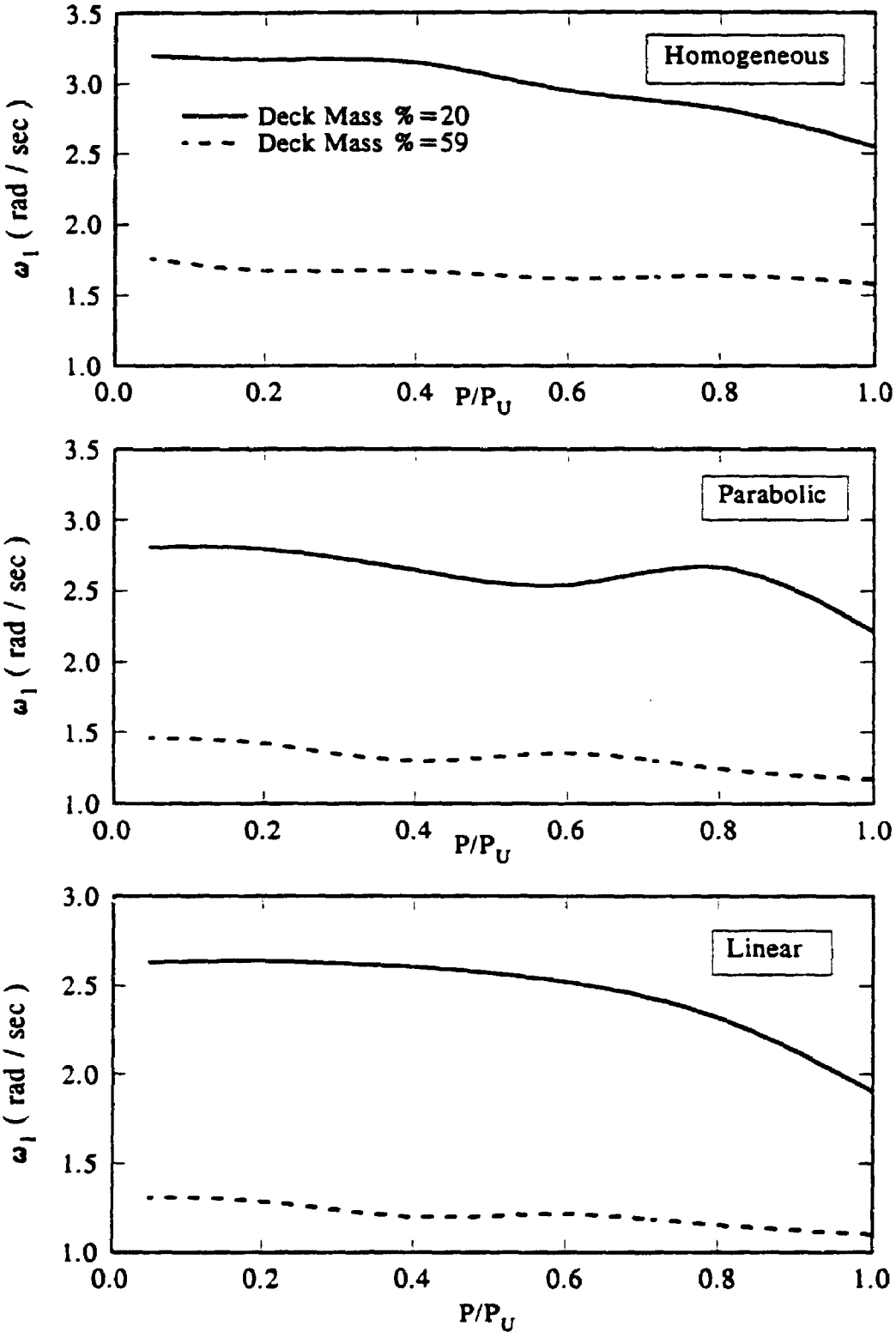

Figure 8.13 Effect of Deck Mass on the First Natural Frequency of the Tower for Three Soil Profiles (V_s(L) = 100 m/s, Interaction Considered)

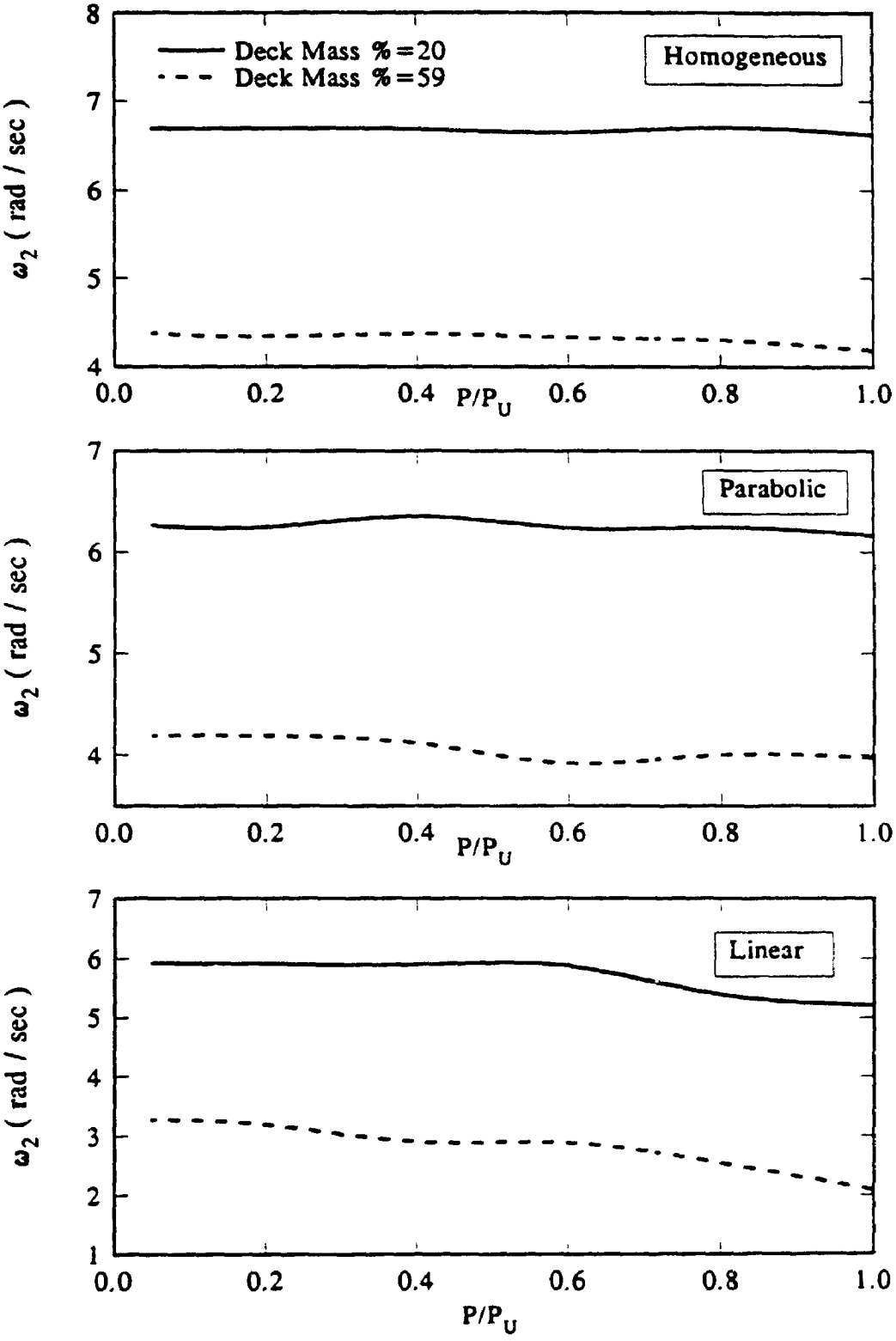

Figure 8.14 Effect of Deck Mass on the Second Natural Frequency of the Tower for Three Soil Profiles ($V_s(L)$ = 100 m/s, Interaction Considered)

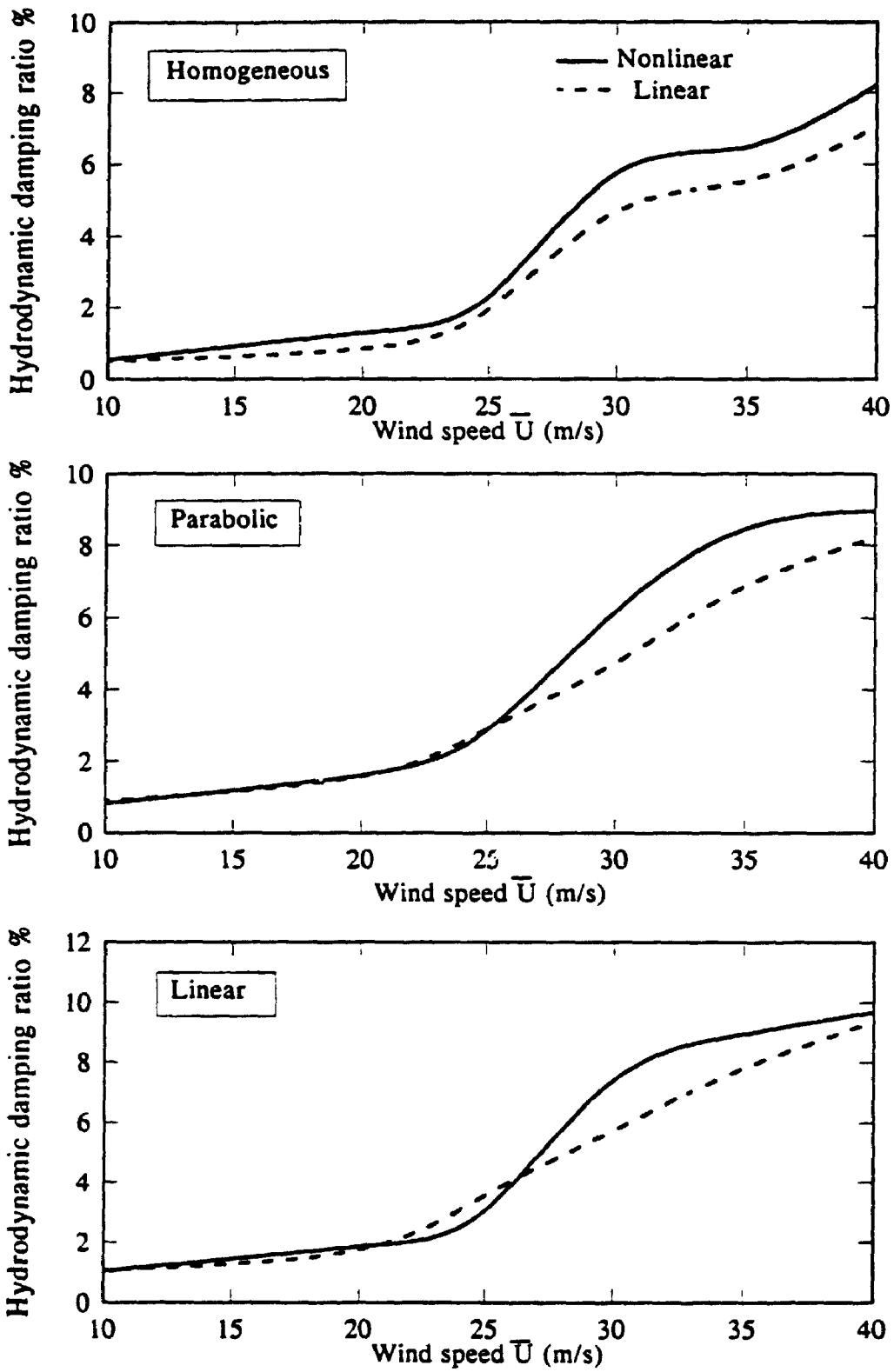

Figure 8.15 Effect of Foundation Nonlinearity on the Hydrodynamic Damping for Three Soil Profiles ($V_s(L)$ = 100 m/s, Interaction Considered)

59.21 % of the total mass of the tower.

8.3.1. Effect of Foundation Nonlinearity

Response of the tower to wave forces is evaluated for the three soil profiles with $V_s(L)$ = 100 m/s and six different wind speeds ranging from 10 to 40 m/s. Hydrodynamic ratios are obtained by both considering and neglecting the nonlinear behavior of the supporting piles. Fig. 8.15 shows the variation of the hydrodynamic damping with the wind speed for the three soil profiles for both cases. It may be noticed from the figure that the hydrodynamic damping increases as the wind speed increases. This is understood because higher wind speeds means larger tower response. Also, considering the nonlinear behavior of the foundation leads to the prediction of higher values of the hydrodynamic damping particularly for higher wind speeds. This is because the assumption of linear foundation overpredicts the tower stiffness and consequently, underpredicts the tower response leading to the evaluation of lower hydrodynamic values.

8.3.2. Effect of Soil Stiffness

The tower is analyzed for two different shear wave velocities, $V_s(L)$ = 100 and 200 m/s assuming a parabolic soil profile. The nonlinear behavior of the soil is considered and the interaction between piles is taken into account. Fig. 8.16 shows the variation of the hydrodynamic damping ratio with the wind speed for the two shear wave velocities. As expected, the figure shows that the hydrodynamic ratios for the stiffer soil are less than those of the softer soil especially for higher wind speeds.

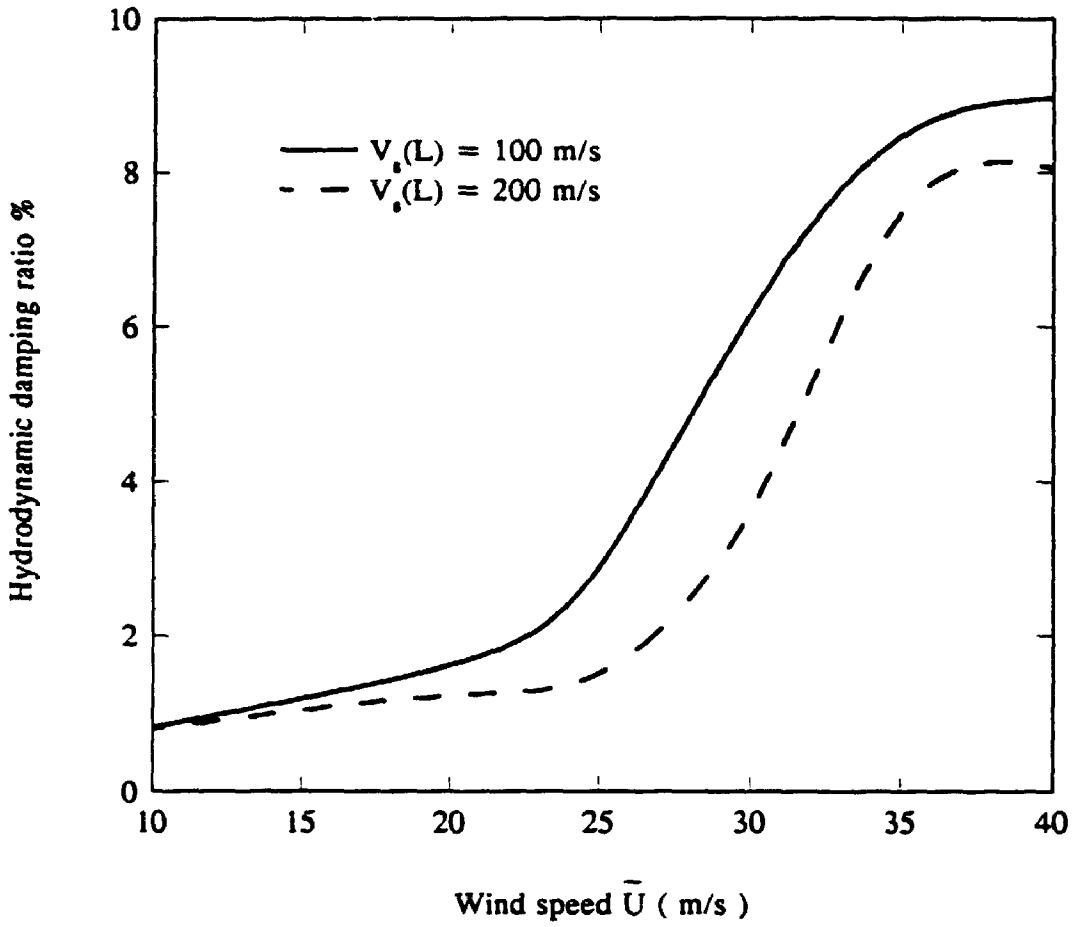

Figure 8.16 Effect of Soil Stiffness on the Hydrodynamic Damping Ratio (Parabolic Profile, Interaction Considered)

8.3.3. Effect of Pile-Soil-Pile Interaction

The hydrodynamic damping is calculated for two soil profiles, homogeneous and parabolic, with $V_s(L)$ = 100 m/s. Fig. 8.17 presents the hydrodynamic ratios as a percentage of the critical damping calculated considering and neglecting the pile-soil-pile interaction for both linear and nonlinear cases. It may be observed from the figure that the effect of the interaction on the ratio of the hydrodynamic damping is such that the interaction decreases the calculated hydrodynamic ratios for lower wind speeds and increases it for higher wind speeds. This is because the interaction increases the structural flexibility leading to larger hydrodynamic damping, but it also increases the total damping significantly.

8.4. Variation in Tower Response to Wave Forces with Different Parameters

The tower response to wave forces is greatly affected by the behavior of the supporting foundations. The effects of different parameters defining the foundation behavior are explored in this section. For all the results presented in this section, the deck mass is assumed to be 59.21 % of the total mass and the exponential decay parameter c is assumed to have a value of 1.

8.4.1. Effect of Foundation Nonlinearity

The tower response is evaluated for the three different soil profiles with the shear wave velocity Vs(L) = 100 m/s and six different wind speeds ranging from 10 to 40 m/s. For all cases the pile-soil-pile interaction is considered. Figs. 8.18, 8.19 and 8.20 show the power spectra of top node deflection for different wind speeds for

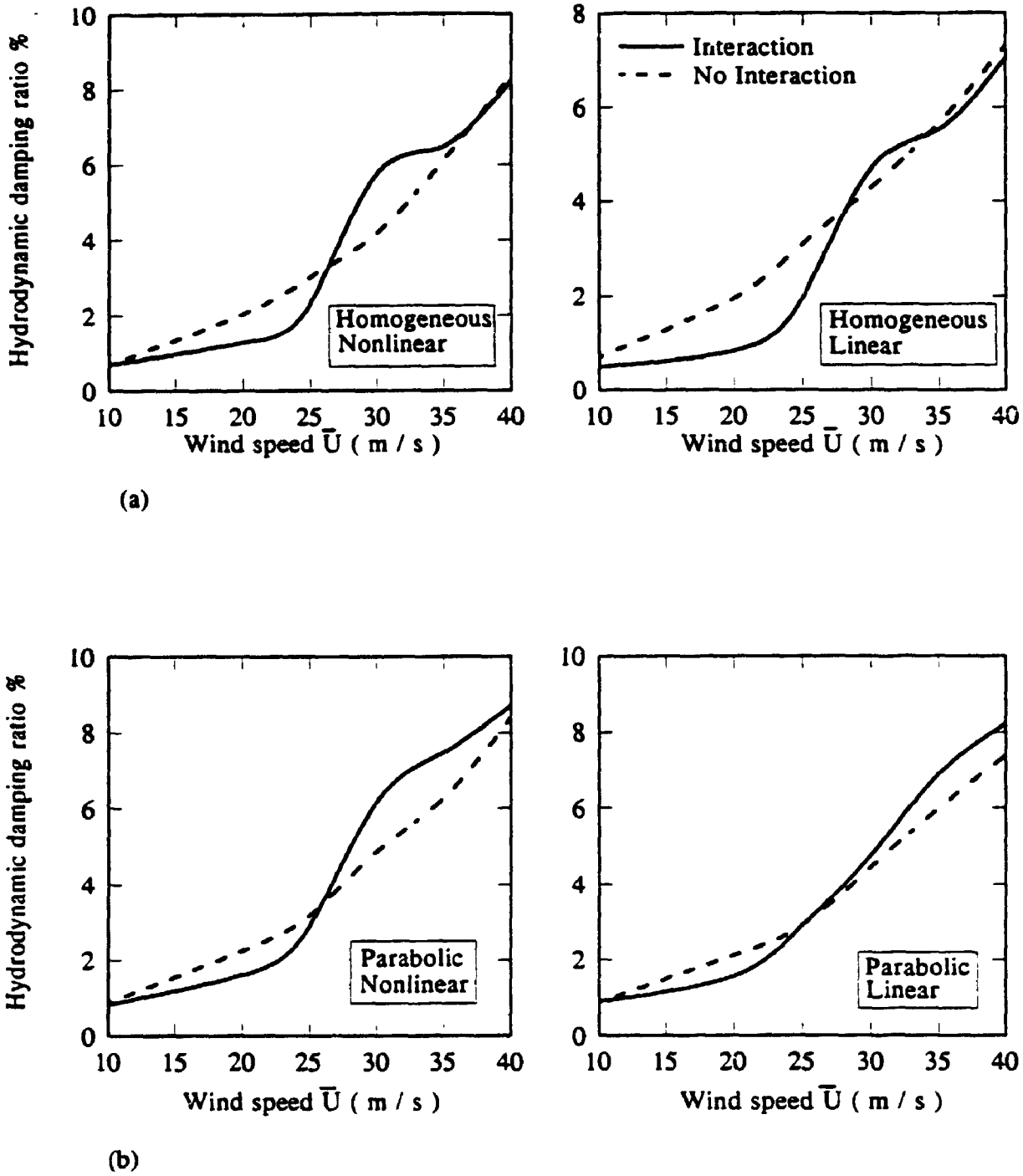

Figure 8.17 Effect of Pile-Soil-Pile Interaction on the Hydrodynamic Damping Ratio for Two Soil Profiles ($V_s(L)$ = 100 m/s, Nonlinear Foundation)

homogeneous, parabolic and linear soil profiles, respectively. In Fig. 8.18, the power spectrum of top node deflection for the homogeneous soil profile evaluated for both linear and nonlinear pile behavior is presented. The figure shows that for wind speed, $\bar{U}$ equal to 10 m/s the response is linear and the spectrum has a pronounced resonance peak and a smaller one, the background response peak, at the wave energy spectral peak frequency, $\bar{\omega}$. As $\bar{U}$ increases, the resonant peak is suppressed and the background peak increases. It may be noticed from the figure that the resonance frequency and resonant peak evaluated from the nonlinear analysis are less than those evaluated from the linear analysis. On the other hand, the background response derived from the nonlinear analysis is almost 30 % higher than that obtained from the linear analysis. Fig. 8.19 displays the power spectrum of the top node deflection for the parabolic case. Similar observations can be made with the exception that the resonant and background peaks are closer to each other and the nonlinear effects for higher wind speeds are more pronounced. Fig. 8.20 presents the power spectrum of the top node deflection for a linear soil profile. It may be noticed from the figure that the background peak is larger than the resonant one and the response spectrum is somewhat broad banded due to the closeness of the dominant natural frequency of the tower, ω_0, and $\bar{\omega}$. As $\bar{U}$ increases, the background response increases with the response evaluated from the nonlinear analysis being higher than the linear response until it becomes almost twice the linear response for $\bar{U}$ = 40 m/s.

To further illustrate the nonlinearity effects on the tower response to wave forces, the variation in the total response amplitude (standard deviation) of the top node

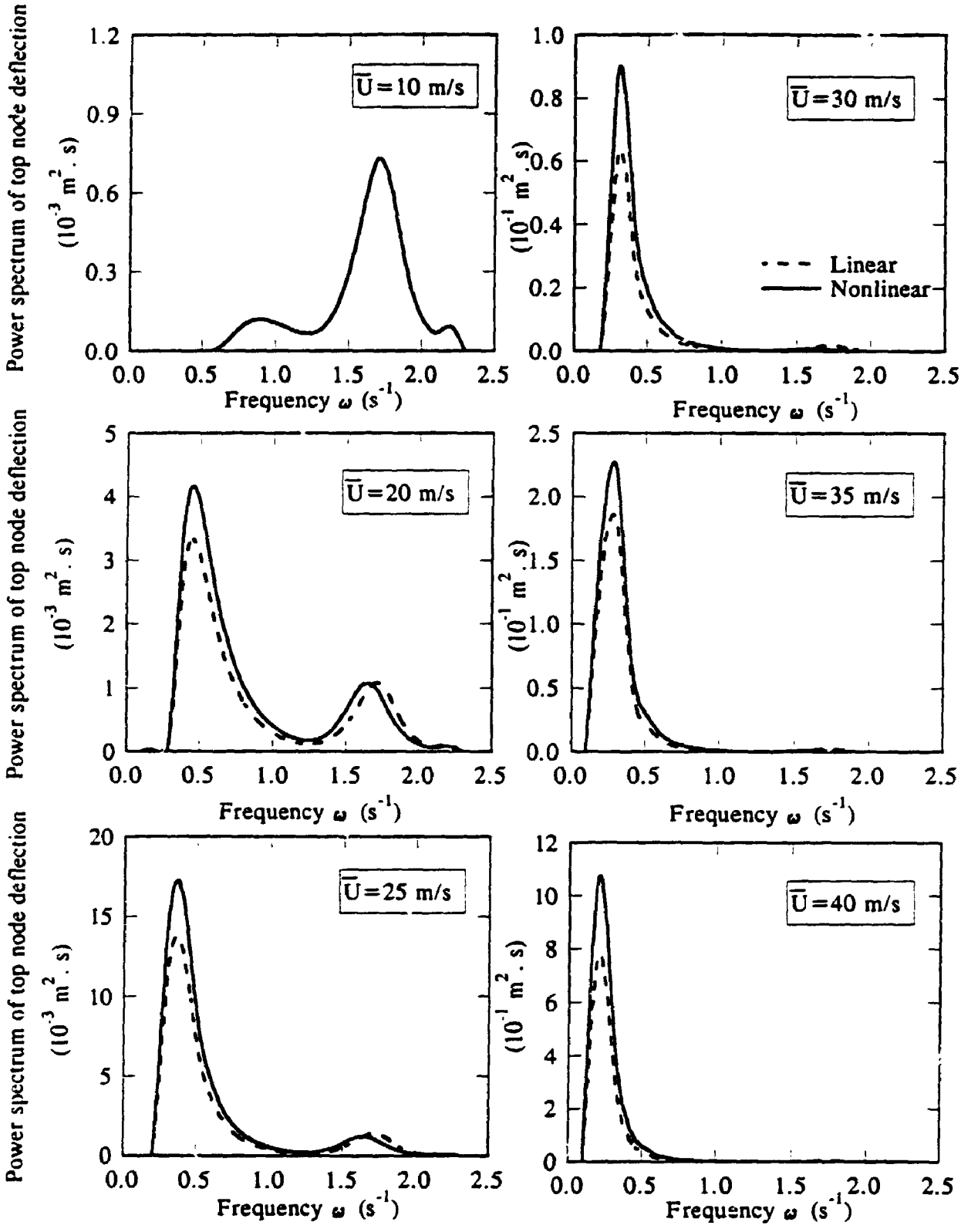

Figure 8.18 Effect of Foundation Nonlinearity on Tower Response Spectrum for Six Wind Speeds (Homogeneous Profile, $V_s(L)$ = 100 m/s, Interaction Considered)

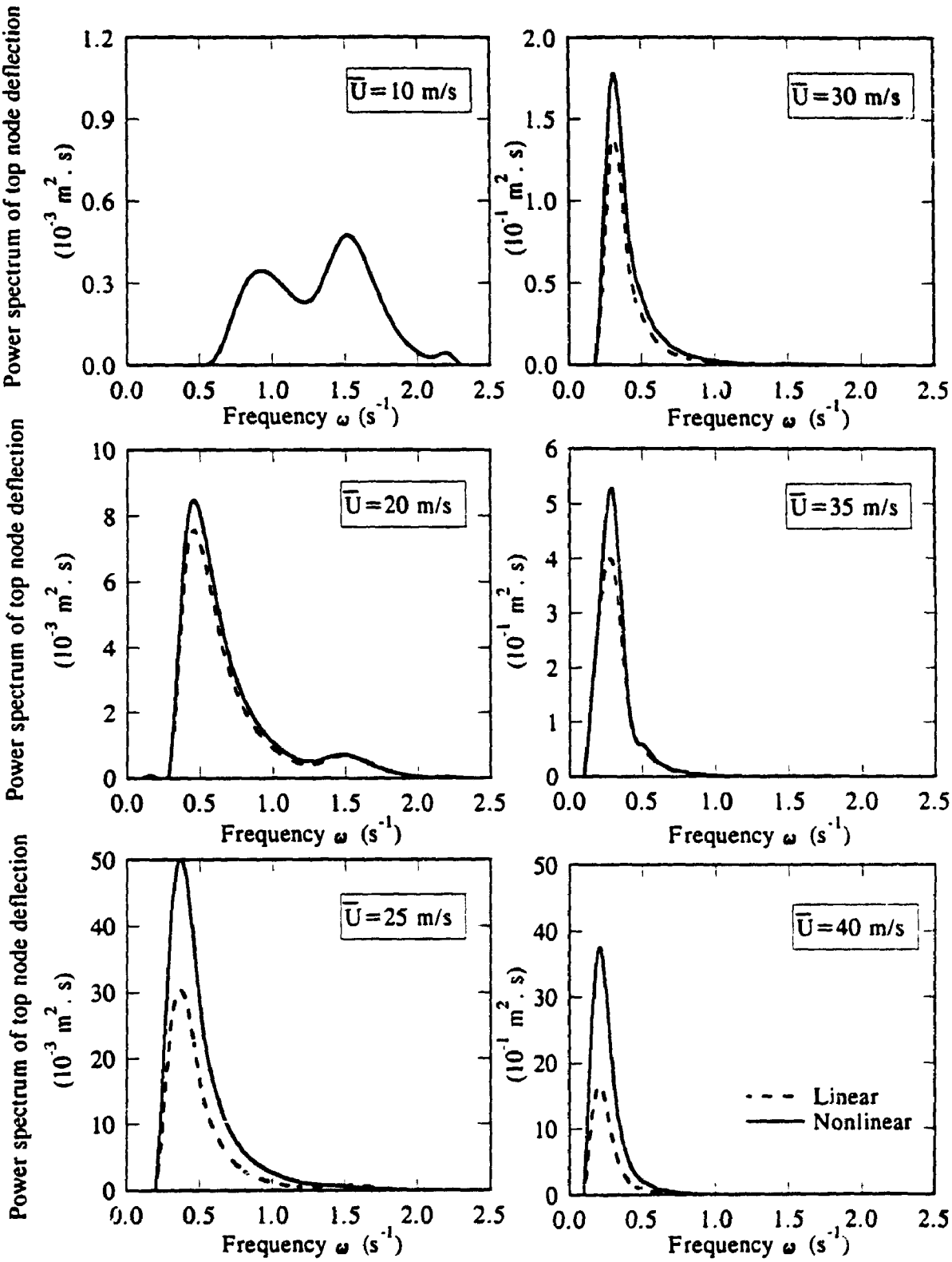

Figure 8.19 Effect of Foundation Nonlinearity on Tower Response Spectrum for Six Wind Speeds (Parabolic Profile, $V_s(L)$ = 100 m/s, Interaction Considered)

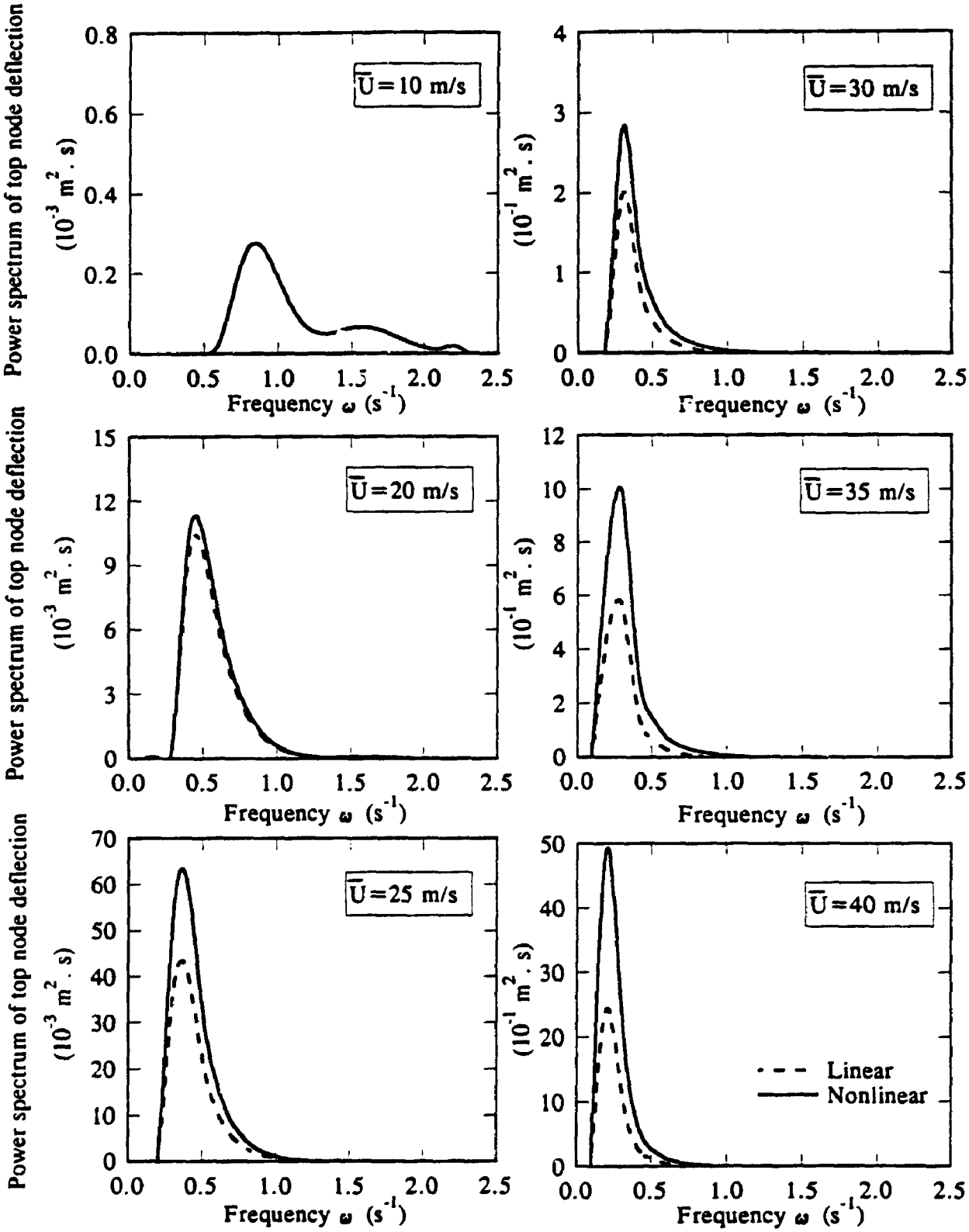

Figure 8.20 Effect of Foundation Nonlinearity on Tower Response Spectrum for Six Wind Speeds (Linear Profile, $V_g(L)$ = 100 m/s, Interaction Considered)

deflection is presented in Fig. 8.21 with the wind speed for the three soil profiles. It may be seen from the figure that the amplitudes for homogeneous soil profile are higher than that of the parabolic one and the linear being the lowest for lower wind speeds with no difference between the results obtained from linear or nonlinear foundation. This is because the resonance component of the response, which is larger for stiffer soils with lower damping ratios, is higher than that of the background component for lower wind speeds. As $\bar{U}$ increases, the response amplitude for the linear case becomes the larger and the response amplitude for the homogeneous case becomes the smaller. This is because the contribution to the total response from the background component is much higher than that of the resonance component. The background response is quasi-static with little or no dynamic amplification. Thus the magnitude of the background response is controlled by the stiffness of the system. Also, the nonlinear effects are more pronounced for higher wind speeds.

To get an insight look into the foundation behavior, the pile head response amplitudes for the pile located on the X axis are presented in Figs. 8.22 and 8.23 for horizontal and vertical deflections, respectively. It may be noticed from Fig. 8.22 that the horizontal deflection at the pile head increases as $\bar{U}$ increases and the inclusion of the nonlinearity in the analysis increases the response for some wind speeds and reduces it for other wind speeds. However, for $\bar{U}$ = 40 m/s the predicted nonlinear response is higher than the linear one especially for nonhomogeneous soils. From Fig. 8.23, it may be observed that a similar behavior occurs for the vertical deflection at the pile head except that the nonlinear response for higher wind speed is lower than the linear

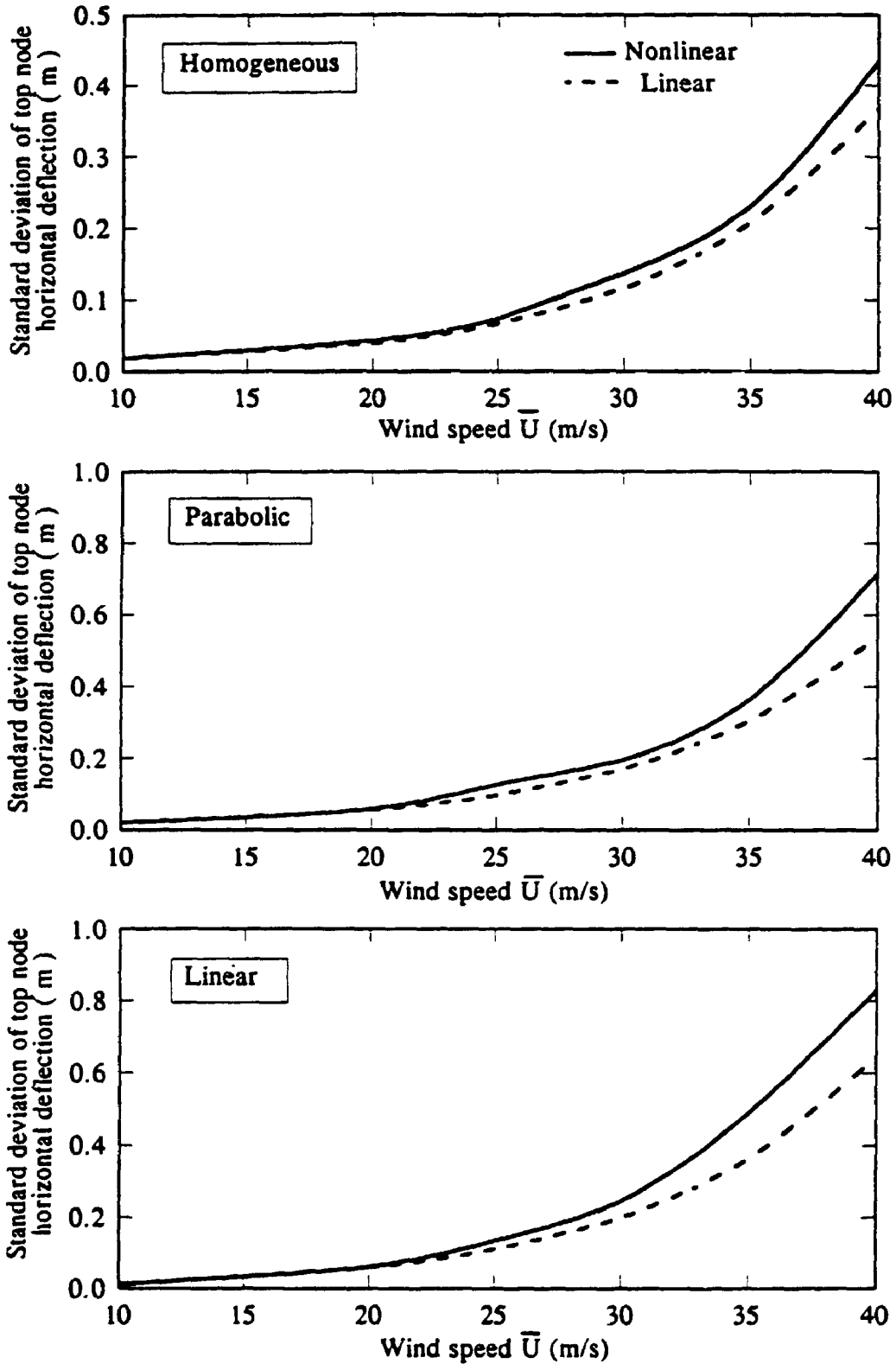

Figure 8.21 Effect of Foundation Nonlinearity on Tower Response Amplitude for Three Soil Profiles ($V_s(L)$ = 100 m/s, Interaction Considered)

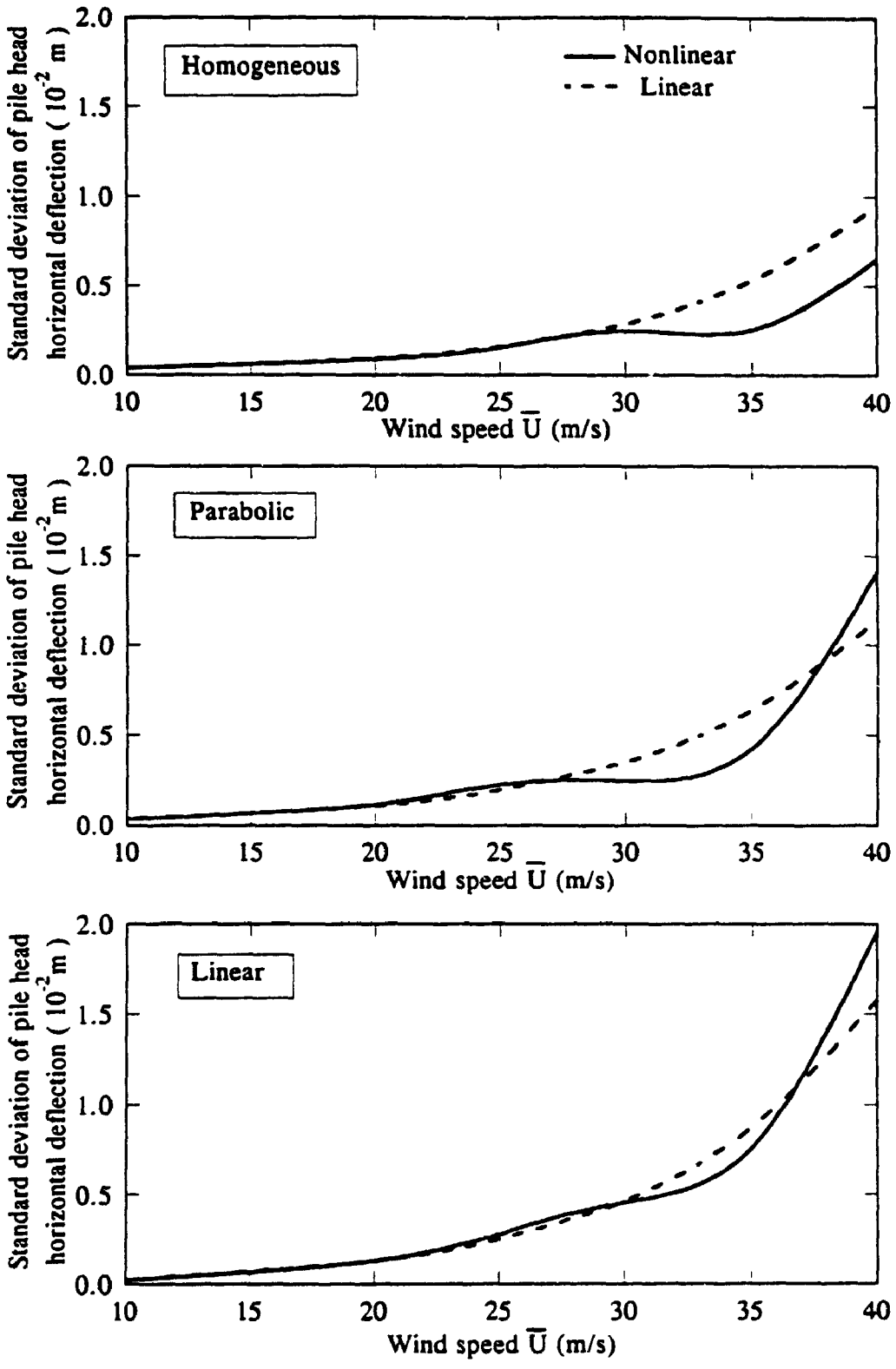

Figure 8.22 Effect of Nonlinearity on the Horizontal Deflection of Supporting Piles for Three Soil Profiles ($V_s(L)$ = 100 m/s, Interaction Considered)

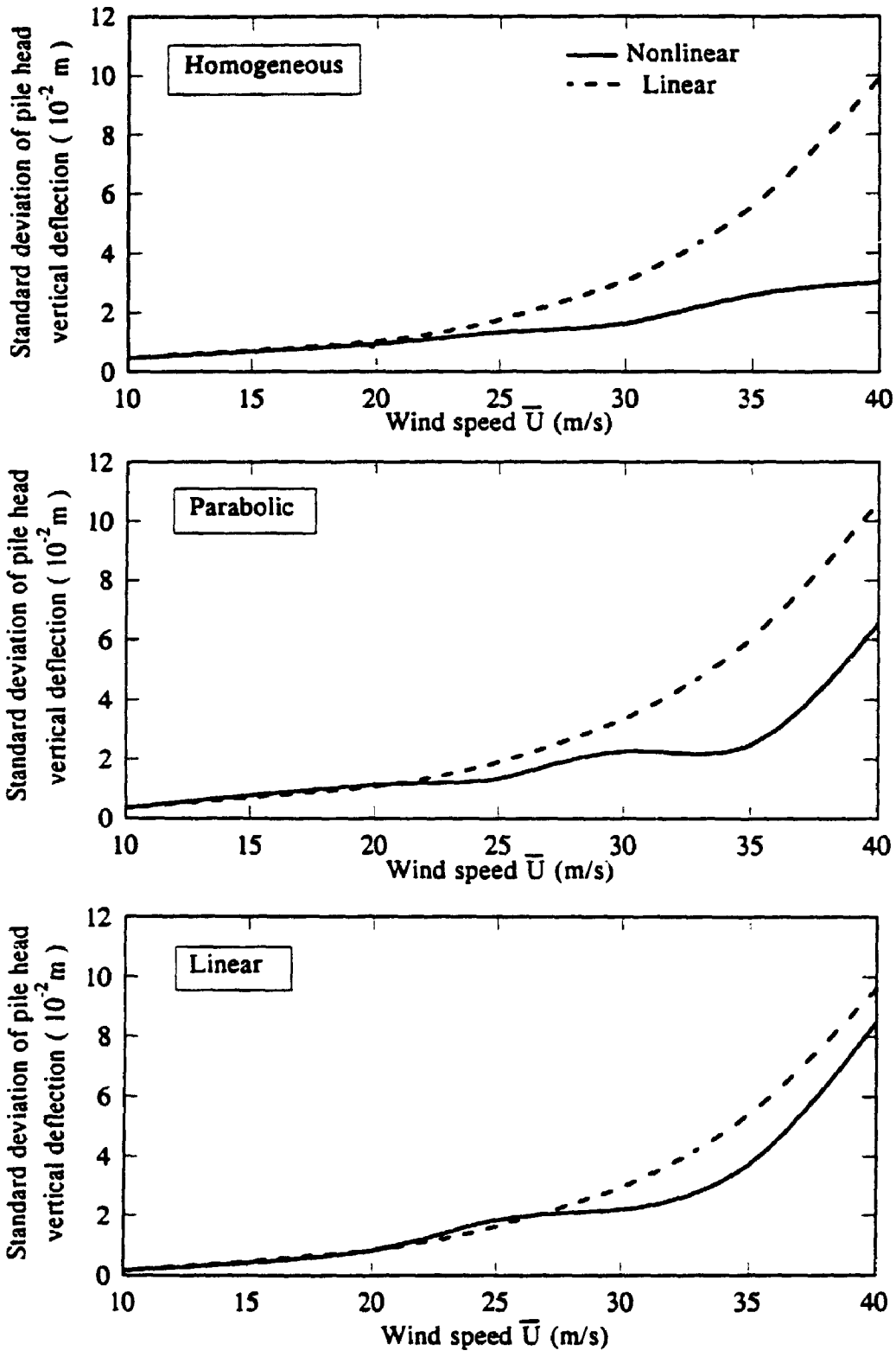

Figure 8.23 Effect of Nonlinearity on the Vertical Deflection of Supporting Piles for Three Soil Profiles ($V_s(L)$ = 100 m/s, Interaction Considered)

response. This is because the tower response predicted, adopting the linear analysis, is essentially rocking due to the overprediction of the horizontal stiffness which reduces the horizontal translation. Also, it may be noticed from Figs. 8.22 and 8.23 that the mean peak deflections calculated using Eq. 7.40 for $\bar{U}$ = 40 m/s are 0.049d and 0.193d for the parabolic soil profile. The mean peak deflections are even higher for the linear soil profile, in the horizontal and vertical directions, respectively, where d is the diameter of the pile. These large displacements confirm that nonlinear effects should be accounted for in the analysis.

8.4.2. Effect of Soil Stiffness

To examine the effect of the soil stiffness on the tower response to wave forces, a parabolic soil profile with $V_s(L)$ = 200 m/s was considered in the analysis and the results obtained are compared to those for the parabolic soil profile with $V_s(L)$ = 100 m/s. The power spectra of the top node horizontal deflection for $V_s(L)$ = 200 m/s for different wind speeds are shown in Fig. 8.24. The figure shows that the response is essentially linear for lower wind speeds and a rather significant peaks are distinguished at ω_0 and $\bar{\omega}$ compared to the case with $V_s(L)$ shown in Fig. 8.19. At $\bar{U}$ = 25 m/s, the resonance peak for the linear case becomes slightly less than the nonlinear case, while the background peak for the linear case becomes slightly higher than the nonlinear case. This may be attributed to the drop of the interaction between piles being much more than the decrease in single piles stiffness for stiffer soils in the intermediate range of loading. This drop in interaction leads to a decrease in the system damping and an increase in the tower stiffness. These two factors, the drop in the damping and the increase in the

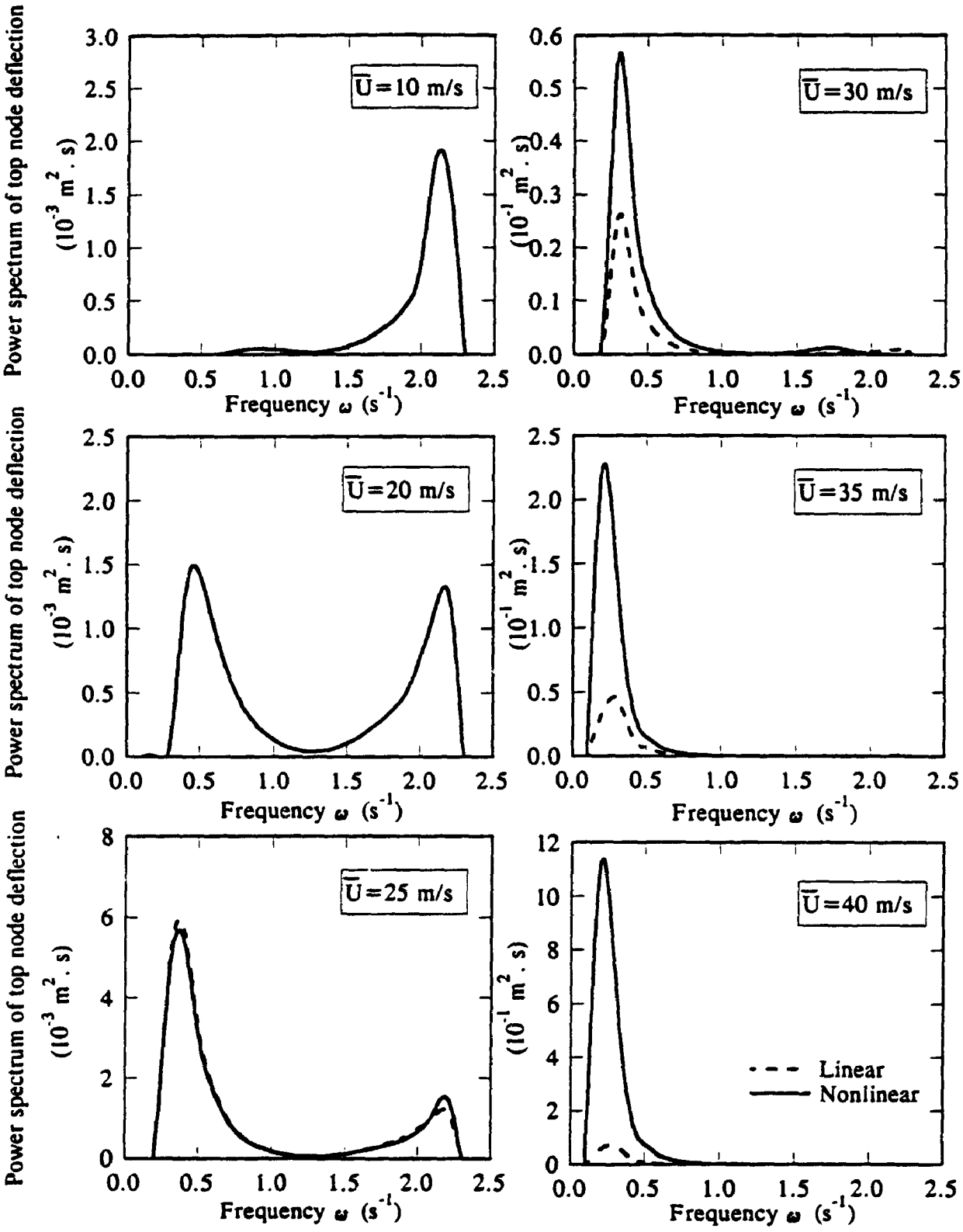

Figure 8.24 Effect of Foundation Nonlinearity on Tower Response Spectrum for Six Wind Speeds (Parabolic Profile, $V_s(L)$ = 200 m/s, Interaction Considered)

stiffness, cause the increase in the resonant peak and the decrease in the background peak for the nonlinear analysis. Also, it may be noticed from the figure that the increase in the response at higher wind speeds is much greater in the nonlinear case than that of the linear case compared to the profile with $V_s(L)$ = 100 m/s shown in Fig. 8.19. The standard deviations of top node horizontal deflection for $V_s(L)$ = 100 and 200 m/s are presented in Fig. 8.25. It may be concluded from the figure that the response amplitudes for the stiffer soil are less than that for the softer soil for all wind speeds and that the nonlinear response amplitudes are higher than the linear ones for all wind speeds. Figs. 8.26 and 8.27 show the variation in the response amplitude of pile head horizontal and vertical deflections, respectively, with $\bar{U}$ for both $V_s(L)$ = 100 and 200 m/s. It may be observed from the figures that response amplitudes derived from the nonlinear analysis are less than those obtained from the linear analysis because the drop in the interaction is much greater than the drop in the single piles stiffness as pointed out earlier.

8.4.3. Effect of Pile-Soil-Pile Interaction

The interaction between piles affects the response of the tower as it alters the values of supporting piles stiffness and damping. Fig . 8.28 shows the power spectrum of top node deflection for a homogeneous soil profile with $V_s(L)$ = 100 m/s for different wind speeds considering and neglecting the pile-soil-pile interaction, respectively. It may be noticed from the figure that, for lower wind speeds, neglecting the interaction leads to significant overprediction of the resonance peak because it reduces the damping dramatically and it also overpredicts the resonant frequency due to the overprediction of the stiffness. On the other hand, the background peak increases dramatically due to the

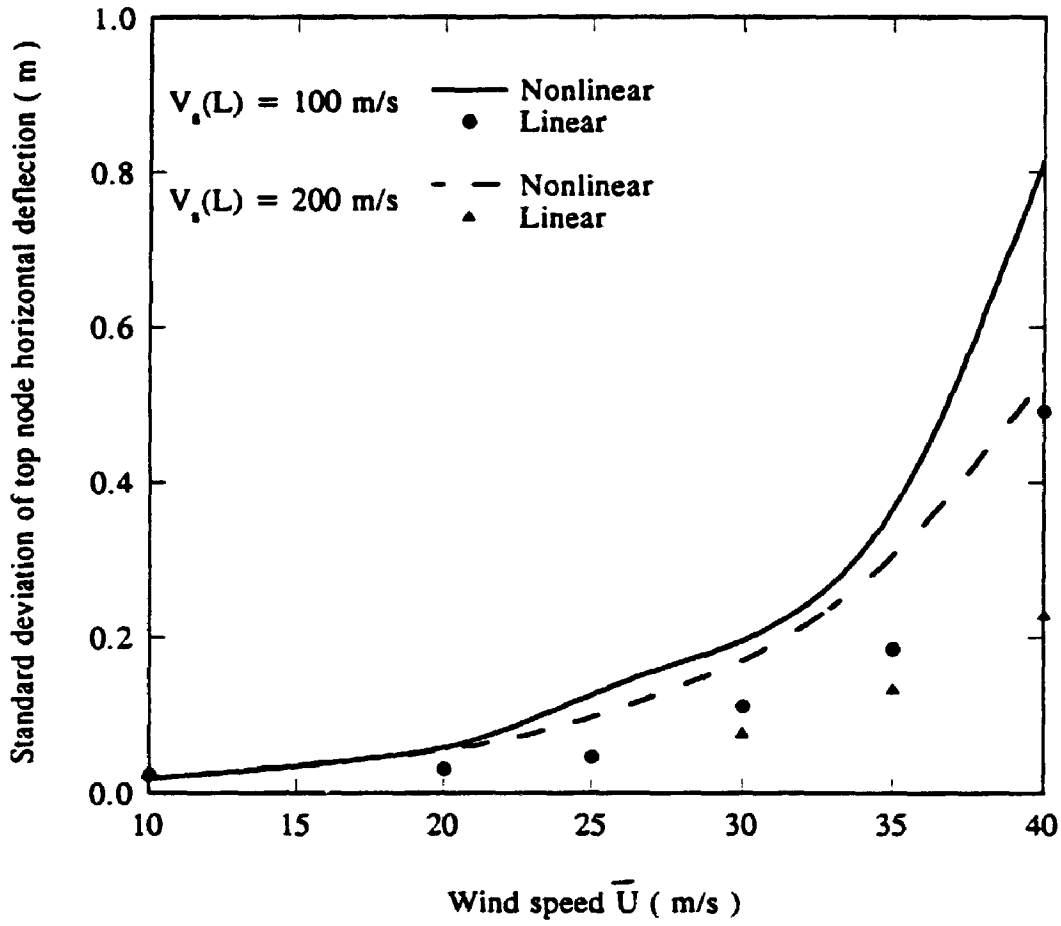

Figure 8.25 Effect of Soil Stiffness on the Tower Response Amplitude (Parabolic Profile, Interaction Considered)

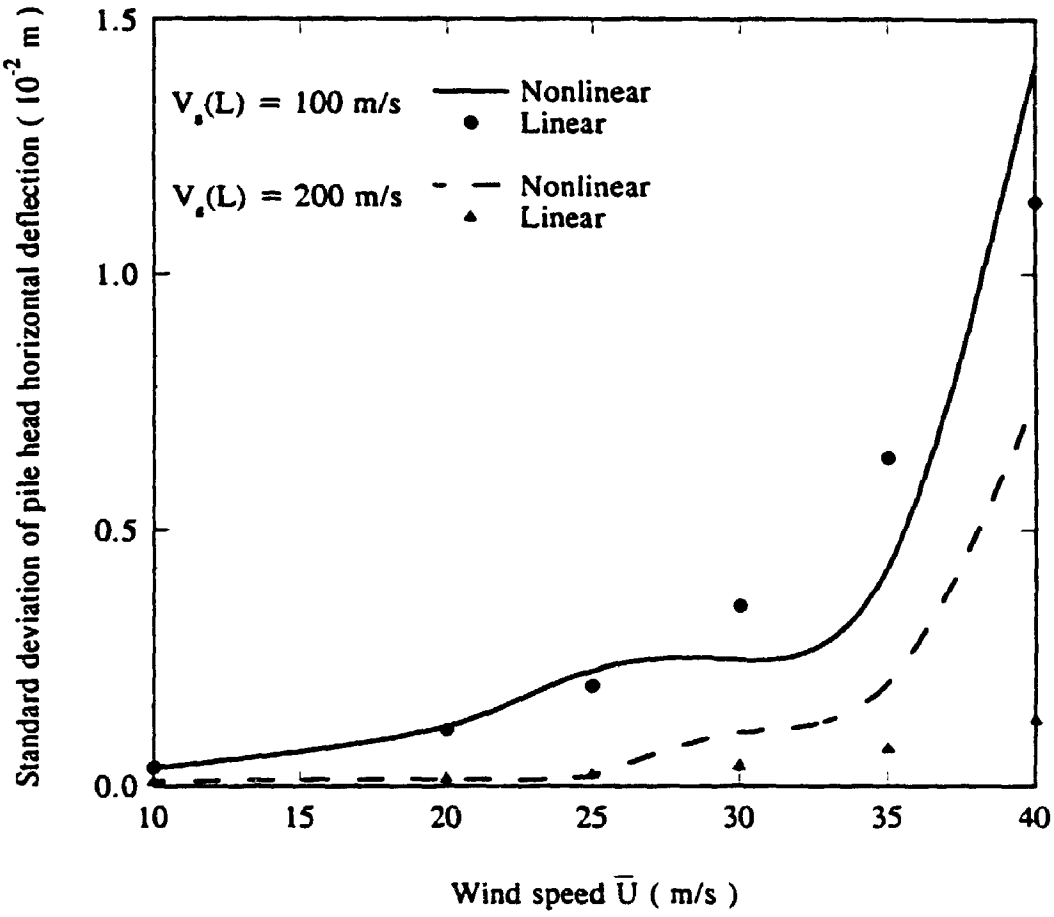

Figure 8.26 Effect of Soil Stiffness on the Horizontal Deflection of Supporting Piles (Parabolic Profile, Interaction Considered)

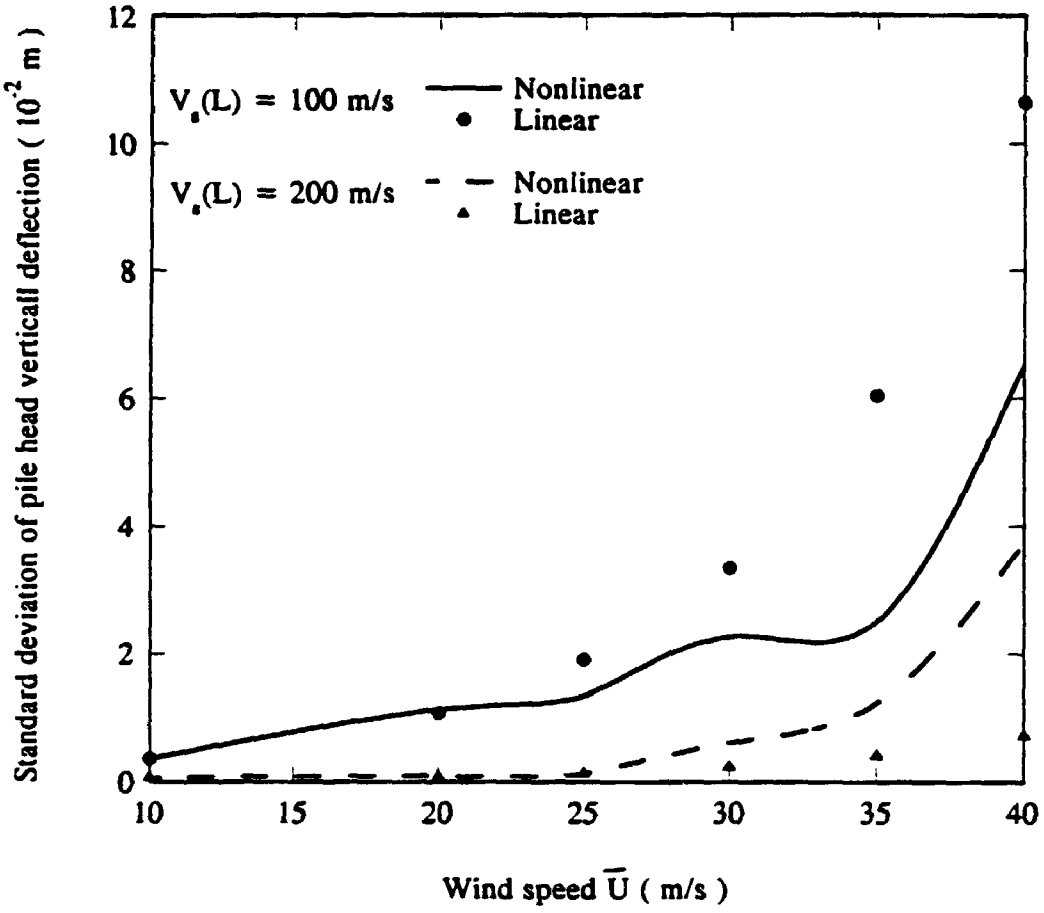

Figure 8.27 Effect of Soil Stiffness on the Vertical Deflection of Supporting Piles (Parabolic Profile, Interaction Considered)

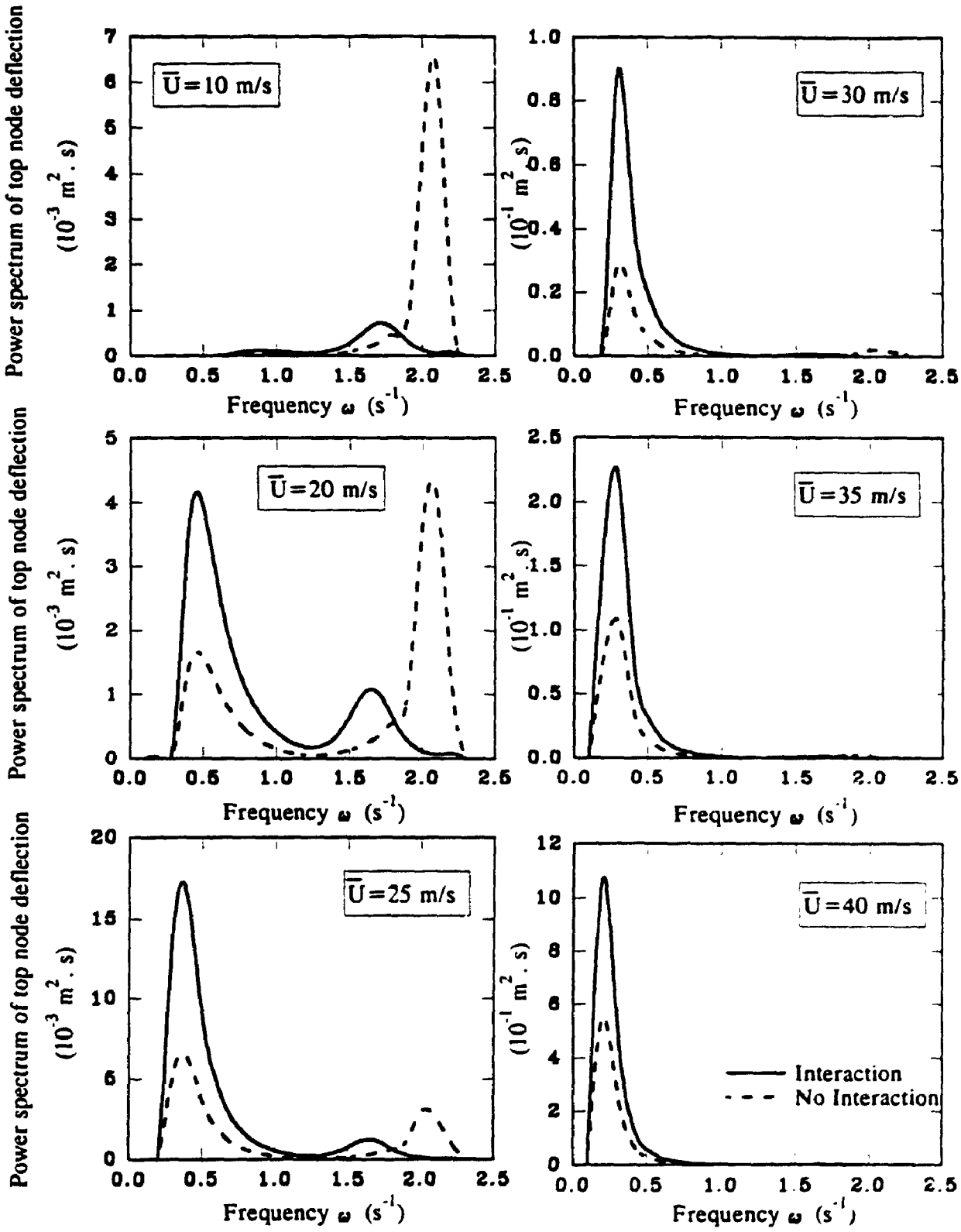

Figure 8.28 Effect of Pile-Soil-Pile Interaction on the Power Spectrum of the Tower Response (Homogeneous Profile, $V_s(L)$ = 100 m/s, Nonlinear Foundation)

interaction between piles. This behavior is further illustrated in Fig. 8.29 which show the variation in the standard deviation of top node horizontal deflection with the wind speed for both the homogeneous and parabolic soil profiles with $V_s(L)$ = 100 m/s. It is evident from the figure that the interaction between piles reduces the response amplitudes for lower wind speeds because it increases the damping in the system. For higher wind speeds, the interaction increases the response amplitudes as the contribution to the total response amplitude from the background component, which depends on the stiffness, is much higher than the contribution from the resonance component. Figs. 8.30 and 8.31 show the variation in the standard deviation of pile head horizontal and vertical deflections, respectively, with different wind speeds for homogeneous and parabolic soil profiles. It may be noticed from the figures that the interaction between piles increases both the horizontal and vertical deflections of the pile for the two soil profiles and all wind speeds. Also, it may be noticed from the figures that the interaction effect is more pronounced in the linear analysis because the linear analysis overpredicts the interaction between piles.

8.5. Conclusions

A parametric study is carried out to illustrate the effect of the foundation system properties on the free vibration characteristics as well as the response of a typical fixed offshore tower to wave forces. The following conclusions are drawn:

1- Natural frequencies decrease due to the nonlinear behavior of the soil.

2- The nonlinear behavior of a foundation decreases the structural damping ratios but it increases the tower damping derived from soil.

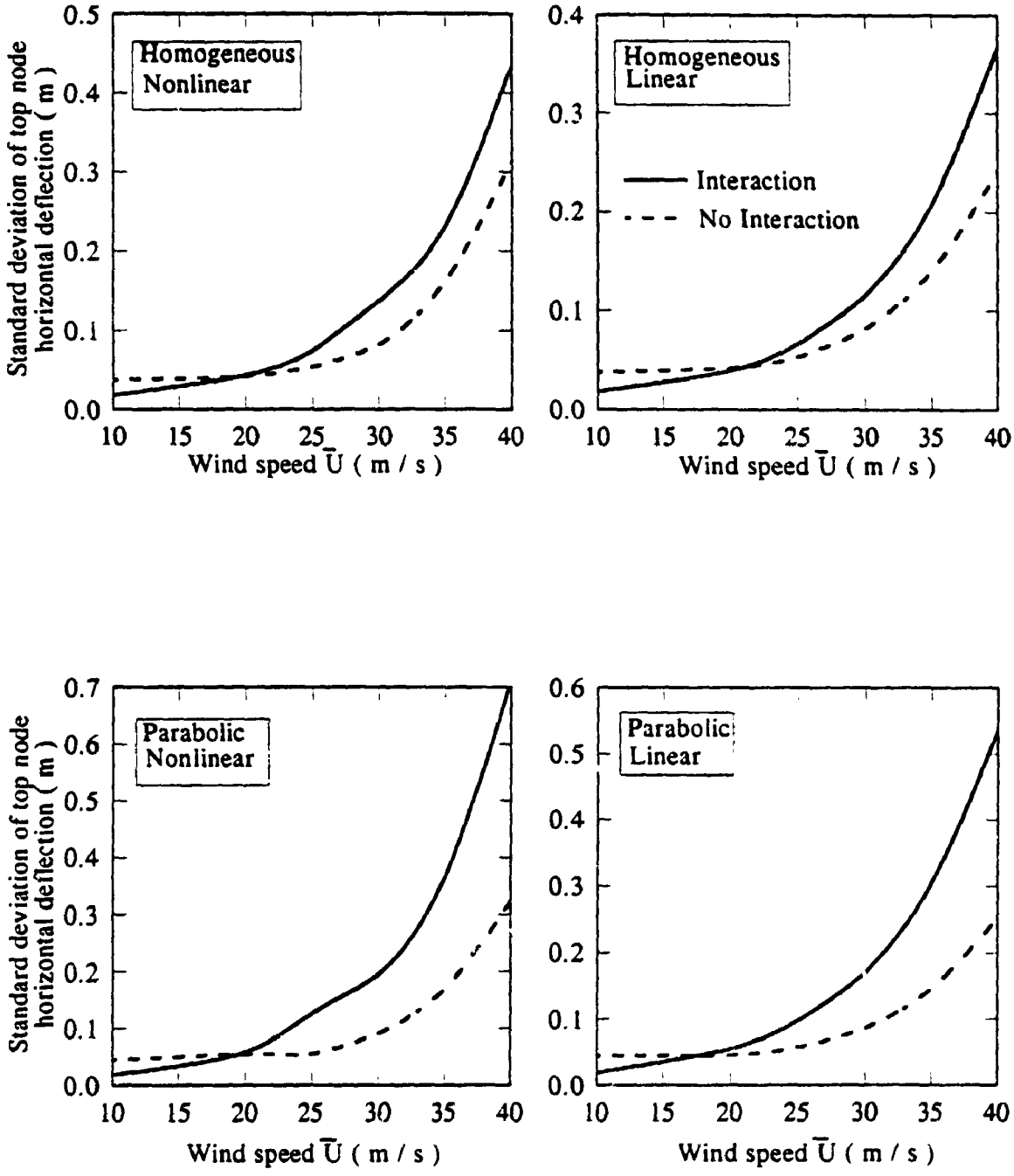

Figure 8.29 Effect of Pile-Soil-Pile Interaction on the Tower Response Amplitude for Two Soil Profiles ($V_s(L)$ = 100 m/s)

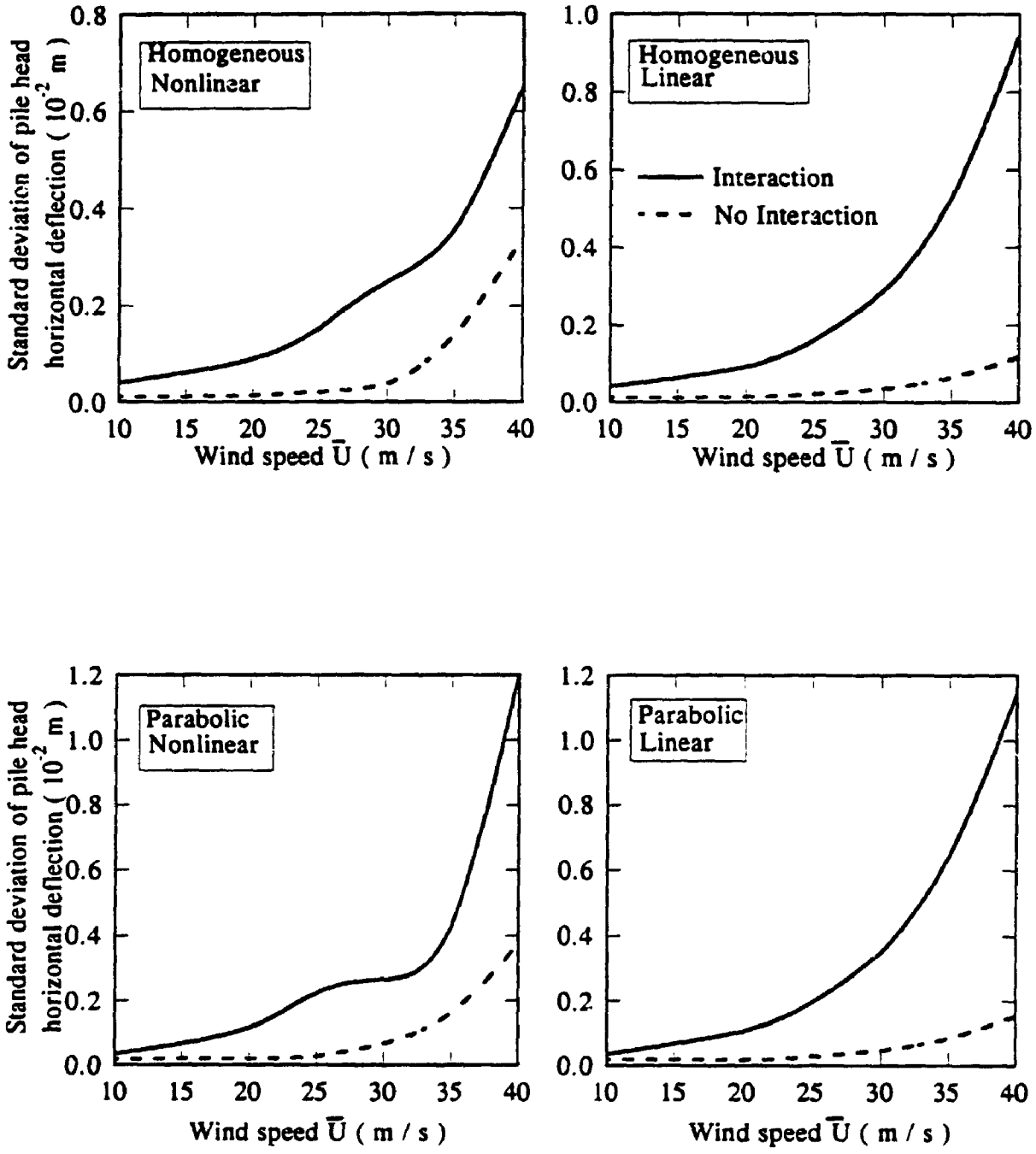

Figure 8.30 Effect of Pile-Soil-Pile Interaction on the Horizontal Deflection of Supporting Piles for Two Soil Profiles ($V_s(L)$ = 100 m/s)

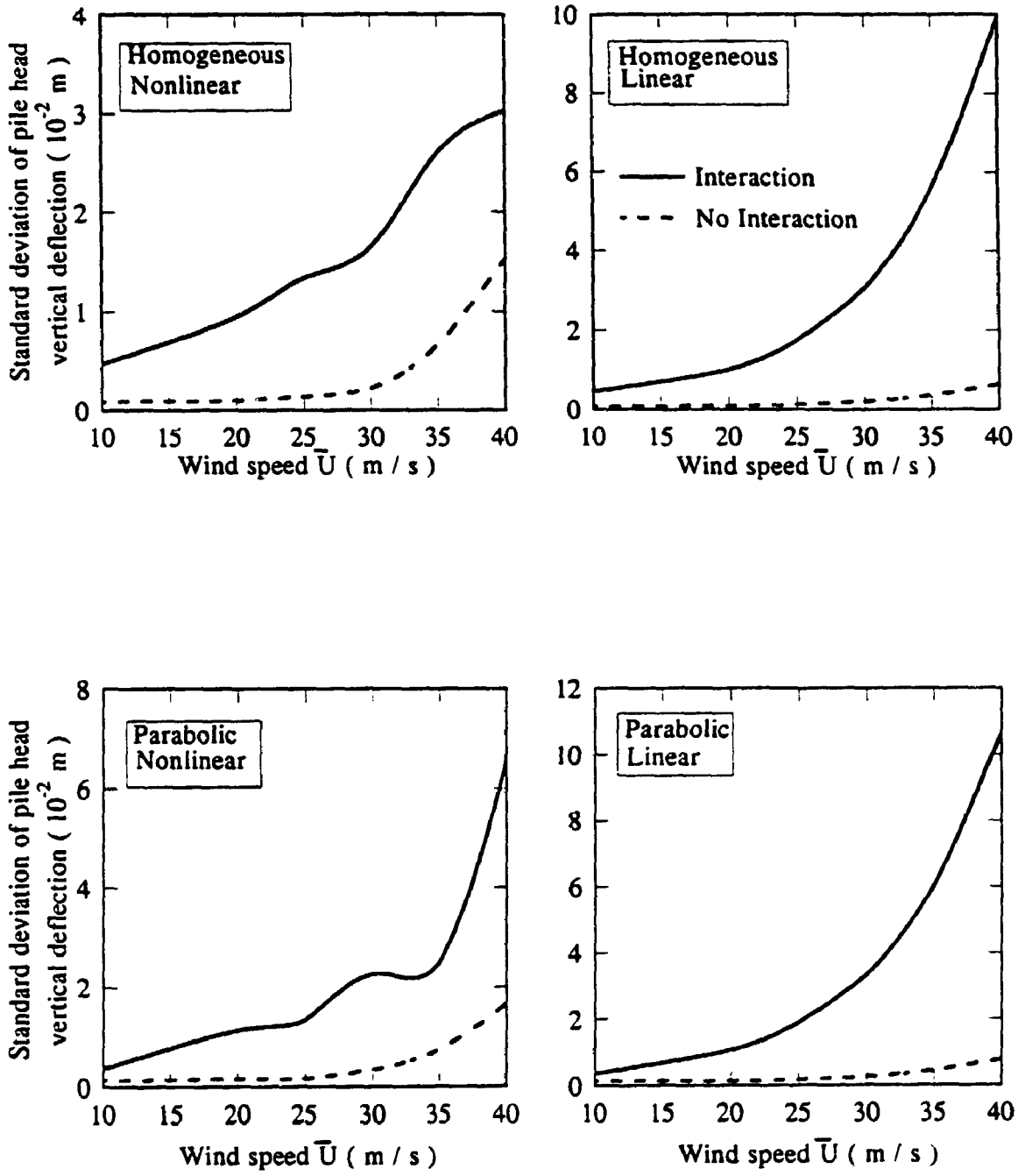

Figure 8.31 Effect of Pile-Soil-Pile Interaction on the Vertical Deflection of Supporting Piles for Two Soil Profiles ($V_s(L)$ = 100 m/s)

3- Foundation damping ratios are much higher than structural damping ratios in the practical range of soil properties encountered in offshore towers and can not be excluded in any realistic analysis.

4- The drop in structural damping ratios due to soil nonlinearity is more than compensated for by the increase in foundation damping ratios.

5- Natural frequencies and structural damping ratios for linear and parabolic soil profiles are lower than those of the homogeneous profile with those of the linear profile being the lowest. Soil damping ratios follow an opposite trend where those of the linear and parabolic soil profiles are higher than those of the homogeneous profile with those of the linear profile being the highest.

6- The nonlinear effects are more pronounced for the nonhomogeneous soil profiles than the homogeneous one and for stiffer soils compared to softer ones.

7- Pile-soil-pile interaction moderately decreases the natural frequencies but dramatically increases foundation damping ratios for linear conditions, however for nonlinear conditions these effects are still there but to a lesser extent.

8- Pile-soil-pile interaction, usually neglected in design, has a significant impact on the dynamic characteristics of the tower even with large spacing and should be considered.

9- The increase in soil shear wave velocity may decrease or increase the tower response at low wind speed, but it decreases the tower response at high wind speeds.

10- Hydrodynamic damping ratios increase due to the soil nonlinearity.

11- Hydrodynamic damping ratios decrease as the shear wave velocity increases.

12- Pile-soil-pile interaction decreases the hydrodynamic damping ratios for lower wind speeds while it increases the hydrodynamic damping ratios for nigher wind speeds.

13- Soil shear wave velocity profile has a significant effect on the tower response. The resonant response for homogeneous profile is higher than the resonant response of the parabolic and linear profiles with the linear profile being the lowest. The background part of the response follows the opposite trend.

14- The nonlinear behavior of the foundation tends to slightly reduce the resonant peak and frequency, while it significantly increases the background part of the response.

15- The total response increases due to nonlinearity for all wind speeds and all soil profiles.

16- At low wind speeds, the total response for stiffer soils is higher than that for softer soils, but for higher wind speeds the total response of the softer soils is much greater than that of the stiffer soils.

17- Pile-soil-pile interaction decreases the resonant response dramatically and significantly increases the background part of the response.

18- Pile-soil-pile interaction decreases the total response of the tower to wave forces at lower wind speeds but it increases the total response significantly for higher wind speeds.

CHAPTER NINE

SUMMARY AND CONCLUSIONS

The research done in this study comprises three main problem areas:

1- The analysis of the STATNAMIC test results and the prediction of the bearing capacity of piles as well as the analysis of pile driving and the pile drivability assessment.

2- The analysis of the nonlinear behavior of single piles and pile groups, including the nonlinear soil behavior, gapping and slippage between pile and soil.

3- The dynamic response of fixed offshore structures taking into account the nonlinear behavior of the supporting piles.

9.1 Statnamic Test and Pile Driving

An improved one dimensional wave equation analysis which accounts for wave propagation in the soil mass, and an approach for the prediction of the bearing capacity from the Statnamic load test are developed. The approach developed in this study is used to analyze some statnamic load tests and to predict the pile capacities and the results are compared with those obtained from the conventional static load test. The following conclusions emerge:

1- The Statnamic load test, along with the theoretical approach developed in this study, represents an efficient tool to predict the capacity of piles in a quick and nondestructive way for both driven and drilled piles.

2- The soil model developed has the advantage of accounting for wave propagation in the soil in a way related to fundamental soil properties and it also accounts for the variation

of the soil resistance to pile motion with the loading rate.

3- The model developed is able to handle the pile driving analysis and to assess the pile drivability in a rational way.

9.2 Nonlinear Behavior of Pile-Soil System

A simplified model was developed in this research work to analyze not only single pile response but also to include the group effects. The nonlinear behavior of the soil adjacent to the pile, gapping and slippage between pile and soil as well as the wave propagation away from the pile were taken into account. The model developed was used to analyze some cyclic and dynamic load tests. Results compared very favourably to the field measured data. Furthermore, the single piles impedance functions and pile-soil-pile interaction factors obtained using this model are similar to those obtained employing more rigorous frequency domain solutions in the linear range. The following conclusions are drawn from results of the analysis of the developed model.

1- The approximate time domain solutions developed in this study can produce sufficiently accurate results for the practical frequency range encountered for offshore piles, i.e. $0.05 < a_0 < 0.5$.

2- The model behavior was compared with the field test results of pile foundations subjected to vertical or horizontal loads. Comparisons between the two results were acceptable.

3- The single piles impedances and interaction between piles are greatly affected by the nonlinear behavior of the soil and discontinuity conditions at the pile-soil interface. These nonlinear effects should be considered in the pile group response analysis,

especially for the limit state considerations.

4- The nonlinear behavior of the soil reduces both the vertical and horizontal single pile stiffness. In addition, it increases the damping in vertical vibration and reduces it in lateral vibration. It also reduces the interaction between piles and that results in a drop in the group damping and slight increase in the group stiffness. However, the resultant effect of the nonlinear soil behavior is a reduction in both the stiffness and damping of the pile group for both the vertical and horizontal vibrations.

9.3. Response of Fixed Offshore Towers

The tower response to random wave forces is carried out incorporating the nonlinear behavior of piles and the coherence function model into the analysis. Pile-soil-pile interaction is accounted for. Drag forces are linearized and the analysis is carried out in terms of the theory of random vibration. The effect of both the foundation and wave loading parameters on the dynamic properties as well as the response of the tower are investigated and the following conclusions are drawn:

1- Foundation nonlinearity significantly affects the dynamic characteristics of the tower. It reduces natural frequencies and structural damping of the tower and increases the tower damping derived from the foundation as well as the hydrodynamic damping.

2- Pile-soil-pile interaction, usually neglected in the design, has a significant effect even with large pile spacing. It markedly increases the damping derived from the foundation and slightly decreases the natural frequencies of the tower.

3- Foundation damping is the major source of damping at low wind speeds while the

hydrodynamic damping is the main source at high wind speeds.

4- Foundation nonlinearity and the pile-soil-pile interaction have the effect that they increase the background response of the tower but they decrease the resonant response.

5- Foundation nonlinearity significantly increases the total response of the tower especially at higher wind speeds.

6- While the total response of the tower increases due to pile-soil-pile interaction at higher wind speeds, it decreases at lower wind speeds.

9.4. Recommendations for Further Research

Many of the offshore structures are located in earthquake active regions all over the world. Large displacements of the structures and supporting foundations due to earthquake excitations exceed the linear limit and nonlinear analysis is called for. The induced excitations due to earthquakes have a high frequency content and their effects on soil behavior are different from those due to waves. A rational analysis for an offshore structure response to earthquake excitations should include the soil nonlinearity as well as the interaction between piles.

Waves are usually accompanied with wind and the response of offshore structures to the mutual action of waves and wind needs to be investigated.

However, it should be noted that the accuracy of the models presented herein depends on the reliability of the input parameters. With regard to the uncertainties associated with these parameters, particularly with the soil properties, safety of offshore structures should be further studied.

REFERENCES

1. Smith, E.A.L., "Pile Driving Analysis by the Wave Equation", ASCE, Transactions, Paper No. 3308, Vol. 127, Part 1, pp. 1145-1170.

2. Tajimi, H., "Dynamic Analysis of Structures Supported on Deep Foundations", Report of the Faculty of Engineering Science, Nihon University, 1966, (in Japanese). See also Tajimi, H., "Dynamic Analysis of a Structure Embedded in an Elastic Stratum", Proceedings, 4th World Conference on Earthquake Engineering, Chile, 1969.

3. Novak, M., "Dynamic Stiffness and Damping of Piles", Canadian Geotechnical Journal, Vol. 11, No. 4, pp.574-598.

4. Nogami, T., and Novak, M., "Soil-Pile Interaction in Vertical Vibration", Earthquake Engineering and Structural Dynamics, Vol. 4, 1976, pp.277,293.

5. Novak, M., and Nogami, T., "Soil-Pile Interaction in Horizontal Vibration", Earthquake Engineering and Structural Dynamics, Vol. 5, 1977, pp.263-281.

6. Kobori, T., Minai, R. and Baba, K., "Dynamic Behavior of a Laterally Loaded Pile Proceedings of Speciality Session 10, 9th ICSMFE, Tokyo, 1977, pp.175-180.

7. Novak, M. and Aboul-Ella, F., "Impedance Functions of Piles in Layered Media", Journal of Engineering Mechanics Division, ASCE, June, 1978, Vol. 104, No. EM3, Proceedings Paper 13847, pp.643-661. See also Novak, M. and Aboul-Ella, F., "Stiffness and Damping of Piles in Layered Media", Proceedings of Earthquake Engineering and Soil Dynamics, ASCE, Speciality Conference, Pasadena, CA, June 19-21, pp.704-719.

8. Novak, M. and Sheta, M., "Approximate Approach to Contact Problems of Piles", Proceedings of Geotechnical Engineering Division, ASCE, National Convention, "Dynamic Response of Pile Foundations: Analytical Aspects", Florida, October 30, 1980, pp.53-79.

9. Akiyoshi, T., "Soil-Pile Interaction in Vertical Vibration Induced through a Frictional Interface", Earthquake Engineering and Structural Dynamics, Vol. 10, 1982, pp.135-148.

10. Banerjee, P.K., "Analysis of Axially and Laterally Loaded Pile Groups", Chapter 9 in "Developments in Soil Mechanics", Editor Scott, C., R., Applied Science Publications, London, 1978, pp. 317-346.

11. Kaynia, A.M. and Kausel, E., "Dynamic Behavior of Pile Groups", Proceedings, 2nd International Conference on Numerical Methods in Offshore Piling, I.C.E., April, 1982, pp.509-532.

12. Sen, R., Davies, T.G. and Banerjee, P.K., "Dynamic Analysis of Piles and Pile Groups Embedded in Homogeneous Soils", Earthquake Engineering and Structural Dynamics, , Vol. 13, 1985, pp.53-65.

13. Mamoon, S.M., Kaynia, A.M. and Banerjee, P.K., "On Frequency Domain Dynamic Analysis of Piles and Pile Groups", Journal of Engineering Mechanics, ASCE, Vol.116, No.10, October, 1990, pp.

14. Sanchez-Salinero, I., "Dynamic Stiffness of Pile Groups, Approximate Solution",

Geotechnical Engineering Report No. G-83-5, Department of Civil Engineering, University of Texas at Austin, 1983.

15. Winkler, E., "Die Lehre Von Der Elastizitet Und Festigkeit, "Dominics, Prague, 1867.

16. Penzien, J., Scheffey, C.F. and Parmlee, R.A., "Seismic Analysis of Bridges on Long Piles", Journal of the Engineering Mechanics Divisi.., ASCE, Vol. 90, No. EM3, June, 1964, pp.223-254.

17. Mindlin, R., D., "Force at Point in the Interior of a Semi Infinite Solid ", Physics, Vol. 7, May, 1936, pp. 195-202.

18. Prakash, S. and Chandrasekaran, V., "Pile Foundation Under Lateral Dynamic Loads", Proceedings of the 8th ICSMFE, Vol. 2, Moscow, 1973, pp. 199-202.

19. Novak, M., "Vertical Vibration of Floating Piles", Journal of the Engineering Mechanics Division, ASCE, Vol. 103, No. EM1, February, 1977, pp.153-167.

20. Baranov, V.A., "On the Calculation of Excited Vibration of an Embedded Foundation", Voprosy Dynamiki Prochnocti, No. 14, Polytech. Institution Riga, 1967, pp.195-209.

21. Novak, M., Nogami, T. and Aboul-Ella, F., "Dynamic Soil Reactions for Plane Strain Case", Journal of the Engineering Mechanics Division, ASCE, Vol. 104, No. EM4, August, 1978, pp.953-959.

22. Kagawa, T. and Kraft, L.M., "Seismic p-y Responses of Flexible Piles", Journal of the Geotechnical Engineering Division, ASCE, Vol. 106, No. GT8, August, 1980, pp. 899-918.

23. Kagawa, T. and Kraft, L.M., "Lateral Pile Response During Earthquakes", Journal of the Geotechnical Engineering Division, ASCE, Vol. 107, No. GT12, December, 1981, pp. 1713-1731.

24. Nogami, T., "Non-Linear Dynamic Winkler Model for Lateral Cyclic Response Analysis of Single Piles", Proceedings, 2nd International Conference on Soil Dynamics and Earthquake Engineering, on Board the Queen Elizabeth 2, June, 1985, pp.4-51-4-60.

25. Matlock, H., Foo, S.H.C. and Bryant, L.M., "Simulation of Lateral Pile Behavior Under Earthquake Motion", Speciality Conference on Earthquake Engineering and Soil Dynamics, Pasadena, June, 1978, pp. 600-619.

26. Nogami, T. and Konagai, K., "Time Domain Axial Response of Dynamically Loaded Single Piles", Journal of Engineering Mechanics Division, ASCE, Vol. 112, No. 11, November, 1986, pp. 1241-1252.

27. Nogami, T. and Konagai, K., "Time Domain Flexural Response of Dynamically Loaded Single Piles", Journal of Engineering Mechanics Division, ASCE, Vol. 114, No.9, September, 1988, pp.1512-1525.

28. Konagai, K., and Nogami, T., "Time Domain Axial Response of Dynamically Loaded Pile Groups", Journal of Engineering Mechanics Division, ASCE, Vol. 13, No. 3, March, 1987, pp.417-430.

29. Nogami, T., "Dynamic Stiffness and Damping of Pile Groups in Inhomogeneous soil", ASCE Special Technical Publications on Dynamic Response of Pile Foundations: Analytical Aspects, 1980, pp.31-52.

30. Nogami, T., "Dynamic Effect in Axial Response of Grouped Piles", Journal of the Geotechnical Division, ASCE, Vol. 109, No. 2, February, 1983, pp.228-243.

31. Sheta, M. and Novak, M., "Vertical vibration of Pile Groups", Journal of the Geotechnical Engineering Division, ASCE, Vol.108, No. GT4, April, 1982, pp.570-589.

32. Dobry, R., Vicente, E., O'Rourke, M.J. and Roesset, J.M., "Horizontal Stiffness and Damping of Single Piles", Journal of the Geotechnical Engineering Division, ASCE, Vol. 108, GT3, March, 1982, pp.439-459.

33. Gazetas, G. and Dobry, R., "Horizontal Response of Piles In Layered Soils", Journal of the Geotechnical Engineering Division, ASCE, Vol. 110, No. 1, January, 1984, pp.20-40.

34. Nogami, T., Konagai, K. and Otani, J., "Nonlinear Time Domain Numerical Model for Pile Group Under Transient Dynamic Forces", Proceedings: 2nd International Conference on Recent Advances in Geotechnical Earthquake Engineering and Soil Dynamics, March, 1991, St. Louis, Missouri, Paper No. 5.51.

35. Blaney, G.W., Kausel, E., and Roesset, J.M., "Dynamic Stiffness of Piles", Proceedings, 2nd International Conference on Numerical Methods in Geomechanics, Vol. 2, 1976, pp.1001-1012.

36. Kausel, E., Roesset, J.M. and Waas, G., "Dynamic Analysis of Footings on Layered Media", Journal of Engineering Mechanics Division, ASCE, Vol. 101, No. EM5, 1975, pp. 679-693.

37. Kuhlemeyer, R.L., "Static and Dynamic Laterally Loaded Floating Piles", Journal of Geotechnical Engineering Division, ASCE, Vol. 105, No. GT2, February, 1979, pp. 325-330.

38. Wolf, J.P. and von Arx, G.P., "Impedance Function of a Group of Vertical Piles", Proceedings, Speciality Conference on Earthquake Engineering and Soil Dynamics, Vol. 2, 1978, pp.1024-1041.

39. Angelides, D.C. and Roesset, J.M., "Nonlinear Lateral Dynamic Stiffness of Piles", Journal of the Geotechnical Engineering Division, Vol. 107, No.GT11, November, 1981, pp.1443-1459.

40. Stevens, J.B. and Audibert, J.M.E., "Re-examination of p-y curve Formulations", Proceedings, 11th Offshore Technology Conference, Paper No. OTC3402, 1979, pp. 397-403.

41. "Planning and Design of Fixed Offshore Platforms", McClelland, B. and Reifel, M.D. (Editors), Van Nostrand Reinhold Company, 1986.

42. Vickery, B.J., "Wind Loads on Compliant Offshore Structures", Proceedings of Symposium on Ocean Structural Dynamics, Dept. of Civil Engineering, Oregon State University, Covillas, Oregon, September 8-10, 1982.

43. Strickland, G.E., Brooks, L.D. and Pearce, J.C., "Ice Forces", Chapter 3 in

"Planning and Design of Fixed Offshore Platforms", McClelland, B. and Reifel, M.D. (Editors), Van Nostrand Reinhold Company, 1986.

44. Forehand, P.W. and Reese, J.L., "Prediction of Pile Capacity by the Wave Equation", Journal of Soil Mechanics and Foundation Division, ASCE, Vol. 90, No.2, 1964, pp. 1-25.

45. Meynard, A. and Corte', J.F., "Experimental Study of Lateral Resistance During Driving", Proceedings 2nd International Conference on Application of stress wave theory on piles., Stockholm, 1984, pp.143-150.

46. Mitwally, H. and Novak, M., "Pile Driving Analysis", 10th Canadian Congress of Applied Mechanics, London, Canada, 1985, pp. A325-A326.

47. Simons, H.A. and Randolph, M.F., "A New Approach to One Dimensional Pile Driving Analysis", Proceedings 5th International Conference on Numerical Methods in Geomechanics, Nagoya, Vol.3 1985, pp.1457-1464.

48. Lee, S.L., Chow, Y.K., Karunaratne, G.P. and Wong, K.Y., "Rational Wave Equation Model for Pile Driving Analysis", Journal of Geotechnical Engineering, ASCE,Vol. 114, No.3, 1988, pp. 306-325.

49. Mitwally, H. and Novak, M., "Pile Driving Analysis Using Shaft Models and FEM", Proc. 3rd International Conference on Application of Stress-Wave Theory to Piles. Ottawa, May, 1988, pp. 455-466

50. Horvath, R.C., Bermingham, P. and Janes, M.,"The Statnamic Loading Test, an Innovative Method for Predicting Capacity of Deep Foundations", Proceedings 43rd Canadian Geotechnique Conference, Laval University, Quebic, 1990, pp.143-150.

51. Janes, M.C., Bermingham, P.D., and Horvath, R.C., "An Innovative Dynamic Test Method for Piles", Proceedings 2nd International Conference on Recent Advances in Geotechnical Earthquake Engineering and Soil Dynamics St. Louis, March, 1991, pp.252-256.

52. Novak, M. and Han, Y., "Impedances of Soil Layer with Boundary Zone", Journal of Geotechnical Engineering Division, ASCE, vol. 116, No.6, 1990, pp.1008-1014.

53. Lysmar, J. and Richart, F.E., "Dynamic Response of Footing to Vertical Loading", Journal of Engineering Mechanics Division, ASCE, Vol. 92, 1966, pp. 65-91.

54. Egorov, K.E., "Calculation of Bed for Foundation with Ring Footing", Proc. 6th International Conference on Soil Mechanics and Foundation Engineering, Montreal, Canada, vol.2, 1965, pp.41-45.

55. Gazetas, G. and Dobry, R., "Simple Radiation Damping Model for Piles and Footings", ASCE, Journal of Engineering Mechanics, Vol. 110, No. EMS, 1984, pp. 937-956

56. Coyle, H.M. and Gibson, G.C., "Empirical Damping Constants for Sands and Clays", Journal of Soil Mechanics and Foundation Division, ASCE, Vol. 96, No. 3, 1970, pp. 949-965

57. Litkouhi, S. and Poskitt, T.J., "Damping Constants for Pile Drivability

Calculations", Geotechnique, Vol. 30, No. 1, 1980, pp. 77-86

58. Heerema, E.P., "Relationships Between Wall Friction, Displacement, Velocity and Horizontal Stress in Clay and in Sand for Pile Drivability Analysis", Ground Engineering, Vol. 12, No. 1, 1979, pp. 55-60

59. Heerema, E.P., "Dynamic Point Resistance in Sand and in Clay for Pile Drivability Analysis", Ground Engineering, Vol. 4, No.6, 1981, pp. 30-46.

60. Bathe, K.J., "Finite Element Procedures in Engineering Analysis", 1982, Prentice-Hall,inc.

61. Chow, Y.K., Karunaratne, G.P., Wong, K.Y. and Lee, S.L., "Prediction of Load-carrying Capacity of Driven Piles", Canadian Geotechnical Journal, Vol. 25, 1988, PP.13-23.

62. Robertson, P.K., Campenella, R.G., Davies, M.P. and Sy, A., "Axial Capacity of Driven piles in Deltaic Soils Using CPT", 1st International Symposium on Penetration Testing, Orlando, March, 1988, pp.919-928.

63. Briaud, J.L., "Dynamic and Static Testing of Nine Drilled Shafts at Texas A&M University Geotechnical Research Sites", Geotechnical News, Canadian Geotechnical Society, Dec., 1991, pp.65-67.

64. Clough, R.W. and Penzien, J., "Dynamics of Structures", 1975, McGraw-Hill.
Coutinho, A.L.G., Costa, A.M., Alves, J.L.D. and Ebecken, N.F.F., "Pile Driveability Simulation and Analysis by the Finite Element Method", Proceedings 3rd International Conference on the Application of Stress-Wave Theory to Piles. Ottawa, 1988, pp. 197-207.

65. Akiyoshi, T. and Fuchida, K., " An Approximate Solution of Vertical Vibration of End-Bearing Piles With Frictional Interface", Proceedings JSCE, No. 324, August, 1982, pp. 31-40 (in Japanese).

66. Holeyman, A.E., "Dynamic Non-Linear Skin Friction of Piles", Proceedings of the International Symposium on Penetrability and Driveability of Piles. San Francisco, vol.1, 1985, pp.173-176.

67. Holeyman, A.E., "Modelling of Dynamic Behaviour at the Pile Base", Proceedings 3rd International Conference of Application of Stress-Wave Theory on Piles, Ottawa, 1988, pp.174-185.

68. Randolph, M.F. and Wroth, C.P., "Analysis of Deformation of Vertically Loaded Piles", Journal of Geotechnical Engineering Division, Vol.104, No.GT12, 1978, pp.1465-1488.

69. Trochanis, A.M., Bielak, J. and Christiano, P., "A Three-Dimensional Non-Linear Study of Piles Leading to the Development of a Simplified Model", Technical Research Report No. R-88-176, Dept. of Civil Engineering, Carnegie Institute of Technology, Pittsburgh, PA, 1988.

70. Kondner, R.L., "Hyperbolic Stress Strain Response : Cohesive Soils", Journal of Soil Mechanics and Foundations Division, ASCE, vol. 89, 1963, pp. 115-143

71. Novak,M. and Beredugo,Y., "Vertical Vibration of Embedded Footings", Journal of Soil Mechanics and Foundations Division, ASCE, Vol. 98, No. SM12, December, 1972, pp.1291-1310

72. Danziger, B.R., "Dynamic Analysis of Pile Driving", Ph.D. Thesis. University of Rio De Janeiro, Brasil, 1991, (in Portuguese).

73. Muster, G.L., II, and O'Neil, M.W., "Dynamically Loaded Pile in Overconsolidated Clay", Geotechnical Testing Journal, American Society for Testing and Materials, Philadelphia, PA, Vol. 9, No. 4, 1986, pp. 189-197.

74. Poulos, H.G., "Analysis and Settlement of Pile Groups", Geotechnique, Vol. 18, 1968, pp. 449-471.

75. El-Marsafawi, H., Kaynia, A.M. and Novak, M., "The Superposition Approach To Pile Group Dynamics", Piles Under Dynamic Loads, ASCE Geotechnical Special Publication No.34, 1992, pp.114-135.

76. American Petroleum Institute, "Recommended Practice for Planning, Designing and Constructing Fixed Offshore Platforms", API Recommended Practice 2A (RP 2A), Nineteenth Edition, Washington, D.C., 1991.

77. Poulos, H.G., "Behaviour of laterally loaded Piles: I-Single Piles", Journal of Soil Mechanics and Foundations Division, ASCE, Vol. 97, SM5, Proceedings Paper 8902, 1971, pp. 711-732.

78. Evangelista and Viggiani, "Accuracy of Numerical Solutions for Laterally Loaded Piles in Elastic Half Space", Proceedings of 2nd International Conference on numerical Methods in Geomechanics, Blacksburg, Vol. 3, 1976, pp. 1367-1370.

79. El Sharnouby, B. and Novak, M., "Static and Low Frequency Response of Pile Groups", Canadian Geotechnical Journal, Vol. 22, No. 2, 1985, pp.79-84.

80. Makris, N. and Gazetas, G., "Dynamic Pile-Soil-Pile Interaction. Part II: Lateral and Seismic Response", Journal of Earthquake Engineering and Strucural Dynamics, Vol. 21, February 1992, pp. 145-162.

81. Poulos, H.G., "Behaviour of laterally loaded Piles: II-Pile Groups", Journal of Soil Mechanics and Foundations Division, ASCE, Vol. 97, SM5, Proceedings Paper 8903, 1971, pp. 733-751

82. O'Neil, M.W. and Dunnavant, T.W., "A Study of the Effects of Seals, Velocity and Cyclic Degradability on Laterally Loaded Single Piles in Overconsolidated Clay", Research Report UHCE84-7. Department of Civil Engineering, University of Houston, 1984.

83. Blaney, G.W. and O'Neil, M.W., "Lateral Response of a Single Pile in Overconsolidated Clay to Relatively Low Frequency Pile-Head Load and Harmonic Ground Surface Loads", Research Report UHCE83-19, Department of Civil Engineering, University of Houston, 1983.

84. Philips, O.M., "The Dynamics of Upper Ocean", Second ed., Cambridge University Press, 1977.

85. Wheeler, J.D., "Method for Calculating Forces Produced by Irregular Waves", First Annual Offshore Technology Conference, Houston, Texas, May 1969, OTC 1008.

86. Morison, J.R., O'Brien, M. P., Johnson, J.W. and Schaaf, S.A., "The Force Exerted by Surface Waves on Piles", Petroleum Transactions, AIME, Vol. 189, 1950, pp. 149-154.

87. Hobgen, N., Miller, B.L., Searle, J.W. and Ward, G., "Estimation of Fluid Loading on Offshore Structures", Proceedings of Institution of Civil Engineering, Part 2, Vol. 63, September 1977, pp. 515-562.

88. Malhorta, A. and Penzien, J., "Non-Deterministic Analysis of Offshore Structures", Journal of Engineering Mechanics Division, ASCE, Vol. 96, No.EM6, December 1970, pp. 985-1003.

89. Dean, R.G., "Hybrid Methods of Computing Wave Loading", Proceedings, Offshore Technology Conference, Houston, May 1977, OTC 3029, pp.483-492.

90. Mitwally, H., "Dynamic Analysis of Offshore Structures", Ph. D. Thesis, University of Western Ontario, London, 1987.

91. Sarpkaya, T. and Isaacson M., "Mechanics of Wave Forces on Offshore Structures", Chapter 4, Van Nostrand Reinhold Co., 1981.

92. St.Denis, M. and Pierson, W.J., "On the Motion of Ships in Confused Seas", Trans. Soc. Naval Architects and Marine Engineers, New York, 1961, pp. 280-357.

93. Pierson, W.J. and Moskowitz, L., "A Proposed Spectral Form for Fully Developed Wind Seas Based on the Similarity Theory of S.A. Kitairorodskii", Journal of Geophysical Research, Vol. 69, No. 24, December 1964.

94. Borgman, L.E., "Directional Spectra Models for Design Use", First Annual Offshore Technology Conference, Houston, Texas, May 1969, OTC 1069.

95. Berge, B., "Three Dimensional Stochastic Response of Offshore Towers to Wave Forces", Ph. D. Thesis, University of California, Berkeley, California, 1973.

96. Novak, M. and Mitwally, H., "Random Response of Offshore Towers with Pile-Soil-Pile Interaction", Journal of Offshore Mechanics and Arctic Engineering, Vol. 112, February 1990, pp.35-41.

97. Davenport, A.G., "Wind Structure and Wind Climate", Paper Presented at the International Research Seminar on Safety of Structures Under Dynamic Loading, Trondheim, June 1977.

98. Bea, R.G., "Earthquake Geotechnology in Offshore Structures", Proceedings of 2nd International Conference on Recent Advances in Geotechnical Earthquake Engineering and Soil Dynamics. St. Louis, March, 1991, Paper No. SOA13.

99. Penzien, J., Kaul, M.K. and Berge, B., "Stochastic Response of Offshore Towers to Random Sea Waves and Strong Motion Earthquakes", Computers and Structures, Vol. 2, 1972, pp. 733-756.

100. Cook, R.D., "Concepts and Applications of Finite Element Analysis", John Wiley,

1974.

101. Novak, M. and Howell, J.I., "Dynamic Response of pile Foundations in Torsion", Journal of Geotechnical Engineering Division, ASCE, Vol. 104, No. GT5, pp. 535-552. Rubinstien, M.F., "Matrix Computer Methods in Structural Analysis", Prentice-Hall, Inc., 1968.

102. Weaver, W. Jr. and Gere, J.M., "Matrix Analysis of Framed Structures", Van Nostrand Reinhold Co., 1965.

103. Godeau, A.J. and Deleuil, G.E., "Dynamic Response and Fatigue Analysis of Fixed Offshore Structures", Annual Offshore Technology Conference, Houston, Texas, OTC 2260.

104. Foster, E.T., "Model for Nonlinear Dynamics of Offshore Towers", Journal of Engineering Mechanics Division, Proceedings, ASCE, Vol. 96, No. EM1, February 1970, pp. 41-67.

105. Pipes, L.A. and Hovanessian, S.A., "Matrix Computer Methods in Engineering", John Wiley, 1969.

106. Novak, M. and El-Hifnawy, L., "Effect of Soil Structure Interaction on Damping of Structures", Journal of Earthquake Engineering and Structural Dynamics, Vol. 11, pp. 595-621.

107. Davenport, A.G., "The Distribution of Largest Values of Random Function with Application to Gust Loading", Proceedings ICE, London, Vol. 28, 1964.

108. Dawson, T.H., "Offs' ore Structural Engineering", Prentice-Hall, Inc., 1983.